INKJET PRINTING OF BIOLOGICAL MACROMOLECULES FOR USE IN BIOLOGY AND MEDICINE

A thesis submitted to The University of Manchester for the degree of

Engineering Doctorate

in the Faculty of Engineering and Physical Sciences

2011

CHRISTOPHER CHARLES COOK

School of Materials Science

TABLE OF CONTENTS

TITLE PAGE ..... - 1 -
TABLE OF CONTENTS ..... - 2 -
TABLE OF FIGURES ..... - 7 -
TABLE OF TABLES ..... - 11 -
ABSTRACT ..... - 12 -
DECLARATION ..... - 13 -
COPYRIGHT STATEMENT ..... - 14 -
ACKNOWLEDGEMENTS ..... - 15 -
CHAPTER 1: INTRODUCTION ..... - 16 -
1.1. Aims and Objectives ..... - 17 -
CHAPTER 2: LITERATURE REVIEW ..... - 19 -
2.1. Overview of Sensors ..... - 19 -
2.1.1. Structure of the sensor ..... - 19 -
2.1.2. Biological Elements ..... - 20 -
2.1.2.1. Enzymes ..... - 21 -
2.1.2.2. Antibodies ..... - 22 -
2.1.2.3. Nucleic Acids ..... - 23 -
2.1.2.4. Receptors ..... - 24 -
2.1.3. Immobilisation of biological component ..... - 24 -
2.1.3.1. Adsorption ..... - 24 -
2.1.3.2. Microencapsulation ..... - 25 -
2.1.3.3. Entrapment ..... - 26 -
2.1.3.4. Cross – Linking ..... - 26 -
2.1.3.5. Covalent Bonding ..... - 26 -
2.1.4. Biosensor Manufacturing Technique ..... - 27 -
2.1.4.1. Screen Printing Procedures ..... - 27 -
2.1.5. Sensor Electrochemistry ..... - 29 -
2.1.5.1. The double layer ..... - 29 -
2.1.5.2. The Potentiostat ..... - 31 -
2.1.5.3. Cyclic Voltammetry ..... - 35 -
2.1.5.4. Hydrodynamic Voltammetry ..... - 37 -
2.1.5.5. Amperometric in stirred solution ..... - 39 -
2.1.5.6. Chronoamperometry ..... - 40 -
2.1.5.7. Flow Injection Analysis with Amperometric Detection ..... - 42 -
2.1.6. Current sensor technology ..... - 44 -
2.1.6.1. Pregnancy sensors ..... - 44 -

2.1.6.2. Glucose sensors ..... - 47 -
2.2. Fundamentals of Proteins ..... - 55 -
2.2.1. Amino Acids ..... - 55 -
2.2.2. Primary structure of proteins ..... - 56 -
2.2.3. Secondary structure of proteins ..... - 57 -
2.2.3.1. Alpha Helix ..... - 57 -
2.2.3.2. β Pleated Sheet ..... - 58 -
2.2.4. Tertiary structure of proteins ..... - 59 -
2.2.5. Glucose Oxidase Structure ..... - 60 -
2.2.6. Enzyme Kinetics ..... - 61 -
2.2.6.1. How enzymes work ..... - 61 -
2.2.6.2. Dehydrogenase Enzymes ..... - 63 -
2.2.6.3. The Michaelis – Menten Mechanism ..... - 63 -
2.2.7 Enzyme Stabilisation ..... - 67 -
2.2.7.1 Influencing Factors ..... - 69 -
2.2.7.2 Mechanism of Stabilisation ..... - 69 -
2.3. Protein Printing Techniques ..... - 71 -
2.3.1. Contact Printing Techniques ..... - 71 -
2.3.1.1. Pin Printing ..... - 72 -
2.3.1.2. Microstamping ..... - 73 -
2.3.1.3. Nano- Tip Printing ..... - 74 -
2.3.2. Non-Contact Printing Techniques ..... - 77 -
2.3.2.1. Photochemistry-Based Printing ..... - 77 -
2.3.2.2. Electro-Printing ..... - 78 -
2.3.2.3. Laser Writing ..... - 78 -
2.3.2.4. Motion Controlled Non-Contact Pin Printing ..... - 80 -
2.3.2.5. Electrospray Deposition (ESD) ..... - 80 -
2.3.2.6. Continuous Inkjet Printing ..... - 82 -
2.3.2.7. Drop on Demand (DOD) Inkjet Printing ..... - 83 -
2.3.2.8. Thermal Drop on Demand Printing ..... - 84 -
2.3.2.9. Piezoelectric Drop on Demand Printing ..... - 86 -
2.4. Solution Parameters ..... - 89 -
2.4.1. Protein Inks ..... - 89 -
2.4.2. Drop impact, spreading and coalescence ..... - 91 -
2.4.3. Drop drying and coffee staining ..... - 93 -
2.5. Current Biosensor Deposition Technology ..... - 96 -

2.5.1. Current deposition techniques for biosensors ..... - 96 -
2.6. Summary and Conclusions ..... - 98 -
CHAPTER 3: BUSINESS JUSTIFICATION ..... - 100 -
3.1. Project Outline and History ..... - 100 -
3.2. Business Case ..... - 101 -
3.3. Exploitation of the technology ..... - 102 -
3.3.1. Chemical Sensors Market ..... - 102 -
3.3.2. Cell Printing ..... - 105 -
CHAPTER 4: METHODS ..... - 106 -
4.1. Protein Preparation ..... - 106 -
4.2. Inkjet Printing ..... - 106 -
4.2.1. The experimental set up ..... - 106 -
4.2.2. Determining the effect of actuating voltage on drop volume ..... - 108 -
4.2.3 Determining the effect of voltage on drop mass ..... - 109 -
4.2.4 General procedure for protein printing ..... - 109 -
4.2.5. Printing Patterns ..... - 109 -
4.3. Protein Characterisation ..... - 110 -
4.3.1. Protein solution viscosity ..... - 110 -
4.3.2. Protein solution surface tension ..... - 110 -
4.3.3. Fluorescence analysis ..... - 110 -
4.3.3.1. Calibration Curve ..... - 111 -
4.3.3.2. Taking a reading ..... - 111 -
4.3.4. Light Scattering ..... - 111 -
4.3.4.1. Theory ..... - 111 -
4.3.4.2. Data Collection ..... - 112 -
4.3.5. Analytical Ultracentrifugation ..... - 112 -
4.3.5.1. Theory ..... - 113 -
4.3.5.2. Data Collection ..... - 113 -
4.3.6. Circular Dichroism ..... - 114 -
4.3.6.1. Theory of secondary structure determination ..... - 114 -
4.3.6.2. Data collection ..... - 114 -
4.4. Surface Characterisation ..... - 115 -
4.4.1. Scanning Electron Microscopy ..... - 115 -
4.4.1.1. Theory ..... - 115 -
4.4.1.2. Data Collection ..... - 116 -

4.4.2. Phase Contrast Optical Microscopy ..... - 116 -
4.4.2.1. Theory ..... - 116 -
4.4.2.2. Data Collection ..... - 117 -
4.4.3. Contact Angle analysis ..... - 117 -
4.4.3.1. Theory ..... - 117 -
4.4.3.2. Data Collection ..... - 118 -
4.4.4. Chronoamperometry Measurements ..... - 118 -
4.4.4.1. Theory ..... - 119 -
4.4.4.2. Data collection ..... - 120 -
4.5. Statistical Analysis ..... - 120 -
4.5.1. Theory ..... - 121 -
CHAPTER 5: RESULTS AND DISCUSSION ..... - 124 -
5.1. Analysis of Printing Parameters ..... - 124 -
5.1.1. Viscosity of printing solution ..... - 124 -
5.1.2. Surface Tension of printing solutions ..... - 125 -
5.1.3. The influence of waveform amplitude on drop volume and mass ..... - 126 -
5.1.4. Retained activity of the enzyme after printing ..... - 128 -
5.2. Printing Associated Protein Damage ..... - 131 -
5.2.1. Effect of printing on protein structure ..... - 131 -
5.2.2. Analytical Ultracentrifugation analysis of the protein structure ..... - 138 -
5.2.3. Analysis of protein conformation after printing ..... - 143 -
5.3. Electrode Characteristics ..... - 147 -
5.3.1. Comparison of the carbon electrode materials ..... - 149 -
5.3.2. Consistency of electrode production ..... - 157 -
5.3.2.1. Analysis of chemical properties of the electrodes ..... - 157 -
5.3.2.2. Analysis of the physical properties of the electrodes ..... - 162 -
5.4. Fluid Properties on the Electrode Surface ..... - 166 -
5.4.1. Comparison of the fluid – electrode interaction with different carbons ..... - 167 -
5.4.2. Effect of the enzyme sugar solution on the electrode – fluid interactions. ..... - 171 -
5.4.3. Effect of the addition of a surfactant to the enzyme solution ..... - 175 -
5.4.4. Drying conditions and optimal concentrations ..... - 181 -
5.5. Method for Production of a Biosensor using Drop on Demand Inkjet Technology - 187 -
5.5.1. Refining the electrochemical properties of the electrode. ..... - 187 -

5.5.2. Protocol for the Production of Electrodes using Inkjet Printing. ..... - 191 -
CHAPTER 6: CONCLUSIONS AND FURTHER WORK ..... - 194 -
6.1. Technical Aspects ..... - 195 -
6.1.1. Current Technologies ..... - 195 -
6.1.2. Market Requirement ..... - 196 -
6.1.3. Effect of the printing technique on the analyte ..... - 197 -
6.1.4. Surface characterisation ..... - 198 -
6.1.5. Reproducibility and Repeatability ..... - 199 -
6.1.6. Overall Conclusions ..... - 200 -
6.1.7. Further work and Recommendations ..... - 201 -
6.2. Business outcomes ..... - 202 -
6.2.1. Xaar ..... - 202 -
6.2.2. AET Ltd ..... - 203 -
6.2.3. Ellis Developments ..... - 204 -
6.2.5. Project Dissemination ..... - 204 -
CHAPTER 7: REFERENCES ..... - 206 -

Total Word Count = 56,654

TABLE OF FIGURES

Figure 2.1.	Schematic Layout of a Biosensor	19
Figure 2.2.	Antibody Structure showing the antigen binding sites as well as the heavy and light chains	23
Figure 2.3.	The basic screen printing process	28
Figure 2.4.	Electrical double layer	30
Figure 2.5.	Setup of the electrode system used in this study	34
Figure 2.6.	Typical CV output signal	35
Figure 2.7.	Cyclic Voltammetry input waveform	36
Figure 2.8.	Typical excitation waveform for Hydrodynamic Voltammogram	38
Figure 2.9.	Representative experimental response obtained using Hydrodynamic Voltammetry at two different stirring speeds	38
Figure 2.10.	Representative current response obtained for amperometry in stirred solutions following multiple addition of the analyte	40
Figure 2.11.	Typical waveform for amperometry in stirred solution	40
Figure 2.12.	Typical waveform for chronoamperometric detection	41
Figure 2.13.	Typical chronoamperometric detection in presence of analyte	41
Figure 2.14.	Representation of wall jet electrodes and relative flow pattern	43
Figure 2.15.	Principle of agglutination inhibition assay	46
Figure 2.16.	Principle of enzyme immunoassay	47
Figure 2.17.	Schematic of a first generation biosensor	50
Figure 2.18.	Sequence of events that occur in second generation (mediated) glucose sensors	53
Figure 2.19.	The basic structure of an amino acid	55
Figure 2.20.	A condensation reaction between two amino acids to form a peptide bond	56
Figure 2.21.	A diagram of an alpha helix.	58
Figure 2.22.	Representation of two Beta pleated sheets	59
Figure 2.23.	Overall topology of GOX	61
Figure 2.24.	Difference in activation energy for catalysed and uncatalysed reaction	62
Figure 2.25.	Plot of reaction rate versus analyte concentration for a reaction obeying Michaelis Menten kinetics	65
Figure 2.26.	Eisenthal-Cornish Bowden plot	67
Figure 2.27.	Polyelectrolyte stabilisation of a protein	70
Figure 2.28.	Microstamp fabrication	74
Figure 2.29.	Schematic diagram of the process of AFM dip-pen lithography	75
Figure 2.30.	Schematic of AFM grating	76
Figure 2.31.	Schematic of an indirect laser writing system	79

Figure 2.32.	Schematic of electrospray deposition	81
Figure 2.33.	The Biodot Jet Printer	83
Figure 2.34.	Schematic diagram for the ink droplet generation cycle in a Thermal Inkjet Printer	85
Figure 2.35.	Squeeze mode actuator design	87
Figure 2.36.	Principle of bend mode actuation	87
Figure 2.37.	Functional principle of a push mode inkjet actuator	88
Figure 2.38.	Inkjet printing is practical for a limited range of fluids and printing conditions	91
Figure 2.39.	Schematic illustration of the timescales appropriate to the processes of drop deformation and spreading on a physical substrate after impact	92
Figure 4.1.	Schematic arrangement of the printer set up	107
Figure 4.2.	(a) Schematic of the printhead (b) Image of the jet in action (c) The waveform applied to the piezoelectric	108
Figure 4.3.	Setup of electrode system used in this study	119
Figure 5.1.	The shear viscosity of solutions measured against the speed of the parallel plates in solution	125
Figure 5.2.	Surface tension of the solutions analysed using the pendant drop method	126
Figure 5.3.	Weight per drop and volume per drop given at three different printing voltages	127
Figure 5.4.	Retained activity of the enzyme after printing at different printer settings in comparison to a control unprinted sample	129
Figure 5.5.	Light scattering refractive index of GOX printed at different voltages.	132
Figure 5.6.	Graph showing the hydrodynamic radius across the different printed samples.	135
Figure 5.7.	Molar mass plots of GOX after printing at different voltages	136
Figure 5.8.	Dimatix DMP 2800 waveform	137
Figure 5.9.	Linear regression analysis of the hydrodynamic radius of GOX after printing through the Dimatix DMP printer	138
Figure 5.10.	AUC graph of GOX before and after printing through the Microfab head	139
Figure 5.11.	AUC raw results of the GOX enzyme before printing	140
Figure 5.12.	AUC analysis of a) Glucose Dehydrogenase b) Glutamate Dehydrogenase	142
Figure 5.13.	Circular Dichroism traces of the GOX enzyme printed at different voltages and without printing	144
Figure 5.14.	CD analysis of the Glucose Dehydrogenase enzyme before and after printing	146

Figure 5.15.	Pictures of the electrodes a) 3mm^2 surface area electrode b) 1mm^2 surface area electrode	147
Figure 5.16.	Setup of electrode system used in this study	148
Figure 5.17.	SEM secondary electron images of the electrode surface of a) 3mm^2 surface area electrode and b) 1mm^2 surface area electrode	150
Figure 5.18.	(1) AFM images of the surface of a) 3mm^2 surface area electrode b) 1mm^2 surface area electrode (2) PCM graphs of relative heights in x and y directions of a) 3mm^2 surface area electrode b) 1mm^2 surface area electrode	151
Figure 5.19.	SEM images of a) Carbon Rod b) Carbon foil c) Carbon spray on glass cover slips	153
Figure 5.20.	AFM representations of the surfaces of the three different carbon samples	154
Figure 5.21.	PCM graphs of the heights across the samples in the x and y direction of a) HOPG carbon b) carbon foil c) carbon spray on glass cover slips	156
Figure 5.22.	SEM image of the electrode ring showing the points of impurity	158
Figure 5.23.	SEM image showing the surface of the bulk of the electrode including indication of the impurities	158
Figure 5.24.	SEM EDAX analysis of two different batches of 3mm^2 surface area electrodes	160
Figure 5.25.	SEM EDAX analysis of two different batches of 1mm^2 surface area electrodes	161
Figure 5.26.	SEM images of two different batches of 1mm^2 surface area electrodes	163
Figure 5.27.	SEM images of two different batches of 3mm^2 surface area electrodes	164
Figure 5.28.	PCM analysis of 1mm^2 surface area electrodes	165
Figure 5.29.	Measurements to be taken of a drop (where a = spread radius, θ = contact angle and h = drop height)	168
Figure 5.30.	Analysis of droplet spreading	170
Figure 5.31.	Contact angle images of solutions on a 1mm^2 surface area electrode	172
Figure 5.32.	Spreading of a GOX plus stabilising solution sessile drop	173
Figure 5.33.	PCM image of the dried GOX solution on the electrode surface	174
Figure 5.34.	Electrochemical comparison of the GOX solution both with and without surfactant	176
Figure 5.35.	Graph showing the degree of spreading encountered when surfactant was added to the enzyme solution.	177
Figure 5.36.	Contact angle analysis of the second drop placed on a saturated electrode.	179

Figure 5.37.	PCM image of dried enzyme on electrode surface showing the enzyme to have spread beyond the original electrode and onto the surrounding reference electrode	180
Figure 5.38.	PCM images after drying of the electrodes at a) 4^0C b) Room temperature c) 37^oC	183
Figure 5.39.	PCM images of electrodes dried in a dessicator at a) 4^0C b) Room temperature c) 37^0C	184
Figure 5.40.	Electrochemical properties of the electrodes that were dried in a dessicator at 4^0C, Room temperature and 37^0C	186
Figure 5.41.	PCM images of enzyme deposited onto the electrode surface at a) 1 unit b) 2 units c) 3 units and d) 4 units	189
Figure 5.42.	Electrochemical analysis of the electrodes with different concentrations of enzyme on the surface	190

TABLE OF TABLES

Table 4.1.	Typical printing parameters used for printing protein suspensions	109
Table 5.1.	Two way analysis of variance with replication test to analyse the effect of voltage and rise time on the fluorescence activity of the protein GOX.	130
Table 5.2.	Concentration of GOX detected at different printing voltages	134
Table 5.3.	Absorption of GOX detected at different printing voltages	134
Table 5.4.	Molar Mass of GOX detected at different printing voltages	136
Table 5.5.	Analysis of percentage of different secondary structure types in GOX.	145

ABSTRACT

Presented by: Christopher Charles Cook at The University of Manchester for the degree of Engineering Doctorate in the subject of 'Inkjet Printing of Biological Macromolecules for use in biology and medicine' in April 2011.

This thesis presents an investigation into the viability of utilising piezoelectric drop on demand printing as a tool for the deposition of proteins for the rapid prototyping of biological sensors. The work has focussed on several main aspects; the effect of printing parameters on drop characteristics, the effect of printing parameters on protein survivability, the influence of surface characteristics on the drop formation at the surface of the sensor, and the electrochemical properties of the sensors after printing. The main objective of this study was to derive a method for the rapid prototyping of sensors using the piezoelectric drop on demand printer.

The first section details the influence of waveform amplitude on the characteristics of the printed drop including droplet weight and volume. It was established that proteins were suitable for printing in both a Phosphate buffered saline solution and a sugar based carrier solution as supplied by AET. Protein survivability experiments suggested that there was some loss of activity during the printing process which required further investigation.

Research into the effect of printing parameters on the viability of proteins, specifically Glucose Oxidase (GOX) has been categorised according to protein structure and protein conformation. No damage was found to occur to either protein conformation or structure after analysis of the samples using light scattering, analytical centrifugation and circular dichroism after printing at 40, 60 and 80V. Further analysis revealed that there was a loss of mass of protein after the printing process compared to a non printed sample.

Surface analysis was employed to quantify the effect of the surface of the electrodes on the drop behaviour after printing through a piezoelectric drop on demand printhead. Proteins were printed onto different carbon surfaces for comparison in different holding solutions and the surfaces analysed for both the drop behaviour when wet and the form and size of the dried enzyme on the carbon surface. Printed samples were observed to spread best with surfactant present in the solution and some evidence of a 'coffee staining effect' was encountered. Further optimisation of the surfactant percentage and the drying conditions ameliorated these effects to produce optimal drying of the solution both on the surface and after drying.

An electrochemical technique was also employed to optimise the number of units of enzyme deposited using the printing technique and to ensure that the current response required was achievable and repeatable. After optimisation, it was possible to demonstrate that the 3 unit sample provided a current response with an R^2 value greater than 0.99, therefore demonstrating reproducible linearity in the current response. This therefore demonstrated that piezoelectric drop on demand printing techniques could be used for the rapid prototyping of biosensors, especially for use in the glucose sensing market.

DECLARATION

No portion of the work referred to in this thesis has been submitted in support of an application for another degree or qualification of this or any other university or other institute of learning.

COPYRIGHT STATEMENT

ACKNOWLEDGEMENTS

To whom it may concern….Thank you.

Special thanks to Professor Brian Derby for his supervision and patience; and to my colleagues and friends at the Material Science Centre. I would also like to acknowledge the invaluable help provided by Andy Wallwork and Rachel Saunders throughout this project.

This thesis would not have materialised without the eternal support of my family and friends. I would particularly like to thank Frances Taylor for her tolerance, support and love and to say that I look forwards to offering her the same in return. Finally I must thank my parents for their positivity and backing in this and in everything I have done in my life.

CHAPTER 1: INTRODUCTION

Biosensors are widely used for the rapid analysis of a sample for diagnosis of medical conditions or for the definition of an impurity from within a sample. The most widely used biosensor is the glucose sensor, which is used for the day-to-day monitoring of glucose levels in the bloodstream of patients with diabetes. This allows the user to monitor their blood sugar level and administer glucose / insulin themselves without the need for hospital admission or medical intervention. However, even these sensors, which have been around for half a century, must constantly evolve to accommodate improvements in medical treatments. This project aims to develop the glucose biosensor further through improving manufacturing technology, which has the potential to reduce the volumes of fluid deposited onto the sensor surface, opening up new possibilities in testing for multiple analytes. This improved technology could assist in the diagnosis of multiple conditions and/or molecules with a single blood sample.

The production of biosensors requires the use of nanomanipulation techniques, the majority of which are limited by an inability to precisely position very small drops of liquid [1]. In this regard, inkjet printing represents a key technological advance because of its potential for accurate deposition of volumes in the 10 pl range. In recent years, there has been an explosion of interest in inkjet printing for use in biology and medicine, and these advances have laid the foundations for a new vista of opportunity in patterning and assembly for biology. Example applications include: cell microarrays for toxicity screening, cell-factory devices to produce pharmaceuticals or biological materials, implantable seeded scaffold structures for regenerative medicine, and implantable devices for reproducing organ function. Within this vista of opportunity, inkjet printing can be applied to the deposition and production of biosensors with the opportunity of depositing multiple solutions on small sensor surfaces so multiple tests can be carried out at once.

This thesis concerns using inkjet printing as a tool for the micromanipulation and dosing of biological materials to create structures that may be useful in the field of biosensors. This can only be carried out by the successful modification of the ink drop generating system

(printhead) to allow free and easy passage of biological materials onto the printed surface without them suffering damage or loss caused by the processes originating within the printhead. Thus, alterations may be required to either the printhead design or the driving electrical signal, or a stabiliser may need to be incorporated, in order to ameliorate or eliminate whatever effect is encountered.

1.1. Aims and Objectives

The work contained within this thesis aims to build upon previous research carried out both within the University of Manchester and elsewhere. It will combine different areas of research including; Drop on Demand Inkjet printing, electrochemistry, protein and biological macromolecules, and protein stabilisation. The project has one major objective:

'To demonstrate and prove the principle that the Drop on Demand Piezoelectric Inkjet printing technique is advantageous for the deposition of enzymes onto electrochemical sensors in comparison to currently used techniques. This will encapsulate both the scientific, and business and economic considerations.'

This objective consists of several aims. The conclusion section will measure the outcomes of the work against these aims in order to outline both the strengths and weaknesses of the work and to inform any further work that could be carried out to move towards a marketable product.

The aims of the work are to:

- Outline the current technologies used in the deposition of biological macromolecules for the purposes of manufacturing electrochemical sensors and the considerations that must be made when designing a new deposition technique,
- Justify the requirement and need for a new deposition technique in business and economic terms,
- Understand the effect the deposition technique may have on the macromolecules which are to be deposited onto the sensors and, if necessary, ameliorate the effect,

- Analyse the characteristics of the physical substrate surface both before and after deposition of the biological macromolecules,
- Analyse the reproducibility and repeatability of the deposition of the biological macromolecules, especially with regards to the properties of the completed sensor,
- Conclude whether or not the deposition technique is viable for the purpose of depositing biological macromolecules for use in electrochemical sensors and why,
- Recommend further work that should be carried out to enable the technique to be taken to market.

CHAPTER 2: LITERATURE REVIEW

2.1. Overview of Sensors

2.1.1. Structure of the sensor

A sensor is an element that responds to a trigger or change in its environment to produce a chemical or electrical response; this is then converted into a signal, which can be interpreted. A good natural example of this is the human nose. The nostrils collect a gas sample, which is then sensed by the olfactory membrane. The responses of the olfactory membrane are then converted by the olfactory nerve cells into electrical signals which pass along the nerve fibre to the brain for interpretation as a smell. An extremely useful source on biomedical sensors has proven to be by B. Eggins [2].

In a biosensor, the sensing element which responds to the substance being measured is biological in nature and is often, but not exclusively, an enzyme. It has to be connected to some form of transducer so that an observable electrical or optical response can be generated and monitored. Biosensors are usually designed for sensing and measuring particular chemicals, which need not necessarily be biological components themselves. Figure 2.1 shows a schematic general arrangement for the components of a biosensor.

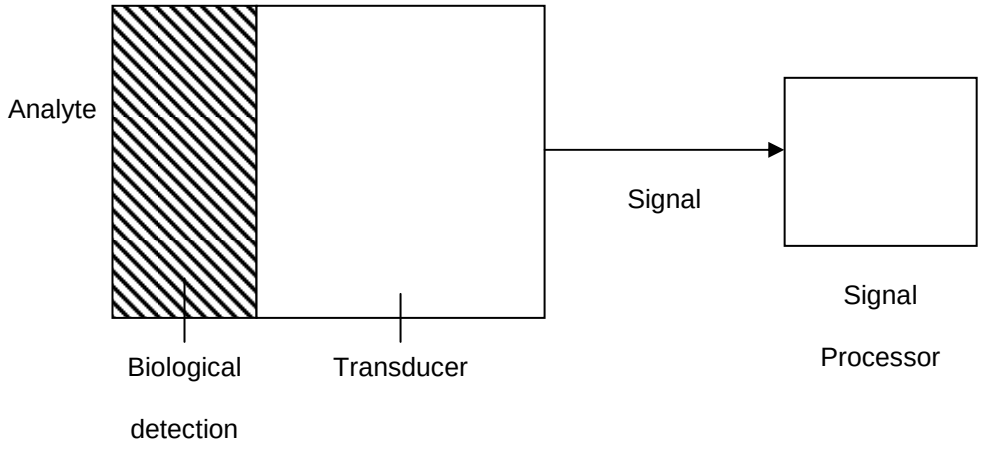

Figure 2.1. Schematic layout of a biosensor [2].

A biosensor can therefore be defined as; ‘a device incorporating a biological sensing element connected to a transducer’. The transducer converts an observed change into a measurable signal, usually an electronic signal whose magnitude is proportional to, or some simple function of, the concentration of a specific chemical or set of chemicals. It is an apparently alien marriage of two contrasting disciplines; it combines the specificity and sensitivity of biological systems with the computing power of the microprocessor [2].

2.1.2. Biological Elements

Biological elements provide the major selective element in biosensors. They must be substances that can attach themselves to one particular analyte but not to others. In this work the analyte is defined as the element that is being tested for e.g. the glucose in a blood sample in a diabetes sensor. The biological elements within the sensor must selectively bind to the appropriate analyte. Four main groups of biological materials that are suited to this purpose are:

- Enzymes
- Antibodies
- Nucleic Acids
- Receptors

The biological elements most regularly used, as they are in this project, are enzymes. These may be used in a purified form, or may be present in microorganisms or in slices of intact tissue. They are biological catalysts for particular purposes and can bind themselves to the specific analyte. This catalytic action is made use of by the biosensor.

Antibodies have a different mode of action. They bind specifically with the corresponding antigen, to remove it from the sphere of activity, but they have no catalytic effect. Despite this, they are capable of achieving ultra-high sensitivity in biosensors. Considerable ingenuity is often needed in sensor design to associate them with the analyte and to provide a signal for the transducer to measure.

Nucleic acids have been much less used so far. They operate selectively because of their base-pairing characteristics. They have great potential use in identifying genetic disorders, particularly in children.

Receptors are proteins that traverse the full breadth of the lipid bilayer plasma membrane surrounding a cell and which have molecular recognition properties. They are difficult to isolate, but will bind solutes with a degree of affinity and specificity to match antibodies [2].

2.1.2.1. Enzymes

An enzyme is a large, complex macromolecule, consisting largely of protein, usually containing a prosthetic group, which often includes one or more metal atoms. In many enzymes, especially in those used in biosensors, the mode of action involves oxidation or reduction which can be detected electrochemically.

A good example of the use of an enzyme in a biosensor and, indeed, the one around which this project is based, is the glucose biosensor. This is the most extensively studied biosensor and the most commercially developed because of its application as a diagnostic tool for diabetics. The original form involved the oxidation of glucose (the analyte) by molecular oxygen, catalysed by the enzyme glucose oxidase (GOX) to give gluconic acid and hydrogen peroxide;

$$C_6H_{12}O_6 + O_2 \xrightarrow{GOX} C_6H_{10}O_6 + H_2O_2 \qquad (1)$$

The reaction was originally followed with a Clark oxygen electrode, which monitors the decrease in oxygen concentration amperometrically [2]. The precise reactions and methodology used in current glucose biosensors will be discussed later.

The advantages of using enzymes in a biosensor are that: they bind to the analyte exclusively, they are highly selective, they have catalytic activity thus improving sensitivity, they are fairly fast acting and they are commonly used as a biological component.

The disadvantages of using enzymes in a biosensor are that they are expensive due to the high cost of extraction, isolation and purification; however there is a wide range available commercially. Enzymes may also suffer a loss in activity when they are immobilised onto a transducer and may also lose activity after a relatively short period of time [2].

2.1.2.2. Antibodies

Organisms develop antibodies (Ab) which are proteins that can bind with an invading antigen (Ag) and remove it from harm, shown in (2) below.

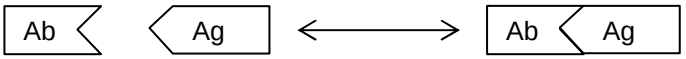

(2)

An unknown Ag can be determined using labelled antibodies. This labelling will enable the antibody to produce a biological signal once it has bound to the unknown compound. Labelling may be achieved with radioisotopes, enzymes, red cells, fluorescent probes, chemiluminescent probes or metal tags. The label may be on either the Ab or Ag, but in biosensors, the emphasis has been on labelling with enzymes. The advantages of using antibodies in biosensors are that they are very selective, ultra-sensitive and they bind very powerfully to their antigen. Figure 2.2 below shows the structure of an antibody.

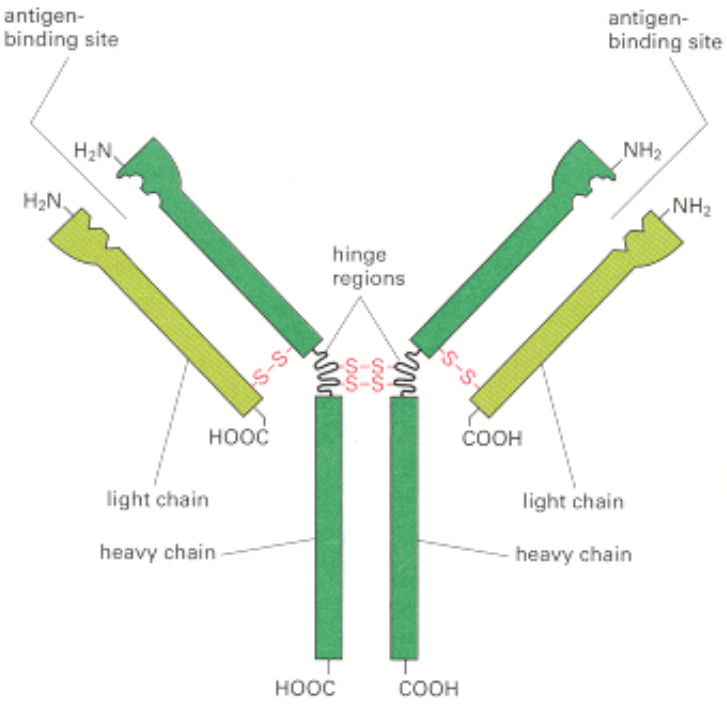

Figure 2.2. Antibody structure showing the antigen binding sites as well as the heavy and light chains. The antigen binding site is the site onto which any antigen would bind in preparation for disposal [2] (copied from source).

2.1.2.3. Nucleic Acids

Nucleic acids operate in many ways like antibodies. The specific base pairing between strands of nucleic acid gives rise to the genetic code, which determines the replicating characteristics of all parts of living cells and thus the inherited characteristics of individual members of a species. A short length of a synthesized nucleic acid can be designed to bind specifically to one site of the DNA in a natural organism.

DNA probes can be used to detect genetic diseases, cancers and viral infections by being designed to match the appropriate target sequence of base pairs. They are used either in the ‘short’ synthetic form or the ‘long’ form produced by cloning. As with antibodies, a DNA assay often involves the addition of labelled DNA to the assay as DNA in itself is ‘Bio-inert’ and cannot produce a signal. The labelling may be radioactive, photometric, enzyme or electro active, giving scope for a range of biosensor types [2].

2.1.2.4. Receptors

Much of the research into receptors has been with neuroreceptors and their recognition of neurotransmitters, neurotransmitter antagonists and neurotoxins. Neurotransmitter and hormonal receptors are the body's own biosensors. An example already referred to earlier is the olfactory membrane in the nose. The binding of a ligand (an agonist) to the receptor triggers an amplified physiological response such as (i) ion channel opening, (ii) second messenger systems and (iii) activation of enzymes. These biological receptors tend to have an affinity for a range of structurally related compounds rather than one specific analyte, which is often an attractive feature for use in biosensors. Often they are used with labelled materials, originally with radioactive labelled ligands but now also with fluorescent or enzyme labelled ligands. Alternatively the label could be on the receptor [3].

2.1.3. Immobilisation of biological component

In order to make a viable biosensor, the biological component has to be in close association to the transducer. There are several methods of doing this as shown below.

2.1.3.1. Adsorption

This is the simplest and involves minimal preparation. However, the bonding is weak and this method is only suitable for exploratory work over a short time span. Many substances adsorb enzymes onto their surfaces, e.g. alumina, charcoal, clay, cellulose, kaolin, silica gel, glass and collagen. No reagents are required, there is no clean up step and there is less disruption to the enzymes [2].

Adsorption can be roughly divided into two classes: physical adsorption (physisorption) and chemical adsorption (chemisorption). Physisorption is usually weak and occurs via the formation of Van der Waals bonds, occasionally with hydrogen bonds or charge-transfer forces. Chemisorption is much stronger and involves the formation of covalent bonds. Adsorption is rarely used on its own, because of its weak and transitory effect. However, it is commonly used along with other methods. Frequently an enzyme is adsorbed onto an

electrode surface and then immobilised there with a membrane or some other form of encapsulation [2].

2.1.3.2. Microencapsulation

Microencapsulation was the method used with early biosensors [4]. The biomaterial is held in place behind a membrane, giving close contact between the biomaterial and transducer. It is adaptable. It does not interfere with the operation of the enzyme. It limits contamination and biodegradation. It is stable towards changes in temperature, pH, ionic strength and chemical composition. It can be permeable to some materials, e.g. small molecules, gas molecules and electrons.

There are two different membranes that can be used for this method; diffusion and exclusion. Diffusion membranes are membranes that allow the passage of molecules from regions of high concentration to regions of low concentration. Exclusion membranes prevent molecules not meeting a certain criteria (e.g. size) from passing through them. Therefore, with regards to the Km of the enzyme, both membranes have the potential to reduce the K_m (the mid point concentration of the analyte across the reaction) and therefore reduce the rate of reaction (see section 2.2.6). In these instances the analyte may be more commonly known as the enzyme substrate to an enzyme chemist.

This method uses an inert membrane to trap the biomaterial on the transducer and was the method used with the first glucose biosensor on the oxygen electrode [4]. A polyethylene membrane, permeable to oxygen, covered the platinum electrode. The Glucose Oxidase (GOX) was then sandwiched between this membrane and a cellulose acetate membrane, which is permeable to both oxygen and glucose. The advantages of this method are that; there is a close attachment between the biomaterial and the transducer, it is very adaptable, it is very reliable, there is a high degree of specificity maintained as well as good stability and there is always the option of bonding the biological component to the sensor via molecules that conduct electrons, such as polypyrrole [2].

2.1.3.3. Entrapment

A polymeric gel is prepared in a solution containing the biomaterial. The enzyme is thus trapped within the gel matrix. The most common polymer used is polyacrylamide. It is prepared by copolymerisation of acrylamide with N, N'-methylenebisacrylamide. Polymerisation can be effected by UV radiation in the presence of vitamin B_1 as the photosensitiser. Other materials used are starch gels, silastic gels and conducting polymers such as polypyrrole. However, there are some problems associated with this method. Large physical barriers are created, inhibiting the diffusion of the analyte, which slows the reaction and hence the response time of the sensor. There is also a loss of enzyme activity through the pores in the gel. This problem may be overcome by cross-linking with glutaraldehyde [2].

2.1.3.4. Cross – Linking

This method uses bifunctional agents to bind the biomaterial to solid supports. It is a useful method to stabilise adsorbed enzymes. There are several disadvantages to this method including; the enzyme getting damaged during the process, limited diffusion of the analyte and poor mechanical strength. The most commonly used materials for this are glutaraldehyde, hexamethylene diisocyanate and 1,5-dinitro-2,4-difluorobenzene. This technique has been used to immobilise urease and penicillinase, as very fine films, directly on the sensitive ends of a glass pH electrode [5] [2].

2.1.3.5. Covalent Bonding

This involves a carefully designed bond between a functional group in the biomaterial and the support matrix. Nucleophilic groups in the amino acids of the biomaterials, which are not essential for the catalytic action of an enzyme, are suitable. Such groups as NH_2, CO_2H, OH, C_6H_4OH, SH and imidazole are used. The reactions need to be performed under mild conditions – low temperature, low ionic strength and with the pH in the physiological range. The advantage is that the enzyme will not be released during use. In order to protect the active site, the reaction is often carried out in the presence of the analyte.

2.1.4. Biosensor Manufacturing Technique

Screen printed electrodes are widely used for the electrochemical determination of various substances. The screen printing technique has two main advantages; it is reproducible for mass manufacture, and low cost, making it ideal to produce disposable sensors. The construction of the sensors is usually an alumina, polyester or PVC physical substrate with layers of conductive and insulative inks printed on top using the screen printing method. The tailoring of the composition of the inks allows for different end uses of the final electrodes. This is done by using different materials such as metals and carbons or by adding enzymes to produce biosensors.

The work in this report is based upon the most widely used disposable screen printed biosensor; that used for the detection of glucose in blood for diabetes detection and treatment [6]. It is also important to recognise the other screen printed biosensors that are used to detect other analytes, as reported by many other publications [7] [8] [9] [10] [11] [12]. The electrochemical technique that is most widely used and associated with the screen printed electrodes is chronoamperometry [13].

2.1.4.1. Screen Printing Procedures

There are many advantages of screen printing over other methods of fabrication. The production of the pattern, including the tooling, is relatively cheap and simple, the machinery need not be too complex and the printing surface does not have to be flat. There are two other advantages that make screen printing the method of choice for sensors however; the thickness of the print is greater than other methods (e.g. lithography and flexographic printing) and can be controlled. This therefore means that it is easier to achieve the desired electrical performance of the film. This is the preferred technique for the production of biosensors due to it being low cost for small volumes of the printing solution and giving a thick film deposit. It can, however, prove to be a more time consuming method when printing more than two films onto the same sheet, hence why the measurement technique used has a pseudo reference electrode instead of a true reference electrode (see section 2.1.5.2). The pseudo reference electrode is also used to reduce the cost of materials used in the base

sensor. Silver and silver salts cost ~£650 per kg compared to carbon based materials at £85 per kg.

The screen printing process requires four essential items; the printing medium (film paste), a screen to define the pattern to be printed, the surface for printing onto (herein termed the physical substrate), and a squeegee which is used to force the paste through the screen mesh of the printer. Figure 2.3 shows the basic process in simple diagrammatic form.

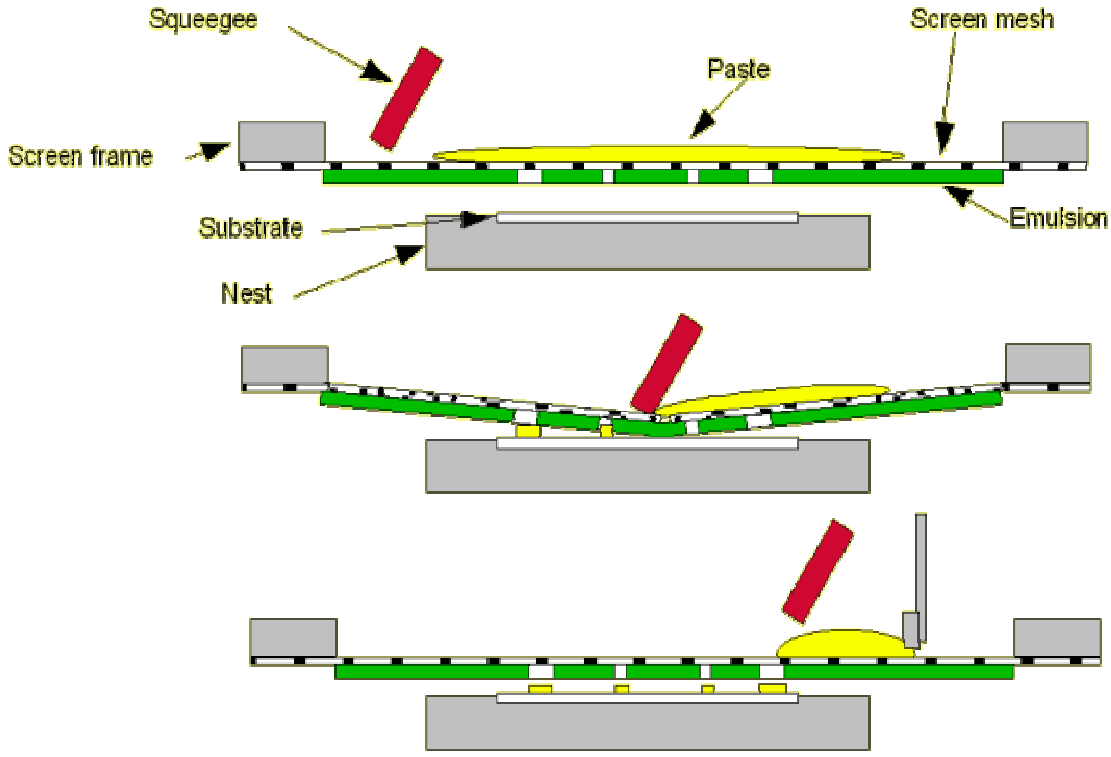

Fig 2.3. The basic screen printing process (copied from source [14])

This figure shows the basic method of screen printing. The steps are as follows: the paste is passed over the screen by the flood blade to fill the open areas, the squeegee then passes over the surface of the screen with pressure which deflects the mesh into contact with the physical substrate which in turn forces the paste through, the paste is then left on the surface of the physical substrate in the same pattern as was used in the emulsion [14].

The most important property of the paste for this process is the rheology. This is because the paste is required to be capable of filling the open areas of the screen mesh without passing

straight through onto the physical substrate. It it also required to be capable of retaining the definition once it has been deposited onto the surface of the physical substrate.

2.1.5. Sensor Electrochemistry

In the case of a sensor the measured current is related to the electrochemical reaction occurring directly at the Working Electrode (WE), while in the case of a biosensor a cascade of reactions is necessary to be able to detect the analyte. In both cases, the current will be proportional to the analyte concentration.

2.1.5.1. The double layer

The peak currents (i_p) obtained with various electrochemical techniques are proportional to the concentration of the analyte of interest and consist of both *faradaic* and *capacitance* current. The electrochemical reaction occurs at the interface between the electrode and the solution and it is in this space that the greatest differences in potential across the electrical circuit appear.

When a potential is applied to an electrode, a net charge appears on the surface which will attract oppositely charged ions. This separation in the charge causes a capacity effect around the interfacial region (double layer), which is measured using impedance techniques. The majority of the electrode surface is therefore covered by polar solvent molecules as a result and by adsorbed electrolyte ions of the same charge. This is known as the Inner Helmholtz Plane (IHP) (see figure 2.4.). There are solvated ions with different polarity near this layer, named the Outer Helmholtz Plane (OHP).

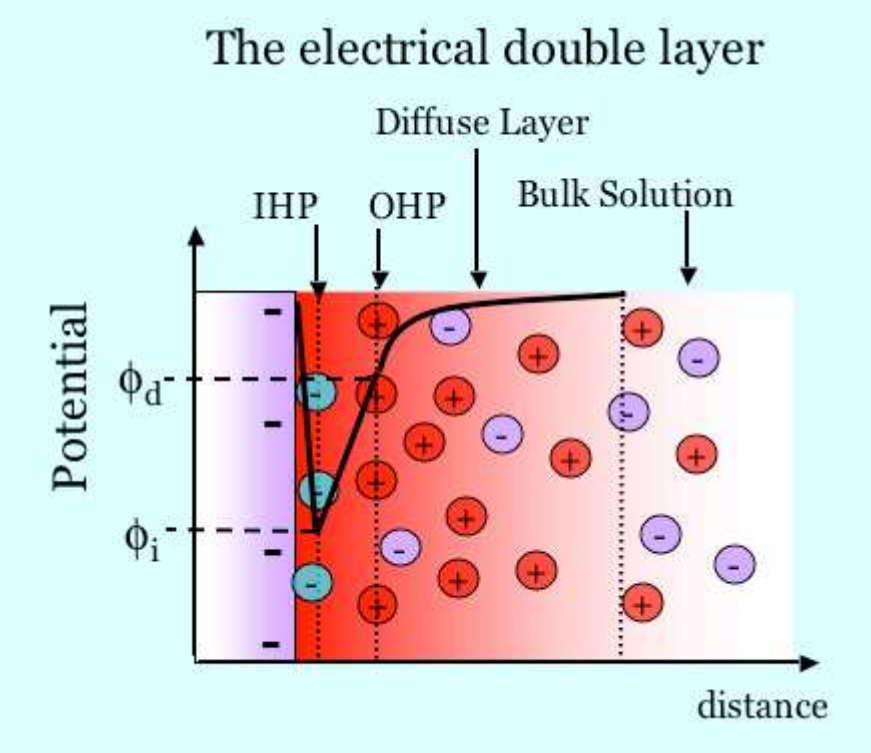

Figure 2.4. Electrical double layer (copied from source [15])

The region beyond this point is a diffuse layer where the ions are arranged following the electrostatic forces between them and their charge. The greater the distance from the electrode surface that is travelled, the less the ions are affected by it, until the point where the bulk solution is not affected by the electrode, is reached. The result of the oxidation-reduction reactions taking place at the electrode surface is the Faradaic current.

In order for the electron shuttle to occur, when the reactant is in a soluble species, the reactant has to get sufficiently close to the electrode surface. It is important for the electrode material to be correct as it will influence the distribution of the electrons in the solid. The interfacial region is crucial for the Faradaic electrochemistry to occur. In order for all the electron energy associated with the electrode to be used to cause the electrochemical reaction, it is important for the layer to be as thin as possible. To achieve this, a sufficiently high electrolyte concentration is required.

There is also a charge separation in the interfacial region which gives rise to a capacitive current. The current is usually unwanted for electrochemical measurements and therefore

needs to be as low as or zero if possible. This can be achieved through different methods; utilise a sufficiently slow rate when changing the applied potential with time, or subtract the background current obtained under identical condition, but without the electroactive species in solution. However, the electroactive species contributes only a small fraction to the species present near the interfacial region [16]. Another approach to avoid this problem is to use pulse and square wave technologies to discriminate the unwanted capacity current from faradaic current.

Figure 2.4 also shows the diffusion gradient at the surface of the electrode (shown by the graph on the figure). The Nernst diffusion layer model shows that the bulk solution at a critical distance from the electrode is of a steady well mixed concentration. As you get closer to the electrode surface, the concentration starts to decay upon the application of a potential to the electrode. This diffusion layer is dependent upon the mass transfer coefficient and is related to time. According to the Cottrell equation:

$$I = nFAc_o\sqrt{D/\Pi t} \qquad (3)$$

Where I is current, n is the number of electrons, F is Faraday's constant, A is electrode area, c_o is concentration, D is diffusion coefficient, π is pi (3.14159) and t is time.

When a potential is applied to the electrode, the electroactive species is oxidised or reduced. The step in potential results in a current which drops off with time, since the electroactive material must diffuse to the electrode surface in order to react. This causes the diffusion layer to become thicker, therefore resulting in a lower, and falling, rate of diffusion and an associated fall in current. This type of diffusion occurs at the surface of a planar electrode [17].

2.1.5.2. The Potentiostat

The potentiostat controls the applied potential in a three-electrode cell. Generally an electrochemical cell consists of 3 electrodes; the working electrode, where the electrochemical reaction takes place, the counter electrode and the reference electrode. The potentiostat operates by applying a potential (voltage) between the counter and working

electrode. The potential delivered to the working electrode is maintained by the reference electrode. The potential is fed back to the potentiostat in real time, with the potentiostat able to stabilise the half-cell by applying extra potential should there be any variance in the values. This therefore means that the working electrode potential will not be influenced by the reactions that take place at its surface.

The typical material used for the construction of a reference electrode is either a saturated calomel electrode or a silver/ silver chloride electrode. The added stability obtained by using an Ag/ AgCl electrode means that it is widely used, it also has a standard redox potential of +0.22 V compared to a standard hydrogen electrode. Recent developments have led to the development of screen printed silver/ silver chloride electrodes (shown in (4)) which are suitable to be used as pseudo reference electrodes in a two electrode system [18]. There will be more on this topic further in this thesis.

$$AgCl + e^- \longleftrightarrow Ag + Cl^- \qquad (4)$$

The role of the counter electrode is to collect and deliver, to the potentiostat, the current generated during the electrochemical reaction at the working electrode. Generally, it is recommended that the size of the counter electrode should be bigger than the size of the working electrode in order to show the maximum efficiency in collecting the current. In many cases the electrochemical cell can be made of only two electrodes: working electrode and common counter and reference electrode.

In the work carried out in this thesis, the printed electrode sheets used were of two different constructions; a carbon black working electrode printed onto one sheet with a separately printed Ag/ AgCl common counter and reference electrode, and a working electrode and a common reference and counter electrode both manufactured from carbon black. The use of one material for both electrodes allows time and cost savings during the manufacturing process as only one screen needs to be used during the screen printing process. The outcome of this is that a two electrode electro-analytical technique needs to be used to

analyse the properties of the system. The method and theory behind this is explored further below.

Two electrode systems

In most electrochemical measurements, it is necessary to keep one of the electrodes in an electrochemical cell at a constant potential. This so-called reference electrode allows control of the potential of a working electrode (e.g. in voltammetry) or the measurement of an indicator electrode. Secondary reference electrodes are preferred in most experiments. A secondary reference electrode must fulfil the following criteria: (i) it should be chemically and electrochemically reversible, i.e. its potential is governed by the Nernst equation and does not change in time; (ii) the potential must remain almost constant when a small current passes through the electrode and reverse to its original value after such small current flow (i.e. a non-polarisable electrode); and (iii) the thermal coefficient of potential should be small. Whereas there is no reference electrode that offers all these properties to the same extent, some electrodes are very close to that ideal behaviour. In general, secondary reference electrodes are electrodes of the second kind, i.e. metal electrodes coupled to a solubility equilibrium of a salt of this metal and an electrolyte solution containing a fixed concentration of the anion of the sparingly soluble metal salt. In addition to this kind of electrode, for some special cases, other reference systems exist. It would be ideal if the reference electrode could be placed in the same electrolyte solution that is used in the electrochemical system.

In this study, one of the other reference systems is used. This is because the system is a two electrode system in a non aqueous reaction i.e. the solution used is placed onto a single electrode containing both working and counter electrode, both made from carbon. When a reading is taken, the reference electrode used is set up as a pseudo reference electrode. This means that the potentiostat reference wire is plugged into the counter wire and both are connected into the counter electrode, with a separate wire in the working electrode. This set up is shown in figure 2.5. The potential is applied through the working electrode, with the

potentiostat measuring the current flow between the working and counter electrode with the reference electrode held at a constant potential.

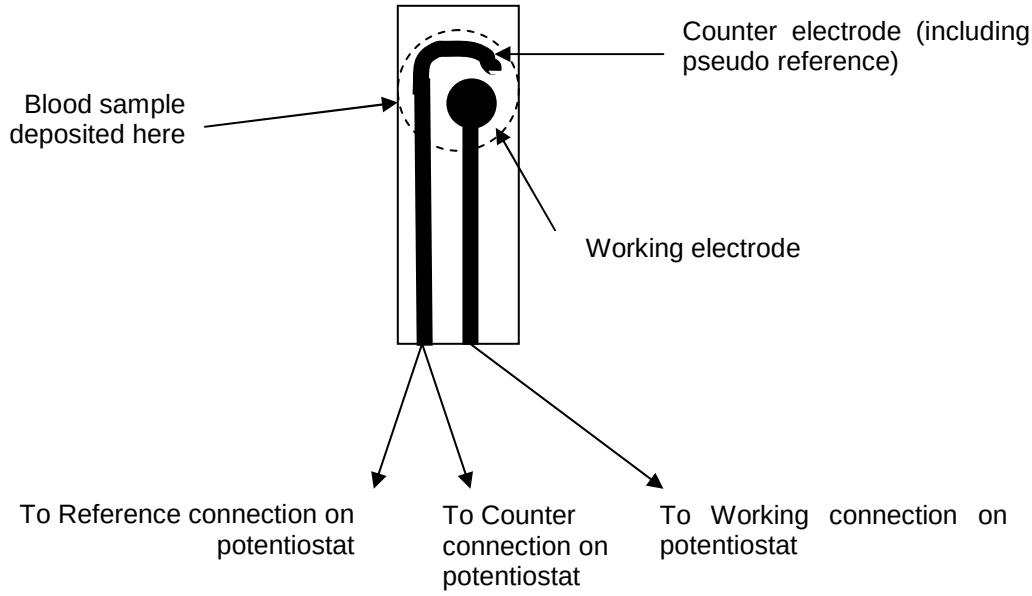

Figure 2.5. Set up of electrode system used in this study.

Pseudo reference electrodes are electrodes that are used as reference electrodes, especially in three-electrode potentiostatic measurements, but do not possess the properties of “real” reference electrodes, i.e. they are not non-polarisable, they do not possess a thermodynamically calculable potential and they do not have a potential, which is independent of the electrolyte in the cell. Nevertheless, such electrodes, normally simple metal wires of platinum or gold, can be used provided that the potential scale is calibrated with an inner standard. A somewhat worse alternative is to measure the potential of the pseudo reference electrode versus a conventional reference electrode in a separate experiment. This is reliable only when one can be sure that the potential of the pseudo reference electrode is the same in the calibration and the application experiment. Since the pseudo reference electrode is directly placed into the cell electrolyte, the impedance is usually small (no salt bridge, no liquid junction potentials etc.), which is desirable for the potentiostat to function properly [19].

2.1.5.3. Cyclic Voltammetry

Cyclic Voltammetry, often referred to as CV, is one of the most versatile electro-analytical techniques used to study electroactive species as it offers experimental information about the kinetic and thermodynamics of many chemical systems.

CV utilises an applied potential that is changed with time at a constant rate up to the point of the pre-determined switching potential being reached when the potential is reversed. This potential as a function of time is known as the scan rate, measured in mV s^{-1} in an unstirred solution. This measured current is then plotted as current versus applied potential (figures 2.6 and 2.7). This method is often used in electrochemistry measurements, inorganic and organic chemistry as well as biochemistry [20].

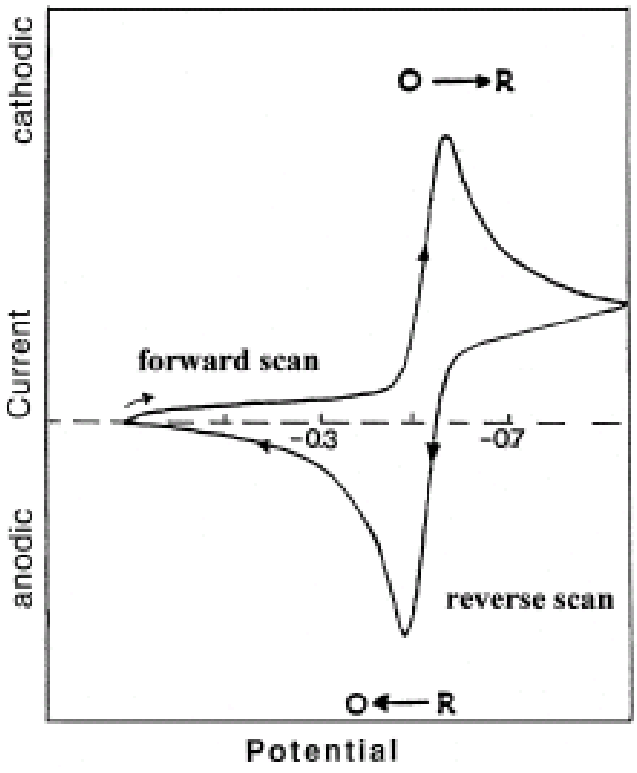

Figure 2.6 Typical CV output signal (copied from source [21]).

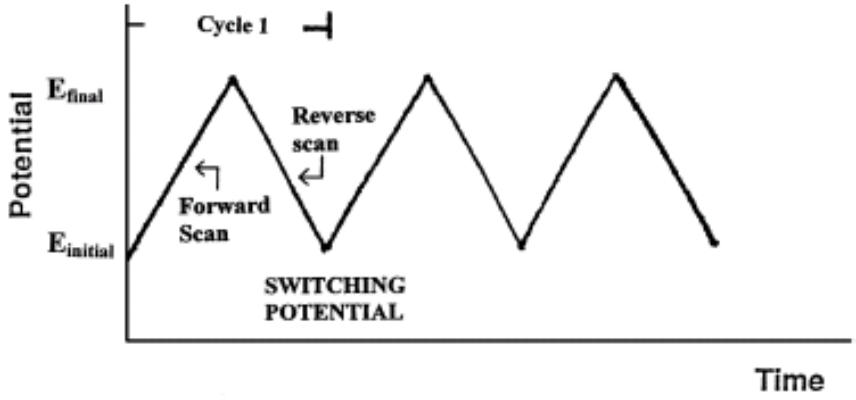

Figure 2.7 Cyclic voltammetry input waveform (copied from source [21])

CV is most commonly carried out in an electrochemical cell consisting of three electrodes: the reference electrode (referred to as RE), the counter electrode (referred to as CE) and the working electrode (referred to as WE), which is where the reaction takes place. The potential difference is monitored by the reference electrode, with the intensity of the current being measured between the counter and working electrodes over the potential range, which provides for the analysis of the redox behaviour of species present in the solution.

The forward scan of the waveform shown in figure 2.6 produces a current peak for any analytes that are reduced through the range of the potential scan. As the potential reaches the reduction potential of the analytes, the current will increase. It then falls off as the concentration of the analyte is depleted close to the surface of the electrode in the diffusion layer. Upon reversal of the potential, and providing the correct potential is reached, the products from the first reaction will become re-oxidised and produce a current of reverse polarity from the forward scan for a totally reversible system. The two peaks, both oxidation and reduction, will have similar shapes when there is no other reaction involving the redox species generated at the electrodes surface. Therefore, information about the redox potential and electrochemical reaction rates of the compounds is obtained. When the reaction at the electrode surface is reversible, the CV presents a reversible peak on the forward and reverse scans (figure 2.7). This data generated through the CV process can be used to obtain important information regarding the electrode reaction, as shown below. The difference in anodic and cathodic peak potential is used to calculate *n* (see below equations).

$$\Delta Ep = Ep_{\alpha} - Ep_{c} = \frac{59}{n} mV \quad (5)$$

Where n= number of electrons exchanged by the redox couple and gives a good indication of the reversibility of the system.

For irreversible or quasi-reversible reactions where n=1 then the numerical value will be much higher than 59 mV.

$$\frac{Ip_{\alpha}}{Ip_{c}} = 1 \quad (6)$$

A redox couple in which both species rapidly exchange electrons with the working electrode is an electrochemically reversible couple, and the formal reduced potential (E^0) is half way between Ep_α and Ep_c [20].

$$E^{0} = \frac{Ep_{\alpha} + Ep_{c}}{2} \quad (7)$$

The peak current is described by the Randles-Sevkic equation for the forward sweep of the first cycle:

$$Ip = (2.69 * 10^{5}) n^{3/2} A D^{1/2} C v^{1/2} \quad (8)$$

Where; I_p is the peak current (Amperes), n is the electron stoichiometry, A is the electrode area (cm^2), D is diffusion coefficient ($cm^2\ s^{-1}$), C is concentration (mol cm^{-3}), and v is the scan rate (V s^{-1}). The peak current I_p increases with $v^{1/2}$ and is directly proportional to concentration [22].

2.1.5.4. Hydrodynamic Voltammetry

This technique involves submerging an electrode into an electrolyte. The solution is then stirred continuously at a fixed rate. Due to frictional forces a thin layer of stagnant solution develops and can be found adjacent to the electrode surface. This layer is called the Nernst diffusion layer and has a discrete thickness, δ [22].

A Hydrodynamic Voltammogram (HDV) is constructed by plotting the current obtained versus the different potentials applied (figures 2.8 and 2.9), all obtained at steady state under stirred conditions. This steady stirring rate causes the Nernst diffusion layer to be of a constant thickness. As the potential applied is increased, the rate of oxidisation of the species in solution increases, therefore giving an increase in current. The Nernst diffusion layer is the limiting factor in the current readings, as the species present in the solution must diffuse through this. Any further increase in the applied potential will, therefore, not result in an increase.

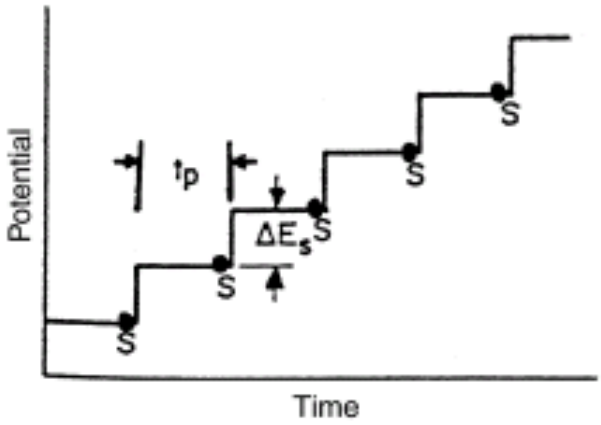

Figure 2.8 Typical excitation waveforms for Hydrodynamic Voltammogram (copied from source [21]).

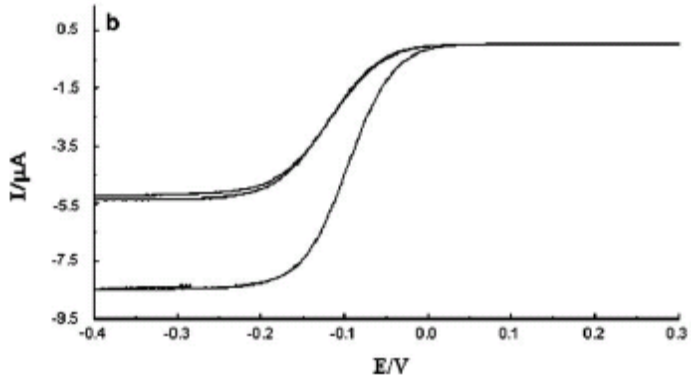

Figure 2.9 Representational experimental response obtained using Hydrodynamic Voltammetry at two different stirring speeds (copied from source [23]).

The constant nature of the current readings, despite the increases in the applied potential, indicates that the maximum sensitivity has been reached and there is no added benefit to using a higher potential. The point at which maximum sensitivity has been reached is usually the point that is chosen for use in biosensor application. This is due to the current being limited by diffusion and being dependent, therefore, on both the discrete thickness of the Nernst diffusion layer (δ) and the bulk analyte concentration.

2.1.5.5. Amperometric in stirred solution

The amperometric method differs from those explored so far in so much as this method measures the current flow through the working electrode at a fixed applied potential. The measured current is proportional to the analyte concentration. This method is often used because it has the advantage that the instruments necessary to take the measurements are simple and comparatively inexpensive.

The electrode surface has a constant potential applied to it which results in a steady state current being produced. Once a steady state current has been achieved, a standard addition of the analyte is performed which results in a typical step shape being obtained. The magnitude of the current for each step obtained is proportional to the concentration of the analyte injected. Figure 2.10 and figure 2.11 show typical response and waveform shapes for this method. All analyte concentrations are determined using the multiple standard addition technique.

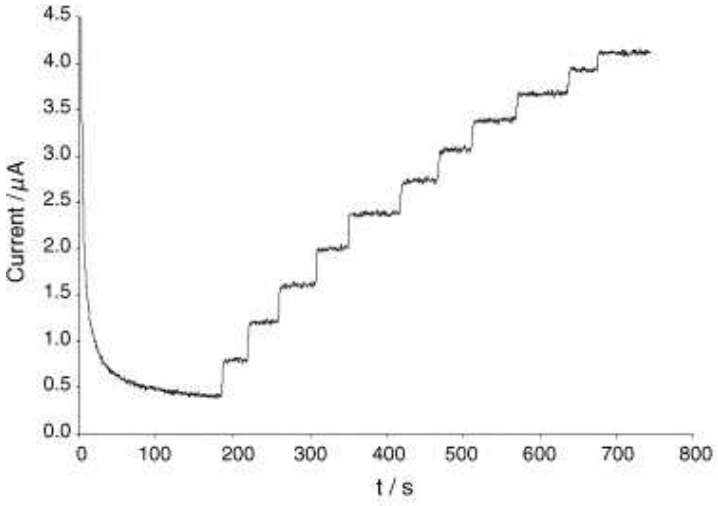

Figure 2.10 Representative current response obtained for amperometry in stirred solution, following multiple addition of the analyte.

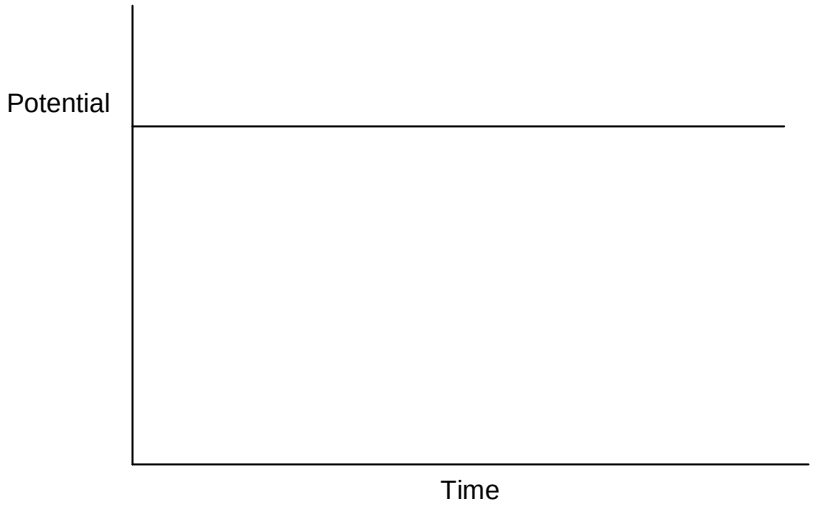

Figure 2.11 Typical waveform for amperometry in stirred solution

2.1.5.6. Chronoamperometry

In this method, the working electrode has its potential stepped from a potential where negligible electrochemistry occurs (usually open circuit) to a potential where the analyte is oxidised or reduced under diffusion control, and the maximum Faradaic current is measurable.

The method relies on the Cottrell equation, which defines the current-time dependence for linear diffusion control, shown below [24].

$$I = nFACD^{1/2}\Pi^{-1/2}t^{-1/2} \quad (9)$$

Where; n= number of electrons transferred/ molecule, F= Faraday's constant (96,500 C mol^{-1}), A= electrode area (cm^2), D= diffusion coefficient ($cm^2\ s^{-1}$), C= concentration (mol cm^{-3}) and π= pi (3.14159).

A typical waveform and response can be seen in the figures below (figure 2.12 and 2.13).

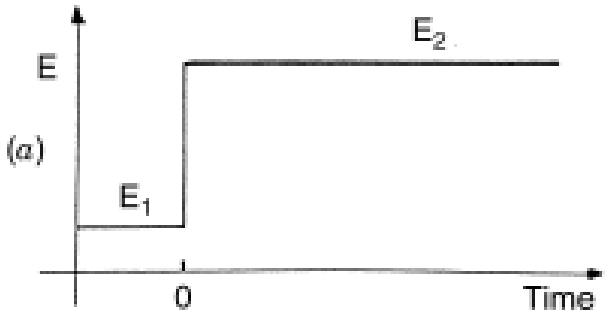

Figure 2.12 Typical waveform for chronoamperometric detection (where E is potential applied) (copied from source [21])

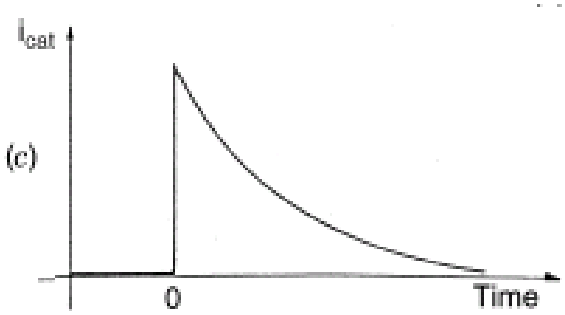

Figure 2,13 Typical chronoamperometric detection in presence of the analyte (i_{cat} is current) (copied from source [21])

This is the preferred method used for this work as it allows for the simple detection and analysis of the sample and the current response is directly proportional to the glucose

(analyte) concentration. In this work the sample is connected up to the potentiostat as shown in figure 2.5 and allowed to acclimatise for 10 seconds prior to any readings being taken.

The readings are taken by maintaining a potential of 0.5 V, with reference to the pseudo reference electrode, for 40 seconds. Measurements are taken along the entire 40 seconds of potential application with the final current response measurement at 40 seconds being the one used to measure the current; this method is known as end point measurement (rather than kinetic measurements.

2.1.5.7. Flow Injection Analysis with Amperometric Detection

Flow Injection Analysis (FIA) is a continuous flow technique that can be ideally suited to rapid automation of the analysis of liquid samples. Ruzicka and Hansen [25] [26] first reported this technique in 1975. A sample, which is usually a small fixed volume of liquid, is injected into the flow using an injection device. There is a liquid carrier also flowing through a narrow tube or conduit, into which the sample is injected. This is then progressively dispersed into the carrier solution, initially by convection. As time passes, this mode changes to axial and radial diffusion as the sample is carried along the conduit under laminar flow conditions. Figure 2.14 shows how the jet directly hits the working electrode area. This type of method is also known as a ‘wall jet’ configuration. It is characterised by a fine jet of solution that hits the centre of a circular disc electrode and spreads out radially. Based on the information in figure 2.14, it is possible to draw the conclusion that only solution from the incoming jet will reach the electrode surface.

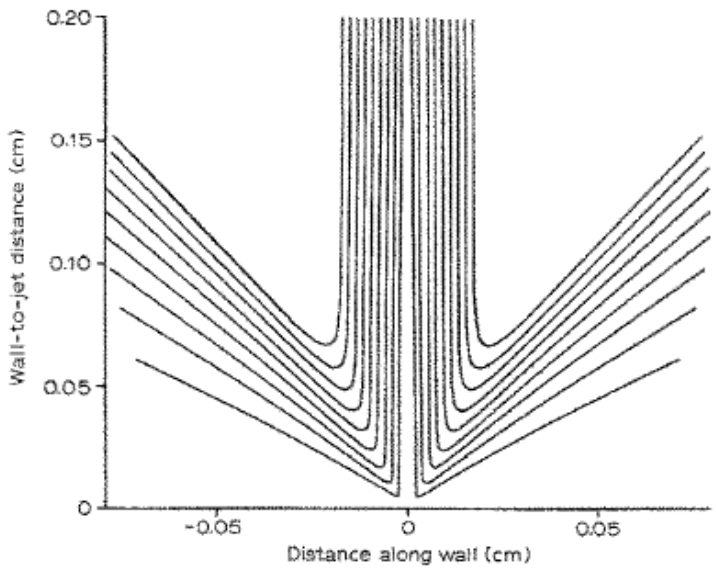

Figure 2.14 Representation of wall jet electrodes and the relative flow pattern (copied from source [27])

In this method the buffer is pushed through the system using a peristaltic pump with the samples injected using an injection valve with a 65 µl sample loop. The buffer pumped to the flow cell impinges on the centre of the working electrode and spreads out radially passing onto the silver/ silver chloride counter/ reference electrode. The sensor is connected to the potentiostat for data acquisition.

The analyte can be quantified using this method by measuring the height or area of the peak-shaped signal obtained after sample injection. This whole process (of sample injection, transport, reagent addition, reaction and detection) can be achieved in a very short time. This method has the advantage of requiring minimum amounts of sample and reagents, and results in very good reproducibility.

The standards and samples are dispersed to the same extent and processed in an identical way. This means that quantitation of unknown samples is possible, therefore a calibration plot of standard sample can be achieved. When the unknown sample is injected, its concentration can be easily deduced from the external calibration plot. This method is compatible with virtually any detection method, is reliable at low volumes of analyte and allows for the completion of rapid experiments. It is therefore used for applications where these characteristics are important, such as on-line monitoring of chemical and biochemical

process [28] [29]. FIA can be used with amperometric biosensors for different analyte detection in complex samples like blood in clinical analysis, fermentation monitoring, and direct sampling of river water [30] [31].

2.1.6. Current sensor technology

There are two types of sensors that currently dominate the mainstream sensor market. They are the pregnancy sensor, used to detect whether a woman is pregnant or not, and the blood glucose sensor, used to detect the levels of glucose in human blood to assist in the diagnosis of diabetes. These both work using different mechanisms but are the two that dominate the consumers' minds most, as they are the most recognisable. Therefore, this section describes the background to the sensors, the sensors themselves and the types of reactions that take place.

2.1.6.1. Pregnancy sensors

Pregnancy sensors can be found on the shelves of most pharmacies and supermarkets, and are one of the most accessible biosensors to the public. They are used to detect and confirm whether a woman is pregnant or not, with some of the more modern ones also being able to confirm the length of time the woman has been pregnant for. The following sections will outline the history and the mode of action of the sensors as well as compare and contrast some of the different types of sensors available today.

2.1.6.1.1. Background

The first pregnancy test kit approved for use in the home entered the market in 1976. Ovulation tests were approved for use in the community in 1984. Since the first home pregnancy test was approved, more than 100 pregnancy tests and several home diagnostic agents have been approved by the Food and Drug Administration (FDA) to assist patients in monitoring and diagnosing various conditions. Sales for home diagnostic agents exceeded $1 billion in 1998, with annual sales of pregnancy tests alone in 1999 estimated at $230 million, approximately 19 million tests [32] [33]. Home diagnostic agents are inexpensive and are convenient means for patients to take ownership of their health care. Home pregnancy

tests allow women to detect pregnancy earlier than waiting for an appointment with a physician. This early knowledge may be important for women to avoid activities that are harmful to foetal development [34] [35].

Home pregnancy tests are designed to detect human chorionic gonadotrophin (hCG) in the urine to predict pregnancy. hCG (the analyte) is a hormone produced by the placenta after the ovum has been fertilised and implanted in the uterus. Production of hCG then stimulates the production of progesterone [33] [35]. The levels of hCG continue to increase until approximately the eighth week and are usually detectable by home pregnancy tests within 10 – 12 days from fertilisation; however, the interval of implantation is variable, and the hormone may not be detected for up to 21 days in some women [36] [37].

The development of the first biological assay for hCG, and hence pregnancy tests, can be attributed to Ascheim and Zondek (1927) [38]. A number of variations on their procedure were used for the next 30 years. In the classic study by Tietz (1965) [39], the frog test showed 12% of positive results in the first week after the missed period, 58% during the second week and 93% in the third week. Corresponding results for the more sensitive rabbit tests were 77%, 90% and 96% [39]. Subsequent developments in bioassays for gonadotrophic activity suggest that it would not be difficult to devise tests with a higher level of accuracy in the first week after the missed period [40]. However, the real disadvantage of the bioassays as clinical tests was that the procedures were cumbersome and expensive, and that it might be several days before results were available. As so often in practical medicine, convenience and cost determine the applicability of a procedure and it is not surprising that the bioassays were rapidly overtaken in the 1960's when immunoassays were introduced [41].

2.1.6.1.2. Biochemistry

The Human chorionic gonadotrophin (hCG) hormone is one of a family of glycoprotein hormones, the other members being luteinizing hormone (LH), follicle stimulating hormone (FSH) and thyrotrophin-stimulating hormone (TSH). Each of these consists of two sub units:

an alpha subunit (92 amino acids) which is virtually identical in all four; and a beta-subunit which is characteristic of the individual hormone [42].

In the circulation, the bulk of hCG is in the form of the intact hormone with only small amounts of free alpha and beta-subunit. In urine, by contrast, a large fraction of the material which reacts in immunoassays for hCG is a metabolic fragment of the hormone commonly known as 'beta-core' [43].

2.1.6.1.3. Detection

Several different forms of immunoassay have been used for qualitative pregnancy tests. The major variants are in the type of label employed and in the specificity of the antibody. The original immunoassays used particles as the label – agglutination assays (figure 2.15).

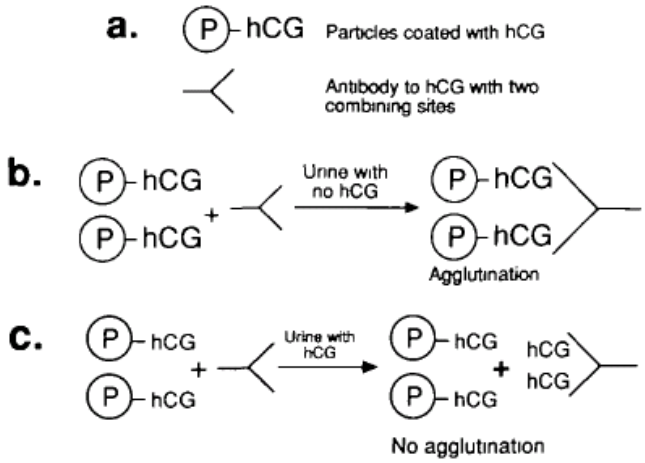

Figure 2.15. The principle of the agglutination inhibition assay: (a) the test reagents are particles (red cells or latex) coated with hCG, and an antibody to hCG; (b) when these are mixed with urine containing no hCG, the antibody binds adjacent particles thus causing agglutination; (c) when the reagents are mixed with urine containing hCG, the latter combines with the antibody and thus prevents it from binding and agglutinating the particles (copied from source [44]).

Agglutination techniques are still widely used because of their familiarity and relatively low cost. The most recent generations of slide tests have a sensitivity of 500 IU l^{-1} and the tube tests of 200 IU l^{-1}. The later ELISA procedures (figure 2.16) occur in a variety of different

sorts of which ‘dipsticks’ offer great user convenience and a sensitivity between 25 and 50 IU l^{-1} [45].

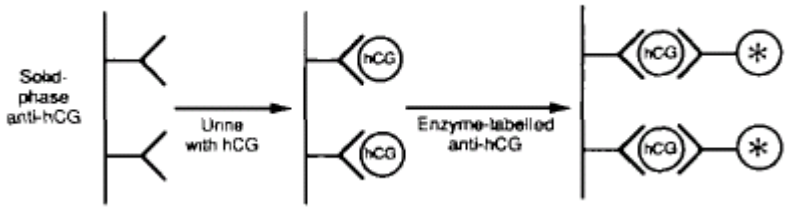

Figure 2.16. The principle of the enzyme immunoassay (enzyme linked immunosorbent assay (ELISA); also sometimes known as ‘sandwich or ‘immunometric’ assays). hCG in urine is captured by a solid phase antibody directed to one site on the hCG molecule. The bound hCG is then identified by a second antibody to a different site on the hCG molecule. This second antibody carries an enzyme: addition of an appropriate substrate yields a colour reaction. There are many variations on this procedure, especially in the solid-phase support and the method of developing the colour reaction: commercial pregnancy tests involve a range of dipsticks, pots, tubes etc. The use of two antibodies confers sensitivity because the capture antibody concentrates the hCG on the surface of the solid phase. It also confers specificity because the two antibodies can be directed to sites which will only be found together in hCG (copied from source [44]).

The earlier assays raised against the whole hCG molecule. Most of these antisera reacted equally well with LH and hCG. The use of antibodies raised against the purified beta-subunit was an important development; such antibodies would react with hCG but not to a significant extent with LH [46]. The resulting ability to measure low levels of hCG in the presence of LH explains the great sensitivity of current pregnancy tests. A further development was the use of monoclonal antibodies. These have two important advantages: first, because of the method of selection it is possible to choose only those antibody producing clones which have the desired specificity; second, they can be produced in large quantities with total consistency from one batch to the next, unlike traditional polyclonal antibodies which vary with each individual antibody producing animal [44].

2.1.6.2. Glucose sensors

This section aims to describe the reactions that take place in order for the glucose biosensor enzyme to correctly sense the glucose analyte.

2.1.6.2.1. Enzymatic Reaction

Glucose can react rapidly in the presence of a catalyst, such as an enzyme. Enzymatic reactions are highly specific. Among the commonly used enzymes for glucose determination are glucose oxidase (GOX), hexokinase, and glucose dehydrogenase (GDH). Hexokinase needs a cofactor, Mg^{2+}, for catalysis, while glucose dehydrogenase (GDH) needs coenzymes such as Nicotinamide adenine dinucleotide (NAD^{+}) or it's reduced form NADH. Given present technology, these cofactors and coenzymes cannot be stably and permanently immobilized. Thus the use of hexokinase, and glucose dehydrogenase for continuous, *in vivo* glucose sensing is not currently practical. Glucose Oxidase (GOX), the most stable of these three enzymes, needs neither cofactors nor coenzymes. Consequently, it was the first to be considered for possible use for *in vivo* glucose sensing [47] and, since then, has been studied extensively. The catalyzed reaction is shown at (10).

$$\text{Glucose} + O_2 \xrightarrow{\text{Glucose Oxidase}} \text{Gluconic acid} + H_2O_2 \quad (10)$$

2.1.6.2.2.. Glucose Biosensor history

The first amperometric enzyme electrode was reported for the determination of glucose [47]. The sensor utilised soluble glucose oxidase (GOX) held between two cuprophane membranes. The oxygen uptake was measured with a Clark oxygen electrode using the same equation shown above. Since then, a large number of glucose sensor devices have been developed for analytical, industrial and clinical purposes [48] [49]. Guilbault and Lubrano reported an improvement over the original Clark glucose electrode, by coating a layer of physically entrapped glucose oxidase in polyacrylamide gel onto an Oxygen electrode [48]. A glucose oxidase electrode based on the electromagnetic entrapment of the enzyme bound to magnetic beads has also been described [50].

The amperometric monitoring of liberated H_2O_2 has achieved much popularity, since H_2O_2 is readily oxidised at platinum, gold, vitreous carbon, and other electrodes by an irreversible, pH-dependent, process (11) [48].

$$H_2O_2 \longrightarrow O_2 + 2H^+ + 2e^- \qquad (11)$$

Guilbault and Lubrano constructed a simple, stable, fast-responding electrode for glucose by covering a Pt electrode [48] with a thin film of immobilized GOX held by a cellophane membrane. When a potential difference of 600mV was applied between the working electrode and the Ag/AgCl reference electrode, the current produced was proportional to the glucose concentration. Good precision and accuracy were obtained when using 100 µl blood samples. A wide range of amperometric enzyme electrodes, differing in the electrode design or material, membrane composition, or immobilization approach have since been described.

2.1.6.2.3.. First Generation Glucose Biosensors

First-generation devices have relied on the use of the natural oxygen cosubstrate, and the production and detection of hydrogen peroxide (Equations 10 and 11). Such measurement of peroxide formation has the advantage of being simple, especially when miniaturized sensors are concerned. A very common configuration is the YSI probe, involving the entrapment of GOX between an outer diffusion-limiting / biocompatible polycarbonate membrane and an inner anti-interference cellulose acetate one (Fig. 2.17).

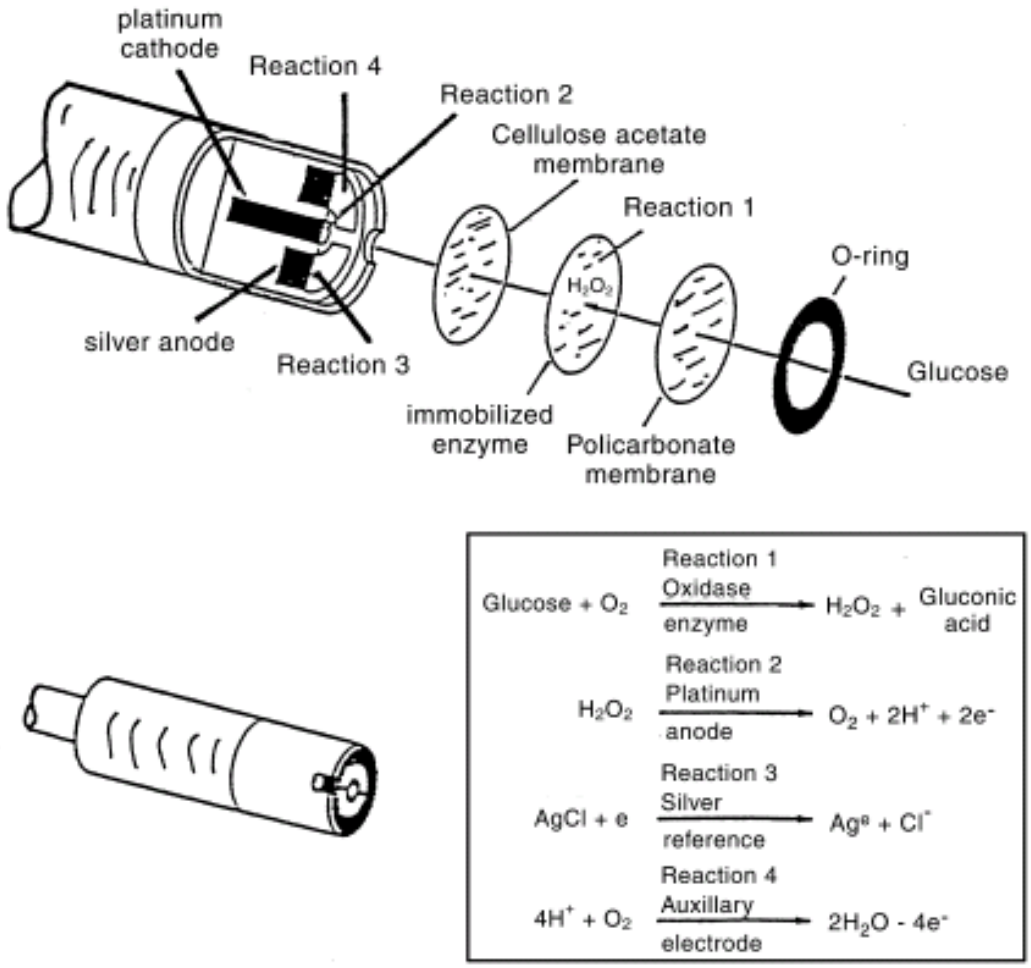

Figure 2.17. Schematic of a first- generation biosensor (based on a probe manufactured by YSI Inc) (copied from source [51]).

Redox Interferences

The amperometric measurement of hydrogen peroxide requires application of a potential at which coexisting species, such as ascorbic and uric acids or acetaminophen, are also electroactive. The anodic contributions of these, and other oxidisable constituents of biological fluids, can compromise the selectivity and hence the overall accuracy of a sensor. Extensive efforts were devoted during the 1980s to minimize the error from electroactive interferences in glucose electrodes. One useful strategy is to employ a permselective coating that minimizes access of such constituents to the transducer surface. Different polymers, multilayers and mixed layers, with transport properties based on size, charge, or polarity of the diffusing species, have thus been used for discriminating against coexisting electroactive compounds [52] [53]. Such films also exclude surface-active macromolecules, hence

imparting higher stability. Electropolymerized films, particularly poly(phenylenediamine) and overoxidized polypyrrole, have been shown particularly useful for imparting high selectivity (based on size exclusion) while confining the GOX onto the surface [54]. Other widely used coatings include the negatively charged (sulfonated) Nafion or Kodak AQ ionomers, size-exclusion cellulose acetate films, and hydrophobic alkanethiol or lipid layers.

The use of multi-(overlaid) layers, combining the properties of different films, offers additional advantages. For example, alternate deposition of cellulose acetate and Nafion (a sulfonated tetrafluoroethylene based fluoropolymer-copolymer) was used for eliminating the interference of the neutral acetaminophen and negatively charged ascorbic and uric acids, respectively [53]. Efforts during the 1990s focused on the preferential electrocatalytic detection of the liberated hydrogen peroxide [54]. This has allowed tuning of the detection potential to the optimal region where most unwanted background reactions are negligible. The remarkably high selectivity thus obtained was coupled with a fast and sensitive response. Metalized (Rh,Ru)-carbon [54] and metalhexacyanoferrate [55] based transducers have been particularly useful for enhancing the selectivity towards the target glucose analyte. Additional improvements can be achieved by combining this preferential catalytic activity with a discriminative layer, e.g., by dispersing rhodium particles within a Nafion film [56].

Oxygen Concentration Dependence

Since oxidase-based devices rely on the use of oxygen as the physiological electron acceptor, they are subject to errors accrued from fluctuations in the oxygen tension and the stoichiometric limitation of oxygen. Such limitation (known as the “oxygen deficit”) reflects the fact that normal oxygen concentrations are about an order of magnitude lower than the physiological level of glucose.

Several routes have been proposed for addressing this oxygen limitation. One strategy relies on the use of mass-transport limiting films (such as polyurethane or polycarbonate) for tailoring the flux of glucose and oxygen, i.e., increasing the oxygen / glucose permeability ratio [58]. An electrode, designed by Gough’s group [59], has been particularly attractive for

addressing the oxygen deficit by allowing oxygen to diffuse into the enzyme region of the sensor from both directions and glucose diffusion only from one direction. The oxygen limitation of glucose biosensors has recently been addressed by designing an oxygen-rich carbon paste enzyme electrode [60]. This new biosensor is based on a fluorocarbon (Kel-F oil) pasting liquid, which has very high oxygen solubility, allowing it to act as an internal source of oxygen. The internal flux of oxygen can thus support the enzymatic reaction even in oxygen-free glucose solutions. It is also possible to circumvent the oxygen demand issue by replacing the GOX with glucose dehydrogenase (GDH) that does not require an oxygen cofactor [61].

2.1.6.2.4.. Second Generation Biosensors

Electron Transfer between GOX and electrode surfaces

Further improvements (and attention to the above errors) can be achieved by replacing the oxygen with a non-physiological (synthetic) electron acceptor, which is able to shuttle electrons from the redox center of the enzyme to the surface of the electrode. Glucose oxidase does not directly transfer electrons to conventional electrodes because a thick protein layer surrounds its flavin redox center. Such a thick protein shell introduces a spatial separation of the electron donor-acceptor pair, and hence presents an intrinsic barrier to direct electron transfer [51]. Accordingly, various innovative strategies have been suggested for establishing and tailoring the electrical contact between the redox center of GOX and electrode surfaces.

Use of Artificial Mediators

Particularly useful has been the use of artificial mediators that shuttle electrons between the flavin adenine dinucleotide (FAD) centre and the surface by the following scheme:

$$\text{Glucose} + GOX_{(ox)} \longrightarrow \text{Gluconic acid} + GOX_{(red)} \qquad (12)$$

$$GOX_{(red)} + 2M_{(ox)} \longrightarrow GOX_{(ox)} + 2M_{(red)} + 2H^{+} \qquad (13)$$

$$2M_{(red)} \longrightarrow 2M_{(ox)} + 2e^{-} \qquad (14)$$

where M(ox) and M(red) are the oxidized and reduced forms of the mediator. Such a mediation cycle produces a current that depends on the glucose concentration. Diffusional electron mediators, such as ferrocene derivatives, ferricyanide, conducting organic salts (particularly tetrathiafulvalene-tetracyanoquinodimethane, TTFTCNQ), phenothiazine and phenoxazine compounds, or quinine compounds have thus been widely used to electrically contact GOX [62] [63] (Fig. 2.18.). As a result of using these electron-carrying mediators, measurements become largely independent of oxygen partial pressure and can be carried out at lower potentials that do not provoke interfering reactions from coexisting electroactive species. In order to function effectively, the mediator should react rapidly with the reduced enzyme (to minimize competition with oxygen), possess good electrochemical properties (such as a low redox potential), have low solubility in aqueous medium, and must be nontoxic and chemically stable (in both reduced and oxidized forms). Commercial blood glucose self-testing meters commonly rely on the use of ferrocene or ferricyanide mediators. Most *in vivo* devices, however, are mediator-less due to potential leaching and toxicity of the mediator [51].

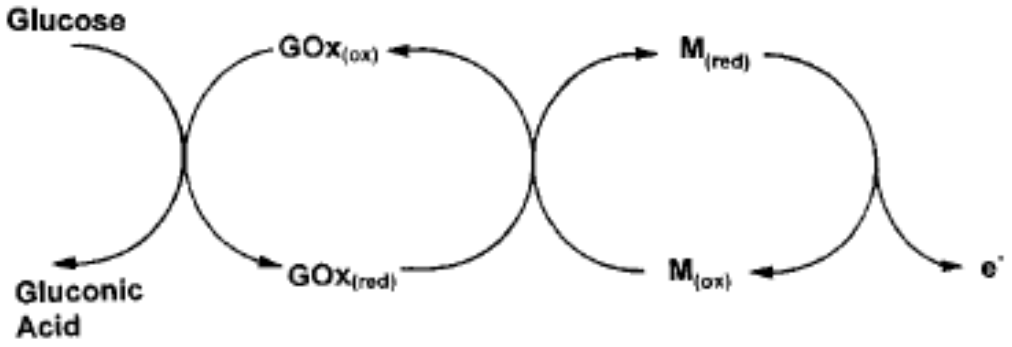

Figure 2.18 Sequence of events that occur in second generation (mediated) glucose sensors (copied from source [51]).

2.1.6.2.5. In Vitro glucose testing

Electrochemical biosensors are well suited for satisfying the needs of home (personal) glucose testing. The majority of personal blood glucose meters are based on disposable (screen printed) enzyme electrode test strips. Such single-use disposable electrode strips are mass produced using thick-film microfabrication technology. Each strip contains the printed working and reference electrodes, with the working electrode coated with the necessary reagents (i.e., enzyme, mediator, stabilizer, linking agent). A counter and an additional ('baseline') working electrode may also be included. Such single-use devices obviate problems of carry over, contamination, or drift, although electronic drift can and does occur in commercial devices, usually due to the drift in amplifier circuits.

The control meter is typically light and small (pocket-size), battery operated, and relies on a potential-step (chronoamperometric) operation. Such devices offer considerable promise for obtaining the desired clinical information in a faster, simpler (''user-friendly''), and cheaper manner compared to traditional assays. The first product was a pen-style device (the Exactech), launched by Medisense Inc. in 1987 (now part of Abbott Laboratories Inc., USA). This relied on the use of a ferrocene-derivative mediator. Various commercial strips and pocket-sized test meters, for self-monitoring of blood glucose – based on the use of ferricyanide or ferrocene mediators – have since been introduced [64]. In most cases the diabetic patient pricks the finger, places the small blood droplet on the sensor strip, and obtains the blood glucose concentration (typically on a digital, liquid crystal display) within 15–30 s. Recent efforts have led to new strips, requiring sub-microlitre blood volumes and enabling ''less painful'' sampling from the arm. In addition to small size, fast response and minimal sample requirements, such modern personal glucose meters have features including extended memory capacity and computer downloading capabilities [51].

2.2. Fundamentals of Proteins

The proteins we observe in nature are polypeptides that have evolved, through selective pressure, to perform specific functions. The functional properties of proteins depend upon their three dimensional structure. The three dimensional structure arises because particular sequences of amino acids in polypeptide chains fold to generate, from linear chains, compact domains with specific three-dimensional structures. The folded domains can serve as modules for building up large assemblies such as virus particles or muscle fibres, or they can provide specific catalytic or binding sites, as found in enzymes or proteins that carry oxygen or that regulate the function of DNA.

2.2.1. Amino Acids

All of the 20 “standard” amino acids that are used in protein structures have in common a central carbon atom, to which are attached a hydrogen atom, an amino group, and a carboxyl group (Figure 2.19). What distinguishes one amino acid from another is the side chain attached to the central carbon atom through its fourth valence. There are 20 different side chains specified by the genetic code and 2 others that occur only in single cell bacteria and archea; others occur, in rare cases, as the products of enzymatic modifications after translation.

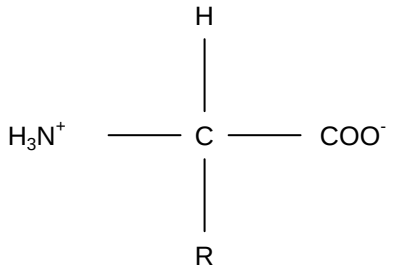

Figure 2.19. The basic structure of an amino acid, where R is the amino acid specific group.

The carbon to which the carboxyl group, the amine group, and the side chain (the R group) are attached is called the alpha carbon (C_α). Each amino acid has the same basic structure as shown in figure 2.19, except for the side chain labelled R. Each of the 20 different amino acids that are used in biological systems is identified by a different 3 letter abbreviation, as well as having their specific chemical name. The complexity of the side group (the R group)

depends on the amino acid name and abbreviation and vice-versa. The simplest is on glycine (GLY) and is a hydrogen atom, with the most complex being lysine (LYS), arginine (ARG) [65] or histidine (HIS) [66].

As is well known, amino acids are the basic building blocks of proteins and govern the overall structure and properties of the protein to which they belong. Within the protein structure each amino acid residue is joined by a peptide bond. This peptide bond, that joins the amino acids, is created between the COO^- and the NH_3^+ groups. This is known as a condensation reaction as it produces a water molecule as a by-product. Figure 2.20 illustrates the reaction schematically:

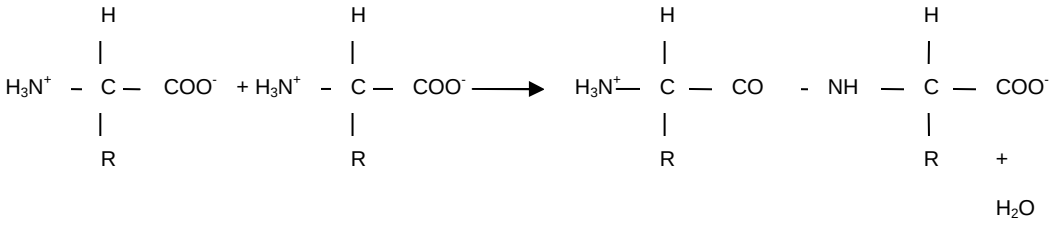

Figure 2.20. A condensation reaction between two amino acids to form a peptide bond.

The condensation of a few amino acids produces small biopolymers which are called peptides; the condensation of peptides in the same manner yield larger polypeptides and the condensation of these yield proteins that can have extremely high molecular weights (of the order of hundreds of thousands of Daltons) [67]. These proteins possess different structural types dependent upon functionality and environment; these are referred to as primary, secondary, tertiary and quaternary structures and will be discussed in the next section.

2.2.2. Primary structure of proteins

The primary structure of a protein is a description of the sequence of the amino acids that make up the protein. By convention this is written by starting at the free amine group (N end) and ending at the free carboxyl group (C end). It includes all references to any disulfide bonds which occur between adjacent chains. It may also be thought of as a complete description of all the covalent bonding in the polypeptide chain or protein. The primary

structure and the amino acid sequence govern the higher levels of structure of the protein or polypeptide molecule.

2.2.3. Secondary structure of proteins

The secondary structure of a protein describes the local 3-dimensional arrangement or structure of the protein peptide chain. This structure normally falls into one of two types: alpha helices or beta sheets. Both structural types are controlled by hydrogen-bonding between the main chain NH and C'=O groups of different amino acids along the chain. The secondary structure elements, formed in this way and held together by the core, provide a rigid and stable framework. They exhibit relatively little flexibility with respect to each other. The functional groups of the protein are attached to this framework, either directly or by their side chains or, more frequently, in loop regions that connect sequentially adjacent secondary structure elements.

2.2.3.1. Alpha Helix

The Alpha (α) helix is the classical element of protein structure. It was first described in 1951 by Linus Pauling [68]. He predicted that it was a structure which would be stable and energetically favourable in proteins. Alpha helices in proteins are found when a stretch of consecutive residues all have the phi, psi angle pair at approximately -60^{o} and -50^{o} (where phi describes rotation around the C(alpha)-N bond and psi denotes rotation around the bond linking the alpha and the carbonyl carbons). The α-helix has 3.5-3.6 residues per turn with hydrogen bonds between C=O of residue *n* and NH of residue *n+4* (figure 2.21). Thus all NH and CO groups are joined with hydrogen bonds except the first NH groups and the last CO groups at the ends of the helix. As a consequence, the ends of α-helices are polar and are almost always at the surface of protein molecules.

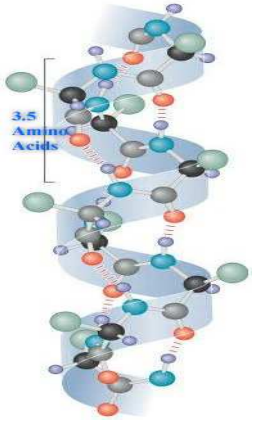

Figure 2.21. A diagram of an alpha helix. It demonstrates the Hydrogen bonding and the 3.5. amino acids per turn (copied from source [69]).

In globular proteins α-helices vary considerably in length, ranging from four or five amino acids to over forty residues. The average length is around ten residues, corresponding to three turns. The rise per residue of an α-helix is 1.5 Å along the helical axis, which corresponds to around 15 Å from one end to the other on an average α-helix. An α-helix can in theory either be right or left handed depending on the screw direction of the chain. A left-handed α-helix is not, however, allowed for L-amino acids due to the close approach of the side chains and the CO group. Thus the α-helix that is observed in proteins is almost always right-handed. Short regions of left-handed α-helices (3-5 residues) occur only occasionally [70].

2.2.3.2. β Pleated Sheet

The second major structural element found in globular proteins is the β-sheet. This structure is built up from a combination of several regions of the polypeptide chain, in contrast to the α-helix, which is built up from one continuous region. These regions are usually from 5 to 10 residues long and are in an almost fully extended conformation. These β-strands are aligned such that the hydrogen bonds can form between C=O groups of one β-strand and NH groups on an adjacent β-strand and vice versa (figure 2.22). The β-sheets that are formed from several such β-strands are 'pleated' with C_α atoms successively a little above and below the plane of the β-sheet. The side chains follow this pattern such that within a β-strand they also point alternately above and below the β-sheet.

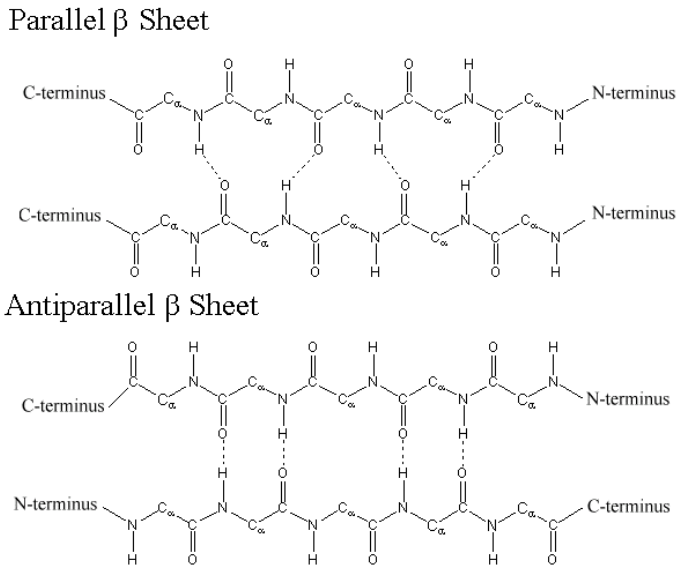

Figure 2.22. Representation of two β pleated sheets; Parallel and Antiparallel (copied from source [71]).

Beta strands can interact in two ways to form a pleated sheet. Either the amino acids in the aligned β-strands can all run in the same biochemical direction, amino terminal to carboxyl terminal, in which case the sheet is described as parallel, or the amino acids in successive strands can have alternating directions, amino terminal to carboxyl terminal followed by carboxyl terminal to amino terminal, followed by amino terminal to carboxyl terminal, and so on, in which case the sheet is called antiparallel. Each of the two forms has a distinctive pattern of hydrogen bonding. The antiparallel β-sheet has narrowly spaced hydrogen bond pairs that alternate with widely spaced pairs. Parallel β-sheets have evenly spaced hydrogen bonds that bridge the β-strands at an angle. Within both types of β-sheets, all possible main-chain hydrogen bonds are formed, except for the two flanking strands of the β-sheet that have only one neighbouring β-strand [70].

2.2.4. Tertiary structure of proteins

Simple combinations of a few secondary structure elements with a specific geometric arrangement have been found to occur frequently in protein structures. These units have been called either supersecondary structures or motifs. Some of these motifs can be

associated with a particular function such as DNA binding; others have no specific biological function alone but are part of larger structural and functional assemblies.

Several motifs usually combine to form compact globular structures, which are called domains. The term tertiary structure is used as a common term both for the way motifs are arranged into domain structures and for the way a single polypeptide chain folds into one or several domains. It is certain motifs that occupy certain roles within the protein structure i.e. enzymatic breakdown of analytes [70].

2.2.5. Glucose Oxidase Structure

GoX is a dimeric protein with a molecular weight of 160 kDa; containing one tightly bound flavin adenine dinucleotide (FAD) per monomer as co-factor. The enzyme is glycosylated, with a carbohydrate content of 16%.

The dimeric protein displays a rather ellipsoidal shape with a high content of secondary structure (28% α-helix, 18% β-sheet; see figure 2.23.). The overall dimensions of the glycosylated dimer are 70 x 55 x 80 Å. The monomers are connected via a rather long but comparatively narrow contact area. The monomer folds into two structural domains; one of them binds FAD, the other one contains the analyte binding site. The tertiary structure of the enzyme is characterised by two separate and distinctly different β-sheet systems, one of which forms part of the FAD binding domain. The second is a large six-stranded antiparallel β-sheet supported by 4 α-helices on its back. The β-sheet forms one side of the active site. The two isoalloxazine moieties are separated by a rather large distance of about 40 Å, a distance which excludes any electrical communication between them [72].

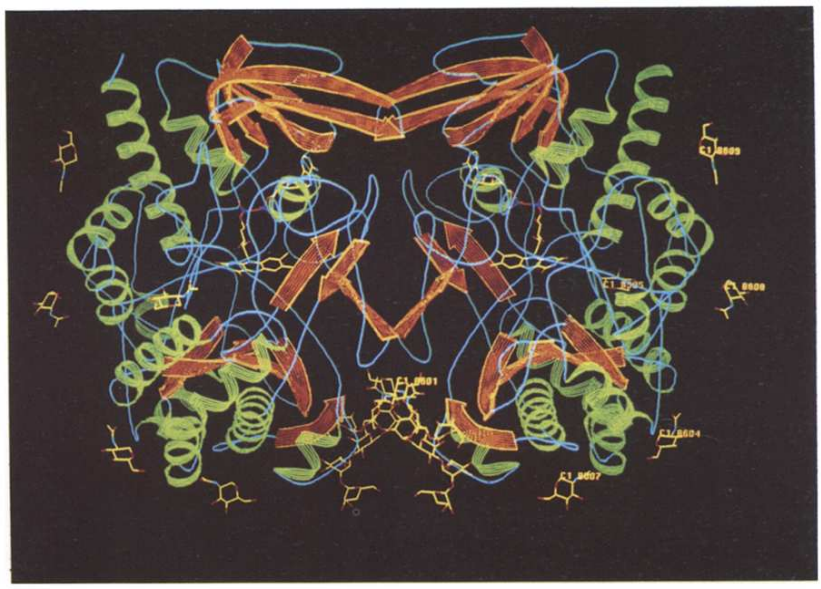

Figure 2.23. Overall topology of GOX: ribbon and secondary structure elements are marked (copied from source [72]).

2.2.6. Enzyme Kinetics

2.2.6.1. How enzymes work

The enzymes present in a living cell have one principal function; to lower the activation energy or free energy that a chemical or biochemical reaction needs to occur. Whilst in a laboratory the activation energy is usually given as heat, this is not possible in a living cell due to the other potential consequences. Therefore, enzymes are used a catalysts within a living cell to decrease the free energy and avoid degradation. They operate by increasing the rate of chemical reaction. Without this, the same reaction may take much longer in time or not occur at all. Figure 2.24 shows the difference in activation energy between a catalysed reaction and an uncatalysed reaction.

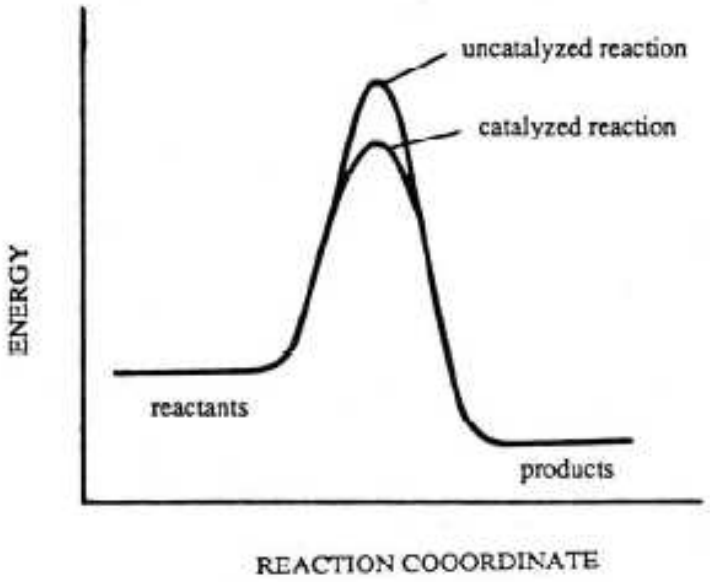

Figure 2.24 Difference in activation energy for catalysed and uncatalysed reaction [73]

The enzymes operate by diminishing the activation energy for a chemical reaction by temporarily binding with the analyte and creating new and efficient reaction pathways for the transformation of reactants into products [73]. The enzymes themselves are extremely specific, only having an affinity for a specific analyte, and have been extensively used for fabricating biosensors because of this [74]. There have been numerous studies carried out on the effect of temperature on the enzymes reaction rate. In 1889, Arrhenius discovered that the temperature dependence of many reactions could be described by the reaction shown in equation 15.

$$k = Ae^{-Ea/RT} \qquad (15)$$

Where k is the rate constant, A is called the pre-exponential factor, E_a is the activation energy, R is the gas constant and T is the absolute temperature.

The quantity A represents the total frequency of collision between reactant molecules. Calculating the natural logarithm of equation 15, the equation shown at 16 is obtained:

$$\ln k = \ln A - \frac{Ea}{RT} \qquad (16)$$

A and E_a have approximately a constant value over a moderate range of temperature (50 K or similar), so that a plot of ln k versus 1/T gives a straight line whose slope (which is negative) is equal to $-E_a/R$ and the intercept on the ordinate gives ln A. Using this equation, A (frequency of collisions between reactant molecules) and E_a (the activation enery) can be calculated.

2.2.6.2. Dehydrogenase Enzymes

This group of enzymes require the cofactor NAD^+ to be attached to the enzyme to become active and react with the analyte. It has been previously shown, in early studies, that dogfish lactate dehydrogenase and the soluble porcine malate dehydrogenase, were almost identical, if the first 20 residues of lactate dehydrogenase are not considered. The conclusion was therefore drawn that these two enzymes evolved from a similar precursor. When two other dehydrogenase enzymes were considered, in this case horse liver alcohol dehydrogenase and lobster glyceraldhehyde 3-phosphate dehydrogenase, they showed a very different structure. It was also noted that all 4 proteins consist of 2 domains, one of which is similar in all of them. This domain that was similar is believed to be the domain responsible for the binding of the nucleotide NAD^+ [75].

2.2.6.3. The Michaelis – Menten Mechanism

The understanding of metabolism is extremely important as it measures the enzyme activity in the steady state condition of the cell. This means that the study of kinetics of biological reactions is also extremely important due to the relationship of them both.

To study enzyme reactions, it is assumed that the concentration of the enzyme is very small compared to the concentration of the analyte. This is generally true considering the high catalytic efficiency of the enzymes. It is then assumed that the initial rate of formation of the product has been measured, that it has not accumulated, and that the analyte is not consumed. Should all these conditions be satisfied, then the change in reagent concentration is generally linear with time. The Michaelis – Menten equation is then used as

the basic equation for studying enzyme kinetics. It was proposed in 1913 by L.Michaelis and M.L. Menten [76] and is shown as equation 17.

$$E + S \underset{K_{-1}}{\overset{K_1}{\rightleftharpoons}} ES \xrightarrow{K_{cat}} E + P \qquad (17)$$

The catalytic reaction is divided into two different processes. Firstly the enzymes and the analyte react together to give an enzyme- analyte complex [ES]. The rate of formation of ES at any time *t*, during the initial period when the product concentration is negligible, is equal to K_1[E][S]. The rate of breakdown of the complex enzyme analyte [ES] at this time is equal to K_1 [ES] + K_{cat} [ES], because the enzyme analyte complex [ES] can breakdown either to form products or to reform reactants. Taking into account a steady state reaction this gives the equation shown at 18.

$$K_1[E][S] = K_{-1}[ES] + K_{cat}[ES] = [ES](K_{-1} + K_{cat}) \qquad (18)$$

When the constant is separated from the variable, the equation shown in 19 is the result. The K_m is another constant.

$$\frac{[E][S]}{[ES]} = \frac{K_{-1} + K_{cat}}{K_1} = K_m \qquad (19)$$

Taking into consideration that the total concentrations of enzyme present [E_0] must be the sum of the concentration of free enzyme [E], and the enzyme in the complex [ES], we can assume that:

$$[E] = [E_0] - [ES] \qquad (20)$$

If equation 20 is substituted into equation 19, equation 21 is obtained.

$$\frac{([E_0] - [ES])[S]}{[ES]} = K_m \qquad (21)$$

From which:

$$[ES] = \frac{[E_0][S]}{[S] + K_m} \quad (22)$$

Since V_0 is equal to K_{cat} [ES], if we substitute this into equation 21, the following is obtained.

$$v_0 = \frac{k_{cat}[E_0][S]}{[S] + K_m} \quad (23)$$

Since $V_{max} = K_{cat}[E_0]$

$$v_0 = \frac{V_{max}[S]}{[S] + K_m} \quad (24)$$

This is the Michaelis- Menten equation, where K_m is the Michaelis constant. If v is plotted against [S], a hyperbola is generated (shown in figure 2.25), consistent with the experimental findings of the enzyme-catalysed reactions. At sufficiently low analyte concentrations [S] the velocity increases linearly with the analyte concentration. As the analyte concentration increases, it does so more rapidly than the velocity. At the point the analyte is at sufficiently high concentration (saturation), the velocity of the reaction will tend towards a limiting value named V_{max}. This can be expressed quantitatively in the Michaelis- Menten equation which is the basic equation of enzyme kinetics.

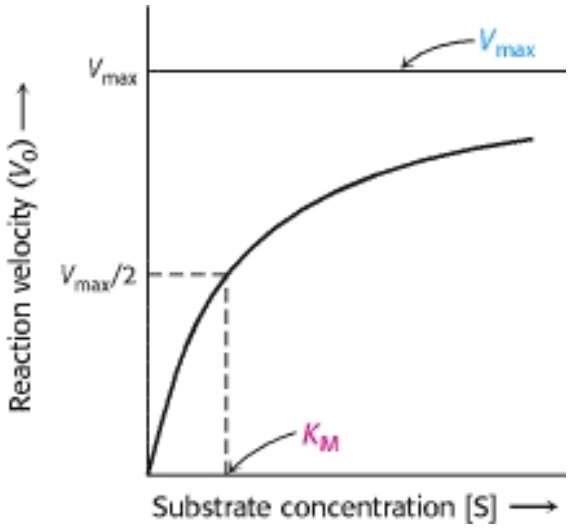

Figure 2.25 Plot of reaction rate v substrate (analyte) concentration [S] for a reaction obeying Michaelis Menten (or saturation) kinetics (copied from source [77]).

Using the graph in figure 2.25 it is possible to obtain V_{max}. K_m can also be obtained using the following equations. When v=1/2V_{max}.

$$\frac{V_{max}}{2} = \frac{V_{max}\,[S]}{[S] + K_m} \tag{25}$$

And:

$$(V_{max})([S] + K_m) = 2(V_{max})[S] \tag{26}$$

Therefore:

$$K_m = [S] \tag{27}$$

Therefore, the K_m value is the value of the analyte concentration [S] which gives the initial velocity equal to ½ of V_{max} and will have the same units as [S]. Taking into consideration the difficulties in calculating a reliable estimate of K_m and V_{max}, Eisenthal and Cornish- Bowden (1974) [78] suggested a different approach based on the Michaelis- Menten equation. They considered $[E_0]$ as a constant and used the reciprocal form of the Michaelis- Menten equation [79].

$$\frac{1}{v_0} = \frac{K_m + [S_0]}{V_{max}\,[S_0]} \tag{28}$$

$$\frac{V_{max}}{v_0} = \frac{K_m + [S_0]}{[S_0]} = \frac{K_m}{[S_0]} + 1 \tag{29}$$

Therefore, if v_0 and $[S_0]$ are constant, a plot of V_{max} against K_m is linear, as shown in figure 2.26.

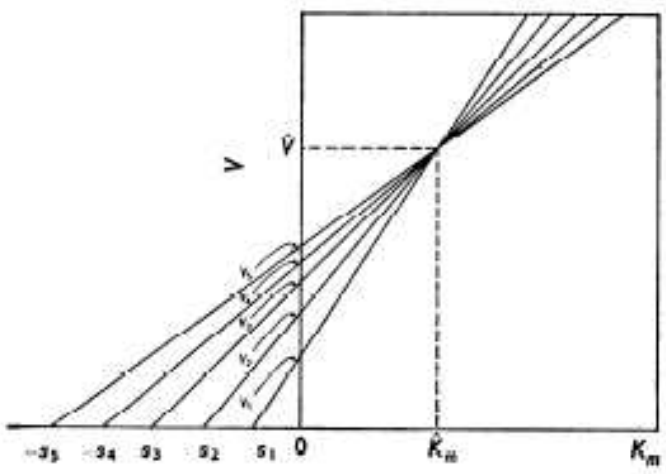

Fig 2.26 Eisenthal- Cornish Bowden plot (copied from source [78])

Taking into account that if K_m=0, V_{max}=0 and when V_{max}=0, K_m=-[S_0], each v_0, [S_0] couple can be used to generate a line by plotting v_0 on the V_{max} axis and –[S_0] on the K_m axis. These two points are then connected and the lines extrapolated. These lines must pass through the 'true value' of K_m and V_{max}, so these values must be given by the point of intersection of all the lines. Considering experimental error, the lines are more likely to intercept over a series of values. The best available estimate of K_m and V_{max} are the medians of the value obtained from the intersection of these lines. This is why the Eisenthal and Cornish- Bowden plot is a useful tool in enzymatic analysis.

2.2.7 Enzyme Stabilisation

Enzyme stabilisation is an important consideration to this programme of work as the current response at the 40 second end point should be repeatable across all samples for set concentrations. There are three different modes of stability that need to be taken into consideration when discussing and contemplating the topic of biosensors and in order to better inform the stabilisation topic. These are:

- Shelf life – All biosensors require a shelf life of at least 6 months, with most modern specifications for biosensors demanding a shelf life of at least 1 – 2 years. If a biosensor cannot be stored for extended periods of time without refrigeration, then the product will never be viable.

- Operational Stability – This is dependent upon the type of the biosensor.
    - A disposable sensor may only require an operational stability of between seconds to several minutes.
    - A reusable sensor may require several days to several months stability (such as a reusable glucose sensor).
- Solution stability – This is required during the manufacturing process of the biosensor.
    - Whether the screen printing technique or a dotting technique is used, the protein can be extremely liable to damage and denaturation when in solution for extended periods. This is relevant to this work, especially where such unknown parameters are introduced in the printing process such as the shear strain within the printhead.
    - There is also the potential for the drying process (extraction of the moisture from enzyme solution on the sensor surface) to be the major process step that will lead to the inactivation of the majority of protein samples.

The work contained within this study has specific interest in the operational stability of the enzyme, as the study is assessing a new manufacturing technique for biosensors which will involve exposing the enzyme to conditions that it has not encountered in other manufacturing techniques that are currently used. More specifically, it is the shear strains within the heads that are of most importance. The method for preventing any damage occurring to the proteins is to use a stabilisation solution to protect the enzyme through the printing process and confer a higher degree of operational stability.

All of the stabilisation solutions were supplied by Applied Enzyme Technologies (AET) and are proprietary solutions to AET. This means the exact content of these solutions cannot be released within this thesis. The stabilisers were all pre-screened using optical methodology and/ or electrophoretic techniques which can interrogate large numbers of stabiliser combinations. The choice of stabiliser, buffer, pH, ionic strength and protein concentration were all critical to producing the correct solution and operational stability.

In order to choose the correct stabiliser for the protein, the isoelectric point of the protein needs to be determined. This enables the correct type of polyelectrolytes to be selected that will bind to the protein of interest. If this proves problematic, then one of two techniques can be used; gel electrophoresis to determine the binding avidity of the protein/ polyelectrolyte complex, or a small panel of positively, negatively or neutrally charged polyelectrolytes can be used.

2.2.7.1 Influencing Factors

The single most important parameter in the promotion of structural stability of proteins is to retain the surface water activity of the protein. The addition of polyhydric alcohols causes the surface water activity to be modified relative to the absolute concentration of the additive.

When this is used in combination with additives that promote electrostatic interactions (polyelectrolytes) or surface chemical reactions that lead to immobilisation or cross linking, then the efficacy of the stabilisation is usually enhanced significantly. This indicates a synergy of action at the surface of the protein structure thereby stabilising the protein overall. Some of these additives such as metal ions are directly related to enzyme structure and as such are not strictly surface interactions. The addition of dilute solutions of metal salts, such as magnesium or calcium, often stabilises proteins to a high degree and causes them to act synergistically with polyelectrolyte combinations.

2.2.7.2 Mechanism of Stabilisation

The stabilisation solutions used are provided by AET, as mentioned earlier. The solutions used consist of one of two types of chemical; polyalcohols or polyelectrolytes, or a combination of the two. The two different chemicals have different modes of action on the proteins in solution.

The polyalcohol family includes sugars and sugar alcohols. They work by modifying the water environment surrounding a protein thus replacing and competing for free water within the system. This modified hydration shell confers extra protection to the protein, helping to

maintain the 3D structure and the biological activity. This therefore enables storage of the biological materials, proteins in this case, both in solution and in the dehydrated state.

The polyelectrolyte family of chemicals include numerous polymers of varying charge and structure. The interactions generated between proteins and the polyelectrolytes are electrostatic in nature and cause the formation of large protein- polyelectrolyte complexes which retain full biological activity. This is because the complexes formed then enable polyhydroxyl compounds to penetrate the structure more effectively and therefore stabilise the solution (figure 2.27). The solutions used in this study, provided by AET, have had the stoichiometry of the protein/ polymer binding calculated, as this is critical for maintaining enzyme activity in stabiliser formulations.

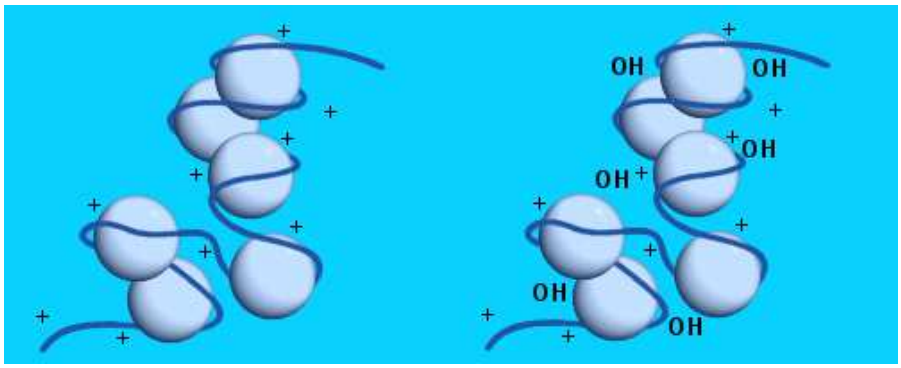

Figure 2.27 Polyelectrolyte stabilisation of a protein (copied from source [14]).

When the two chemical families above (polyalcohols and polyelectrolytes) are used in combination in the same solution, a synergistic effect is usually observed. The important parameter in the solution, when using these chemicals in combination, is the ratio of the polyelectrolyte and polyalcohol. The buffer type, pH, ionic strength, concentration and ratio of stabilisers to protein/ enzyme all play crucial roles in protein stabilisation both in solution and in the dehydrated state.

2.3. Protein Printing Techniques

Inkjet printing is the only current technique that will allow for the deposition of picolitre volumes of ink accurately and reliably onto a physical substrate. Currently, the most accurate method used in manufacturing for the deposition of proteins onto biosensors is to use a pin printing machine (Biodot), which can accurately deposit drops with volumes in the region of nanolitres. There are many different types of Biodot devices (e.g. Innovadyne) that are used within the biosensor industry. Therefore, inkjet printing offers an opportunity for the miniaturisation of sensors with a potential for a reduction in printed drop volume by a factor of approximately 10^3.

Printing is a major business for the reproduction of graphics or artwork through a visual media. Over the last twenty years or so, printing has also given rise to a whole new series of technologies, enabling scientists to develop methods for producing polymeric and metallic structures using precise deposition of the product through a printer and printhead under computer control. Examples of this include the printing of transistors, solar cells and printed circuit boards [80] [81]. This has recently expanded to include biological printing with the aim of building whole biological structures, including the possibility of organs, using the basic building blocks of cells and biological macromolecules [82] [83]. Printing methods can broadly be categorized into two different types; contact and non-contact printing.

2.3.1. Contact Printing Techniques

During contact printing, a printing device comes into physical contact with the physical substrate, transferring “ink” from the carrier or printing plate onto the surface. This can then be further sub- classified as serial or parallel deposition. With serial deposition, fabrication throughput is limited by serially repeated movements of the printing device. Hence, parallel deposition techniques are a better choice for large-scale fabrication; however, most of the parallel techniques for depositing biomolecules are newer and thus, less developed than serial techniques [84].

Contact printing methods can be used to form arrays (patterns of drops) of biochemicals and biological materials by means of direct contact between the printing device and the physical substrate [85]. In order to achieve high spatial resolution, contact printing technologies must provide a method of containing and isolating small volumes of liquid on the plate. To achieve this, high resolution contact printing techniques employ solid pins, split pins, nano-tips, and microstamps to hold the ink. One of the first approaches used for microarray fabrication was contact printing with a single pin, which evolved into methods relying on an array of pins. While pin printing is a serial deposition method, microstamps are used for depositing a large number of proteins or DNA molecules in a parallel fashion. Nano-tip printing is the most recent technology based on Scanning Probe Microscopy (SPM) and yields arrays with submicron spots [85].

2.3.1.1. Pin Printing

Pin printing is a widely used technique for microarray fabrication. Accurate quantitative analysis of printed microarrays is only possible if spot uniformity and positional accuracy is achieved [86]. Spot uniformity is primarily determined by the sample viscosity, pin contact area, pin surface properties, physical substrate surface properties, and physical substrate planarity. Additional factors include pin velocity, the precision of robotic controls, and environmental control of humidity, temperature and contamination. A high pin velocity can induce high inertial forces that drive large sample volumes out of the pin, making the size of the spots very large [87]. However, inertia typically does not play a large role in pin printing. Pin printing is governed by the surface tension of the solution, and the wettability of the solution on the physical substrate controlling transfer of the ink from the pin to the printing surface. Maintaining a high, stable humidity prevents the sample from evaporating from the wells and pin channels. Temperature affects the sample viscosity and, therefore, the dispensed volume. Contamination and dust must be controlled if high-quality arrays are to be produced with minimal risk of split pin clogging [85].

2.3.1.2. Microstamping

Pin printing is an inherently serial technique, in which a single pin or groups of pins are iteratively loaded for spotting. An alternative to pin printing is microstamping. With microstamps, hundreds of spots are printed in parallel, enabling high throughput microarray fabrication. The microstamping process is simple and inexpensive and can be readily conducted in a laboratory. A sample is first adsorbed on the patterned surface of a stamp and then transferred to a physical substrate by physical contact. In order to obtain good contact, microstamps are generally made from elastomeric materials, such as poly (dimethylsiloxane) (PDMS), which conform to surface roughness under an applied load during printing.

Microcontact printing with elastomeric stamps, along with other soft lithographic microfabrication techniques, was developed by Whitesides' group [88] and first demonstrated for self- assembled monolayers (SAMs) of alkanethiols on gold [89]. Elastomeric stamps are manufactured by a micromoulding technique that requires only a single photolithography step (figure 2.28). Mould masters are fabricated by photolithography to define a pattern of the stamp. Then, an uncured liquid elastomer is cast on the master. After curing, the stamp is released from the master. This process enables reproducible, low-cost batch production, resulting in inexpensive and disposable microstamps. Using disposable stamps minimizes the problems of sample carry-over, cross- contamination, and the time consuming cleaning processes that is required for pin printing. Hydrogels have also been used as a stamp material for protein patterning [90].

Microstamping has the capacity to form arrays with very high spatial resolution [91]. However, some disadvantages of microstamping are related to the sample volume transferred. In microstamping, the amount of sample transferred from the stamp to the printing surface is not well controlled and depends upon both surface and sample properties. Additionally, for the same amount of printed sample, microstamping requires larger initial sample volumes, as only a small amount of solution in a well is adsorbed onto the stamp surface, and only a small fraction of the adsorbed solution is transferred from the stamp to the surface due to

strong non-specific adsorption to the hydrophobic stamp material. Likewise, if microstamps are to be reused, the washing process is more tedious than for pins because of non-specific adsorption [92].

Microstamping techniques used with biomolecules can be categorized into indirect stamping [93] and the more recently developed direct stamping [94]. Both categories utilize similar tools but with different stamping procedures. In indirect stamping, the SAM is first patterned on the physical substrate, which is then exposed to the sample solution. In direct microstamping, samples are simply transferred from an inked stamp to the physical substrate in a single step.

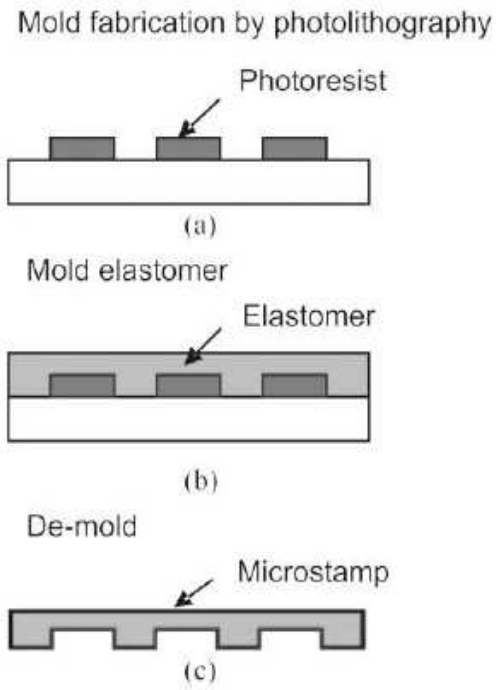

Figure 2.28. Microstamp Fabrication. The master is fabricated by photolithography to define the feature of the stamp. The liquid elastomer is then cast on the master to produce designed patterns. After the curing process, the stamp is released from the master (copied from source [95])

2.3.1.3. Nano- Tip Printing

In order to achieve a higher spot density and more complex arrays, spot sizes must be reduced. The technologies developed for printing spots at the submicron scale are based on atomic force microscopy (AFM). These methods employ an AFM nano-tip for; adding a

sample or its binding molecules to the physical substrate, or removing SAM molecules- known as AFM grafting [96]. When an AFM tip that has been coated with a mobile species, it is brought into contact with a surface and the solution flows from the coated tip to the surface or vice-versa by capillary action.

In dip-pen lithography (figure 2.29) a sample that binds proteins or other biomolecules is transferred from the tip to the surface creating nanometre scale patterns. The rest of the surface is blocked with molecules that do not bind biomolecules and the surface is then exposed to the biomolecule solution. Lee *et al* [97] used dip-pen lithography to print a solution of Retronectin and demonstrated cell adhesion to the resulting submicron spots. The resolution of the printed nano-patterns depends on the tip-physical substrate contact time and relative humidity, as well as physical substrate roughness being an important parameter [98]. When printing 20 nm wide lines of alkanethiols on a gold substrate, they found that the lines were discontinuous and followed the physical substrate grain shape.

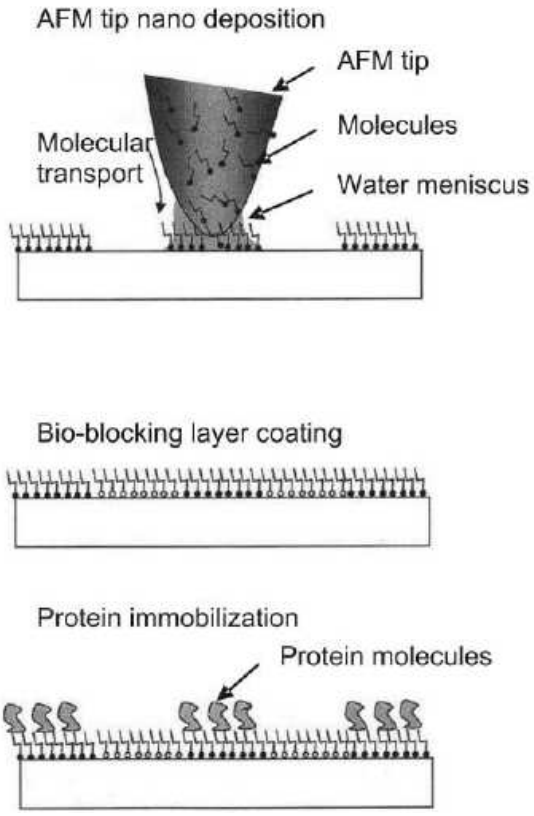

Figure 2.29. Schematic diagram of the process of AFM dip-pen lithography (copied from source [99]).

The AFM grafting method utilizes an AFM tip to remove one SAM layer on selected areas and simultaneously add another SAM [95], as shown in figure 2.30. Thus nano-patterns can be modified and improved *in situ*, without repeating the whole fabrication procedure. AFM printing technology is a serial printing method, and is therefore slow compared to microstamping. Slow printing reduces fabrication efficiency and also limits device functionality because sample volumes are very small and tend to dry out quickly. Furthermore, non-specific binding becomes a serious issue because the size of spots approaches the size of protein molecules. Nevertheless, these techniques are useful for printing nanometer sized features in complex microarrays, where different types of molecules are placed selectively at different sites. The great advantage of AFM printing is that the same tip is used for both printing and reading. By utilizing AFM reading, molecular and physical properties can be directly detected [96].

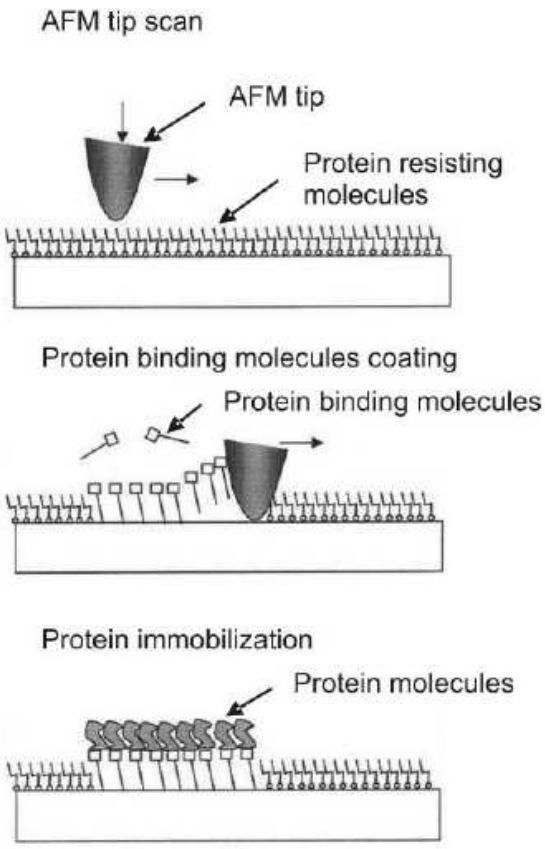

Figure 2.30. Schematic of AFM grating (copied from source [99]).

2.3.2. Non-Contact Printing Techniques

Contact Printing methods include a variety of techniques, but all methods ultimately involve contact between the physical substrate surface and a plate, stamp or pin. In contrast, non-contact printing techniques vary considerably in principle, from photochemistry-based methods to fluid droplet dispensing. There are two main advantages to non-contact printing: reduced contamination and higher throughput. By keeping the printing device and the surface on which the pattern is formed separated at all times, the likelihood of contamination is greatly reduced. Hence, the need to constantly clean the printing device between uses is eliminated. Furthermore, non-contact printing methods hold the greatest potential for increasing microarray fabrication throughput. Many non-contact methods deposit solutions in parallel, allowing entire arrays to be produced simultaneously [85].

2.3.2.1. Photochemistry-Based Printing

Photochemistry microarray printing is based on chemical treatment of the surface by UV light exposure through a photomask. The two main methods are photolithography and direct photochemical patterning [100]. In photolithography a positive photoresist layer is spin-coated onto the surface, exposed to UV light through a photomask and then developed to form micrometer sized patterns with open regions where adhesion-promoting molecules are bound. The physical substrate is then immersed in a solvent to remove the remaining photoresist, and adhesion-resistant molecules are then bound to the newly exposed surface. Direct photo-chemical patterning is very similar to photolithography except that it does not require a photoresist layer. A physical substrate is coated with photochemical molecules and exposed to UV light through a photo mask. UV-exposed molecules are either activated or deactivated to bind biological molecules of interest. Photochemistry-based fabrication methods are mainly applied to protein and DNA arrays although cell adhesion regions can also be fabricated in this way [101]. Similar to all parallel patterning methods, photochemistry features high throughput. The disadvantages include the risk of biomolecule denaturation by photoresist solvents and the difficulty in patterning different chemicals in a single sample [99].

Photolithographic printing is commonly used in generating DNA microarrays of *in situ* synthesised oligonucleotides [102]. For example, the Affymetrix Inc. (Santa Clara, CA, USA) process comprises serial light exposures through different photolithographic masks followed by the chemical synthesis of DNA bases at the exposed/ activated sites. After each exposure a single DNA base is coupled to the activated sites and the process is repeated until the sequences are generated. As a serial process, this method can be time consuming for longer sequences of oligonucleotides, but it provides high-density arrays. The GeneChip® (Affymetrix Inc), a high-density oligonucleotide array, is generated on fused silica surfaces that carry 50 to 400 replicate arrays. Each has up to 400,000 probes on a 1.6 cm^2 area [103].

2.3.2.2. Electro-Printing

The NanoChip® (Nanogen, San Diego, CA) utilizes the negative charges of DNA and RNA molecules to immobilize them on an array of positively charged microelectrodes [104]. Electrodes are coated with a streptavidin-agarose permeation layer and probes are biotinylated such that after the field is turned off, the probe molecules remain non-covalently bound to the surface. In addition, positive charge at individual test sites attracts target DNA molecules whose rapid concentration enables reduced hybridization times. Dense and complex arrays require more sophisticated technology, with integrated complementary metal-oxide-semiconductor field-effect transistor (CMOS) features [85].

Livache *et al* (1998) [66] demonstrated immobilization of DNA in a microarray by electrochemical means. By sequentially activating 50 x 50 µm gold electrodes fabricated on silicon, a mixture of conductive polypyrrole (PPy) and PPy modified by a specific oligonucleotide probe is electro-oxidised which results in copolymerisation of a PPy film carrying covalently linked oligonucleotides immobilised onto the electrodes.

2.3.2.3. Laser Writing

Laser ablation fabrication has recently been used to produce microarrays of protein solutions [99] by means of direct and indirect spot deposition. For direct writing, a quartz disk is coated with a mixture of biological samples, glycerol and buffer [105]. A 150 fs pulsed laser is

scanned across the surface of the disk, locally evaporating small regions of the coating. The sample evaporates and releases liquid droplets that accumulate on the physical substrate. Droplets deposited in this manner are much smaller than those deposited by conventional contact printing. Ringeisen *et al* [105] produced uniform 50 μm spots and claimed that spots less than 10 μm can be formed using this method. This method requires the use of very little sample, which is an advantage over conventional pin printing methods that often induce significant sample waste [105].

Indirect laser writing (fig 2.31) makes use of the established micromachining process of lift-off. A laminate or photoresist is applied to a physical substrate and selectively removed with laser and a mask. A biological solution is then applied to the surface, and the remaining laminate is removed, leaving a patterned sample on the physical substrate [106].

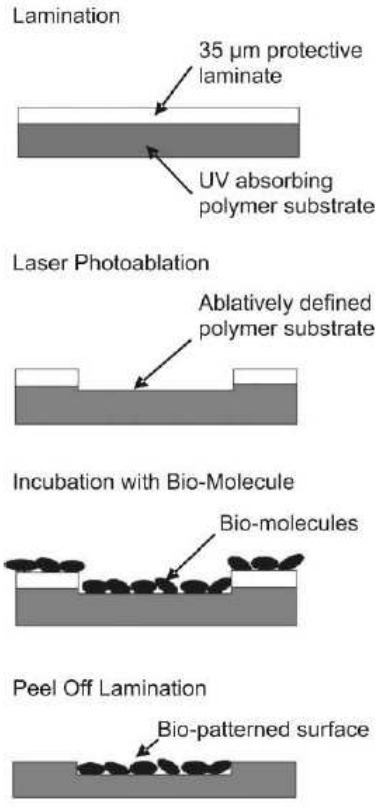

Figure 2.31. Schematic of an indirect laser writing system. A laminate or photoresist deposited on a substrate is selectively removed with laser and a mask using lift-off technique (copied from source [106])

2.3.2.4. Motion Controlled Non-Contact Pin Printing

This is the first of three methods that can be placed under the collective heading of Droplet Dispensing; the others are electrospray deposition (ESD) and inkjet printing.

Zeng *et al* [107] proposed the use of existing contact pin printing technologies to produce microarrays without contacting the physical substrate. This motion controlled non-contact pin printing method uses conventional split pins. Sample solution is loaded into a split pin by capillary forces and the pin is accelerated towards the physical substrate. It is abruptly stopped before contact, driving the solution within the pin out by momentum and forming a liquid bridge between the pin and the physical substrate. Finally, as the pin is drawn away, the liquid bridge pinches off and a droplet is left behind on the physical substrate surface.

Motion controlled non-contact pin printing relies on precise control of pin acceleration, velocity, and position. The pin tip must be stopped a minimum of 2 μm from the physical substrate [107]. The deposited spot volume is strongly dependent on the velocity of the pin as it is retracted from the surface. According to numerical simulation, the entire process takes less than 4ms. No experimental results were reported to confirm the feasibility of this approach [107]. This method solves the problems of pin-tapping, and is most likely compatible with existing contact printing equipment controlled with highly precise robotics. Some difficulties associated with motion controlled printing can be foreseen with the use of even smaller printing pins because surface tension effects scale as L^2, while inertial effects scale with fluid volume (L^3), where L is length [108].

2.3.2.5. Electrospray Deposition (ESD)

As with inkjet printing, electrospray deposition (ESD) is a technique borrowed from an existing application and applied to microarray fabrication. ESD is most commonly used to deposit thin films of polymers, semiconducting ceramics, and radioactive sources [85]. In recent years, there have been a variety of studies using this technique to deposit biological solutions [85]. In ESD, a dielectric mask is placed between a capillary tube containing the solution to be deposited and the physical substrate (figure 2.32.). An electrostatic field is

applied between the capillary and the physical substrate, which drives the solution out of the capillary nozzle. The competition between the induced repulsive surface charge and the interfacial tension leads to the formation of a characteristic conical shape – the Taylor cone. As the applied potential increases the tip of the cone breaks up into a spray of fine, charged droplets and these are attracted to the oppositely charged surface. The solution droplets are attracted to the physical substrate through the holes in the mask. The size of the deposit on the surface is controlled by the size of the holes in the mask, because the drops are much smaller than the mask size. A microarray is created by filling a series of capillaries each with a different solution to be spotted. The array is then created by spraying from one capillary, moving the physical substrate or mask, and then spraying from a different capillary [86].

ESD (fig 2.32) allows for fast and parallel fabrication of microarrays. The use of a single capillary tube for each solution reduces the reservoir filling time. In addition to the high efficiency, ESD is also capable of producing very small spots. To produce spots of 2 - 6 μm in diameter, mask openings are about 25 μm [85]. The shortcomings of the ESD method are that the inner-spot distance is inherently large because the mask holes are much larger than spot sizes. Thus, although ESD can produce microarrays quickly with uniform sized spots; spot density is poor [86].

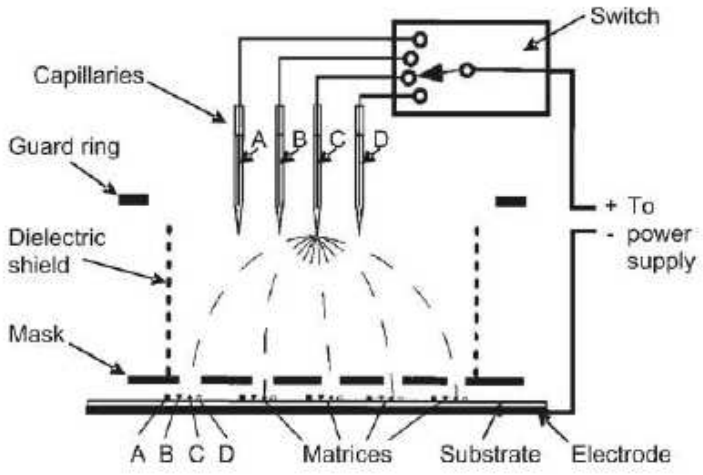

Figure 2.32. Schematic of electrospray deposition. Biomolecule solution loaded in capillaries is dispersed through the dielectric mask onto the substrate by applying electrical fluid between the capillaries and the physical substrate (copied from source [85])

In addition to limited spot density, the ESD method is also limited by significant challenges related to electrofluidics. The droplet distribution within an ESD spray is not uniform. The highest density of droplets occurs directly below the capillary and decreases with radial distance from the centre line. One solution involves moving the mask and physical substrate to allow for uniform deposition. However, this technique still results in the formation of irregularly shaped spots [85], which is an indication of either droplet splashing during impact or the deposition of satellite droplets. Since the inter-spot spacing is large, the possibility of contamination between neighbouring spots is low.

As with inkjet printing, ESD is also limited by possible damage to biomolecules during deposition. The droplets undergo significant shear rates during expulsion from the nozzle and during impact. Additionally, the solution becomes charged when the electrostatic field is activated, and some proteins may deform under such conditions. Finally, the electric field can cause electrochemical reactions that can affect pH levels of the solution. When using ESD, it is important to select solutions that are inert under these conditions [86].

2.3.2.6. Continuous Inkjet Printing

Continuous inkjet printing is a high speed process in which uniform sized drops of ink are deflected from a recycled stream onto a surface. The latter may be uneven or deformable since the printer makes no contact with it. The ability to add material in a controlled fashion to provide net or near net shapes without a mask or pattern also offers an opportunity for the computer controlled generation of microstructures by the use of multi-nozzle printers.

An example of a continuous inkjet printer can be seen in figure 2.33. (Biodot continuous electrostatic jet printer, Biodot, Huntingdon, UK). In this system, fluid is forced under pressure through a 60 µm diameter nozzle. As the fluid passes through the gun body and nozzle it is subjected to vibrations by a piezoelectric drive rod at a frequency of 64 kHz. This regulates the break up of the stream by Rayleigh instability into individual droplets. The fluid is held at an elevated potential in the range 50 – 285 V and hence the drops are formed with a surface charge. The nozzle is aligned so that if no droplet deflection takes place the drops

enter a return tube and are collected, potentially for recycling. Printing is achieved by deflecting drops of fluid from the main jet. As the charged drops pass between parallel high voltage deflector plates they are deflected. The greater the charge on the droplet, the more it is deflected. This is a rapid and robust process used widely in date labelling for food packaging applications. The printed image is built up by an array of printed drops or pixels. As the print table moves past the print head, droplets of fluid are deflected towards the table in a pattern determined by the control unit. The optical sensor in the table accurately detects the position of the table and allows registration so that multiple layers can be built up by over-printing [109].

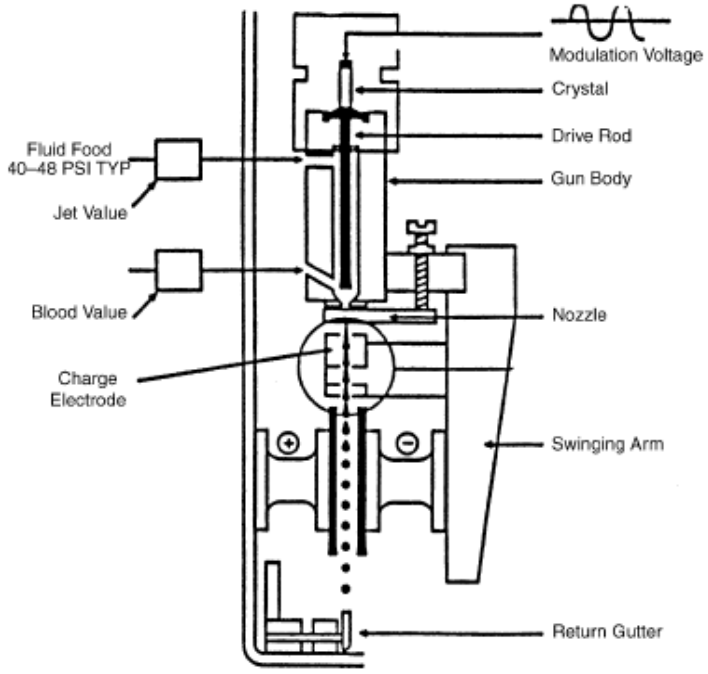

Figure 2.33. The Biodot jet printer (copied from source [109]), where Fluid Food should be Fluid Feed and Blood Value should be Bleed Valve.

2.3.2.7. Drop on Demand (DOD) Inkjet Printing

A Drop on Demand (DOD) inkjet printhead typically comprises an ink chamber with a nozzle at one end, from where droplets are produced under mechanical actuation. The other end comprises an ink inlet from an external reservoir [110]. It is a promising technology for printing of biological materials because it allows deposition of microdroplets of volumes between 2 - 12 pl on any surface with very high precision. Moreover, the use of an array of

inkjet nozzles connected to a device-driving electronic system, which constitutes the typical configuration of a commercial printhead, permits control of the layout of a specific sequence of microdots. Finally, the absence of direct contact between the printhead and the support makes this technique particularly suitable for the deposition of materials on contact-sensitive physical substrates [111]. Actuation of the printer is achieved typically either through a mechanical piezoelectric driven displacement or by a small heater vaporising the ink to form a local bubble, with the growth of the bubble causing the ejection of the ink.

Inkjet printing has been already used for the development of biosensors [112], biochips [113], and DNA arrays [114]. It has to be noted that up to now, the vast majority of the published literature on inkjet printing for the deposition of organic and biological molecules has used the piezoelectric actuation technology [115], due to the high temperature (about 300^{o}C) reached inside the nozzles of thermal printers, which could induce a thermal stress on the ink, in turn damaging the biological and/ or synthetic organic ink components.

2.3.2.8. Thermal Drop on Demand Printing

A typical thermal inkjet (TIJ) printhead is composed of a thin-film heater driven by a power-input controller and an ink nozzle for storing the ink. The operation cycle of the TIJ printhead can be simply divided into three sequential steps, as shown in Fig. 2.34. In the first step, the thin film resistor of the heater is rapidly heated by an electrical pulse of several microseconds. Such a pulse can generate power densities in the order of several megawatts per square meter. Consequently, a sharp temperature rise in the ink results from the high heat flux coming from the thin-film resistor, as shown in Fig 2.34 (a). The ink temperature near the heater-ink interface quickly reaches the threshold temperature, T_t, above which homogeneous nucleation of a phase transformation takes place in the ink. Once the homogeneous nucleation occurs, a vapour bubble with high pressure (> 10 atm) is formed in the ink. The second step of the operation cycle starts from the moment that a vapour bubble is formed. As the vapour bubble grows, it causes ink flow in the nozzle and ink ejection at the exit, as illustrated in Fig 2.34 (b). Due to the fast growth of the vapour bubble and the evaporation of ink, the temperature and pressure in the vapour bubble quickly decrease. At

the end of the second step, a droplet then breaks away from the ejected ink, as shown in Fig 2.34 (c). The break-off of the droplet from the ejected ink occurs nearly simultaneously with the collapse of the bubble. In the third step, the nozzle is refilled with ink after the collapse of the bubble, as shown in Fig 2.34 (d).

The characteristics of the ejected drop are significantly affected by ink properties, heat conduction in the heater, heating pulse conditions, and induced ink motion in the nozzle. To obtain good print quality, the aforementioned characteristics in the micro-scale thin-film structure should be carefully studied. In the last 10 years, several articles have reported both numerical and experimental results which are related to the bubble jet printhead. There are two kinds of thermal bubble inkjet printheads on the market: one has the heater on the ink nozzle side wall (side shooters), and the other has the heater on the nozzle bottom wall (front shooters) [116].

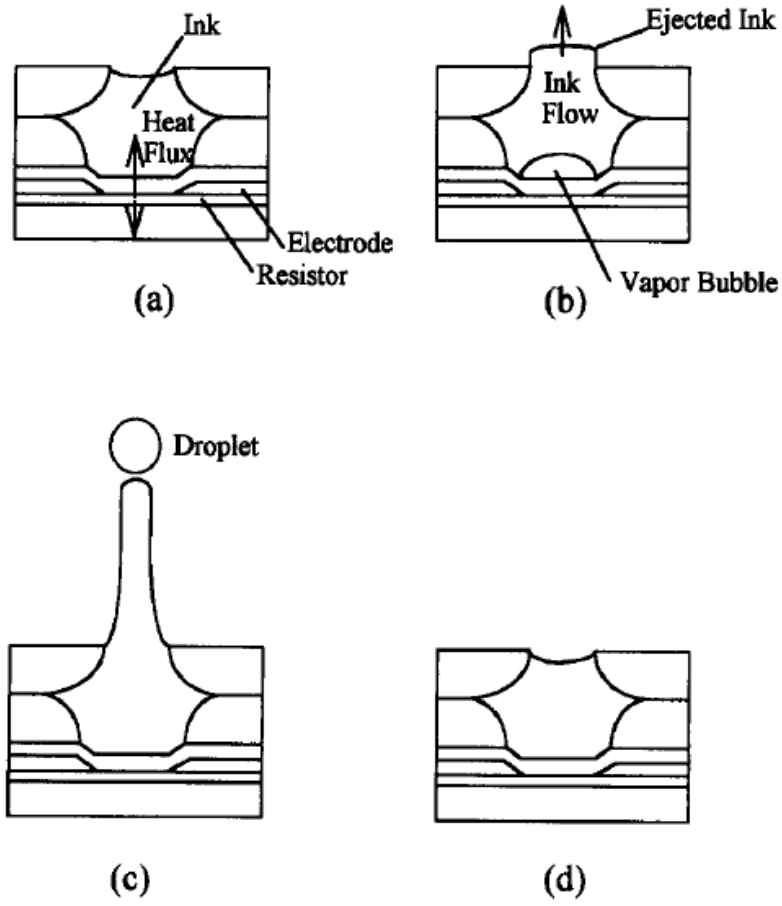

Figure 2.34. Schematic diagram for the ink droplet generation cycle in a TIJ printer (a) heating of ink (b,c) bubble growth and ink ejection (d) ink refill (copied from source [116]).

For side-shooter printheads, a series of studies have been conducted by researchers at Canon Inc. Asai et al. [117] used a one-dimensional model to perform numerical calculations to predict the bubble growth and collapse, as well as ink flow motion in the nozzle. To determine the required heating conditions for bubble jet operation, Asai et al. [118] conducted experiments in which they observed boiling types for different printheads under various heat pulse conditions. Their measured results showed that only homogeneous nucleation could be capable of propelling an ink droplet in the typical printhead. To improve the understanding of the boiling process, Asai [119] presented a theoretical model to predict the incipient boiling time. A refined model was also proposed by Asai [120] to predict the bubble behaviour after the occurrence of homogeneous nucleation. In addition, Asai [121] employed a finite-difference method to solve the three-dimensional Navier-Stokes equations to predict the fluid motion of the inkjet [116].

2.3.2.9. Piezoelectric Drop on Demand Printing

Piezoelectric inkjet printers harness the inverse piezoelectric effect, which causes certain crystalline materials to change shape when a voltage is applied across them. A small electrical pulse makes the crystal contract slightly, squeezing ink out of the nozzle onto the media. Depending on the piezoelectric ceramics' deformation mode, the technology can be classified into four main types: squeeze, bend, push, and shear. For squeeze mode, radially polarized ceramic tubes are used. In both bend and push mode design, the electric field is generated between the electrodes parallel to the polarization of the piezoelectric material. In a shear mode printhead, the electric field is designed to be perpendicular to the polarization of the piezoelectric ceramics [122].

Squeeze Mode Actuator

The actuator of a printhead working in squeeze mode, as displayed in Fig. 2.35, comprises piezoelectric ceramic tubing with a diameter of about 1 mm. The tube, which is polarized radially, is provided with electrodes on its inner and outer surface. When it is desired to have a droplet expelled from the orifice, a short rise time voltage pulse is applied to the transducer, the polarity being selected to cause a contraction of the transducer. The resulting sudden

decrease in the enclosed volume causes a small amount of liquid to be expelled from the orifice. Due to the pressure pulse, some of the ink is also forced back into the tube, but the amount is relatively small due to the high acoustic impedance created by the length and small bore of the tube. The voltage pulse is allowed to decay relatively slowly and the transducer, therefore, expands slowly to its initial volume. Due to the small rate of change of volume during the decay, the accompanying pressure reduction is too small to overcome the surface tension at the orifice. Consequently, liquid flows into the transducer to replace the liquid previously expelled without drawing in air through the orifice. This printhead design was implemented, as an example, in the Siemens PT-80 printer [122].

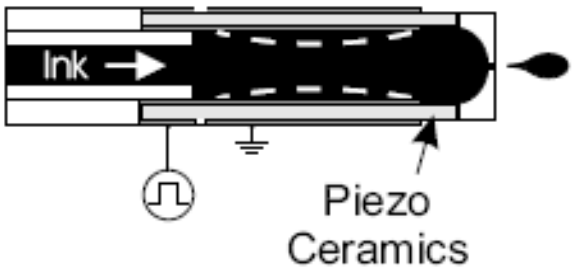

Figure 2.35. Squeeze mode actuator design (copied from source [122]).

Bend Mode Actuator

Fig. 2.36 shows a piezoelectric inkjet printhead operating in bend mode. It consists of a pressure chamber including an ink inlet and an outlet passage terminated in an orifice. A conductive diaphragm forms one side of the chamber with a deflection plate made of piezoelectric ceramic attached. The outer surface of the plate is covered by a conductive coating, which provides an electrical connection to the plate. The application of a voltage to the piezoelectric plate results in a contraction of the plate, thereby causing the diaphragm to flex inwardly into the pressure chamber. This, of course, applies pressure to the printing fluid in the chamber, which forces a droplet to be expelled from the orifice. The size of the droplets is defined by the voltage applied to the deflection plate, the pulse duration, and the diameter of the orifice [123]. The printheads in Tektronix's Phaser and Epson's Color Stylus inkjet printers are based on this design principle [122].

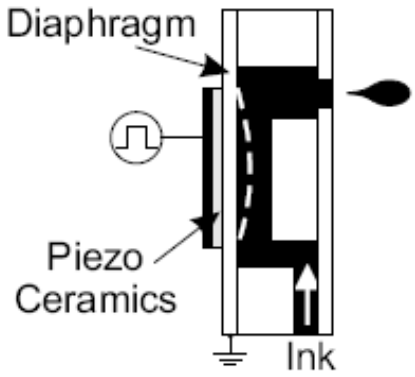

Figure 2.36. Principle of bend mode actuation (copied from source [122]).

Push Mode Actuator

In a push mode design (Fig. 2.37), as the piezoelectric ceramic rod expands, it pushes against a diaphragm to eject the droplets from an orifice. In theory, the piezoelectric actuators can directly contact and push against the ink. However, in practical implementation, a thin diaphragm between the piezoelectric actuators and the ink is incorporated to prevent the undesirable interaction between ink and actuator materials [124]. Successful implementation of the push mode piezoelectric inkjet is found in printheads from companies such as DataProducts, Trident, and Epson [122].

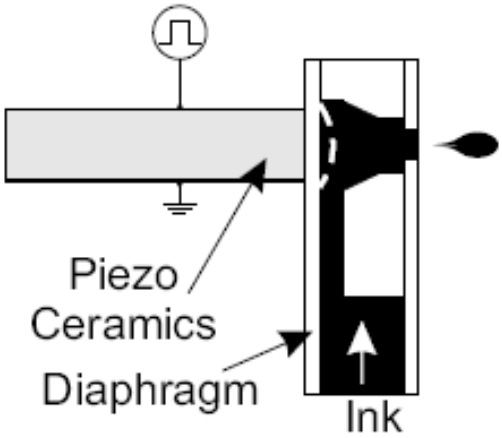

Figure 2.37. Functional principle of a push mode inkjet actuator (copied from source [122]).

2.4. Solution Parameters

In order to fabricate the biosensors required in this study using inkjet printing, it is necessary to satisfy a number of requirements. First there is a need to produce stable protein suspensions with defined fluid properties such that they can be passed through a droplet generator and form regular drops. Second, these suspensions need to be delivered onto a physical substrate. Finally, the printed protein solution must undergo phase transition to a solid even deposit. This chapter considers each of these requirements and their optimisation for the direct printing of protein solutions.

2.4.1. Protein Inks

Manufacturers of DOD inkjet printing equipment normally state a range of viscosity and surface tension within which inks may be successfully printed. However, this information is normally provided for the benefit of formulating graphics inks and may not be directly applicable to the development of aqueous inks. This is because graphical inks are normally oil based inks, the protein suspensions used in this study are aqueous based and therefore have different viscosity and surface tension characteristics.

The fluid rheological requirements for a printable ink are determined by the physics and fluid mechanics of the drop generation process [125] [126]. The behaviour of fluids during inkjet printing can be represented by the Reynolds (Re), Weber (We) and Ohnesorge (Oh) numbers (equations 30, 31 and 32).

$$\mathrm{Re} = \frac{v\rho\alpha}{\eta} \qquad (30)$$

$$We = \frac{v^2\rho\alpha}{\gamma} \qquad (31)$$

$$Oh = \frac{\sqrt{We}}{\mathrm{Re}} = \frac{\eta}{(\gamma\rho\alpha)^{1/2}} \qquad (32)$$

Where ρ, η and γ are the density, dynamic viscosity and surface tension of the fluid respectively, v is the velocity and α is a characteristic length.

The Ohnesorge number (*Oh*) was identified by Fromm as being the appropriate grouping of physical constants to characterise the drop generation in an inkjet printer [127]. *Oh* is independent of fluid velocity and is commonly used in analyses describing the behaviour of liquid drops. However, in Fromm's publication, he defined the parameter $Z=1/Oh$ and from a simple model of fluid flow in a drop generator of simplified geometry, he proposed that $Z>2$ for stable drop generation [127]. This research was extended by Reis through numerical simulation. He proposed that stable drop formulation would occur between the range of $10>Z>1$ [128]. If $Z<1$, viscous dissipation prevents drop ejection from the printer and if $Z>10$, droplets are accompanied by unwanted satellite drops.

The suitability of a fluid for inkjet printing can be roughly assessed by its Ohnesorge number. However, there are other limits of fluid behaviour that impose additional limits to practical drop generation. In order to generate a small radius drop, the surface tension and associated Laplace pressure must be overcome before a drop can be ejected from the printer. Duineveld proposed that this can be described by a minimum value of the Weber number, $We>4$, below which there is insufficient fluid flow to overcome surface tension [129]. A final bound to printability is given by the onset of splashing that occurs if a drop hits the physical substrate with velocity above a critical threshold. This occurs when $We^{1/2}Re^{1/4}>50$ [130]. These limiting bounds define a region of the parameter space of *We* and *Re*, within which DOD inkjet printing is possible [125]. Figure 2.38 shows this parameter space and the region suitable for DOD inkjet printing. Drop velocity increases diagonally, as indicated and has lower and upper bounds that are defined by the appropriate limits of drop ejection and splashing, orthogonal to velocity is the Ohnesorge number, which defines the limits of the fluid properties, thus figure 2.38 can be considered to represent a guide to the limits of both fluid characteristics and drop dynamics consistent with the practical use of piezoelectric DOD inkjet printing.

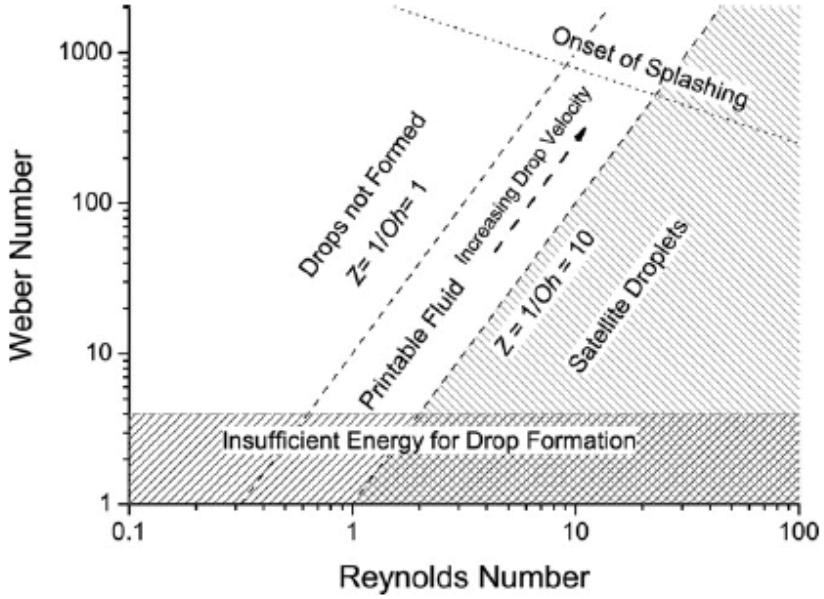

Figure 2.38 Inkjet printing is practical for a limited range of fluids and printing conditions. This is illustrated here in a parameter space defined by axes of Reynolds and Weber numbers (copied from source [131]).

2.4.2. Drop impact, spreading and coalescence

In all cases, the drop will interact with a solid physical substrate. Following deposition, there will be a period when the drop's shape is controlled by fluid processes prior to solidification. Thus an important consideration is the appropriate time constants that apply to the mechanisms of surface spreading and solidification. This discussion confines the mode of moisture loss to be evaporation and to printing from a stationary head, which is what is used in this work.

When a liquid drop impacts a planar physical substrate it will deform and spread to cover the substrate, ultimately achieving an equilibrium sessile drop configuration. Yarin has recently reviewed the impact of drops over a size and velocity range that intersects those relevant to DOD printing [132]. The typical range of drop size (radius from 5 μm to 50 μm) and velocity ($1<v<10$ ms^{-1}) is such that the initial deformation of the drop will be controlled by dynamic impact and viscous dissipation processes [125] [132]. However, this initial stage of drop deformation is expected to have finished after a few μs and subsequent spreading to

equilibrium will be driven by capillary forces [133]. A schematic representation of the timescales associated with drop deformation after impact is presented in figure 2.39.

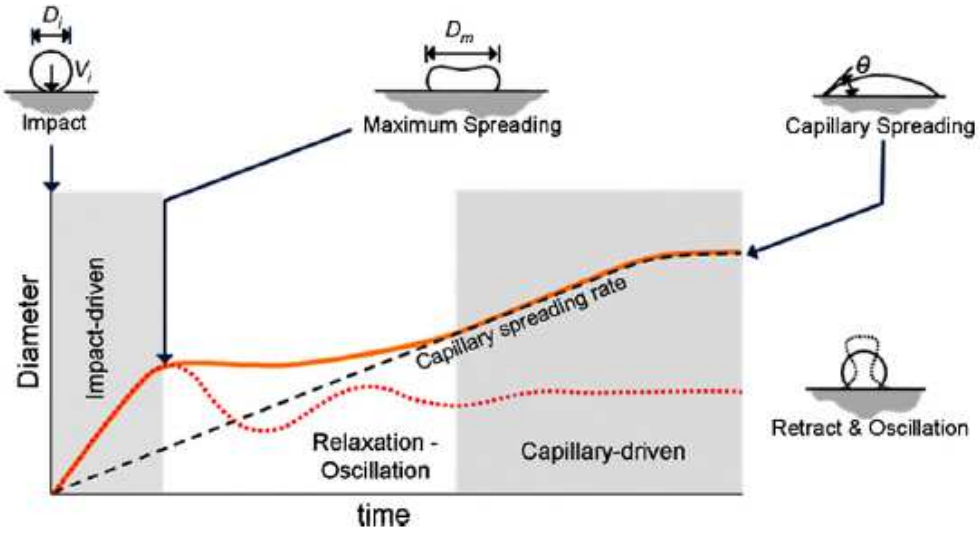

Figure 2.39. Schematic illustration of the time scales appropriate to the processes of drop deformation and spreading on a physical substrate after impact. Axes of time are to arbitrary non-linear scales (copied from source [131]).

The dynamic processes of drop impact occur over a time scale of μs [132]. First the drop deforms on impact with its kinetic energy converted into new surface area as the drop deforms, some energy is absorbed through viscous dissipation. If the impact conditions are such that splashing does not occur (as is normal with the conditions of inkjet printing), the drop may recoil after expansion and oscillate briefly, dissipating energy. Meanwhile, the process of capillary spreading will occur, this has a time scale of ms for drop dimensions consistent with inkjet printing and the final equilibrium drop shape is normally controlled by this process.

Once equilibrium has been reached, the drop can be modelled as a spherical cap because the Bond number is sufficiently low that the influence of gravity may be ignored. In this case, the equilibrium contact diameter of the drop, d_{eqm}, can be calculated with:

$$d_{eqm} = \beta d_{o,} \tag{33}$$

$$\beta = 2\{\tan\frac{\theta_{eqm}}{2}(3+\tan^2\frac{\theta_{eqm}}{2})\}^{-1/3} \tag{34}$$

Where d_o is the diameter of the drop in flight and θ_{eqm} is the equilibrium contact angle.

For an isolated drop of pure solvent, we would expect the drop diameter to decrease and the contact line to retract at a constant receding contact angle during evaporation. However, for the case of particles in suspension, the behaviour of the liquid drop is different. Solvent evaporation does not occur uniformly from the sessile drop. At low contact angles, the fluid close to the contact line is adjacent to a large dry surface and this enhances the transport of the solvent vapour, promoting faster evaporation. This leads to a ring of particles coming out of suspension and the presence of this dried deposit pins the contact line and prevents it retracting. This contact line pinning results in the receding contact angle decreasing as solvent is removed. It can also result in a flow of particles to the contact line, leading to suspension segregation and a ring deposit; this is a phenomenon known as the coffee stain effect [134]. This is the subject of the next section. One of the effects of contact line pinning during drying, is that the footprint or equilibrium diameter of the spread drop of ceramic ink will define the diameter of the dried deposit on the surface after solvent evaporation [131].

2.4.3. Drop drying and coffee staining

The final process to consider that is important in controlling deposit shape is drop drying and coffee staining. Deegan explained this phenomenon as being caused by a combination of contact line pinning preventing an evaporating drop receding, as volume is lost through evaporation, and the enhanced evaporation that occurs at the bounding contact line of a well spread drop, which is driven by the large region of dry physical substrate surrounding the drop that enhances diffusion of the evaporating vapour from the drop surface [134]. In a later publication, Deegan et al. presented a detailed study of coffee staining and developed a numerical model for the process that agreed well with experimentation [135].

It was concluded that coffee staining is the normal behaviour for a drying drop over all length scales studied for both solute and suspended particles. It is not caused by the surrounding dry surface, as originally proposed [134], but occurs if the following two conditions are obeyed;

(1) the edge of the drying drop (the contact line) is pinned, and

(2) evaporation is possible from the edge of the drop.

For solutions or suspensions, condition 1 is normally met if there is any significant roughness to the surface and at small contact angles when rapid solid deposition occurs at the contact line. Deegan observed that on smooth PTFE physical substrates, contact line pinning was absent and drops contracted during evaporation to leave a uniform deposit [135]. Deegan also explored the constraining evaporation through a hole positioned above a drying drop, which severely reduces evaporation from the edge of the drop, and this too eliminated coffee staining [135] [132].

Coffee staining has been observed in a number of prior studies using inkjet printing and methods to counter its effects have been proposed and studied. First it is important to note that coffee staining is only a problem when the liquid solidifies through evaporation and is not significant when a liquid drop solidifies through a phase change on impact [136] [137]. Deegan noted that it may be possible to counter the fluid flow caused by differential evaporation through inducing an opposing flow from the Marangoni effect [135]. He noted that the main source of heat to drive evaporation arises from contact with the physical substrate hence the centre of the drop is expected to be cooler than the edge. In most fluids surface tension decreases with increasing temperature thus there is expected to be a gradient in surface tension that increases to a maximum at the drop centre. Deegan did observe a flow opposing coffee staining during evaporation but this decreases with time and is insufficient to prevent coffee staining.

De Gans and Schubert exploited the Marangoni effect through the use of solvent mixtures [138]. Two solvents were selected, with different vapour pressure and surface tension values, such that a high vapour pressure solvent evaporated at the drop edge causing a local decrease in surface tension and thus generated a surface tension gradient increasing towards the drop centre. Such solvent mixtures can generate much larger surface tension gradients than are attainable through temperature gradients and they were able to

completely suppress coffee staining following inkjet printing of polystyrene solutions. A number of other parameters have been shown to influence coffee staining including the spacing of droplets [138], local partial pressure of the solvent [139], and even the impact velocity of the drops [140].

The importance of Marangoni flows during droplet drying can be estimated using the dimensionless Marangoni number, M_a, defined as:

$$M_a = \frac{\Delta \gamma r}{\eta D} \qquad (35)$$

Where $\Delta\gamma$ is the difference in surface tension (taken here to be the difference between the two pure solvents), *r* is a characteristic length (assumed to be the radius of the spread drop on the physical substrate), η is the fluid viscosity and *D* is the solute diffusion coefficient.

It is generally believed that Marangoni flows are significant if M_a>100, Both de Gans and Zhao computed very large values for M_a in their studies of approximately 10^6 x $\Delta\gamma$ (using SI units) [138] [139]. This result implies that even very small differences in surface tension of around 10^{-4} Jm^{-2} should be sufficient to impede coffee staining and this would appear to be at odds with the common observation of coffee staining reported in the literature. The influence of Marangoni convection on coffee staining was investigated in considerable detail by Hu and Larson [141]. It was found that when clean organic solvents were used in drop drying experiments, coffee staining was never observed and that Marangoni flow dominated the evaporation driven flow proposed by Deegan [142]. It was further proposed that the suppression of Marangoni flow is a necessary condition for the observation of coffee staining. It was suggested that the reason coffee staining is observed in most aqueous systems studied in the literature is because the Marangoni number is drastically reduced (M_a<<100) because of the strong influence of surface contaminants on the surface properties of water.

From this survey of recent work it is clear that solute or particle segregation during the drying of drops is an extremely complex process with a number of competing mechanisms in addition to evaporation and Marangoni flow. These effects may merit consideration later in

this work, especially where drops of protein in suspension are being placed onto a small sensor area. However, the effects of coffee staining also need to be taken with the functionality of the sensor in mind.

2.5. Current Biosensor Deposition Technology

There are four significant drawbacks to inkjet printing for the manufacture of sensors. 1) Commercial printers are not designed to print on glass slides or other surfaces of interest for sensor applications. 2) Inkjet nozzles have a tendency to produce undesirable satellite droplets that may contaminate surrounding spots and thus reduce printing resolution [107]. 3) It is difficult to completely flush printing nozzles before a new solution is loaded [143]; this is more serious in piezoelectric printers since the nozzle is separated from the ink reservoir and all linking channels must be flushed clean. 4) The droplets experience high shear rates while passing through the nozzle and impacting the physical substrate surface; under these shear rates, or high temperatures, there is a risk of denaturing biomolecules in the solution [85].

2.5.1. Current deposition techniques for biosensors

There has been some prior work carried out using DOD inkjet technologies to print proteins. The potential applications of the process are various, from the production of biosensors to producing scaffolds with cells and/or proteins integrated into them. Setti [144] used DOD technology for the development of biosensors and in the process examined the damage to the protein β-galactosidase (GAL). Setti [144] used an ink containing GAL in phosphate buffer, using EDTA as the antimicrobial agent and glycerol as the stabiliser and ink viscosity regulator. The inkjet printer was a TIJ system from Olivetti Tecnost (Ivrea, Italy), with the ink ejected using a printhead supplied from Olivetti I-Jet (Aosta, Italy) which is characterized by 208 nozzles having a roof-shutter design. The activity loss of the microdeposited enzyme after the ink ejection was evaluated through a spectrophotometric assay. Setti (2004) [144] demonstrated that only around 15% of the enzyme activity was lost after the printing, i.e. no significant denaturation effects due to the printhead heater were evidenced. Setti ascribed this finding to the fact that the heater into the nozzle generates a bubble of fluid at high pressure (>10 atm), which in turn presents a gradient of decreasing temperature from the

surface of the heater to the bulk of the ink solution. This gradient permits the enzyme in the bulk to feel an actual temperature not as high as the one on the surface of the resistor, decreasing with the time elapsed from the initial heating event.

This work is supported by other work carried out by Setti (2005) [145] using Glucose Oxidase from *Aspergillus Niger* to assess the suitability of TIJ printing for deposition of proteins. This ink was obtained by dissolving 6 mg ml^{-1} Log GOX in a 0.1 M phosphate buffer, pH 6.5, which contained EDTA 1.5 mM as antimicrobial agent and 10% (w v^{-1}) of glycerol as stabiliser. The same printer was used that was used in similar work carried out by Setti in 2004 [144] (detailed above). The addition of a food dye (Brilliant Blue FCF, E133) as a colorimetric probe enabled visualisation of the printed area as well as the determination of the volume of the ejected ink spectrophotometrically. Setti [145] found that there was no denaturation effect due to the printhead heater, since the enzyme activity values in the biological ink before and after the print were respectively 210.3 and 238.0 U ml^{-1}. On this basis the printed activity resulted in 0.18 U cm^{-2}, corresponding to 2.38×10^{-5} U dot^{-1}.

Both of these experiments were carried out using a modified TIJ printer. Work has also been carried out using a piezoelectric actuated printer by Nishioka *et al* (2004) [146]. Nishioka printed an aqueous solution of peroxidise enzyme buffered with fluorescein sodium salt and sugar (trehalose/glucose) into a 96 microwell plate. The fluorescence of each well was measured, reaction solutions added and absorbance measured after 30 and 45 minutes. The compression rates of the printer were varied by altering the rise time of the actuating 85 V pulse from 14 to 70 μs, using nonresonance conditions at 100 Hz and an asymmetric waveform, consisting of compression over microseconds and expansion over milliseconds.

Using this method, Nishioka found that the absorbance and hence activity increased linearly with the quantity of peroxidase printed at each compression rate. It was also discovered that for a solution printed using a compression rate of 5.48×10^{4} μm^{3} μs^{-1} yielded an absorbance of 1.2 for 1 ng of peroxidase. When compared to the control curve, obtaining an absorbance reading of 1.2 should have required approximately 0.45 ng of peroxidase. Thus, it is

postulated that of the 1ng of peroxidase to have been printed at this compression rate, only 0.45 ng remained active. This result is typical of the work carried out by Nishioka (2004) [146], with the percentage retained activity in the peroxidase changing with the differing compression rates used which was calculated from the horizontal distance between the sample curve and the control curve.

Nishioka also assessed the effect of a stabilising solution on the mode of damage found by using a piezoelectric printer. It was found that the addition of the stabilising sugar solution significantly reduced damage to the peroxidase, and that there was no significant difference between the 10% trehalose/ 1% glucose solution and the 20% trehalose/ 2% glucose solution. It is known that trehalose is an exceptional stabiliser of protein conformation due to its extensive hydrogen bonding with proteins and its effect on the structure of water [147]. This extensive hydrogen bonding may also stabilise peroxidase in the liquid state during the printing process, presumably by cushioning the enzyme against pressure induced denaturing.

2.6. Summary and Conclusions

Inkjet Printing of proteins is an area which has undergone a transformation from a science fiction idea to a possibility. Research has so far been undertaken on a fairly small scale, with the majority of it being used to confirm a proof of principle. That is that the inkjet printing method, whether thermal or piezoelectric, is suitable as a deposition method for proteins. There has also been some research, which has been detailed above, looking at the ability of a printed sensor to function and offer a response which is comparable to a sensor constructed in the usual way.

This project aims to further this work by analysing the suitability of a piezoelectric DOD printing platform as a tool for the deposition of proteins onto small sensor surfaces with the possibility of miniaturization of the sensors. The project will differentiate itself by analysing the fluid properties when depositing onto the surface of the biosensor, as well as the biosensor itself, and the fluid properties once on the surface including its drying and

attachment mechanism. The project will also aim to prove a method by which a whole sensor can be produced relatively easily using a piezoelectric printer as the deposition mechanism.

This will be achieved by using a variety of different characterisation techniques including some for protein characterisation, some physical and chemical characterisation techniques for the sensor surface and the fluid as well as some electrochemical characterisation of the whole printed sensor to optimise the production technique. All of this is outlined further on in the thesis as well as a definition of the industry support on the project.

CHAPTER 3: BUSINESS JUSTIFICATION

3.1. Project Outline and History

This work is based around a Technology Strategy Board sponsored project entitled 'Biomedical Inkjet Printing'. This project consists of a group of companies working in collaboration with the University of Manchester, namely; Applied Enzyme Technologies Ltd, Xaar plc, Ellis Developments and Oxford Biomaterials Ltd. The intended roles of each company were as follows; Applied Enzyme Technologies (AET) expertise lay in the packaging of proteins and the thermal stabilisation of proteins using specially designed solutions and kits. Xaar plc are an Original Equipment Manufacturer (OEM) of printheads and inks, which, for this project, are designed to operate with hardware supplied by Xennia, a systems integrator and printer hardware manufacturer. Ellis Developments is a small consultancy company specialising in woven materials, especially those for use in medical applications such as tissue engineering. Oxford Biomaterials are a company which research into modified natural silks which offer possible applications in tissue engineering.

The project had two distinct objectives – the deposition of proteins for sensor applications and the deposition of cells on embroidered silk physical substrates. Both applications were seen by Xaar as possible future markets. These proteins, cells and physical substrates would be produced for market by the other partners on the project for sale alongside the printing platform. However, due to various factors, Xaar's position on the project was re-assessed internally and they withdrew from the project management role. This led to Julian Ellis (Ellis Developments) taking on the role.

The project objective as it stands for this piece of work is to prove that a piezoelectric drop on demand printer offers the capabilities to deposit small volumes of proteins very accurately with the specific future aim of producing a prototype system which can offer companies the opportunity for a more accurate deposition system for the construction of multiple analyte arrays, for testing for multiple analytes, for use in biosensors. Thus, this piece of work

selected one specific well known and mass produced enzyme biosensor and demonstrates that inkjet printing can be used as an alternative manufacturing route for the production of said biosensor. In this case the enzyme biosensor chosen is that of the glucose oxidase enzyme for the home glucose testing (diabetes) market. The business need for a quicker more accurate deposition method in the biosensor market is outlined in the next section.

3.2. Business Case

The glucose sensing market is currently a diverging market with two clear paths for manufacturers to take: Implantable glucose sensors which can continuously monitor blood glucose levels and provide insulin where necessary or disposable testing strips which use lower volumes of blood and multiple lancets in one machine. This helps with lower pain levels and discomfort as well as increasing ease of use for the patient. They may also aim to produce smaller sensor structures which would open a pathway for the development of multi-enzyme sensors on a small footprint, which can be used to detect multiple analytes from a single test solution.

Within the disposables market, there is also a slight divergence in manufacturers' positions within the market. They are either opting for a reduction in the volume of blood to be used for home testing with volumes currently as low as 200 nl being required for an accurate result or they are looking for an alternative testing site which will reduce the discomfort for the patient.

The final perspective on the biosensor market places an emphasis on the long term future of the marketplace and is taken from a review on the possible future of the glucose sensing market. With the current valuation of the glucose sensing market standing at 85% of the world biosensor market which is valued at $5 billion [148], any innovations that produce improved technology could be extremely profitable. It states that;

'The most important next range of home blood glucose monitoring devices will be integrated. Integration will take several forms and include instruments offering multiple glucose tests, multiple analytes, lancing combined with testing, testing combined with

injectors and pumps combined with sensors. The most successful formats will address real needs, sizeable patient groups and offer un-rivalled convenience in simplicity of use and portability' [148].

From the perspective of continuing this work, the use of inkjet printing offers many advantages over the current process for deposition; it is able to deposit volumes in the range required for current glucose sensors, they are able to do it accurately and in a highly repeatable manner, and they can do it quickly with motion, either of the physical substrate or of the printhead. The ability of the printhead to deposit smaller volumes of liquid than the current method, whilst being advantageous, does not offer an advantage for miniaturisation of the sensors due to associated limitations in the sampling size required to get an accurate result on the biosensor head during analysis of the sample.

Perhaps the largest area of expansion which inkjet printing offers the opportunity to expand into, is that of multiple sensor arrays on a single sensor that allow for the diagnosis of multiple conditions with a single sample. This is due to the ability to accurately (within 5 μm) deposit small volumes of liquid (as low as 10 pl per drop) onto a physical substrate in a highly repeatable manner. With the addition of the ability to manipulate the head by small amounts (10 μm) in any direction through control software and the ability to have multiple heads on a system (up to 4 on the system used in this work), the inkjet printer is well suited to depositing multiple enzymes onto a single biosensor for multiple analyte testing.

3.3. Exploitation of the technology

3.3.1. Chemical Sensors Market

The global biosensors market was worth over $7000 million in 2006. This represents phenomenal growth from a market of $5 million in 1987. Of this market biosensors represent by far the largest share, of which the market for glucose sensors is the most important. The greatest growth of this sector is expected to remain in the medical sensors market, although significant growth is predicted in chemical sensors and industrial sensors [148].

Current fabrication technology for enzyme based sensors combines screen printing for electrode fabrication with either a second screen printing stage for enzyme deposition or direct pin-printing of the enzyme onto the electrode pads. Both these methods require large volumes of liquid with minimum dosage of the enzyme in the µl range. Although this is tolerable with current sensor designs, there is a commercial driver to miniaturise the electrode configuration in biosensors to allow more complex multi-component analysis on a single drop of fluid. In this project we have demonstrated the practicality of using inkjet printing to fabricate glucose sensor structures using inkjet printing of suitably stabilised enzyme solutions. This has reduced the dosing unit to individual drops of 60 picolitres, with a consequential potential decrease in sensor structure size or increase in the number of analytes under test per chip.

AET's products offer the opportunity to stabilise the enzyme whilst in solution but not affect the properties of the biosensor itself. This is beneficial to most biosensor producers as it means that the shelf life and operational stability of the enzymes is improved. AET is in discussions with a major international printhead supplier to validate its enzyme suspensions for application. AET and the University of Manchester have (with funding from BBSRC) agreed to continue collaborating to develop further inkjet printable enzyme suspensions for other sensor applications and to seek OEM partners for printing equipment supply. AET plan to develop new inkjet compatible enzyme systems for commercial release at a rate of two per year until 2012.

Current sales of stabiliser solutions for proteins in solution for AET are expected to reach the £10,000 threshold by the end of this financial year. With the development of stabiliser solutions that are applicable to most commercially available enzymes required for the manufacture of biosensors we expect to see increasing interest in these product lines. With the drive towards smaller structures being printed onto biosensors to allow more complex structures to be developed, there will be increased demand for technologies that can deliver highly accurate enzyme deposition in the picolitre range.

AET predicts initial interest from University research departments world-wide. These institutes will possess lower cost desktop printing technologies. Further commercial interest is expected from the emerging production markets located in the Far-East. These markets are based around printing base electrodes in print houses and each production company being in control of the deposition technology. Further commercial sales are expected from Europe and the US. These will be in the form of older established technology which will need miniaturising for the reduction of production costs. Further commercial interest is likely from the clinical chemistry sector. These instruments are used within pathology and clinical chemistry departments within hospitals. The requirement is for the size reduction in multiple biosensor analytical chips in order to fit more technology within the same chip surface.

There is also the possibility of using the knowledge gained from this work in order to manufacture and use AET solutions for in vivo sensing with various different types of biosensors. The increased stability which the solution confers on enzymes would make this well suited to the products of AET, and the ability of the inkjet technique to manufacture multiple enzyme biosensors would make in vivo testing, continuous or otherwise, a more appealing and cost effective approach.

In terms of the current glucose market, AET predicts that the market size for the sale of stabiliser solutions for ink jetting will increase stabiliser solution sales from £10,000 in 2009 to £50,000 over the next 3 years. If the technology is taken up in collaboration with an ink jet head manufacturer then we predict a sales increase of £100,000 to £200,000 over the next 3 years.

If the future markets, including that of the in vivo sensing and the multiple enzyme sensors are included in the forecasts, it becomes more difficult to place a figure on the income that could be generated. However, with the current biosensor market worldwide manufacturing and selling 20-30 billion sensors per annum, then there is obviously a large opportunity in

existence. If AET were to position their solutions for use in just 5% of these markets, but gain 60-70% of the market, then the margins could be much higher than predicted above.

3.3.2. Cell Printing

The cell printing market is at a much earlier stage of development than the biosensor market with no commercial products available. The project has highlighted some difficulties in using industrial inkjet printheads, which are optimised for work with graphic inks, for the printing of cell suspensions. These are related to the complex internal fluid delivery mechanism and the fact that the ink is fed into a dead volume behind the printer orifice and this can lead to cells coming out of suspension and blocking the printer. However, we have demonstrated that in simpler printer designs, this is not a problem.

In discussions with UK companies working in inkjet printing we have found one OEM that is working on the fabrication of DNA and peptide arrays. We have identified IP external to the project, developed for other applications in the life sciences, that is possibly transferable to our application. We propose to initiate discussions to initiate proof of principle studies and if appropriate determine whether joint development of cell printing is appropriate.

Preliminary data has indicated that cell printing on embroidered physical substrates is sensitive to the fibre density in the embroidered structure. We anticipate further work in optimising embroidered scaffold design for cell printing applications.

CHAPTER 4: METHODS

This chapter outlines the experimental methods used to characterise the effect of printing parameters on proteins. It can be divided into four sections: protein preparation, ink jet printing, protein characterisation and electrode characterisation.

4.1. Protein Preparation

The protein solutions were prepared by taking the original activity of the enzyme in U mg^{-1} and making up a 12000 U ml^{-1} concentration of the enzyme (supplied by AET Ltd., Pontypool, UK) in either PBS (Sigma Aldrich, Gillingham, UK) or a stabilising solution supplied by AET Ltd. The solution used was dependant upon the work to be carried out and will be specified in the results section where appropriate. Where surfactant is also present in the solution, a specific amount of Triton-X 100 (Sigma Aldrich,) was added dependant upon the work to be carried out. Again, the amounts used will be specified in the results section where appropriate.

4.2. Inkjet Printing

The general principles of operation of the drop-on-demand piezoelectric printer were outlined in Section 2.3.2.9. The contraction of the piezoelectric ceramic and subsequent generation of drops are dependent on the application of a voltage pulse or repeating waveform; the precise shape and amplitude of the pulse is defined to control the size and velocity of an ejected drop. All experiments were carried out using inkjet equipment sourced from Microfab Inc. (Plano, TX, USA). Microjet printheads (MJ-AT-01-60, Microfab) were either mounted on a laboratory clamp or in a complete printing system (the in-house designed and built MPP1000, using Microfab electronics). The printhead consists of a drawn glass capillary with an internal diameter of 60 µm surrounded by a piezoelectric actuator.

4.2.1. The experimental set up

The test station referred to throughout this chapter consists of a stationary Microfab printhead clamped into place. All physical substrates, such as tissue culture well plates, were

manually placed underneath the printhead. A complete printing system was used to print patterns and arrays.

A schematic diagram of the test station can be seen in Figure 4.1. The fluid reservoir is attached to a pressure controller and positioned directly above the printhead. A slight back pressure is applied to the reservoir during printing to control the meniscus position at the printing orifice. The position of the meniscus is important to prevent problems such as dripping during quiescence or bubble ingestion during printing. The pressure control system is also used to flush or purge the printing system, when required.

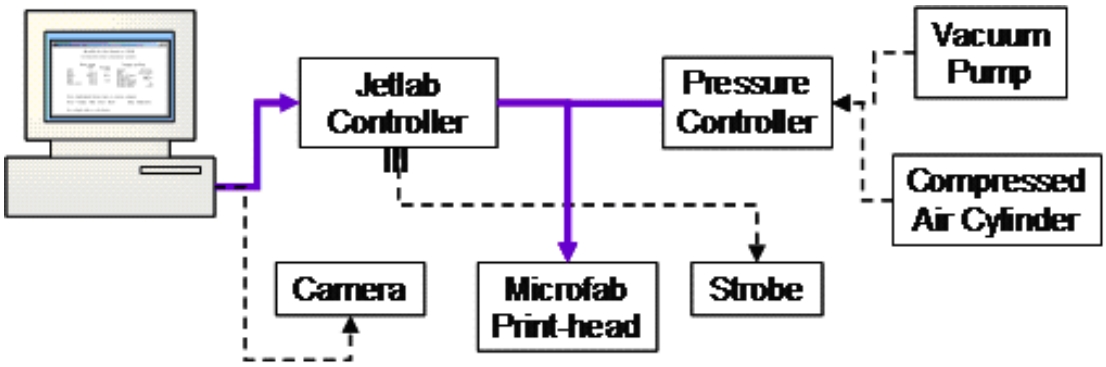

Figure 4.1 Schematic arrangement of the printer set up

The application of a driving waveform to the printhead is computer controlled through the drive electronics (Jet Drive II, Microfab). This also triggers a stroboscopic light emitting diode (LED), which operates at the same frequency as the printhead. This allows the capture of stroboscopic images of the drops to monitor printing performance. The driving waveform used in this study is unipolar and trapezoidal in form. It is shown schematically in Figure 4.2c and is characterised by four parameters, pulse rise time, pulse amplitude, pulse duration and pulse fall time. The driving waveform also has a constant frequency.

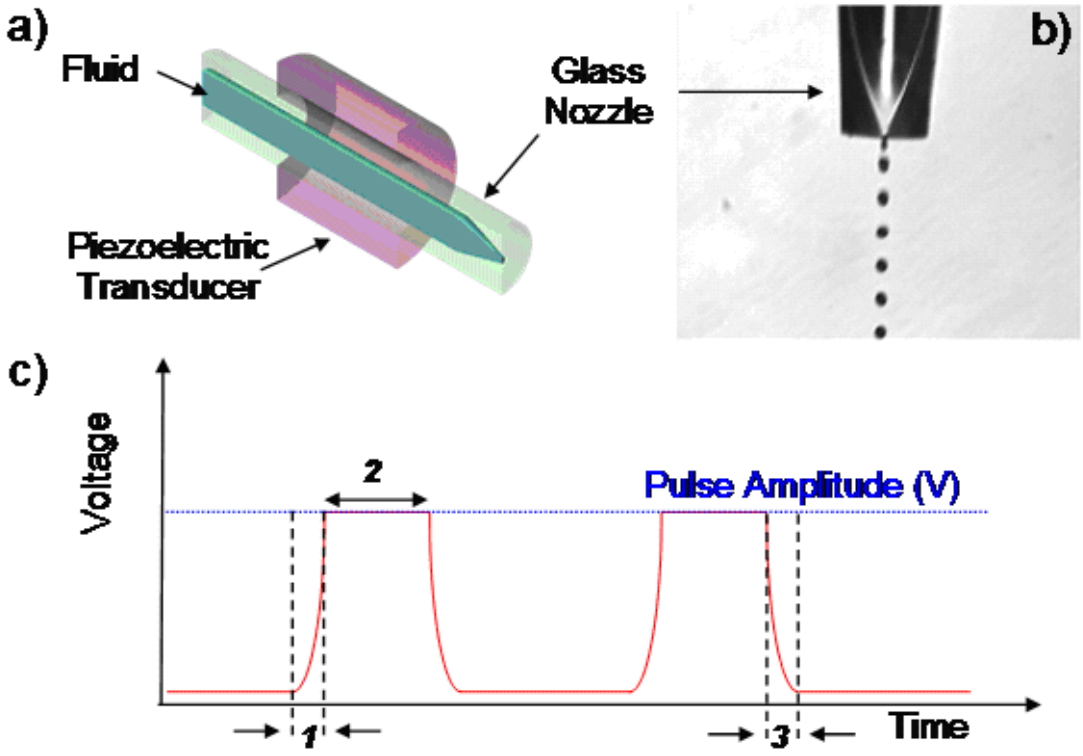

Figure 4.2 a) Schematic of the printhead; b) Image of the jet in action; c) The waveform applied to the piezoelectric 1 - Rise time, 2 - Pulse duration, 3-Fall time

It is known from earlier work that both the velocity and the volume of a drop ejected from an inkjet printhead are controlled by the driving waveform [149]. It is reasonable to expect that the stresses and strains experienced by complex biological macromolecules during inkjet printing will be in some part related to drop velocity and volume. Hence the relationship between driving waveform shape and frequency and the resulting drop parameters must be established.

4.2.2. Determining the effect of actuating voltage on drop volume

An image of a 1 mm graticule was taken as close to the jet as possible. The distance and camera focus remained unchanged after this data was captured to allow analysis of drop size. Cell culture media was printed at a frequency of 10 kHz and the pulse voltage was increased from 40 V to 80 V at 20 V intervals. The rise and fall times remained constant at 3 µs. The drops were illuminated by a strobing LED and a series of equally spaced droplets were captured by a camera. Drop volume can be estimated by measuring the diameter of the droplets and calculating the volume from this.

4.2.3 Determining the effect of voltage on drop mass

The influence of inkjet actuating waveform parameters on drop size was determined by weighing a known number of drops. Phosphate Buffered Saline (PBS) containing enzyme was printed into a container, with the container placed on a weighing scale, for a set period of time (30 s) at a constant frequency of 10 kHz with voltage amplitude varying from 40 V to 80 V at 20 V intervals. The weight of the printed liquid was measured after each 30 s printing run and this was repeated six times for each voltage to ensure adequate statistical data.

4.2.4 General procedure for protein printing

Prior to each printing run, protein suspensions were prepared as detailed in section 4.1. The suspension was then loaded into the reservoir and briefly purged through the connecting tubing to fill the printhead. The suspensions were then printed either directly into well plates or onto electrode sheets, which were manually positioned below the jet. The protein suspensions were typically printed according to the parameters shown in Table 4.1. These were chosen to investigate the influence of the printing parameters on enzyme viability after printing. Once printed, the well plates were analysed using the fluorescence method described in section 4.3.3. If the protein was printed onto the electrode sheets, these were analysed using one of the characterisation methods detailed in section 4.4.

Table 4.1. Typical printing parameters used for printing protein suspensions.

Voltage (V)	Rise and Fall Times (microseconds)		
40	1.5	3	4.5
60	1.5	3	4.5
80	1.5	3	4.5

4.2.5. Printing Patterns

The MPP 1000 printing station was used to print 2-dimensional patterns, in this case onto the electrode sheets, to predefined designs. The MPP 1000 employs a system to drive the printheads with the addition of an XY table to allow positioning of drops to a stated accuracy

of ± 10 µm. The ability to pattern proteins was one of the demonstrable outcomes for this project.

4.3. Protein Characterisation

4.3.1. Protein solution viscosity

This experiment aims to ascertain the effect of protein concentration on the viscosity of the containing solution as well as the effect of the addition of a surfactant. A Brookfield DV-I rheometer (Brookfield Engineering, Middleboro, MA, USA) was used to measure the viscosity of a 17 ml sample of solution at a concentration of 12000 U ml^{-1} enzyme activity. This instrument uses either concentric cylinder or cone and plate load cells, it can operate through a torque range of 0 and 350 mN m.

4.3.2. Protein solution surface tension

This experiment aims to ascertain the effect of biomass on the surface tension of the containing solution as well as the effect of the addition of a surfactant. The surface tension was measured using a pendant drop method with the drop being recorded photographically before measurements being taken using computer software. The surface tension was then calculated using the Young-Laplace equation.

4.3.3. Fluorescence analysis

In this assay, glucose oxidase reacts with D-glucose to form D-gluconolactone and H_2O_2. In the presence of horseradish peroxidase (HRP), the H_2O_2 then reacts with the Amplex Red Reagent in a 1:1 stoichiometry to generate the red fluorescent oxidation product, resorufin. Resorufin has absorption and fluorescence emission maxima of approximately 571 nm and 585 nm, respectively, and because the extinction coefficient is high (54,000 cm^{-1} M^{-1}), the assay can be performed either fluorometrically or spectrophotometrically (Sigma-Aldrich).

4.3.3.1. Calibration Curve

A calibration curve for the fluorescence assay is essential to be able to determine the concentration of protein present in the printed sample. A calibration curve was obtained by pipetting known concentrations of the enzyme into a multiwell plate before exposing it to the correct concentration and volumes of the reagents. This plate was then read in a fluorescence plate reader to generate a standard curve which could be used to estimate the concentration of protein present in future samples.

4.3.3.2. Taking a reading

The plates were printed using the method laid out in section 4.2. The protein was printed into multiwell plates with each sample being printed in replicates of 5 to provide adequate statistics. The necessary reagents were then added to each well in order to produce the reaction necessary to induce fluorescence. The plate was then read at the appropriate wavelength and time intervals to give an indication of the difference between samples. Because of the way the reaction works, the fluorescence of the sample can be directly linked to the activity of the enzyme by a 1:1 stoichiometric reaction.

4.3.4. Light Scattering

Classical light scattering can be used to define the structure of the protein. This technique provides a direct measure of the proteins molar mass and is therefore very useful to define whether the native state of a protein is a monomer or a higher oligomer, and for measuring the masses of the aggregates or other non-native species.

4.3.4.1. Theory

Classical light scattering involves measuring the amount of light scattered by a solution at some angle relative to the incident laser beam. For globular proteins smaller than ~500 kDa, the intensity of the scattered light is uniform in all directions, so it is normal to measure scattering at a single angle to the incident radiation (normally 90º). Theory tells us that the intensity of this scattered light will be proportional to the product of the protein concentration (in mg/ml) times its molecular mass [151].

The technique is also used in conjunction with Size Exclusion Chromatography (SEC-MALS). Since the signal from the light scattering detector is directly proportional to the molecular mass of the protein times the concentration (in mg ml^{-1}), by combining this signal with that from a concentration detector it is possible to measure the molecular mass of each peak coming off the column. Unlike conventional SEC methods, these molecular masses measured from light scattering are independent of the elution volume. Thus, this technique can be used with 'sticky' proteins that elute unusually late as a result of their interactions with the column matrix, and also with highly elongated proteins which elute unusually early for their molecular mass. The molecular masses derived by this technique are generally accurate to ± 3% or better [151].

4.3.4.2. Data Collection

The samples were prepared by printing the protein solution into an Eppendorf tube at a concentration of 12000 U ml^{-1}. Once all samples were printed, each sample was diluted down to a concentration of 200 U ml^{-1} using the appropriate buffer in preparation for testing. A native protein sample was also prepared at a 200 U ml^{-1} concentration to be used as a control. Purified Get3 or Get3 (C317T) (200 µl) (0.5 mg ml^{-1} in 50 mM Tris-HCl (pH 7.5), 150 mM NaCl) were injected onto a Superdex 200 10/300 size exclusion column (GE healthcare, address, USA) at 0.71 ml min^{-1} using the same buffer. The refractive index and the scattering signal of the eluted protein were measured using a refractive index detector (Wyatt Optilab rEX, Wyatt, address, country) and a Wyatt EOS 18-angle laser photometer. The hydrodynamic radius, molecular mass moments, and concentration of the resulting peaks were analyzed by using the computer program Astra 5.3.2 (Wyatt Technology, Santa Barbera, USA).

4.3.5. Analytical Ultracentrifugation

In this project a process known as sedimentation velocity was used. This is an analytical ultracentrifugation method that measures the rate at which molecules move in response to a centrifugal force generated in a centrifuge. This sedimentation rate provides information about both the molecular mass and the shape of the molecules.

4.3.5.1. Theory

In the sedimentation velocity method a sample is spun at very high speed in an analytical ultracentrifuge. The high centrifugal force rapidly depletes all the protein from the region nearest to the centre of the rotor (the meniscus region at the air/solution interface), forming a boundary which moves toward the outside of the rotor with time, until finally all of the protein forms a pellet at the outside of the cell. The concentration distribution across the cell at various times during the experiment is measured while the sample is still spinning, using either absorbance or refractive index detection.

The rate at which the sedimentation boundary moves is a measure of the sedimentation coefficient of the protein. The sedimentation coefficient depends on the molecular weight (larger proteins sediment faster) and also on molecular shape. Unfolded proteins or one with highly elongated shapes will experience more hydrodynamic friction, and thus will have smaller sedimentation coefficients than a folded, globular protein of the same molecular weight. In order to calculate how much material is sedimenting at various sedimentation coefficients, many scans can be taken closely together in time. These can then be subtracted in pairs and some mathematical manipulation carried out to transform them into a sedimentation coefficient distribution. This distribution resembles a chromatogram, and in many ways is similar to a size-exclusion chromatogram except the peaks come in the opposite order. Like a chromatogram, the area under each peak gives the total amount of each species present [151].

4.3.5.2. Data Collection

The samples were prepared by printing the protein solution into an Eppendorf tube at a concentration of 12000 U ml^{-1}. Once all samples were printed, each sample was diluted down to a concentration of 200 U ml^{-1} using the appropriate buffer in preparation for testing. A native protein sample was also prepared at a 200 U ml^{-1} concentration to be used as a control. Sedimentation experiments were performed in an Optima XL-A analytical ultracentrifuge (Beckman Coulter, High Wycombe, UK) equipped with an absorbance optical system. For velocity analysis the protein sample (0.25 mg ml^{-1} of recombinant protein

solution in 50 mM Tris-HCl (pH 7.5), 150 mM NaCl) and buffer only (as a reference) were centrifuged in a 2-sector centrepiece, in an An-60 Ti 4-hole rotor at 45,000 rpm at 20ºC. The sedimentation boundary was monitored every 90 sec at 230 nm for a total of 150 scans. Data was interpreted with the model- based distribution of Lamm equation solutions C(s) using the software Sednterp (freeware available at http://www.jphilo.mailway.com/download.htm#SEDNTERP) [152].

4.3.6. Circular Dichroism

Circular dichroism (CD) spectroscopy measures differences in the absorption of left-handed polarized light versus right-handed polarized light which arise due to structural asymmetry. The absence of regular structure results in zero CD intensity, while an ordered structure results in a spectrum which can contain both positive and negative signals.

4.3.6.1. Theory of secondary structure determination

Secondary structure can be determined by CD spectroscopy in the "far-UV" spectral region (190 - 250 nm). At these wavelengths the chromophore is the peptide bond, and the signal arises when it is located in a regular, folded environment. Alpha-helix, beta-sheet, and random coil structures each give rise to a characteristic shape and magnitude of CD spectrum. The approximate fraction of each secondary structure type that is present in any protein can thus be determined by analyzing its far-UV CD spectrum as a sum of fractional multiples of such reference spectra for each structural type. Like all spectroscopic techniques, the CD signal reflects an average of the entire molecular population. Thus, whilst CD can determine that a protein contains about 50% alpha-helix, it cannot determine which specific residues are involved in the alpha-helical portion [153].

4.3.6.2. Data collection

The samples were prepared by printing the protein solution into an Eppendorf tube at a concentration of 12000 U ml^{-1}. Once all samples were printed, each sample was diluted down to a concentration of 200 U ml^{-1} using the appropriate buffer in preparation for testing. A native protein sample was also prepared at a 200 U ml^{-1} concentration to be used as a

control. Circular dichroism spectroscopy experiments were performed using 250 µg ml^{-1} of recombinant protein (in 50 mM Tris-HCl (pH 7.5), 150 mM NaCl). CD spectra were measured between 190 - 260 nm by a J-810 spectropolarimeter (Jasco, Great Dunnow, Essex, UK) using a 0.05 cm path length and 0.2 nm step increments, and an average of 10 scans. Deconvolution of the spectra was achieved with the help of the CDSSTR software (Jasco) [153] within dichroweb.

4.4. Surface Characterisation

4.4.1. Scanning Electron Microscopy

The scanning electron microscope (SEM) uses a focused beam of high-energy electrons to generate a variety of signals at the surface of solid specimens. The signals that derive from electron-sample interactions reveal information about the sample including surface topology (texture), chemical composition, and crystalline structure and orientation of materials making up the sample. In most applications, data are collected over a selected area of the surface of the sample, and a 2-dimensional image is generated that displays spatial variations in these properties. Areas ranging from approximately 1 cm to 5 µm in width can be imaged in a scanning mode using conventional SEM techniques (magnification ranging from 20X to approximately 30,000X, spatial resolution of 50 to 100 nm). The SEM is also capable of performing analysis of selected point locations on the sample; this approach is especially useful in quantitatively or semi-quantitatively determining chemical compositions (using EDS), crystalline structure, and crystal orientations (using EBSD).

4.4.1.1. Theory

Accelerated electrons in an SEM carry significant amounts of kinetic energy and this energy is dissipated as a variety of signals produced by electron-sample interactions when the incident electrons are decelerated in the solid sample. These signals include secondary electrons (that produce SEM images), backscattered electrons (BSE), diffracted backscattered electrons (EBSD that are used to determine crystal structures and orientations of minerals), photons (characteristic X-rays that are used for elemental analysis and

continuum X-rays), visible light (cathodoluminescence--CL), and heat. Secondary electrons and backscattered electrons are commonly used for imaging samples: secondary electrons are most valuable for showing morphology and topography on samples and backscattered electrons are most valuable for illustrating contrasts in composition in multiphase samples (i.e. for rapid phase discrimination). X-ray generation is produced by inelastic collisions of the incident electrons with electrons in discrete orbits (shells) of atoms in the sample. As the excited electrons return to lower energy states, they yield X-rays that are of a fixed wavelength (that is related to the difference in energy levels of electrons in different shells for a given element). Thus, characteristic X-rays are produced for each element in a mineral that is "excited" by the electron beam [154].

4.4.1.2. Data Collection

The electrodes to be analysed were cut into the appropriate shape and were stuck to the sample holders to prevent them from moving once in the microscope. The microscope used was a Philips 525 with an EDAX EDS X-ray analysis system and the samples were examined using a standard protocol for SEM analysis using secondary electrons. The chemical composition analysis was carried out by analysing any bright spots found on the surface using the EDAX EDS X-ray analysis system.

4.4.2. Phase Contrast Optical Microscopy

The phase contrast technique employs an optical mechanism to translate minute variations in light phase into corresponding changes in amplitude, which can be visualized as differences in image contrast. This then gives an indication of the differences in the relative heights across the sample as well as the shape and structure of the sample.

4.4.2.1. Theory

Partially coherent illumination produced by the tungsten-halogen lamp is directed through a collector lens and focused on a specialized annulus (labeled condenser annulus) positioned in the sub stage condenser front focal plane. Wave fronts passing through the annulus illuminate the specimen and either pass through undeviated or are diffracted and retarded in

phase by structures and phase gradients present in the specimen. Undeviated and diffracted light collected by the objective is segregated at the rear focal plane by a phase plate and focused at the intermediate image plane to form the final phase contrast image observed in the eyepieces.

Prior to the invention of phase contrast techniques, transmitted brightfield illumination was one of the most commonly utilized observation modes in optical microscopy, especially for fixed, stained specimens or other types of samples having high natural absorption of visible light. Collectively, specimens readily imaged with brightfield illumination are termed amplitude objects (or specimens) because the amplitude or intensity of the illuminating wavefronts is reduced when light passes through the specimen [155].

4.4.2.2. Data Collection

The samples were prepared by printing the protein solution onto the electrode surface and drying as required and as specified in the results section. The samples were analysed using a standard PCM method on the ADE Phaseshift MicroXam, (Phoenix, AZ, USA) which gave diffraction images which were then interpreted using MapVue software.

4.4.3. Contact Angle analysis

Contact angle measurement (CA) is a simple-to-adopt method for surface analysis related to surface energy and tension. Contact angle describes the shape of a liquid droplet resting on a solid surface. When drawing a tangent line from the droplet to the touch of the solid surface, the contact angle is the angle between the tangent line and the solid surface.

4.4.3.1. Theory

When a droplet of liquid rests on the surface of a solid, the shape of the droplet is determined by the balance of the interfacial liquid/ vapor/ solid forces. Contact Angle can be used to detect the presence of films, coating, or contaminants with a surface energy different from that of the underlying physical substrate. The Young-Dupre equation can be used to determine the interfacial energy.

$$\gamma(1+\cos\theta_C) = \Delta W_{SLV} \quad (36)$$

(where ΔW_{SLV} is the adhesion energy per unit area of the solid and liquid surfaces when in the medium V.)

When a droplet of high surface tension liquid is placed on a solid of low surface energy, the liquid surface tension will cause the droplet to form a spherical shape (lowest energy shape). The measurement provides information regarding the bonding energy of the solid surface and surface tension of the droplet. Because of its simplicity, Contact Angle has been broadly accepted for material surface analysis related to wetting, adhesion, and absorption.

4.4.3.2. Data Collection

A solution of protein in buffer is prepared at a concentration of 12000 U ml^{-1}, unless specified otherwise, in preparation for deposition onto the electrode surface. The printer head is used to deposit this solution with a syringe used as a make shift pressure controller and the driving electronics and laptop programme still used as described previously. The electrode sheet is then manually positioned under the printhead on a moveable platform and the platform brought to within a few millimetres of the head itself. A droplet of liquid is then dispensed consisting of a known number of drops, as defined in the results, using the printhead control electronics. A CCD camera reveals the profile of the droplet on the computer screen. Software calculates the tangent to the droplet shape and the contact angle. Data and the image are collected, analyzed, and saved on computer. Each sample was measured in triplicate to ensure that the results would be reliable. .

4.4.4. Chronoamperometry Measurements

This method involves the glucose oxidase-catalysed reaction in which 1 mol of oxygen is consumed per 1 mol of glucose oxidised, and 1 mol each of gluconic acid and hydrogen peroxide is produced. Chronoamperometry can be used to measure the consumption of oxygen via a mediator called ferricyanide.

4.4.4.1. Theory

In amperometry, a potential, with respect to a stable reference electrode (pseudo reference in this set up as explained earlier), is applied to the detection electrode, which is called the working electrode. The applied potential between these two electrodes causes an electrochemical oxidation or reduction of the measured substance at the working electrode. Modern amperometry uses a three electrode system in which the applied potential between the working and reference electrodes causes a current flow to a third electrode, the counter electrode. No amperometric current is allowed to flow to the reference electrode; thus the stability of the reference electrode can be assured [156].

In this method, a two electrode set up is used. This is because the system is a two electrode system in a non aqueous reaction i.e. the solution used is placed onto a single electrode containing both working and counter electrode, both made from carbon. When a reading is taken, the reference electrode used is set up as a pseudo reference electrode. This means that the potentiostat reference wire is plugged into the counter wire and both are connected into the counter electrode, with a separate wire in the working electrode. This set up is shown in figure 4.3.

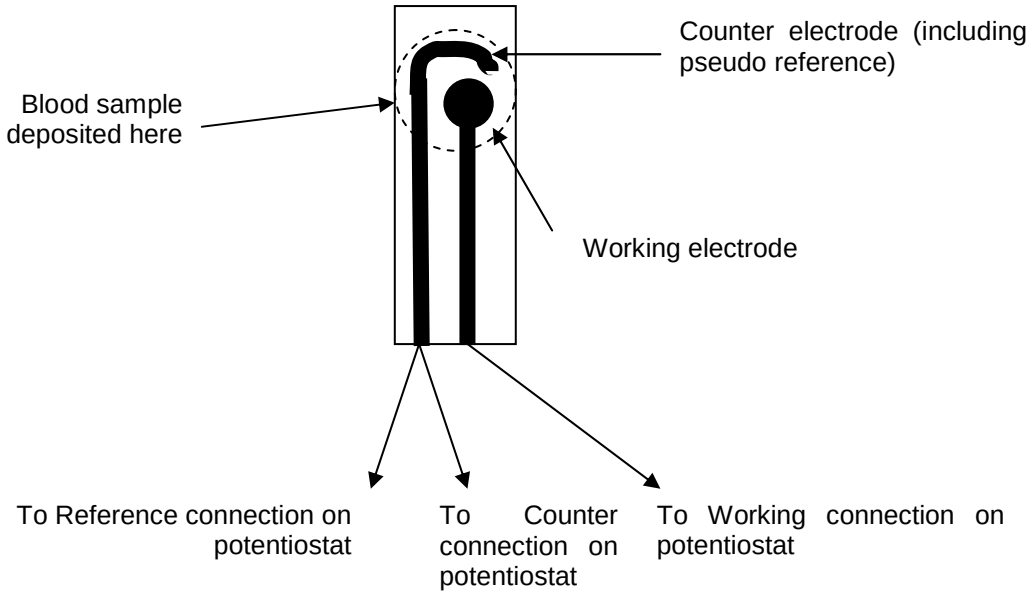

Figure 4.3. Set up of electrode system used in this study.

Pseudo reference electrodes are electrodes that are used as reference electrodes, especially in three-electrode potentiostatic measurements, but do not possess the properties of “real” reference electrodes, i.e. they are not non-polarisable, they do not possess a thermodynamically calculable potential and they do not have a potential, which is independent of the electrolyte in the cell. Nevertheless, such electrodes, normally simple metal wires of platinum or gold, can be used provided that the potential scale is calibrated with an inner standard. A somewhat worse alternative is to measure the potential of the pseudo reference electrode versus a conventional reference electrode in a separate experiment. This is reliable only when one can be sure that the potential of the pseudo reference electrode is the same in the calibration and the application experiment. Since the pseudo reference electrode is directly placed into the cell electrolyte, the impedance is usually small (no salt bridge, no liquid junction potentials etc.), which is desirable for the potentiostat to function properly [19]. The potential is applied through the working electrode, with the potentiostat measuring the current flow between the working and counter electrode with the reference electrode held at a constant potential.

4.4.4.2. Data collection

In this method a mediator is used called ferricyanide which helps in the transfer of electrons from the enzyme and therefore the current produced. The electrodes were prepared using the printing method as outlined above and then dried. These were then placed into a holder with electrical connections inside ready for testing along with a counter electrode, if there was not one already present. Chronoamperometry experiments were performed using 200 µl of glucose buffer solution (0.005 M Potassium Ferricyanide in Phosphate buffer pH 7.5 with glucose concentrations between 0 and 10 mM). Amperometry measurements were taken over a 40 s period at a potential of 0.5 V with a 10 s equilibration time with each reading taken at 40 s. Each sample was run in triplicate to minimise errors.

4.5. Statistical Analysis

Unless otherwise stated, all error bars displayed represent the standard error of the mean. Statistical analysis of results was performed where appropriate including single and double

factor Analysis of Variance (ANOVA) and linear regression. The statistical package within the Excel spreadsheet (Microsoft, Redmond, CA, USA) was used to analyse the data to the standard significance level of 5%.

Due to the number of conditions involved Analysis of Variance (ANOVA) statistics were favoured over the standard T-Test. The T-test is a valid test for comparing a pair of datasets, however as the number of compared conditions increases the chance of an individual T-Test returning a type I or type II error gets higher. Single factor ANOVA overcomes this by comparing the conditions of a series of experiments as a whole. Double factor ANOVA can identify which of two experimental variables has the greatest influence on the measured data and can indicate whether there is any interaction between these parameters. ANOVA makes the assumption that each population set of the data being confirmed has approximately equal variance. Throughout this thesis the level of significance was set at 5% for double tailed tests.

4.5.1. Theory

The variability in a set of data quantifies the scatter of the data points around the mean. To calculate a variance, first the mean is calculated, then the deviation of each point from the mean. Deviations will be both positive and negative; and the sum will be zero. This will be true regardless of the size of the dataset, or amount of variability within a dataset, and so the raw deviations are not useful as a measure of variability. If the deviations are squared before summation then this sum is a useful measure of variability, which will increase the greater the scatter of the data points around the mean. This quantity is referred to as a sum of squares (SS), and is central to the analyses. The SS however, cannot be used as a comparative measure between groups, because clearly it will be influenced by the number of data points in the group; the more data points, the greater the SS. Instead, this quantity is converted to a variance by dividing by $n-1$, where n equals the number of data points in the group. A variance is therefore a measure of variability, taking account of the dataset.

Once the mean is calculated, the second step is to calculate the variance with reference to that mean. If *n-1* deviations are calculated, it is known what the final deviation must be, for they must all add up to zero by definition. So there are only *n-1* independent pieces of information on the variability about the mean. Consequently it can be seen that it makes more sense to divide the SS by *n-1* than *n* to obtain an average squared deviation around the mean. The number of independent pieces of information contributing to a statistic is referred to as degrees of freedom.

There are three measures of variability that are important:

- SSY – Total Sum of Squares – Sum of Squares of the deviations around the grand mean. This is a measure of the total variability in the dataset.
- SSE – Error Sum of Squares – Sum of Squares of the deviations of the data around the three separate group means.
- SSF – Variable Sum of Squares – Sum of Squares of the deviations of the group means from the grand mean.

Variability is measured in terms of sums of squares rather than variances because these three quantities have the simple relationship:

$$SSY = SSF + SSE \qquad (37)$$

So the total variability has been divided into two components; that due to differences between plots given different treatments, and that due to differences between plots given the same treatment. Variability must be due to one or other of these two causes. Separating the total SS into its component SS is referred to as partitioning the sum of squares.

Every SS was calculated using a number of independent pieces of information. The first step in any analysis of variance is to calculate SSY. The second step is to calculate the three treatment means. When the deviations of two of these treatment means from the grand mean have been calculated, the third is predetermined, as again by definition, the three

deviations must sum to zero. Therefore, SSF, which measures the extent to which the group means deviate from the grand mean, has two df associated with it. Finally, SSE measures variation around the three group means. Just as the SS are additive, so are the df.

Combining the information on SS and df, it is possible to arrive at a measure of variability per df. This is equivalent to a variance, and in the context of ANOVA is called a mean square (MS). Unlike the SS, the MS is not additive. The ratio of the two mean squares is the ***F-ratio***, and is the end result of the ANOVA. Even if the experimental results are identical, it is unlikely that the F ratio would equal 1, it could by chance take a whole range of values. The F distribution represents the range and likelihood of all possible F ratios under the null hypothesis, i.e. when all experimental results are identical.

Just as with other test statistics, the traditional threshold probability of making a mistake is 0.05. In other words, it is accepted that the F ratio is significantly greater than 1 if it will be that large or larger under the null hypothesis only 5% of the time. If there was inside knowledge that the null hypothesis was in fact true, then 5% of the time there would still be an F ratio that large. When an experiment is conducted however, nothing can be predicted or known and evidence is being collected against the null hypothesis. The *p-value* is a measure of the strength of evidence against the null hypothesis. Only when it is less than 0.05 do we consider the evidence great enough to accept [157].

CHAPTER 5: RESULTS AND DISCUSSION

5.1. Analysis of Printing Parameters

The focus of this chapter is on the influence of inkjet printing parameters on droplet characteristics and establishing the conditions appropriate for printing and patterning with protein and enzyme suspensions. A Phosphate Buffered Saline (PBS) solution, a sugar solution (Q2090113D3, supplied by Applied Enzyme Technologies limited, Newport, Wales) and a GOX enzyme solution at 12000 U ml^{-1} were tested for their suitability for printing through characterising their rheological behaviour and surface tension. They were printed through a Microfab (Microfab Ltd, Plano, Texas, USA) printhead and the mass and volume of the resulting drops measured and calculated over a range of printing conditions. Arrays of drops were also printed into well plates in order to investigate the ease of printing and the ability of the protein to survive the printing process.

Inkjet printheads are designed to operate with inks within a limited range of viscosity and surface tension. This limit is in the order of 1 - 40 mPa s for viscosity and 20 – 70 mN m^{-1} for surface tension. Thus it was necessary to measure the shear viscosity and the surface tension of the different fluids used in this study.

5.1.1. Viscosity of printing solution

The viscosity of all the fluids used in this study was measured over a range of shear rates. This was achieved using a rheometer fitted with a low force transducer and Couette flow adapter (parallel plates) (Brookfield DV-III+ Rheometer with waterbath and temperature controller). The shear viscosity was measured over a range of rotation rates from from 150 to 250 revolutions per minute (rpm) at 10 rpm iterations. This gave a shear strain rate in the range 200 – 330 s^{-1}. The resulting shear viscosity data is shown in figure 5.1.

The shear viscosity values are shown to be fairly constant for each sample over the range of spindle speeds used but different between samples, as is to be expected. The relationship between the spindle speed and shear strain rate indicates that the viscosity of the samples

remains largely unchanged over the range tested. The addition of enzymes to the solution, whether a sugar stabilisation solution or a simple phosphate buffered saline (PBS) solution, increases the shear viscosity by approximately 10% of the buffer's original value. Addition of a surfactant at 0.05% is seen to reduce this shear viscosity back down to a value in line with the original buffer solution value. All of the solutions tested gave values which fall within the limits of printability and, therefore, for the purpose of this project they should enable the printing process and parameters to be defined for each solution. The error bars shown on the graph are the standard deviation over the 5 samples analysed per data point, with the data point shown being the mean of these samples. The standard deviation shown by the error bars is within the accuracy of the viscometer and therefore does not warrant any further action/ analysis.

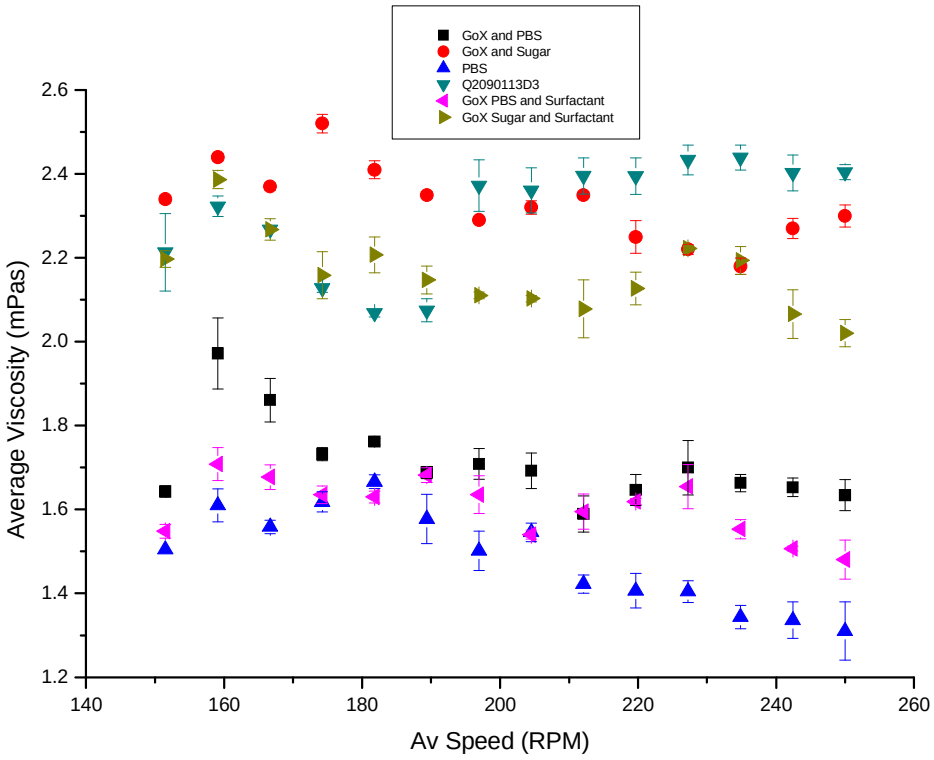

Figure 5.1. The shear viscosity of solutions measured against the speed of the parallel plates in solution.

5.1.2. Surface Tension of printing solutions

Surface Tension data, obtained using the pendant drop method, are displayed in figure 5.2. The solutions all have a surface tension close to that of water, at approximately 70 mN m^{-1}.

The addition of the enzyme has a slight effect on the surface tension with it reducing by about 10% of its initial value. Upon the addition of a surfactant, there is a noticeable drop in the surface tension of the solutions to around 28 mN m^{-1}. All of the surface tensions measured are within the range that are believed to be suitable for use with the Microfab printer, however the addition of a surfactant and the associated drop in surface tension allows the ink to be used with inkjet equipment from other manufacturers, where the ink criteria for printability are more restricted. Again, these results were an average of 5 samples per data point.

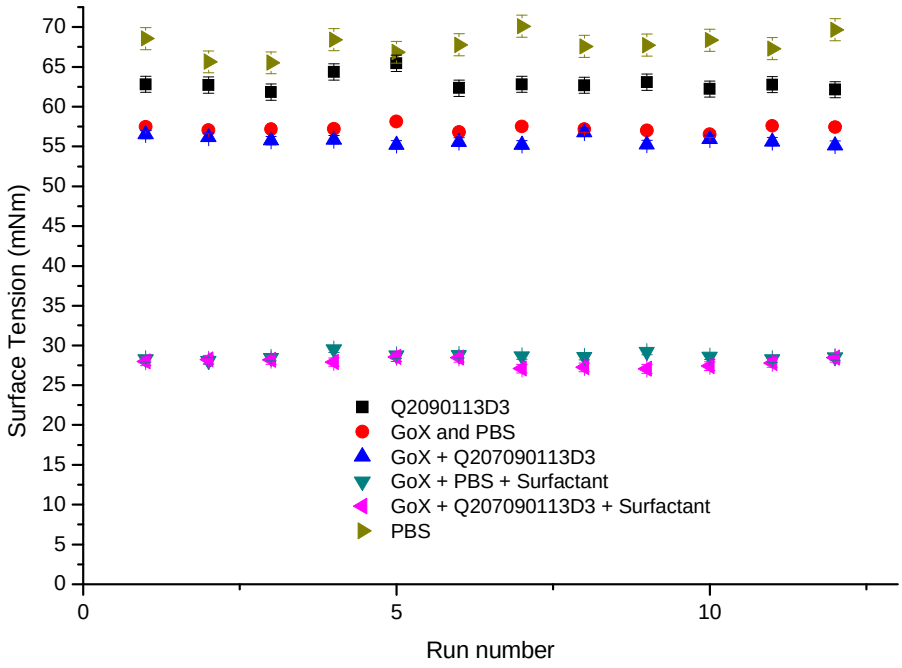

Figure 5.2. Surface tension of the solutions analysed using the pendant drop method.

5.1.3. The influence of waveform amplitude on drop volume and mass

In order to investigate the influence of the printing parameters on drop volume and weight, a series of experiments were undertaken using a simple PBS solution containing GOX enzyme at a 12000 U ml^{-1} concentration. These experiments were completed using an isolated inkjet printhead as described in section 4.2. Experiments were carried out using a waveform frequency of 5 kHz, a rise time of 3us, pulse duration of 25 µs, a fall time of 3 µs and the amplitude of the pulse being 40V, 60V and 80V as previous work has shown that these are suitable for printing biological molecules [158].

The measurements were taken using a set of weighing scales placed underneath the printhead. The printer was then set to print a defined number of drops and the mass recorded. The mass per drop could then be calculated and is plotted in figure 5.3. The volume was calculated using the same method given in section 4.4.3 with each drop measured giving a sessile volume figure. Because of the complexities of the procedure it was only possible to do this over three samples for each voltage and the figures shown in the graph are the averages of these figures and were not measured on the same drops that were measured to give the weight. Figure 5.3 shows the volume and weight printed per drop, at each pulse amplitude.

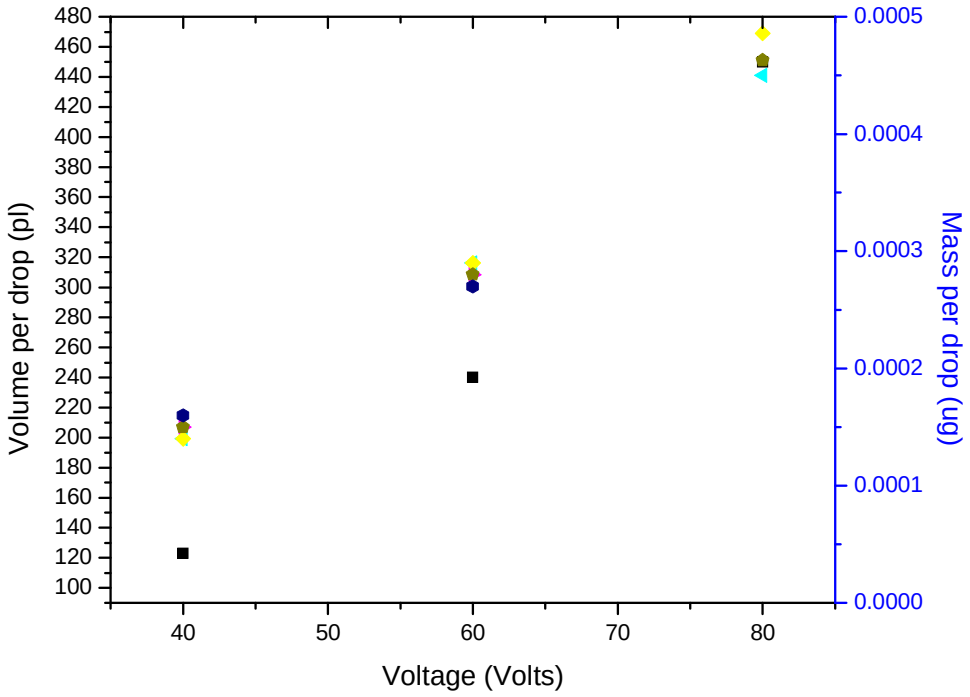

Figure 5.3. Weight per drop and volume per drop given at three different printing voltages.

It is found that the volume and weight of each drop increases as the voltage of the printhead increases, which is expected due to the mode of action of the printhead. As the driving voltage is increased, the pressure applied on the capillary tubing is increased via the piezoelectric actuator which produces a larger drop. This information will be used to calibrate the printer later in the project when there is a requirement to deposit a known volume of fluid.

The methods used herein to measure the size of the drops, namely the printed weight and photography, are limited in their accuracy to determine the size. The method of photographing the drops in order to determine size relies on a repeatable set up for each drop and an accurate reference to measure the drop against. By weighing the total mass of a known number of drops, it is possible to calculate the weight of individual drops. However, this method relies on the printer producing a stream of identical drops, with no satellite drops present, and relies on the setting of the frequency of drops of the printhead being a true reflection of the number of drops deposited.

Neither of these methods are perfect for these measurements, however, use of the mass of a stream of drops is more reliable and will show lower degrees of error as it is carried out over a large number of drops, rather than a single drop. Therefore, even if there are satellite drops in the stream, the individual masses of the drops will be proportionally lower in error than the overall mass of the total drops. It is also much easier to carry out this method over a larger sample size than the visual measurement, therefore giving a lower degree of error and more opportunities to confirm the results against other samples.

5.1.4. Retained activity of the enzyme after printing

It was reported earlier that previous work had found there to be a reduction in the retained activity of the enzyme after printing through a drop on demand inkjet printhead [145] [146]. This project aims to explore methods to negate this drop in retained activity. However, because this prior work used different printing equipment, it is important to confirm whether there is a drop in the retained activity of the protein after printing with our equipment. In order to do this, a known volume of enzyme was printed into a number of wells of a 96 well plate at peak actuation voltages of 40, 60 and 80 V with peak rise times of 3, 4.5 and 6 µs. These samples were then analysed using the Amplex Red method described in section 4.3.3 in a standard Phosphate Buffered Saline solution, the results are presented in Figure 5.4.

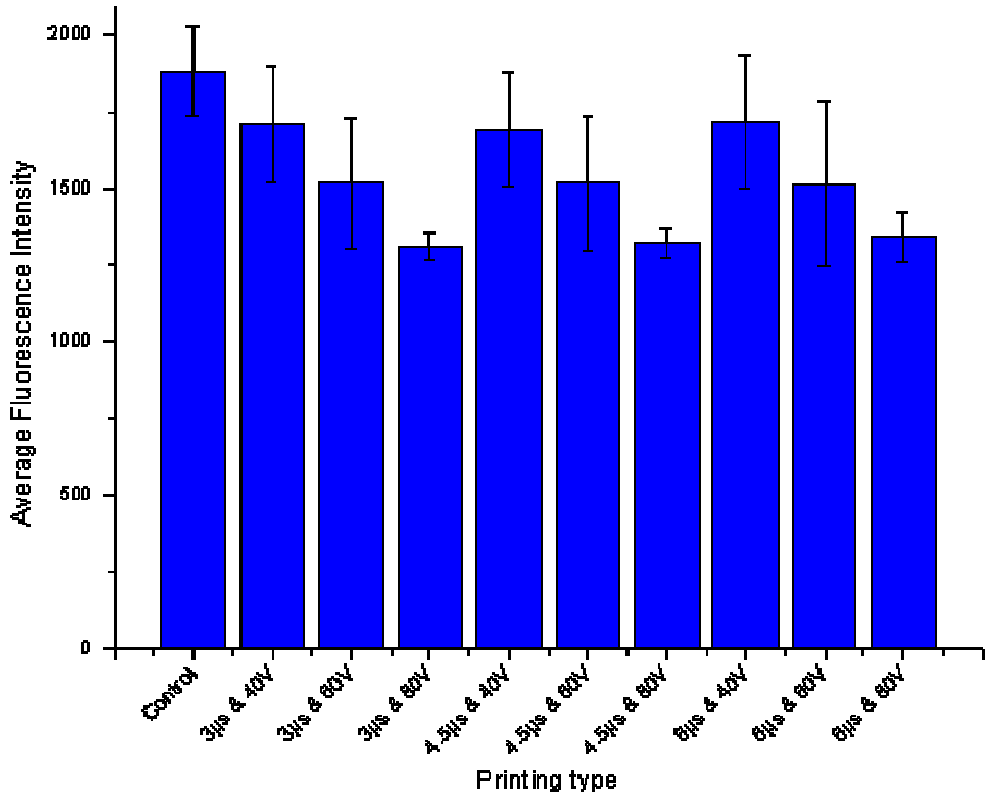

Figure 5.4. Retained activity of the enzyme after printing at different printer settings in comparison to a control unprinted sample.

The retained activity of the protein is seen to decrease in comparison to the control, which was not printed but pipetted. The relative drop in retained activity of the enzyme is seen to be fairly consistent at each voltage and the rise time of the printer does not appear to have any obvious effect on it. This data was analysed for statistical significance using two way analysis of variance (ANOVA) with replication (Table 5.1) over the 5 samples read per measurement point. It can be seen that the difference in behaviour with changing voltage cannot be distinguished from the null (P=0.97), whilst the variation in the rise time data has a P value <<0.05. Thus, it can be concluded that the retained activity of the protein is affected by the actuation voltage but the rise time has no significant effect. It is unclear whether this is due to an alteration of structure or conformation of the protein or purely a drop in concentration of the protein present. In order to confirm whether or not there should be allowances made for the loss of activity in the enzyme when printed, the structure and conformation of the enzyme will be analysed using a variety of methods.

This agrees with previous work carried out on the effect of printing on programmed cell death [158]. The retained activity drop becomes more marked as the actuation voltage increases. This agrees with the general postulation that the higher the driving voltage that is used, the higher the shear strain on the liquid and therefore the more opportunity there is for the denaturation of the proteins.

Table 5.1. Two way analysis of variance with replication test to analyse the effect of voltage and rise time on the fluorescence activity of the protein GOX.

ANOVA

Source of Variation	*SS*	*df*	*MS*	*F*	*P-value*	*F crit*
Voltage	1681.733	2	840.8667	0.025825	0.974523	3.25945
Rise Time	1093289	2	546644.6	16.78887	7.06E-06	3.25945
Interaction	2395.467	4	598.8667	0.018393	0.999305	2.63353

5.2. Printing Associated Protein Damage

As previously mentioned, the printing process may be the main factor behind the drop in the activity of the enzyme after printing, when analysed using a fluorescence assay. This could be due to either a change in the conformation of the protein's tertiary structure or a change in the tertiary structure itself, either through the destruction of one or several peptide chains, or the cleaving of some active site molecules. Either of these processes has the potential to affect the structure of the active site of the protein, which would mean that the analyte is no longer able to fit into the active site and be cleaved to give the reactions necessary at the electrode surface.

Several analytical tools were used to detect whether the drop in activity was related to an alteration to the structure or conformation of the protein. These techniques compared the structure and conformation of the natural GOX protein in its as-received state with the same enzyme after printing. These methods were:

- Light scattering, which gives an idea of the molecular weight of the protein and its general structure.
- Analytical ultra-centrifugation, which gives a more in depth idea of structure;
- Circular dichroism, which presents data to give an indication of the conformation of the protein including the percentage of the protein made up of alpha helices, beta pleated sheets and amorphous structures.

5.2.1. Effect of printing on protein structure

There are two different variants of the light scattering method which can be used in analysis of proteins. The method described here is classical light scattering that measures the amount of light scattered by a solution at some angle relative to the incident laser beam. For the proteins used in these experiments, the intensity of scattered light is uniform and therefore the scattering only needs to be measured at one angle to the incident beam (usually 90º). Since the signal from the light scattering detector is directly proportional to the molecular mass of the protein times the concentration (mg ml^{-1}), combining this signal with

that from a concentration detector makes it possible to measure the molecular mass associated with each peak. This will in turn allow for the examination of the relative size of each molecule and therefore whether they have been denatured by a mechanism (e.g. chain scission or cleavage) that reduces protein mass during the different processes. This will then allow for the assessment of the mode of denaturation using other characterization methods. Samples were printed at a concentration of 12000 U ml^{-1} and analysed at a concentration of 200 U ml^{-1}.

The light scattering data can be analysed to give results in a number of different ways, each of which provides information about different physical properties of the protein. From these results it is possible to determine the hydrodynamic radius of the protein (the radius calculated from the diffusional properties of the particle and is indicative of the apparent size of the dynamic hydrated/ solvated particle), the molar mass of the protein, and the relative structure of the enzyme and the concentration present. Figure 5.5 shows the refractive index chromatogram of the GOX enzyme. This is related to the actual amount of protein present within the sample where the peak sizes are relative to each other.

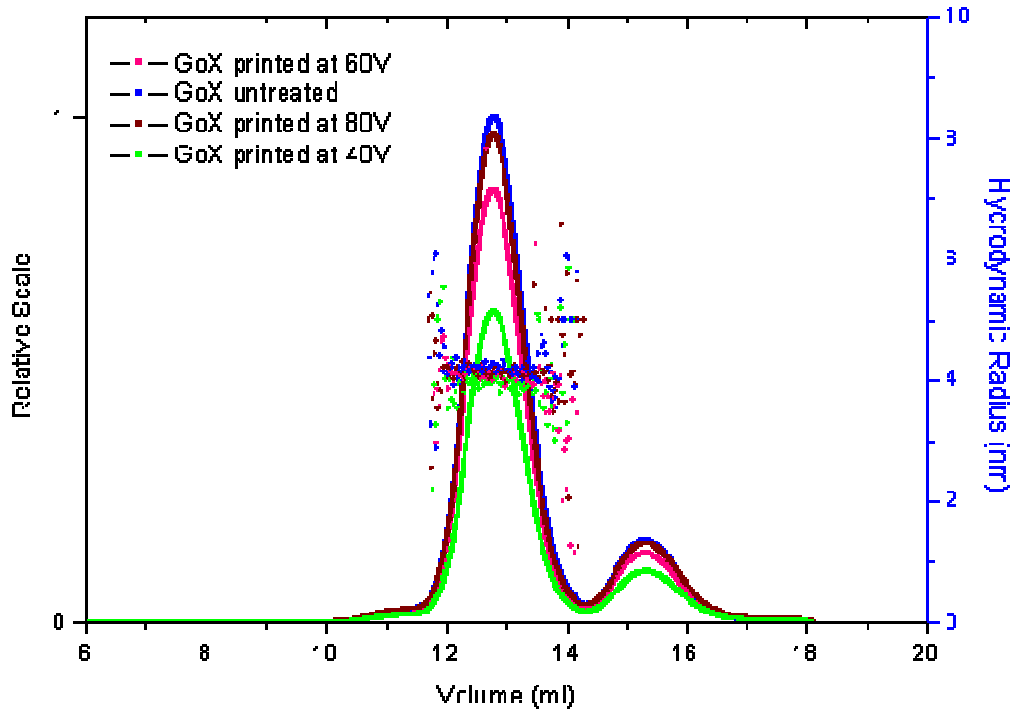

Figure 5.5. Light Scattering refractive index of GOX printed at different voltages. Also showing the hydrodynamic radius of the different samples.

Figure 5.5 shows results from a number of different samples that have been printed at different voltages through the printer. There is also an un-printed sample present which can be used as a control; this is represented by the blue line in the figure. This un-printed sample consists of one main peak, the dimeric form of the enzyme, and is accompanied by a small second peak which is a small substance of molecular weight around 5000 Daltons. This may be an unrelated impurity present in the enzyme or test solution; however this is not thought to have any bearing on the actual results for the GOX enzyme. The main peak of the enzyme has a molecular weight of around 147 kDa with approximately 76 µg of enzyme detected out of a sample of 100 µg, or 76%. This was hypothesised to be due to small losses within the test equipment or the enzyme coming out of solution during the test procedure. For the purposes of this project this is not important as it is the relative percentages of enzyme remaining in solution after printing in comparison to the un-printed sample that will define whether changes need to be made to the printing process.

The refractive index analysis shown in figure 5.5 gives a good indication of any structural changes taking place within the protein during or after printing, because it allows for the analysis of the molar mass, hydrodynamic radius and relative concentrations of enzyme to be measured. The relative molar mass is shown by the relative peak positions on the x-axis, as defined by the volume at which the particles were eluted on the size exclusion chromatography column with the large particles on the far left position and the smaller ones to the right. As can be seen from the graph, there is no identifiable difference in the x-axis position of the peaks of the samples printed at different voltages. Therefore, we conclude that there is no measurable change in the molar mass of the enzyme after printing.

Figure 5.5 also gives some indication of the relative concentration of enzyme present in the sample by the relative height of the peaks on the y-axis. Within the peaks there is a large difference in height with 40 V being the smallest peak rising up to 80 V which is close to the un-printed sample. The actual amounts present in each sample determined from the peak intensity are shown in Table 5.2.

Table 5.2. Concentration of GOX detected at different printing voltages

Printing Voltage (V)	Concentration of GOX detected in a 100ug sample (ug)
40	38
60	54
80	60

Therefore, it can be concluded that there is a loss of some concentration of enzyme through the printing process. A further experiment was carried out to assess whether the protein concentration was affected during printing by measuring optical absorption in the Ultra Violet spectrum at 280nm. Using this software and the enzymes code from PubMed, the predicted absorption of enzyme per mg ml^{-1} at 280 nm is approximately 1.4 in a water solution. The solution on test was a 12000 U ml^{-1} (which equates to 30 mg ml^{-1}) solution and, therefore, the absorption should be around 42 for each sample unless some was lost during the printing process. The actual results were found to be as follows:

Table 5.3. Absorption of GOX detected at different printing voltages

Printing Voltage (V)	Absorption of GOX detected in a 30mgml^{-1} sample
Unprinted	41
40	17.5
60	20.37
80	25.23

These values tally with the values taken from the Light Scattering method to give an approximate percentage of the enzyme remaining in solution after printing of approximately 62% at 80 V, 49% at 60 V and 44% at 40 V. These figures will need to be taken into account in future work where the level of protein being printed becomes important.

Figure 5.5 also shows the measurement of the hydrodynamic radius of the protein after printing at different voltages in comparison with its unprinted value. Upon closer inspection of these results it can be seen that the hydrodynamic radius of the untreated sample (4.3 nm) is greater than that of the printed samples (2.7 nm), except for that of the 40 V printed sample

which appears to remain relatively intact. This is better shown in figure 5.6. It is hypothesised that this is due to one of two issues; either the shear strain within the printhead causes a deformation in the ionic structure of the protein, or the light scattering method and the associated size exclusion chromatography process has too high a margin of error to be able to measure such small hydrodynamic radii as are present within the GOX protein. Thus another test method was used to distinguish between the hydrodynamic radiuses for each sample and to confirm whether there is this change in the radius due to the printing process. This method is discussed later.

The final protein property that defines the protein structure and may be affected by the printing process is the molecular weight of the protein. It has already been stated that the GOX protein has a molecular weight of around 147 kDa, which consists of a Dimer molecule made up of two monomer units of approximately 70 kDa each. With the printing process hypothesised to have a detrimental effect on the protein's hydrodynamic radius, there is a possibility that this may have also caused a drop in the molar mass. Figure 5.7 shows the molar mass of each sample at the three printing voltages and an unprinted control measurement.

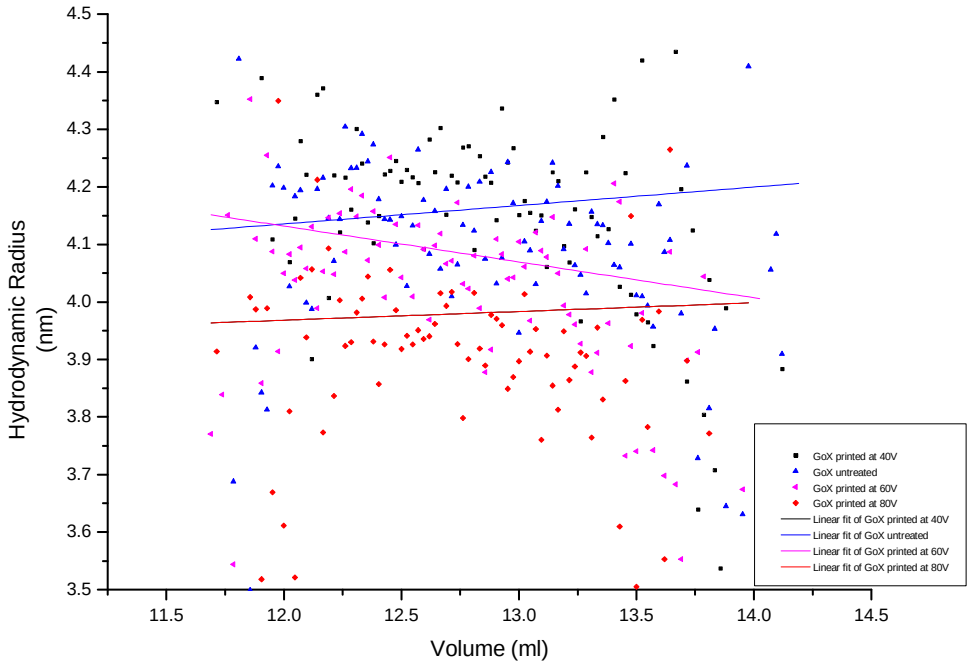

Figure 5.6. Graph showing hydrodynamic radius across the different printed samples.

Although there is a small difference between the values for the untreated glucose and the printed values, there is no significant change ($p < 0.05$) in the molar mass due to printing. What is detected is due to the instrumentations error range across the samples. The actual measured molar mass of each sample is as follows:

Table 5.4. Molar Mass of GOX detected at different printing voltages

Printing Voltage (V)	Molar Mass of GOX detected (kDa)
Unprinted	147kDa ± 4.5kDa
40	144kDa ± 4.5kDa
60	147kDa ± 4.5kDa
80	1 43kDa ± 4.5kDa

This clearly demonstrates that the molar mass differences between the samples is due to the standard error of the machine and all four samples retain the dimer form of the protein whether printed or not due to the standard error being of the order of the separation of the means.

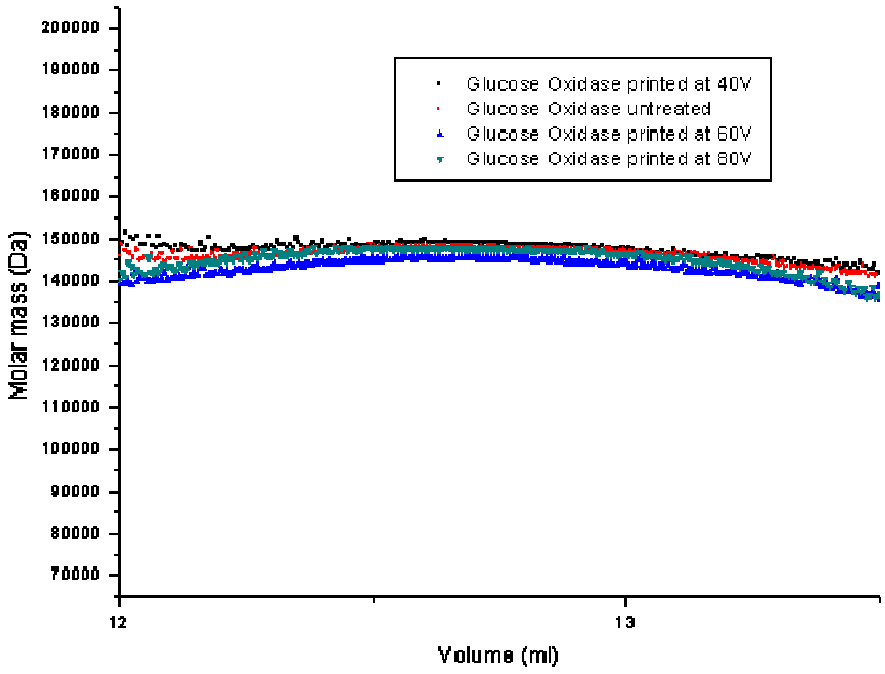

Figure 5.7. Molar mass plots of GOX after printing at different voltages.

It is clear from the work carried out that the only protein characteristic that appears to be affected by printing is the hydrodynamic radius. In order to quantify the degree of damage as well as to confirm whether these results were erroneous and whether the protein damage through the Microfab printer is unique or visible in other printers, another measurement of hydrodynamic radius was taken using the light scattering method after printing the GOX enzyme through a Dimatix DMP 2800 materials printer (Fujifilm Inc, Santa Rosa, California, USA). This printer was set up to mimic the properties of the Microfab printer with a waveform as shown in figure 5.8.

The waveform shown was used to print the samples through the Dimatix DMP 2800 materials printer with an amplitude of 23 V, a slew rate of 0.65 and a frequency of 2 kHz. The sample was in a Phosphate Buffered Saline solution at a concentration of 12000 U ml^{-1} and was printed into an Eppendorf tube in preparation for measurement using the light scattering technique. After printing, the solution was diluted down to a 200 U ml^{-1} solution for testing.

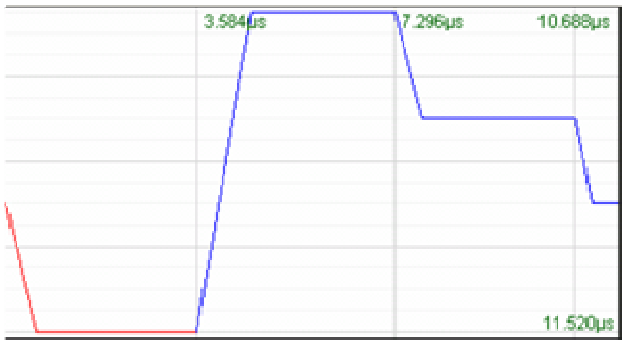

Figure 5.8. Dimatix DMP 2800 waveform

The solutions were analysed in the same way as for the hydrodynamic radius of the Microfab printed samples to produce a graph showing the hydrodynamic radius with a linear fit line. The results in figure 5.9 show that the hydrodynamic radius has been reduced to a greater extent after printing through the Dimatix than occurred after printing through the Microfab printhead, suggesting that the shear strain of the printheads does have significant influence over the hydrodynamic radius of the protein. The linear fit line shows that there is a defined and statistically relevant difference between the two radii and therefore suggests that the printing process is affecting the proteins radius. This is defined by the x-axis which shows

the elution volume of the solution on test. One further test was carried out using a more sensitive piece of equipment to ensure that these results are reliable and representative.

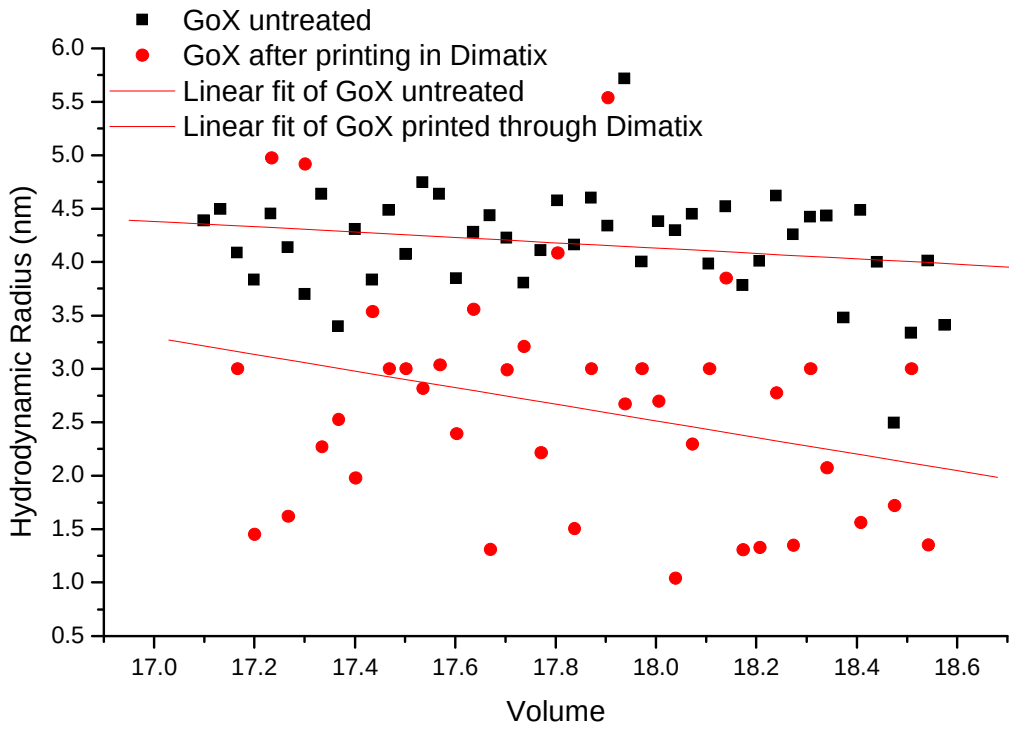

Figure 5.9. Linear regression analysis of the hydrodynamic radius of GOX after printing through the Dimatix DMP printer

5.2.2. Analytical Ultracentrifugation analysis of the protein structure

In an analytical ultracentrifuge, a sample being spun can be monitored in real time through an optical detection system, using ultraviolet light absorption and/or an interference optical refractive index sensitive system. This allows for the observation of the evolution of the sample concentration versus the axis of rotation profile as a result of the radial centripetal force. Sedimentation velocity experiments aim to interpret the entire time course of sedimentation, and report on the shape and molar mass of the dissolved macromolecules, as well as their size distribution. The size resolution of this method scales approximately with the square of the particle radii, and by adjusting the rotor speed of the experiment, size-ranges from 100 Da to 10 GDa can be investigated [159]. This means that as well as giving an indication of molar mass and hydrodynamic radius, this method will also give an indication of the protein's approximate shape in relation to a sphere.

The analytical ultracentrifugation method (AUC) was used to test the GOX enzyme structure after printing to confirm whether or not the drop in hydrodynamic radius is due to the printing process. Figure 5.10 shows the AUC results for the GOX enzyme with the sample printed at 60 V through the Microfab printing head.

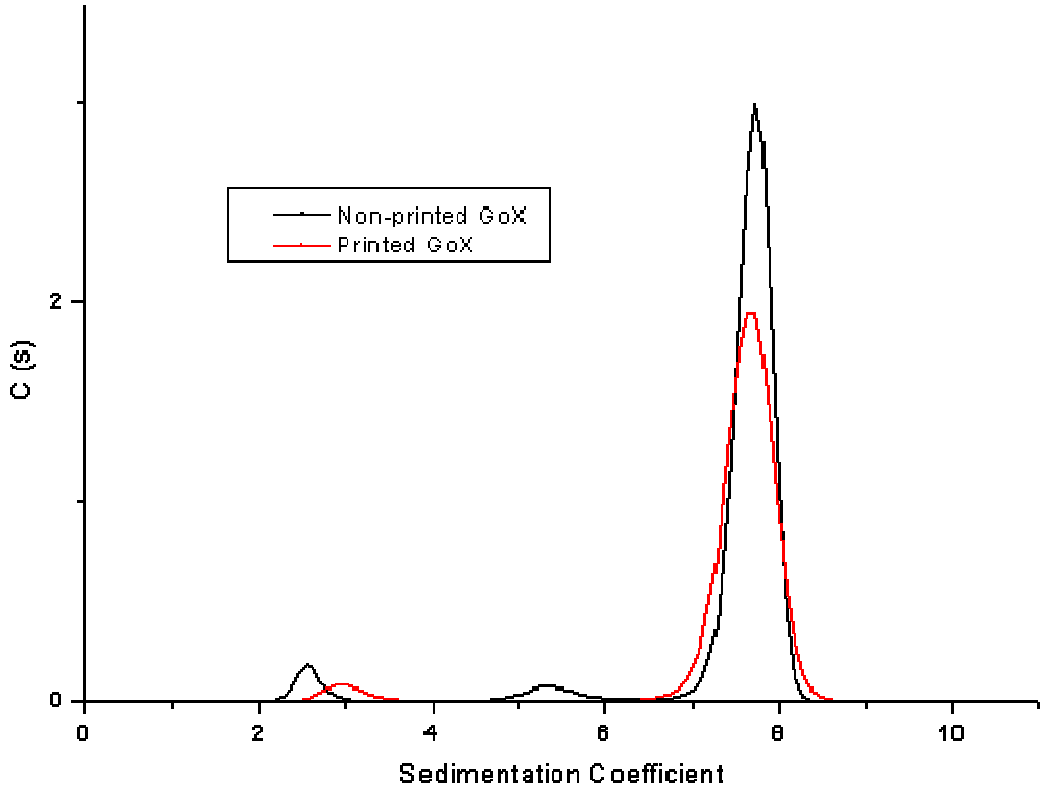

Figure 5.10. AUC graph of GOX before and after printing through the Microfab head.

The application of a centripetal force causes the depletion of macromolecules at the meniscus and the formation of a concentration boundary that moves towards the bottom of the centrifuge cell as a function of time. The definition of the sedimentation coefficient of a macromolecule, *s,* and the molecular parameters that determine the *s*-value are given by the well known Svedberg equation:

$$s = \frac{u}{\omega^2 r} = \frac{M(1-\overline{\upsilon}\rho)}{N_A f} = \frac{MD(1-\overline{\upsilon}\rho)}{RT} \qquad (38)$$

where *u* is the observed radial velocity of the macromolecule, ω is the angular velocity of the rotor, *r* is the radial position, $\omega^2 r$ is the centripetal field, *M* is the molar mass, $\bar{\upsilon}$ is the partial specific volume, ρ is the density of the solvent, N_A is Avogadro's number, *f* is the frictional coefficient, *D* is the diffusion coefficient, and *R* is the gas constant. The relationship $D=RT/N_A f$ was used to obtain the right hand side of the Svedberg equation. The *s*-values are commonly reported in Svedberg (S) units, which correspond to 10^{-13} sec.

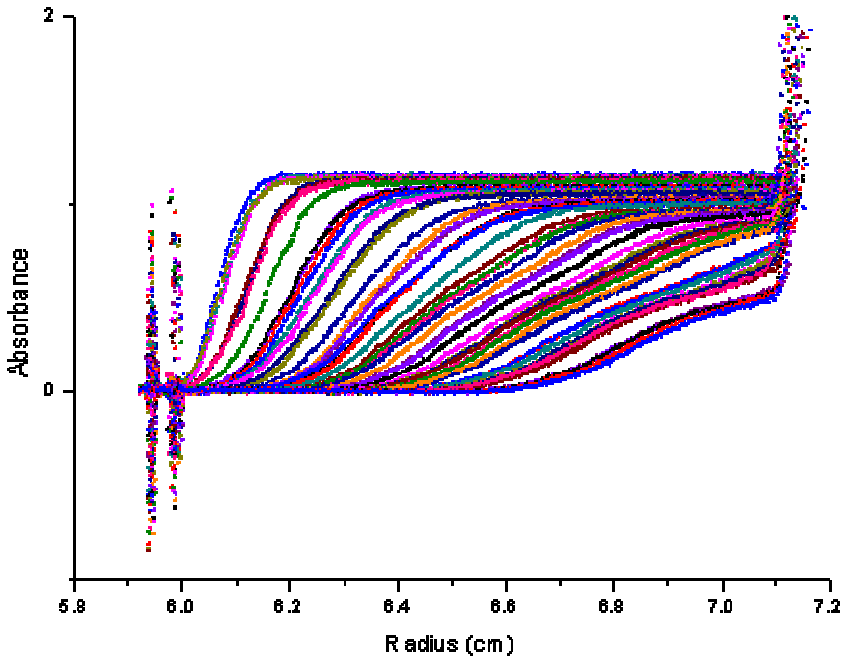

Figure 5.11. AUC raw results of the GOX enzyme before printing.

The sedimentation coefficient as displayed in figure 5.10 is obtained from the time derivative of the raw results shown in figure 5.11. One of these graphs is generated for each sample tested. These results show the radius from the liquid meniscus to the cell bottom against the absorbance, with each different plot showing a different time point; in this case they were read every 90 seconds. The following equation was used to calculate the sedimentation coefficient from the mid point of each curve shown in figure 5.11 to generate the graph in figure 5.10.

$$s^* = \frac{1}{\omega^2 t} \ln\left(\frac{r}{r_m}\right) \quad (39)$$

From the resulting calculation and graph it is possible to analyse the structure of the protein using a program called Sednterp. This program enables the calculation of molar mass and radius, as well as the calculation of the *f* value, which is the relative frictional coefficient of the protein compared to a sphere. Using this program it can be shown that the molar mass, the shape and, most importantly, the hydrodynamic radius of the protein remain unchanged after printing. The reason for the discrepancy between this measurement system and the light scattering system is probably due to the additional analysis required when using the light scattering system to determine the molecular weight of any UV absorbing peaks and hence multimeric protein states. The relative heights of the peaks on the y-axis of figure 5.10 is again due to the concentration of protein within the sample being reduced through the printing process, an effect which has already been explored and understood.

In order to clarify the accuracy of this test method with regards to the measurement of the hydrodynamic radius and molar mass, two other proteins were tested to confirm that there is no change experienced in hydrodynamic radius through the printing process. The proteins chosen were both enzymes to enable comparison between these and GOX. They were: Glucose Dehydrogenase (GDH) as it offered a potential alternative to the GOX enzyme for this project and Glutamate Dehydrogenase (GluDH) as it is known to be a less resilient enzyme and would therefore provide a more sensitive test for protein damage after printing. Results from both of these enzymes are shown in figure 5.12 after analysis using the AUC method and refining of the results to give the sedimentation coefficients.

It is obvious from the graphs in figure 5.12 that there is no measurable change in Sedimentation Coefficients for the proteins under test and therefore no influence of the printing process on the proteins. This is also shown when the hydrodynamic radius is calculated, with both of the enzymes maintaining the same radius within the standard errors of the equipment between the samples. Thus inkjet printing does not change the proteins

structure when printing at 60V through the Microfab system. This reinforces the results obtained for the GOX enzyme through the AUC testing and contradicts the results found through the light scattering test method.

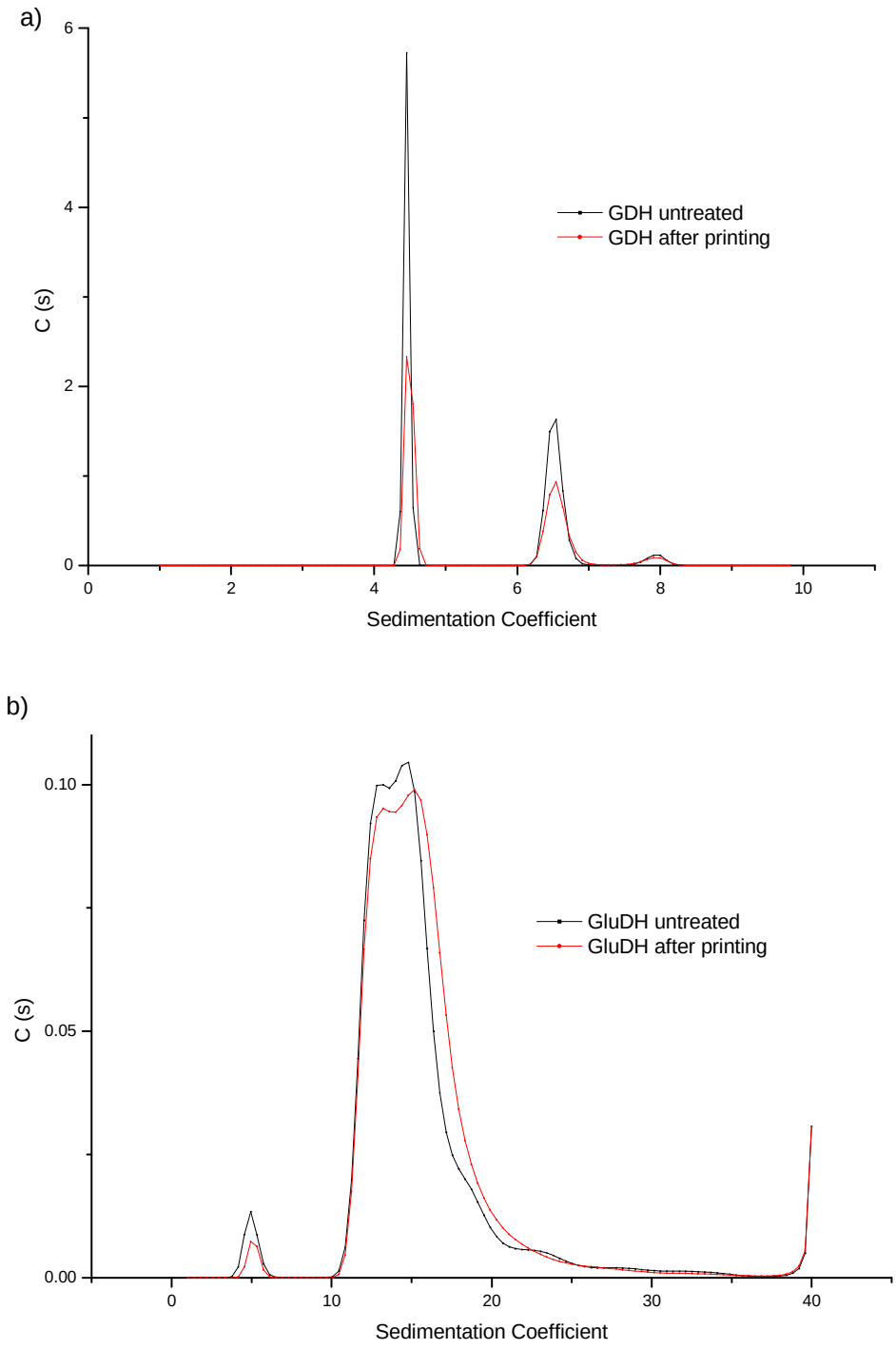

Figure 5.12. AUC analysis of a) Glucose Dehydrogenase and b) Glutamate Dehydrogenase.

GluDH appears to sediment at a much higher sedimentation coefficient than the other two enzymes and appears to have a much higher retained concentration (C (s) value). The higher sedimentation coefficient means that the enzyme is larger (approximately 220 kDa compared to 150 kDa) than the GOX or GDH and it may be this that is causing more of the enzyme to be printed in the same volume of liquid when using the same 60 μm diameter head compared to the other enzymes tested. It is difficult to be accurate with the conclusions about the form the enzyme takes from the results shown, due to the peaks not being clear and there being several forms present. Each peak on the graph shows a form of the enzyme, whether a monomer, dimer etc. Under the constraints of this project it is not necessary to understand either this or as to why there is a greater concentration of the GluDH protein being retained than the GOX protein as it is only necessary to ensure that there is no damage occurring so that the proteins may be used for the production of electrochemical sensors by inkjet printing.

5.2.3. Analysis of protein conformation after printing

With the knowledge that the structure of the protein is not affected adversely by the printing process, it is necessary to ensure that there is no alteration of the conformation of the protein. Any change in conformation could affect the mode of action of the enzyme through an alteration in the active site shape, which would prevent the analyte from accessing the active site as easily and therefore decrease the enzyme's rate of cleavage. It has already been shown that the shape of the enzyme remains the same through the AUC testing carried out earlier. Thus, it is expected that the enzyme's conformation will remain unchanged after printing.

The samples were analysed using Circular Dichroism (CD), a technique that measures the differences in the absorption of left-handed polarized light versus right handed polarized light, which arise due to structural asymmetry. In the case of this project, the technique is used to analyse the secondary structure of the protein to ensure that there is no alteration in this conformation and therefore the way in which the protein is arranged after printing. This secondary structure can be determined by CD spectroscopy in the 'far-UV' spectral region

(190 – 250 nm). At these wavelengths the chromophore is the peptide bond, and the signal arises when it is located in a regular, folded environment. Alpha-helix, beta-sheet, and random coil structures each give rise to a characteristic shape and magnitude of the CD spectrum. The approximate fraction of each secondary structure type that is present in any protein can thus be determined by analyzing its far-UV CD spectrum as a sum of fractional multiples of such reference spectra for each structural type. Like all spectroscopic techniques, the CD signal reflects an average of the entire molecular population. Thus, while CD can determine that a protein contains a certain proportion of alpha-helix, it cannot determine which specific residues are involved in the alpha-helical portion [151].

The enzyme was tested in a standard Phosphate Buffered Saline solution (PBS) at a concentration of 200 U ml^{-1} after printing and as an unprinted sample. The enzyme used was GOX and this was printed at a concentration of 12000 U ml^{-1} and then diluted using PBS to the appropriate test concentration of 200 U ml^{-1}. Printing was carried out using the same settings as for the light scattering experiments, with the actuating printing voltage varied between 40 V and 80 V at 20 V intervals. Figure 5.13 shows the CD traces for the printed samples compared with the unprinted control sample.

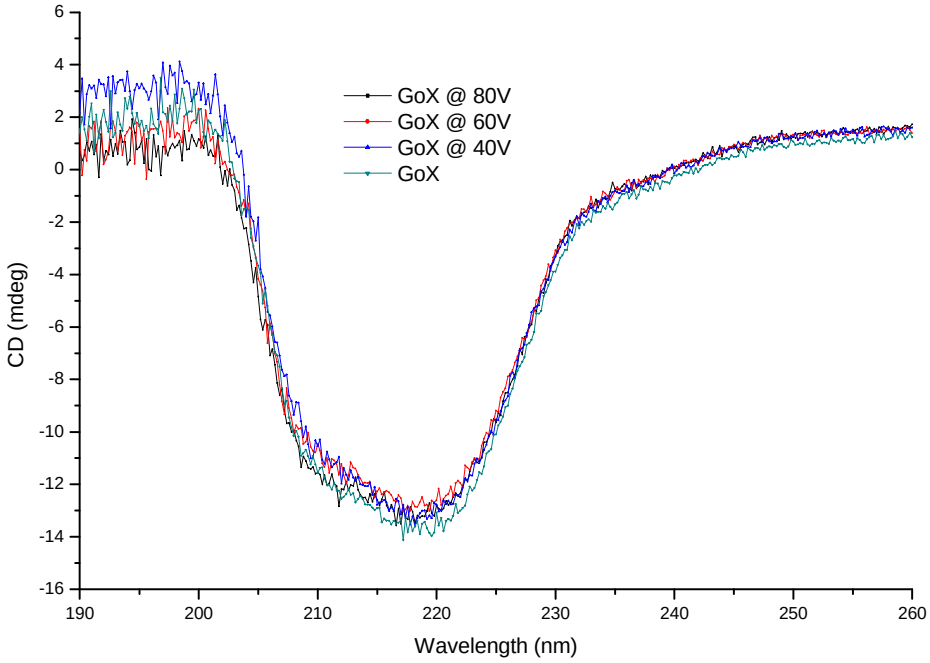

Figure 5.13. Circular Dichroism traces of the GOX enzyme printed at different voltages and without printing.

The CD results produce a picture of the structure of the protein in both its natural state and after printing, thus allowing for comparison. It can be seen from the CD graph shown in figure 5.13 that there is no discernable difference between the traces of the natural GOX and the GOX after printing. After checking, these results are within the standard error of the equipment, therefore it is believed that there is no change in the conformation or the constituent structure of the protein. Further analysis of the structures shown in figure 5.13 using software supplied with the test equipment gives a breakdown of the different secondary structures present within the samples on test. These are displayed in table 5.3 below. Previous studies of the thermal deactivation of GOX have found significant changes in the circular dichroism in the region 200 – 230 nm, that is associated with the unfolding of the protein and disruption of the α-helix structural units at temperatures above 60º C [160]. The absence of any changes in this region of the spectrum after printing indicates that the GOX remains in its folded state and is unaffected by the shears associated with inkjet printing.

Table 5.5. Analysis of percentage of different secondary structure types in GOX.

Helix1	Helix2	Strand1	Strand2	Turns	Unordered	Total
0.00	*0.03*	*0.23*	*0.13*	*0.22*	*0.36*	*0.97*

This analysis is broken down into constituent parts where helix 1 and helix 2 represent the percentage of alpha helix present in the structure, strand 1 and strand 2 represent the percentage of beta pleated sheet present in the structure, turns represents the percentage of random coils present and unordered represents the percentage of amorphous structure present. Therefore, the GOX enzyme is seen to contain approximately 3% alpha helix, 36% beta pleated sheet, 22% random coils and 36% amorphous structure. The figures given here were found to be unchanged between the samples, reinforcing the claim that the enzyme remains in the same structure and conformation as before it is printed, thus implying that the printing process does not damage the protein structure. In order to confirm that the circular dichroism test method is reliable and accurate, a second protein was tested after printing. The protein used was the Glucose Dehydrogenase as used during the AUC testing and was again printed at 60V with the results shown in figure 5.14.

The CD analysis of the GDH sample conclusively shows that there is no change in the conformation of the protein between the two samples and therefore reinforces the findings for the GOX enzyme that piezoelectric drop on demand inkjet printing is not a destructive process to the proteins at any driving voltage tested. The results also show a different secondary structure conformation to the GDH compared to that of the GOX. According to the CD results, it appears that the GDH has more alpha helix domains present than the GOX enzyme but has lower relative percentages of beta pleated sheet. Therefore, this also demonstrates that there does not appear to be any dependency upon the original conformation of the protein prior to printing as to how the protein responds to being printed.

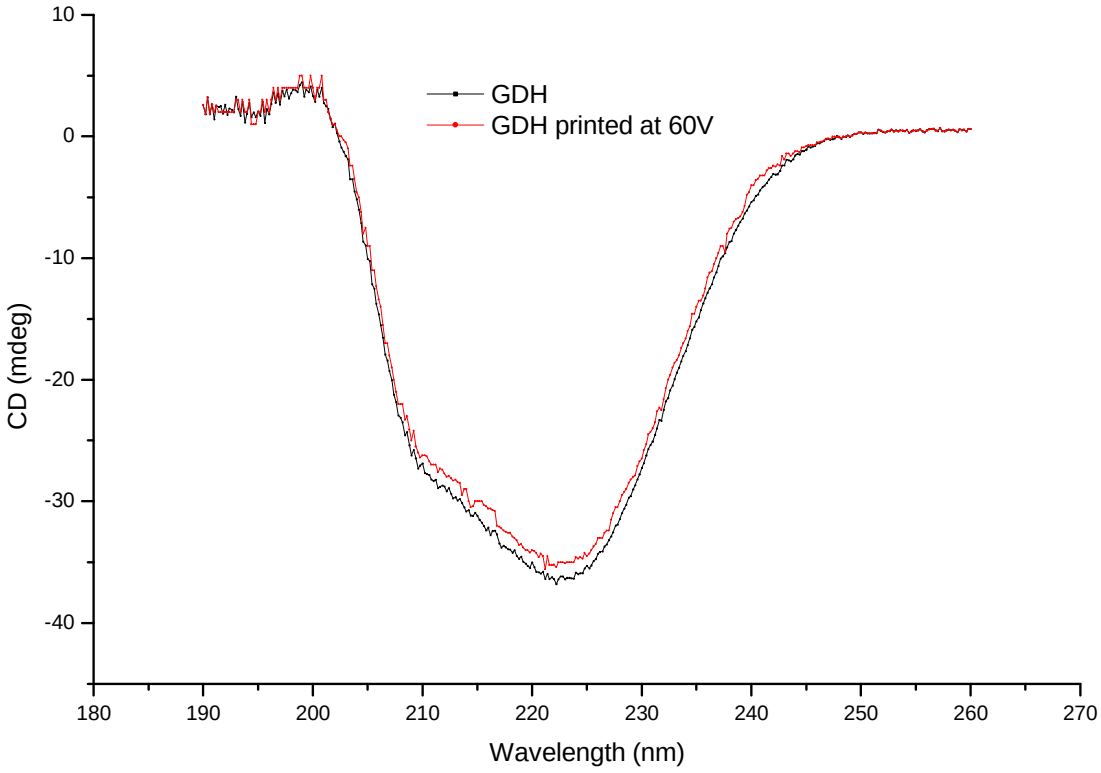

Figure 5.14. CD analysis of the Glucose Dehydrogenase (GDH) enzyme before and after printing.

5.3. Electrode Characteristics

Having established an understanding of the proteins' response to the printing process, as well as some understanding of the proteins' natural form, the remainder of the project focuses on the characteristics, both physical and chemical, of the electrodes and their surface. The electrodes are supplied by AET Ltd. (Newport, Wales, UK) and are the same electrodes as are used in a current glucose sensor that is commercially available for monitoring blood sugar levels in diabetics. The electrodes are made from a carbon black suspension screen printed onto a polyester substrate and are available as two different types. One is a working electrode, with a counter electrode made from Silver Chloride that is on a different sheet from the working electrode. The working electrode has a square node of 9 mm^2 surface area and is shown in figure 5.15 (a). The second type of electrode consists of a working electrode with a circular node of approximately 1 mm^2 surface area surrounded by a counter electrode, with both being manufactured from carbon black using screen printing. This type of electrode is shown in figure 5.15 (b).

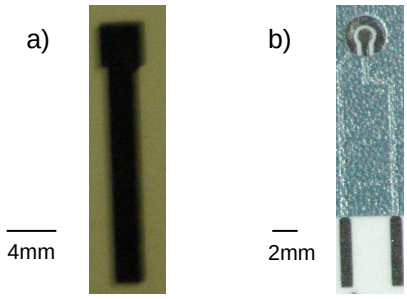

Figure 5.15. Pictures of the electrodes (a) 9 mm^2 surface area electrode (b) 1 mm^2 surface area electrode.

These electrodes are produced in large batches before being cut into the appropriate number required for the appropriate job or customer. Because of this, it is important to assess two aspects of the electrodes and their surface. Firstly, whether there is a better alternative to the current carbon black used by comparing it to the carbons used in other areas of science and engineering; and secondly whether there is a problem in the consistency of the production between the batches and size of electrodes which may adversely affect the electrochemical properties of the printed electrodes. The techniques

used to assess both of these questions were Scanning Electron Microscopy (SEM), Phase Contrast Optical Microscopy (PCM) and Atomic Force Microscopy (AFM). SEM was used to examine the surface structure and composition. PCM and AFM were used to characterise and quantify the surface in terms of the surface roughness, peak heights and total surface area of the electrode. These techniques allow a full surface characterisation and may also be used to determine the ability of the electrode to hold the printed protein samples on its surface and thus act as an effective electrochemical testing tool.

The two electrode samples are used in an identical manner, as both have only a counter and working electrode, necessitating the use of a pseudo-reference two electrode system as described in section 2.1.5.2. The setup of the electrode system for electrochemical testing is shown below in figure 5.16.

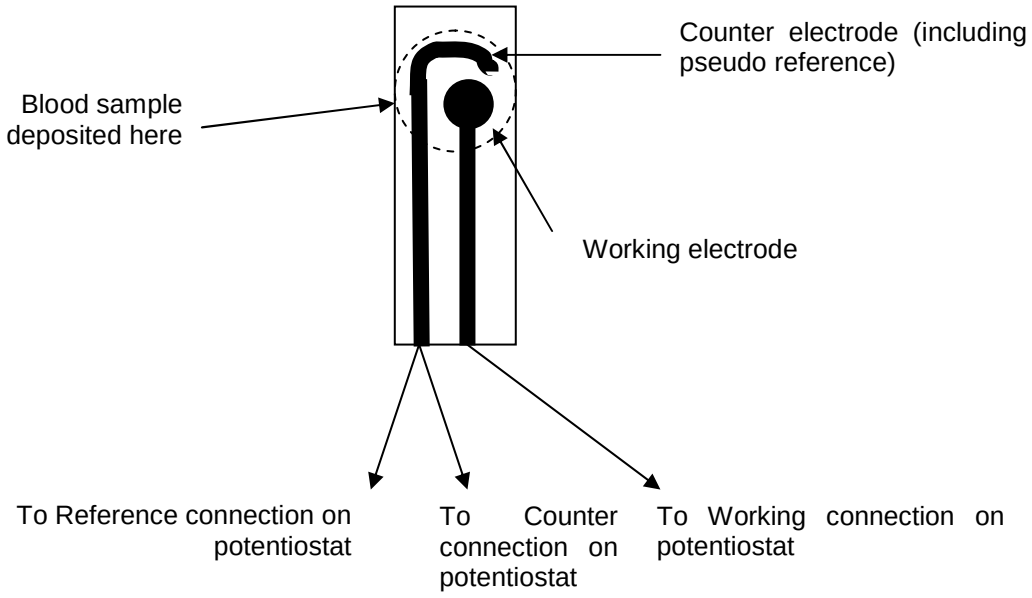

Figure 5.16. Set up of electrode system used in this study.

In a two electrode system, as this is, the reference electrode connection on the potentiostat is connected to the counter electrode which doubles as a pseudo reference electrode. The applied potential is applied through the working electrode with reference to a second applied potential through the pseudo reference electrode. The current response generated from the oxidation or reduction of the sample on the sensor surface (caused by the application of the

applied potential through the working electrode) is then measured at the counter electrode and directly links to the concentration of glucose present in the sample placed onto the sensor surface. This setup is used as it means that both electrodes can be manufactured at the same time using the same material, negating the need for a separate material for a separate reference electrode and therefore increased material use, time to manufacture and cost to the manufacturer and the end user.

5.3.1. Comparison of the carbon electrode materials

The two electrodes mentioned above were analysed and compared with three other carbon samples. These were: Highly Oriented Pyrolitic Graphite (HOPG), a thin carbon foil and finally a carbon nanospray. HOPG was in the form of a highly compressed and stiff rod of approximately 20 mm in radius which had thin transverse cross sections cut from it of approximately 5 mm in thickness and polished. The thin carbon foil was received with one side highly polished and dull on the other, this was extremely flexible but easy to tear. The carbon nanospray is normally used to produce an electrically conducting surface on samples for thermal diffusivity testing, this was sprayed onto two glass cover slips. All of these samples were prepared and the polished sides analysed and compared with the carbon electrodes using SEM, PCM and AFM.

The first samples to be analysed were the two AET electrodes (9 mm^2 and 1 mm^2 surface area) electrodes. These were examined using SEM and PCM as outlined in the methods section. Because of the nature of the analytical techniques, only part of the area of each electrode could be analysed but this area was kept consistent between the electrodes to ensure any images were from similar locations and hence consistent between samples. 5 samples from each type of electrode were analysed with representative images shown below. SEM images of the electrodes are shown in figure 5.17.

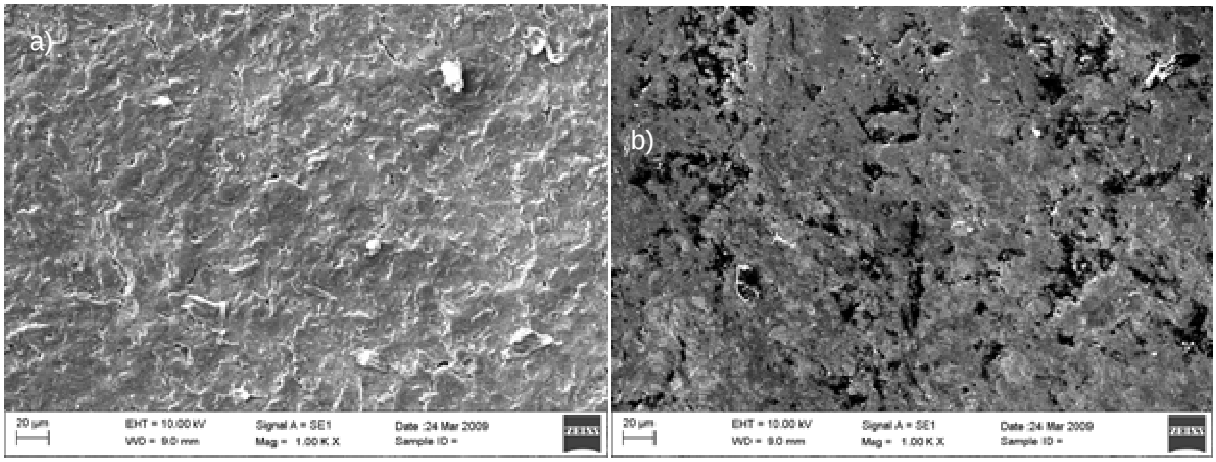

Figure 5.17. SEM secondary electron images of the electrode surface of: a) 9 mm^2 surface area electrode, b) 1 mm^2 surface area electrode.

The SEM pictures show the graphite flake morphology of the two electrode surfaces, which are seen to be fairly smooth, which is believed to be characteristic of the screen printing fabrication process. There does not appear to be an associated flake direction as would be expected with screen printing due to the action of the squeegee across the physical substrate surface. The sample shown for the 1 mm^2 surface area electrode does appear to have more of an uneven surface from the SEM pictures, possibly due to the screen printing procedure depositing a thinner layer of carbon on the surface because of the more complex pattern used. These flakes have an approximate mean size of 20 µm and the surface does not appear to have a great deal of porosity. The level of porosity as well as the surface roughness can be analysed further using a combination of atomic force microscopy and phase contrast microscopy. These two tools can give a quantitative analysis of the surface roughness as well as an indication of the height of the surfaces. These results are shown in figure 5.18 overleaf.

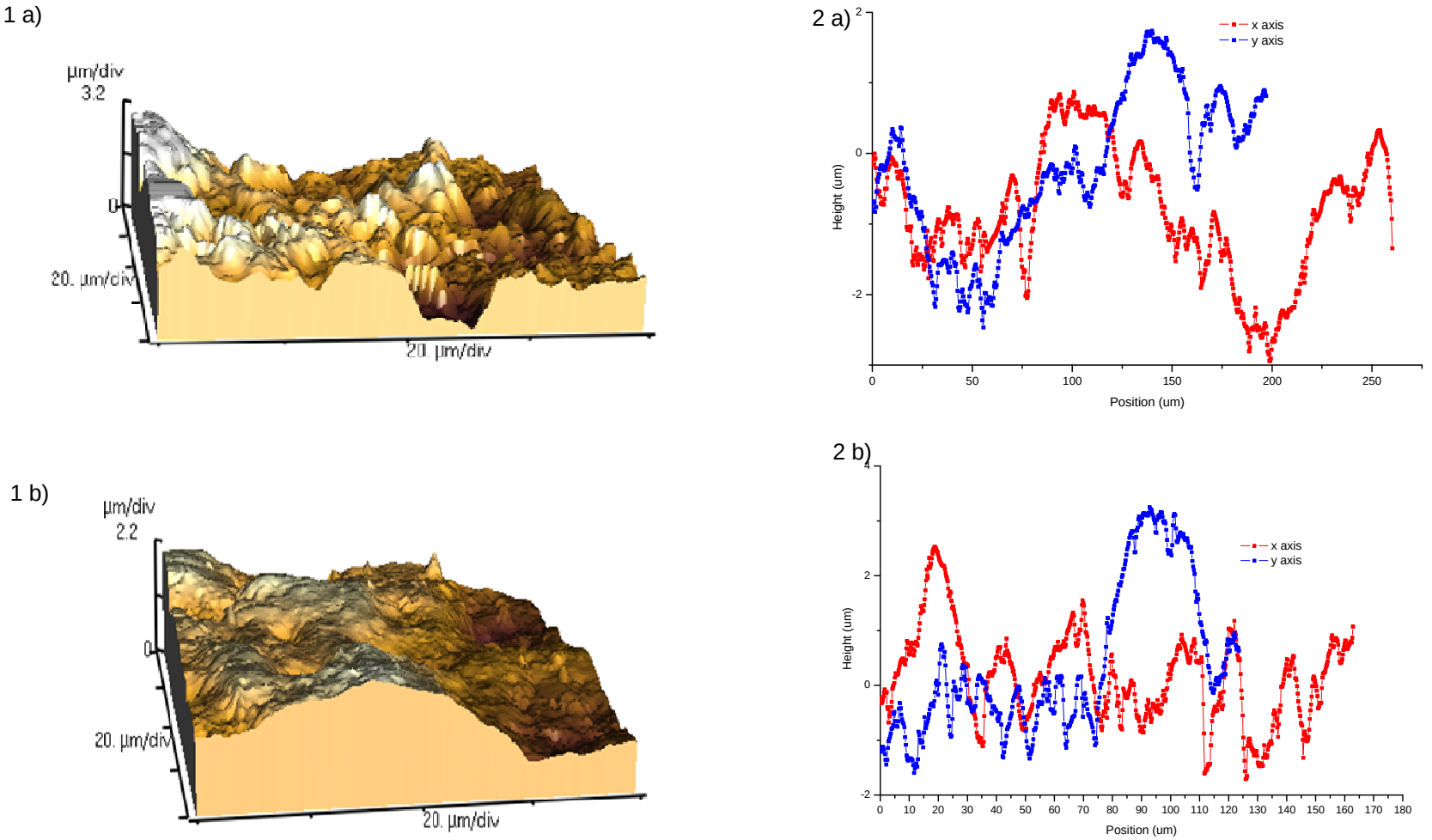

Figure 5.18. [1] AFM images of the surface of a) 9 mm^2 surface area electrode, b) 1 mm^2 surface area electrode [2] PCM graphs of relative heights in x and y directions of a) 9 mm^2 surface area electrode, b) 1 mm^2 surface area electrode.

The data and images shown in figure 5.18 clearly show the differences between the two surfaces. The 9 mm^2 surface area electrode possesses a fairly rough surface, which has a height of around 6.4 µm, compared to the 1 mm^2 surface area electrode, which has a height of around 4.4 µm. Both of these electrodes are known to have a carbon film thickness of approximately 15 µm measured from the polyester substrate surface to highest point on the carbon film. When the data from the PCM is analysed, it is noted that the average surface roughness of the two different electrodes are fairly similar. The Rq value, which indicates the average surface roughness, is 1.19 µm for the 9 mm^2 surface area electrode and 1.22 µm for the 1 mm^2 surface area electrode. However, the peak to trough height, that is the lowest point on the sample to the highest point on the sample, is shown to be much larger on the 9 mm^2 surface area electrode than the 1 mm^2 surface area electrode. This value is referred to as the PV value and is 8.08 µm for the 9 mm^2 surface area electrode and 6.86 µm for the 1 mm^2 surface area electrode. Therefore, the 9 mm^2 surface area electrode may be slightly smoother overall but has a far greater peak to trough height in comparison to the 1 mm^2 surface area electrode which has a relatively smooth surface profile. This indicates that although the 9 mm^2 surface area electrode is smoother, it has occasional large defects when compared to the smaller electrode.

If the sample size were to be increased to cover the entire sample, then the figures above would be shown to be representative. This means that the average height and roughness would remain similar, with small variations. The peak to trough height is more of an unknown entity and may be found to increase the closer to the edge of the electrode the sample is analysed. The theory behind this is that as the squeegee is moved across the physical substrate surface and contacts the mask pattern, then there will be an element of physical ‘pull’ on the ink which draws it up the side of the mask and leaves a slightly higher peak height than in the centre. This occurrence can be checked through the use of PCM later on in this thesis. If true, it may also be found to contribute to any contact pinning that is encountered, increasing the required surface energy of the drop to overcome the edge of the working electrode.

In order to compare the surface structure of these samples to other types of carbon preparation, the same characterization steps were carried out on the three other carbon samples; namely the carbon foil, the HOPG carbon rod and the carbon conductive spray. SEM images from these three samples are shown in figure 5.19. Again five different samples were analysed with the images being representative images taken.

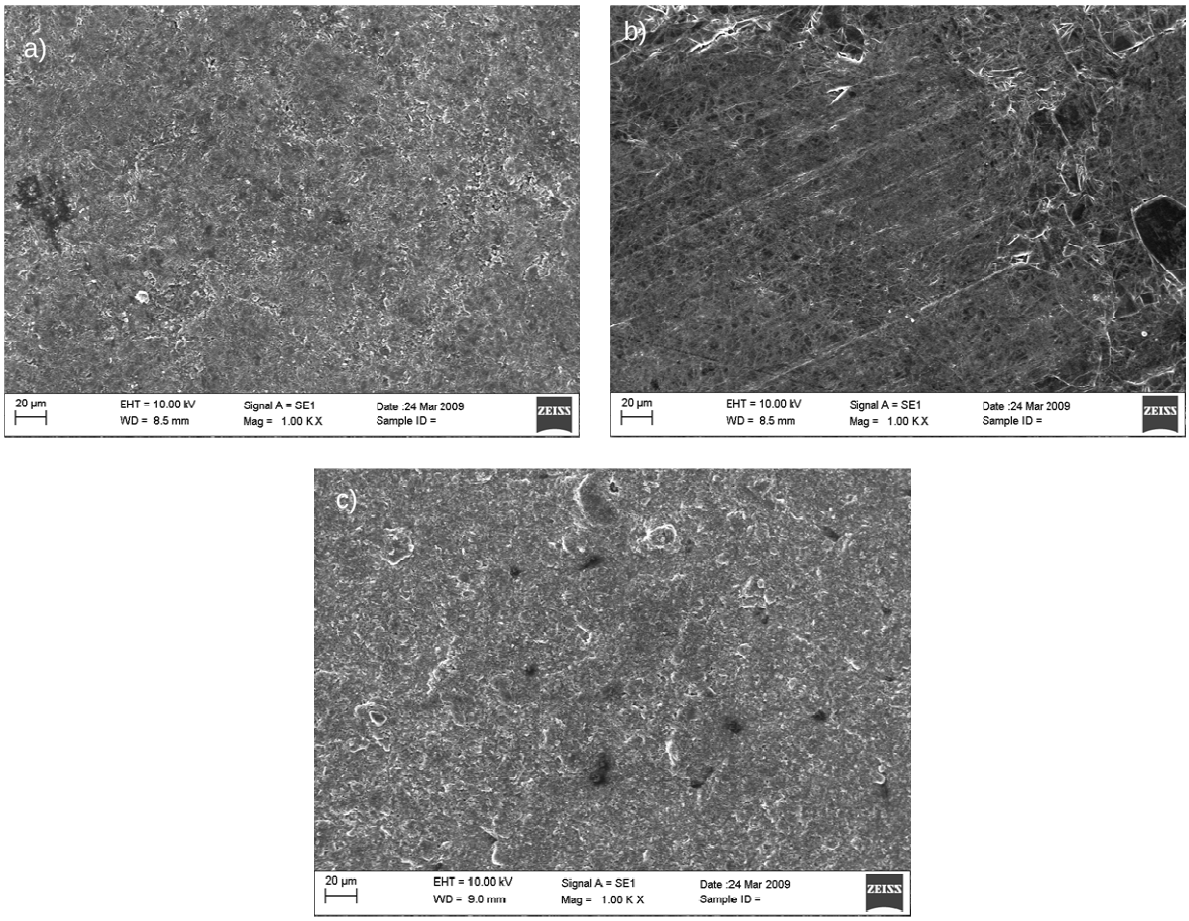

Figure 5.19. SEM images of a) Carbon Rod b) Carbon Foil c) Carbon Spray on Glass cover slips.

The SEM images of the three other carbon samples are shown at the same magnification as the SEM images of the AET carbon electrodes. As can be seen from a comparison of the electrode and non-electrode samples, the surfaces differ in their characteristics, with the rod and spray samples appearing to be rougher than the electrode surfaces. The rolling direction can also be seen in the foil sample with no obvious flakes visible compared to the electrode samples. To get an accurate representation of the roughness and height of the surface the

AFM was used. This would also allow for direct comparison between the AFM diagrams for the electrodes and for the three carbon samples. These are shown in figure 5.20.

a)

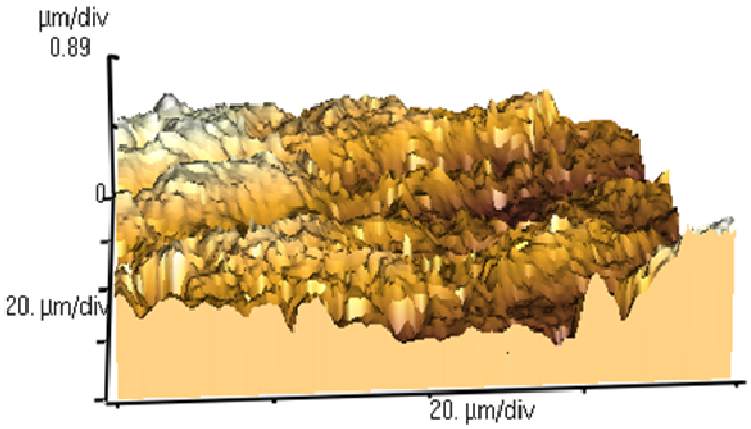

b)

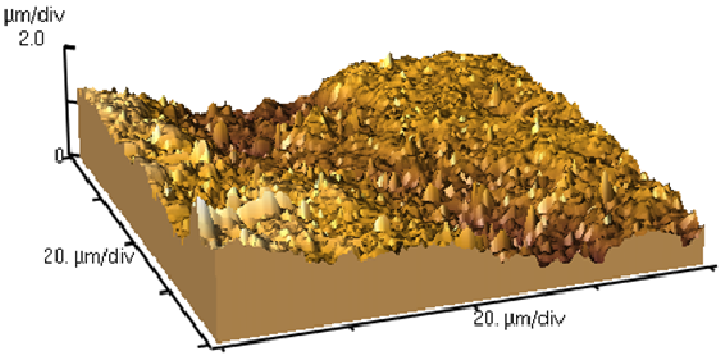

c)

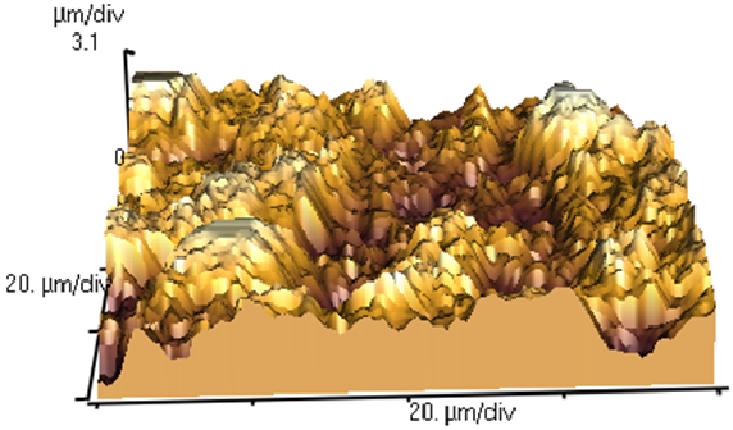

Figure 5.20. AFM representations of the surfaces of the three different carbon samples, namely a) Carbon foil b) Carbon rod and c) Carbon spray

As suggested previously, the rod and spray appear to have a rougher surface than the electrodes and the foil appears to be smoother. It can also be seen that the foil has a much smaller height difference across the sample than either the rod or the spray, leading to the conclusion that the carbon foil is generally a much smoother surface. The diagrams shown above are only of a small cross section of the samples, in the order of 80 μm^2, so give a small representation of the overall sample. In order to accurately compare these samples using a much larger sample area, it is necessary to refer to the PCM graphs and to attain the Rq values and the PV values for these three samples (figure 5.21).

The PCM graphs show the different surface topography of each sample and the relative smoothness in the x and y directions at a certain point on the sample. As can be seen from the graphs, the HOPG carbon appears to be relatively smooth. When the PV (14.26 µm) and Rq (0.60 µm) values are analysed it can be seen that the sample is very smooth but has a high trough to peak height. The carbon foil is seen to be fairly similar to the electrodes with a PV value of 12.35 µm and an Rq value of 1.51 µm, which was expected due to the manufacturing techniques used in both being similar. The carbon spray is the least smooth of the samples with a PV value of 18.57 µm and an Rq value of 2.32 µm.

When comparing this data and using it to predict the way the different surfaces may behave when a solution is placed onto them then it is predicted that those with a higher average surface roughness may cause a more pronounced beading effect of the drop, producing a higher contact angle and therefore make evaporation and absorption more difficult. Conversely, those with a lower average surface roughness may have greater difficulty retaining aqueous solutions on the surface due to the lower degree of contact pinning, leading to lower contact angles and increased spreading.

a)

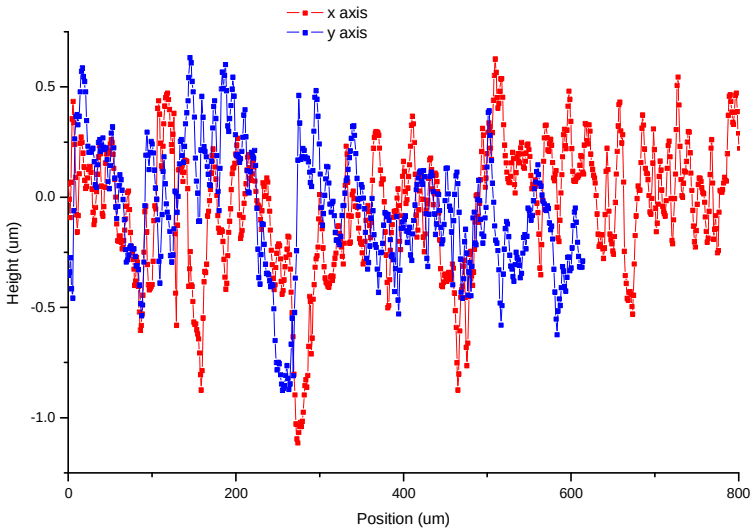

b)

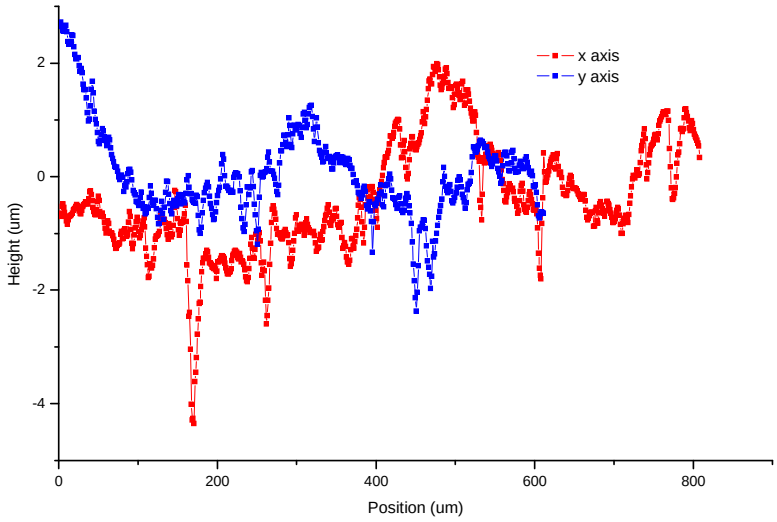

c)

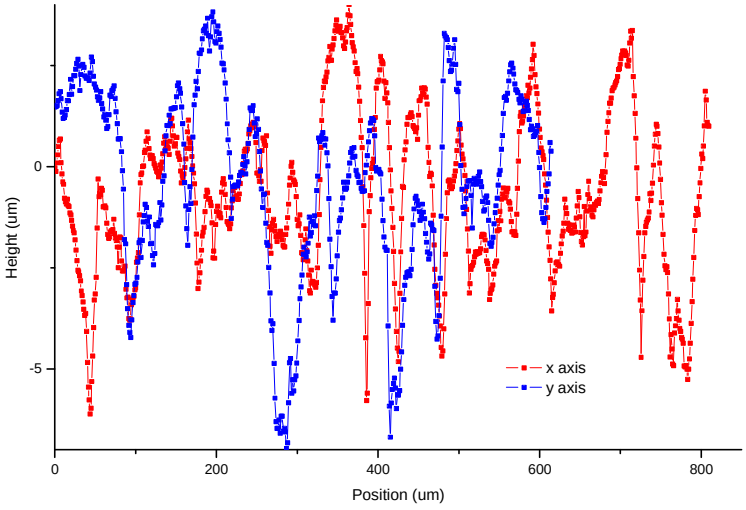

Figure 5.21. PCM graphs of the heights across the samples in the x and y direction of a) HOPG carbon rod b) carbon foil c) carbon spray on glass cover slips.

The electrodes appear to be very similar in surface properties to the other carbon samples. They have a similar surface roughness and peak heights at the surface, with a comparable structure in terms of carbon flake size. The electrodes are expected to have sufficient surface roughness to retain the enzyme solution and allow the enzyme to bind to the surface and give sufficient surface area to provide a good rate of reaction and therefore analyte breakdown and electron production for good electrochemical properties. However, the electrodes can only possess good electrochemical properties for the designed use if there are very few or no impurities present. Any impurities present in large amounts on the electrode surface may lead to errors in the electrochemical properties and therefore different results between identical samples. This could in turn prevent the electrodes from being used due to a lack of repeatability across a production batch. In order to prevent this problem, some analysis was carried out to test the contents of the electrode surface using SEM.

5.3.2. Consistency of electrode production

The importance of carrying out this testing has already been outlined and is split into two sections; the analysis of the chemical properties of the electrodes between batches, to test for impurities, and the analysis of the physical properties of the electrodes to test the consistency in production, with particular reference to such properties as surface roughness and flake size. Any large differences in any of these properties may lead to a different degree of absorption of the enzyme onto the surface, as well as different electrochemical properties. In terms of the end goal of this project, any of these things would be disastrous to the use of the technology as a biosensor and may require some alterations to the screen printing technique used for the production of the electrodes.

5.3.2.1. Analysis of chemical properties of the electrodes

The chemical properties were analysed using SEM and an associated energy-dispersive X-ray spectroscopy technique (EDX) to assess what compounds and elements were present within the surface of the electrode. The EDX was utilised once a bright spot was found (shown in figure 5.22) using a separate piece of software to detect what was present.

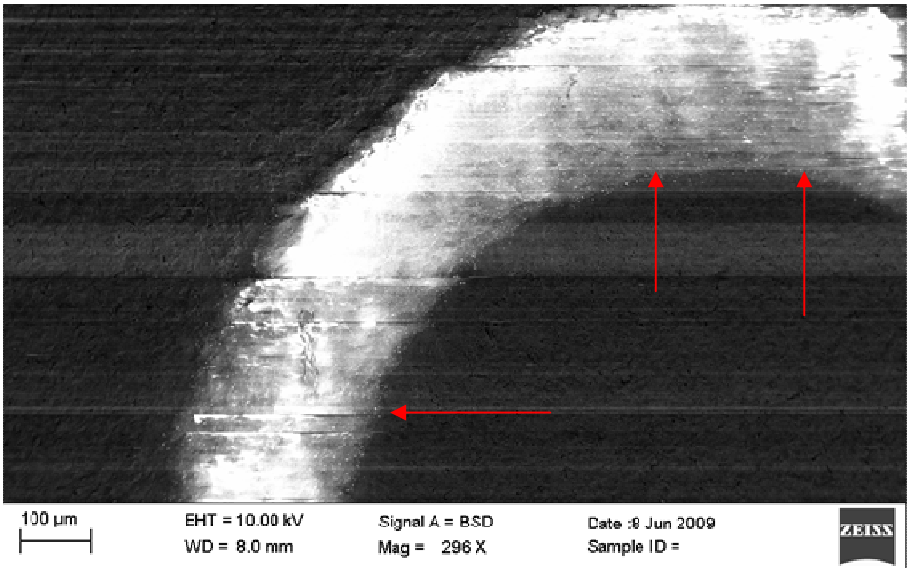

Figure 5.22. SEM image of the electrode ring showing the points of impurity (red arrows).

Figure 5.22 clearly shows what an impurity looks like upon examination by SEM. It also clearly shows that there is a significant quantity present on the boundary between the Carbon and the polyester, possibly due to the way in which the screen printing method is used to produce the electrodes. However, when the main bulk of the electrode is analysed, it can be seen that there is a very low proportion of impurities over the surface, demonstrating that the structure is fairly repeatable across one sample. Figure 5.23 shows the level of impurities across the sample of one electrode surface.

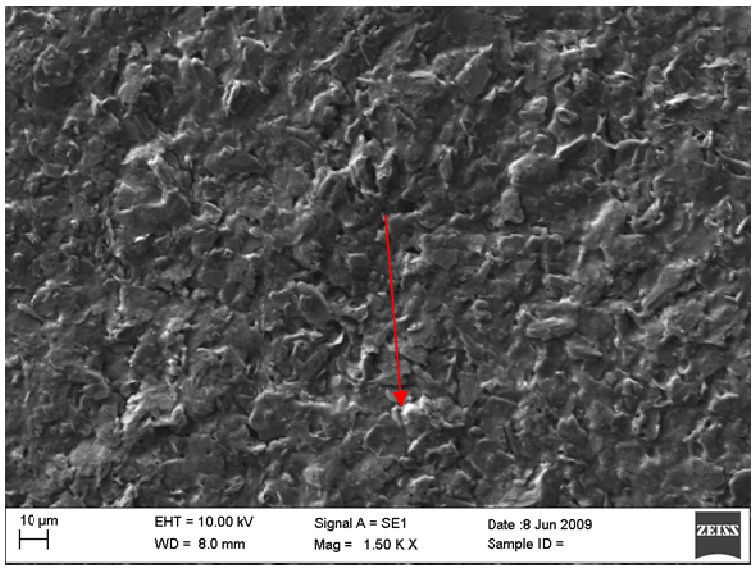

Figure 5.23. SEM image showing the surface of the bulk of the electrode including indication of impurities (red arrows)

The surface shown in figure 5.23 is representative of all of the samples that were provided of which a cross section of 5 from each batch were analysed. In the knowledge that the numbers of impurity spots across the electrode samples are low and consistent, it is important to determine what compounds and elements are present within these bright spots. This will give a direct comparison between the electrodes and an indication of where the impurities are coming from. If the electrodes all have similar levels of similar impurities then it could be postulated that the impurities are due to the manufacturing technique and are present on the screen printer when printing the electrodes. If the electrodes have different impurities present between the batches, then it could be concluded that the impurities are found in the original ink and are laid down as part of the screen printing of this ink. The electrodes were analysed in terms of batches, with two different batches of each of the 9 mm^2 surface area and 1 mm^2 surface area electrodes being analysed to give a breakdown of the elements present. The 3 mm^2 surface area electrodes were analysed first and are shown in figure 5.24.

It should be noted that the EDX technique used below is not able to identify compounds, only elements. Therefore it is important to compare the overall construction of the chart, not just the elements in isolation, as there may be compounds such as oxides present. This data should also have been presented in terms of the relative atomic percentages of the elements to help inform the discussion. However, due to the mistaken destruction of the raw data prior to the writing this report, it has been impossible to convert the chart to show the relative atomic percentages.

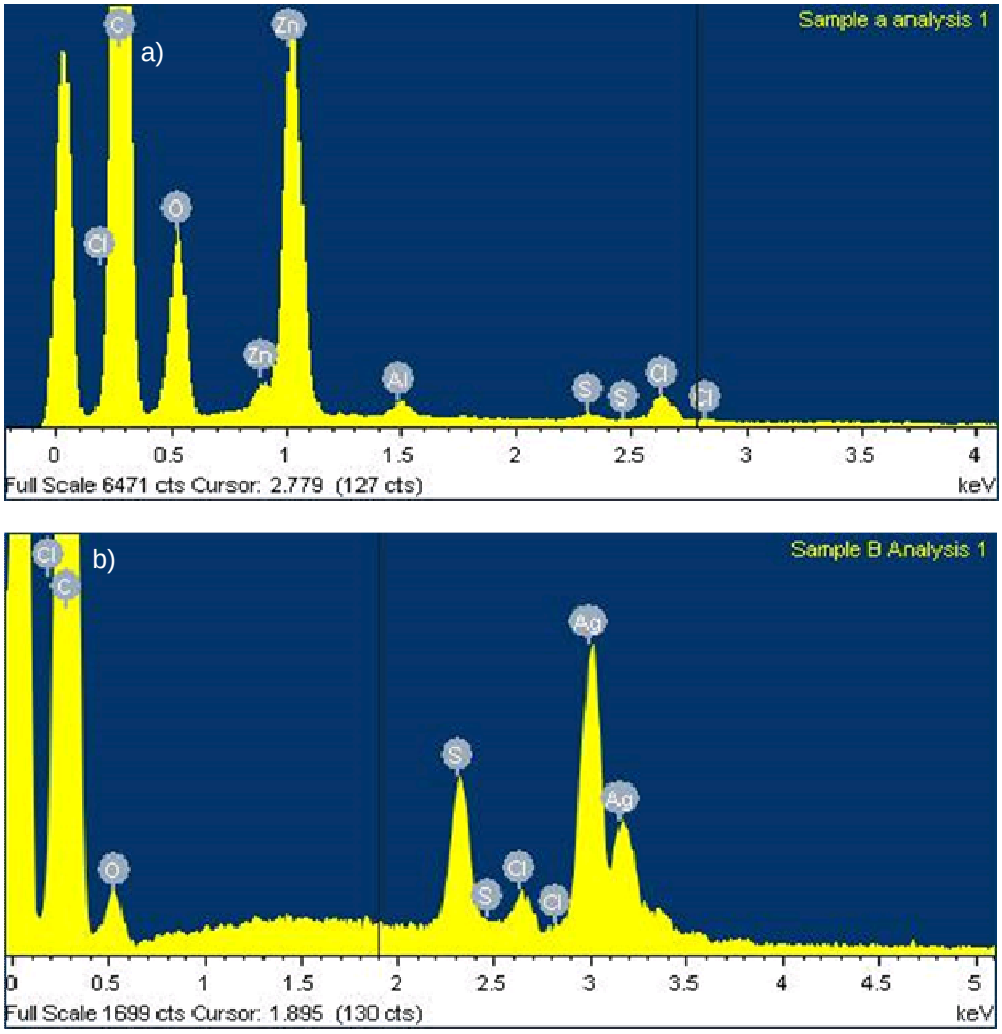

Figure 5.24. SEM EDX analysis of two different batches of 3 mm^2 electrodes (a) 2090407.02 (b) 2071107.28.

As can be seen from figure 5.24, there is a wide range of elements present in the two batches. Not surprisingly, the Carbon is the dominant peak on both graphs. Surprisingly, however, the two samples do have some similar impurities with Chlorine and Sulphur being present in small levels. The main difference between the impurities present in each sample is Zinc. This has the potential to cause disruption to the electrochemical properties as it is conductive when in metallic form. However, it is highly unlikely that the Zn found in this sample is in its metallic form and will therefore not affect the electrochemical properties of the electrode. The 1 mm^2 surface area electrodes were also analysed to give a comparison of the two electrodes as well as a comparison of any differences between batches (fig 5.25).

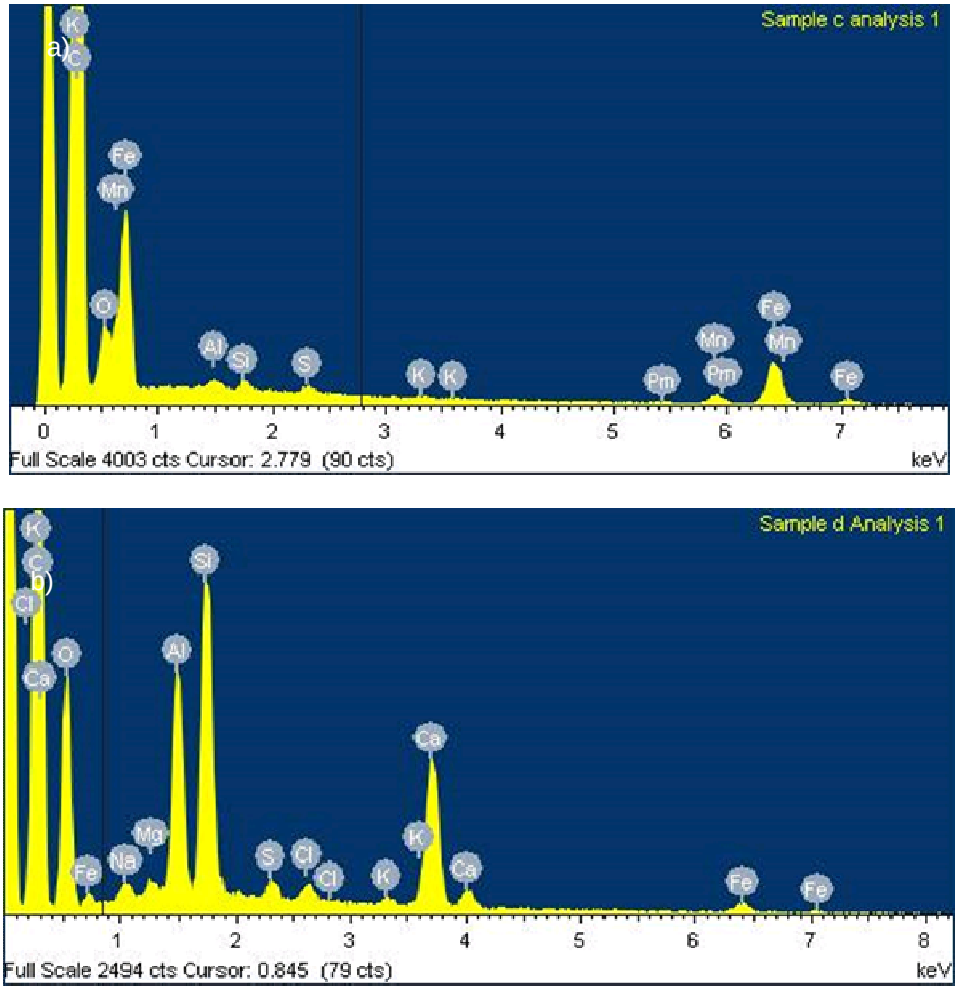

Figure 5.25. SEM EDAX analysis of two different batches of 1 mm^2 electrodes (a) 2071030.20 (b) 2090407.02.

The 9 mm^2 surface area electrodes had different impurities present between the batches, with there being Silicon and Aluminium in one and Iron in the other. The presence of Oxygen within the sample leads to the conclusion that these elements are not likely to be present in their purest form, but as an oxide. Therefore they are unlikely to interfere with the electrochemical properties of the Carbon electrode.

To conclude, from the elemental analysis carried out thus far, it is difficult to identify the origin of the impurities. The difference in the impurities present between samples more or less rules out the screen printer being responsible for their source. Therefore, they could either come from the ink or be present on the polyester prior to printing. Due to the low volumes of these impurities present and the combination of different elements postulated to

be in various non-conductive compounds, no further investigation was thought necessary to discover the origin of the contamination.

5.3.2.2. Analysis of the physical properties of the electrodes

The physical properties of the electrode will help define whether the screen printing process is reliable and repeatable. Using SEM, an image of the surface can be taken and this will give an idea of the surface roughness and the flake size of the electrodes, both between the different electrode sizes and the batches. Figure 5.26 shows representative SEM pictures of the two different batches of the 1 mm^2 surface area electrodes.

It can be seen from these images that the surface morphology is comparable between the two different batches, with each having a flake size of approximately 20 µm. The flake alignment is the same and is associated with the direction of the “squeegee” motion during screen printing. In both cases it appears that this direction is the same, suggesting that a standard production procedure was used for each batch. This is supported by the fact that the surface roughness is similar for both samples upon visual assessment of the SEM images. The final point to note is the relative dearth of impurities within the samples, demonstrating the point made earlier that the relative proportion of the impurities compared to the surface area of the carbon within the electrodes is small.

Analysis of the images of the 9 mm^2 surface area electrodes (figure 5.27) shows similar findings to the 1 mm^2 surface area electrodes, whereby the surfaces appear very similar between batches and there is a very low level of impurities present. There is also a similar alignment of the flakes and they are of a similar size as found with the 9 mm^2 surface area electrodes. Again, there is a definite difference in the roughness of the surfaces when visually comparing the 1 mm^2 and 9 mm^2 surface area electrodes, whereby the surface of the 9 mm^2 surface area electrode appears rougher. From the analysis of this data, the 1 mm^2 surface area electrode was selected as the electrode to be used in this project because the 1 mm^2 surface area electrode also offers a smoother and more impurity free surface than the 3 mm^2 surface area electrode. This is also the electrode that is currently used for production

purposes at AET. It contains a counter electrode printed onto the same sheet, so can be produced using the same material on one screen printing screen. They are also more representative of the electrode types that are used in currently marketed glucose biosensors.

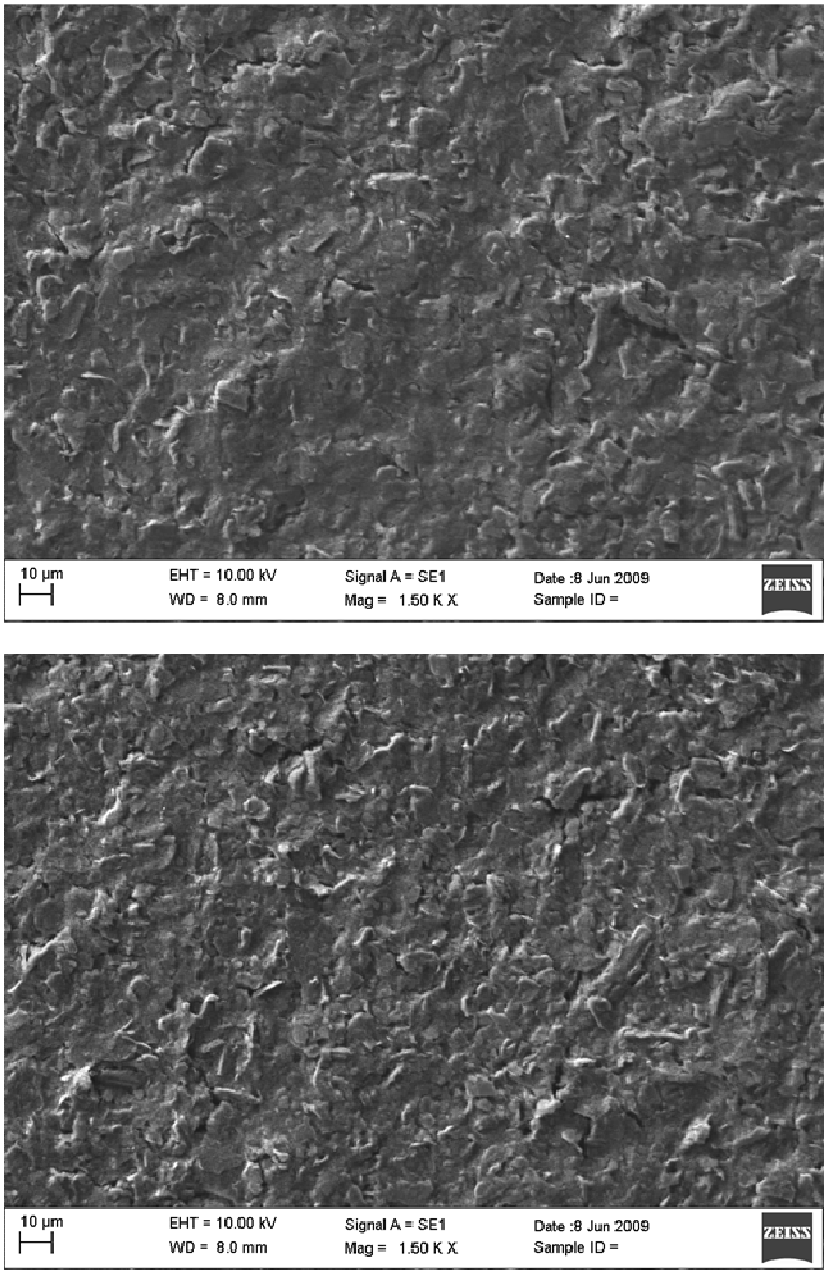

Figure 5.26. SEM images of two different batches of 1 mm^2 surface area electrodes.

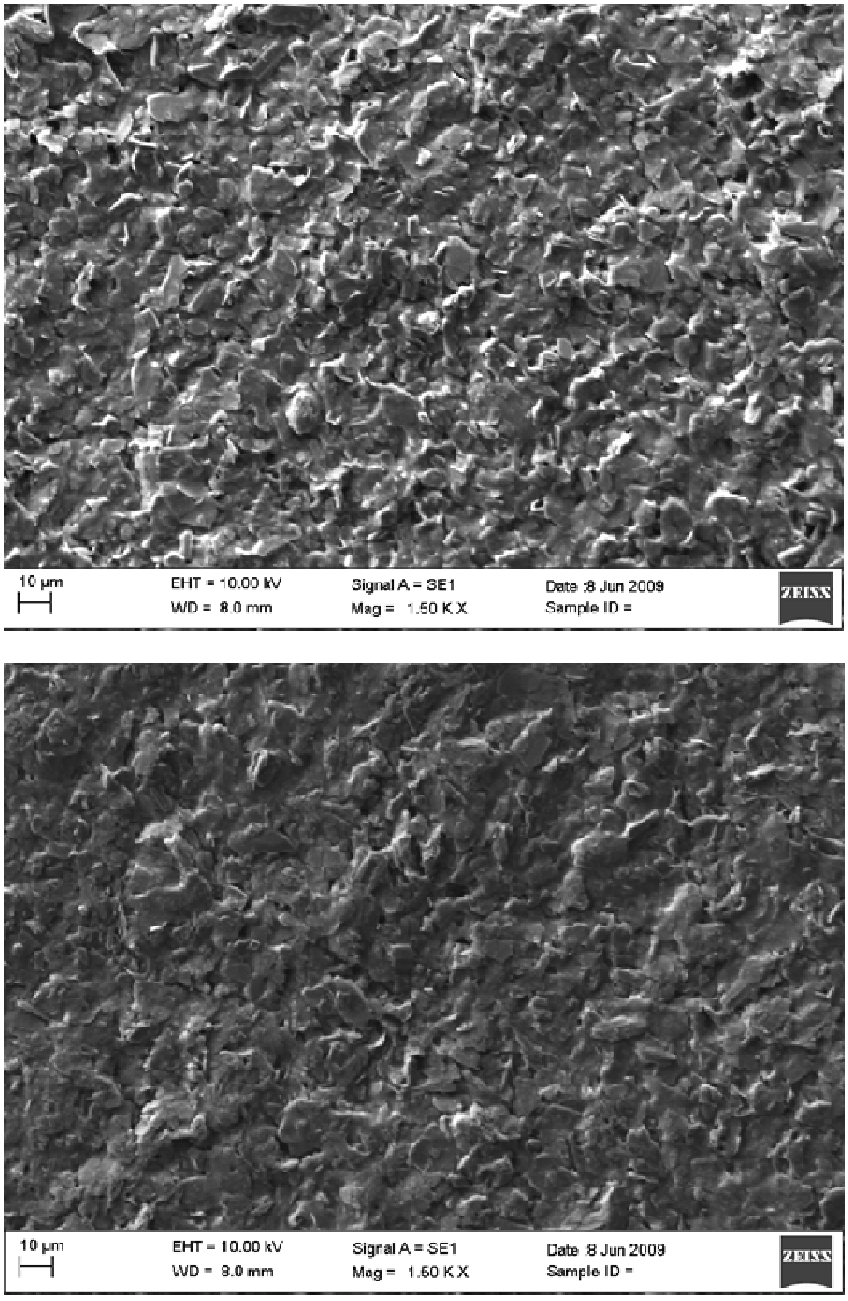

Figure 5.27. SEM images of two different batches of 9 mm^2 surface area electrodes.

Closer analysis of the surface morphologies of the 1 mm^2 surface area electrodes can be carried out using the PCM method, which gives a quantified measure of surface height. This allows for a more detailed picture to be built up of the electrode surface including surface roughness. Several pictures can also be stitched together to produce a more complex 3-dimensional picture of the whole surface, which will allow comparison of this to later work where protein is placed onto the surface. It will also allow for more detailed analysis of the repeatability of the screen printing method and the consistency of the electrodes after

production. Figure 5.28 shows PCM images from the two batches of 1 mm^2 surface area electrodes.

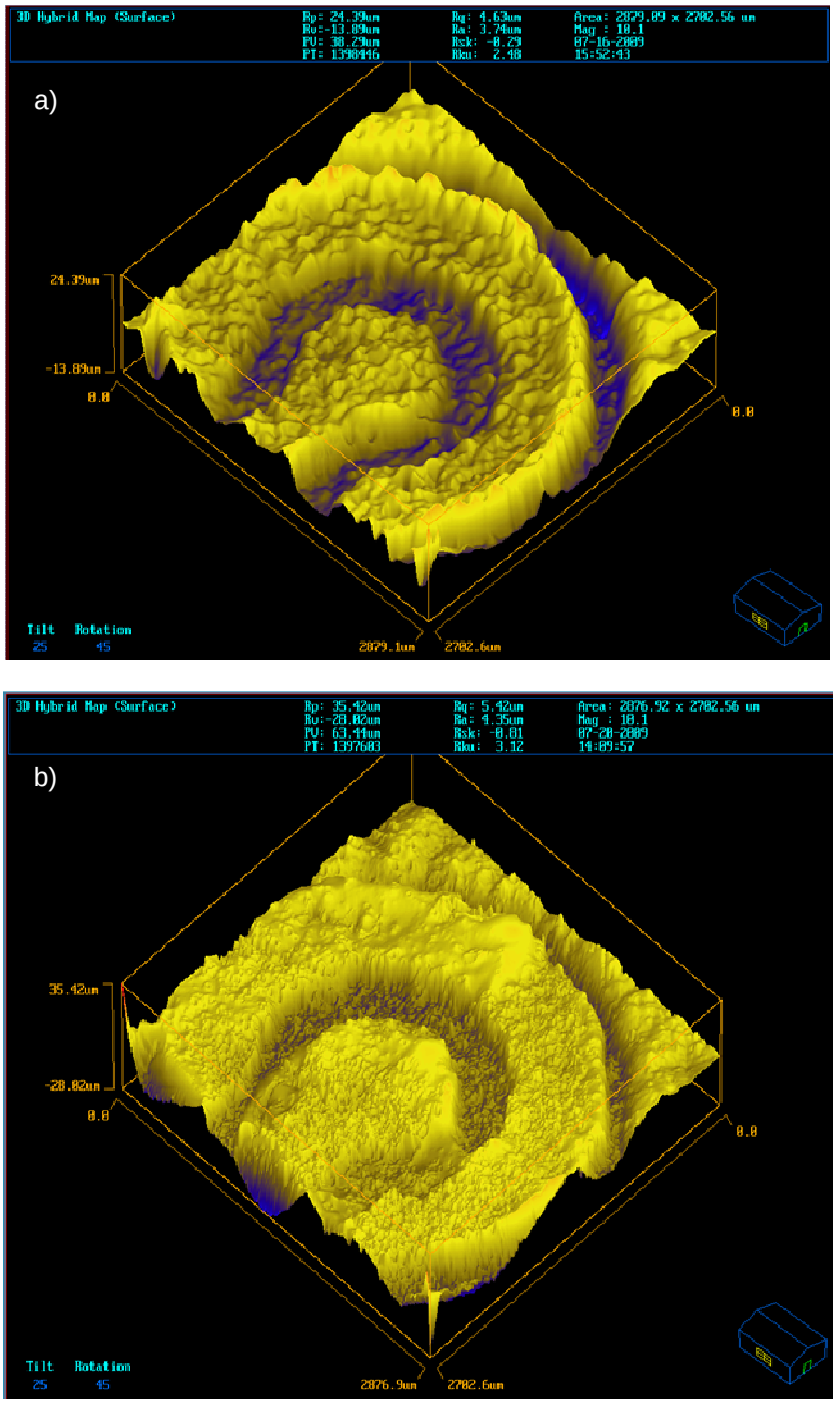

Figure 5.28. PCM analysis of 1mm^2 electrodes batch numbers (a) 2090407.02 (b) 2071030.20

It can be seen from figure 5.28 that the surface roughness of the batches is slightly different. Figure 5.28 (b) appears to have a much smoother surface than figure 5.28 (a). However, when the figures are analysed in detail and the data is quantified, it can be seen that both the average roughness and the peak to trough height of figure 5.28 (b) is in fact greater. This

is hypothesised to be because a deeper layer of material is present in figure 5.28 (b) than 5.28 (a). This can be seen in the figure by the blue layer shown in between the yellow regions (yellow represents the carbon). This blue layer represents the polyester physical substrate onto which the carbon is deposited.

The difference in the amount of carbon deposited onto the polyester is interesting but is not thought to cause a problem when concerned with deposition of the enzyme for the electrochemical properties. This is because the enzyme is only placed onto the surface of the electrode and the carbon will have the same level of conductivity when it comes to testing the electrochemical properties of the electrodes. There is, however, a danger that the presence of exposed polymer film means that the Carbon electrode may not be fully connected and part of it may be electrically isolated which may cause a drop in the current response. This is something that may have to be accounted for when carrying out the electrochemical testing.

With the analysis of the surface of the electrode complete and the decision made to use the 1 mm^2 surface area electrodes, further investigations of the deposition of the enzyme can be begun, in order to calculate the ideal deposition technique, in terms of the printer settings, as well as the ideal drying conditions in order to give the best electrochemical properties. In order to utilise the PCM method above in further chapters, the data captured here (in terms of roughness and height) will be used as a baseline to help differentiate between the carbon electrode and the parts of the electrode onto which the enzyme has been deposited. This will help inform the optimal method for the deposition of the enzyme onto the carbon electrode and the optimal drying technique to prevent coffee staining.

5.4. Fluid Properties on the Electrode Surface

In section 5.3 we identified the chemical and physical properties of the carbon electrodes, paying particular attention to variations between and within batches. This section reports on the interaction between the electrode surfaces and the enzyme solutions during and after deposition with emphasis on the wetting, spreading of the solutions after printing and the

subsequent drying of the deposit. The final morphology of the printed enzyme is expected to control the electrochemical performance of the enzyme and thus an understanding of the interaction processes during printing and drying is critical in defining the manufacturing protocol for sensor fabrication. This will be achieved by assessing the way in which the solution behaves on the surface after deposition and how drying occurs. It is also important to assess what portion of the electrode surface the dried solution occupies and whether it remains contained within the working electrode or spreads across onto the underlying carrier material or the adjacent reference electrode.

The interaction between the fluid and the electrode surface will be characterised by analysing the change in contact angle of the enzyme solution on the surface of the electrode with time. This will be compared with the behaviour of the fluid on other reference carbon surfaces to determine the relation between fluid behaviour and the specific surface properties. The deposited and dried solutions are analysed using a combination of PCM images and quantified roughness data, combined with some further contact angle analysis. This will give a complete and overall picture of the solution drying process as well as the best solution make-up for optimal functional properties. These can then be tested electrochemically to produce an optimal solution formulation that can be used with inkjet printing to produce working electrodes for use in biosensors.

5.4.1. Comparison of the fluid – electrode interaction with different carbons

The objective of this task is to attempt to formulate an enzyme solution, or ink, to enable the appropriate degree of spreading over the electrode surface. The optimum formulation will achieve complete coverage of the working electrode without further spreading of the solution onto the polyester physical substrate. Spreading of the solution onto the polyester physical substrate may interfere with the reference electrode and therefore give an incorrect reading for any sample. In order to complete this work the analysis of the solutions was carried out on the electrode surface using contact analysis software after 999 drops were printed onto the surface in one complete trigger.

An important method of analysis is to characterise the behaviour of a sessile drop on the carbon surface. The geometry of a sessile drop is illustrated in figure 5.29.

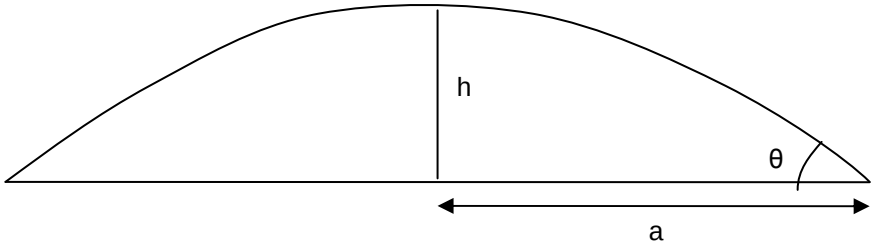

Figure 5.29. Measurements to be taken of a drop (where a = spread radius, θ = contact angle and h = drop height). These will be used to calculate the drop area.

If the drop is small the influence of gravitational forces can be neglected and the shape approximated to that of a spherical cap. The surface area and volume of the drop are given by:

$$A = \pi\left(a^2 + h^2\right) \qquad (40)$$

$$V = \frac{1}{6}\pi h\left(3a^2 + h^2\right) \qquad (41)$$

Should the drop volume change over time and the area remain constant then it can be assumed that mass loss by evaporation dominates with any difference being a difference in absorption rate.

The volume of the sessile drop will be equal to the volume of the drops placed on the surface and it can be shown that the radius of the spread drop is related to the original spherical drop radius by the contact angle (where a_{eqm}= the spread area of the drop, a_0= the initial area of the drop and θ_{eqm}= the contact angle after spreading).

$$\frac{a_{eqm}}{a_0} = \sqrt[3]{\frac{8}{\tan\frac{\theta_{eqm}}{2}\left(3+\tan^2\frac{\theta_{eqm}}{2}\right)}} \qquad (42)$$

It is thus possible to redefine the volume of the drop in terms of the contact angle.

$$V = \frac{1}{6}\pi h\left(3a^2 + h^2\right) = \frac{\pi a^3}{3}\left(2\cos ec^3\theta_{eqm} - \cos ec^2\theta_{eqm} + 1\right) \quad . (43)$$

Figure 5.30 shows the change in sessile drop radius and volume with time of a PBS solution on all the carbon surfaces. All printing was carried out using 999 drops per trigger and a single trigger for each electrode. The printer was set to print at 60 V with a pulse width of 25 µs and a rise and fall time of 3 µs. A frequency of 5000 Hz was used. The sessile volume of the samples shown below was calculated using the above equation.

The data shown in figure 5.30 was captured by depositing a stream of 999 drops onto the working electrode and analysing them using the contact angle method described earlier. A video was taken of the drop on the electrode surface for the whole 90 second period using a high speed camera at 4 frames per second. The analysis was then done in slow time by using computer software to track the spread radius and volume over this time period frame by frame. Each data point is a mean of 5 data points for both the sessile volume and the spread radius.

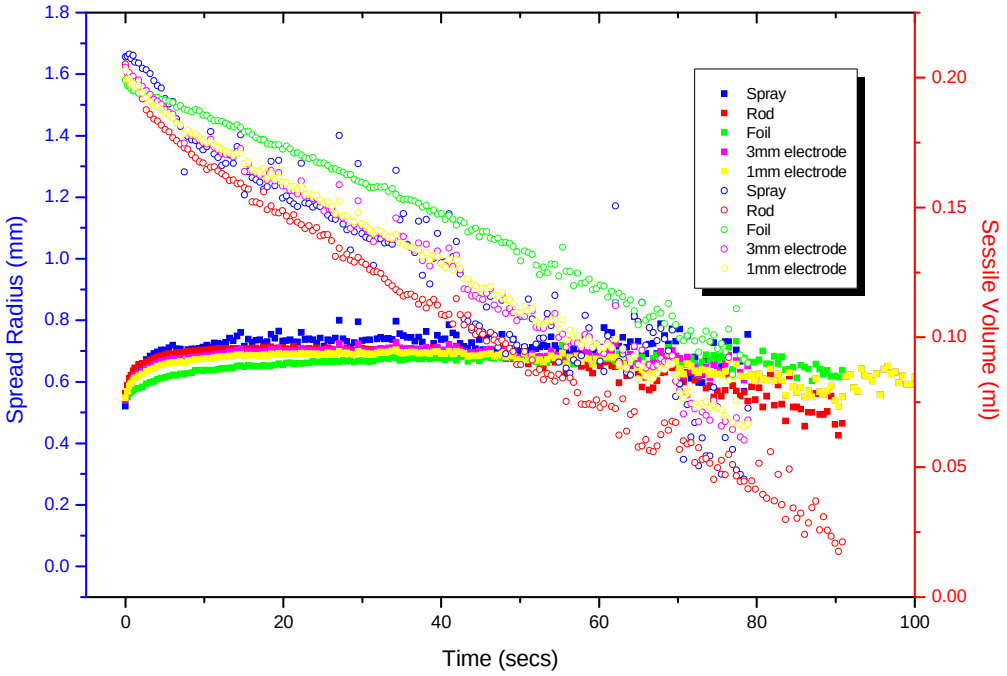

Figure 5.30. Analysis of droplet spreading (where spread radius is shown by the filled symbols and sessile volume is shown by the hollow symbols).

It can be seen from figure 5.30 that the drop spreads fairly slowly with a decreasing rate. This is consistent with Tanners law which states that the spreading rate of a drop is proportional to $1/t^n$ where n is around 9 [133]. As this spreading occurs, the volume of the drop decreases. If this was caused by evaporation it would be expected that the rate would be proportional to the area of the drop surface. This same principal applies if the reduction in volume was caused by absorption. It has not been possible to test Tanner's law with this data, as the volume of the drop is decreasing with time and Tanner's law assumes a constant drop volume.

As the rate of change in drop volume is fairly constant with time, then it would suggest that the surface area of the drop is not changing much. The decrease in the spread radius is only small which demonstrates that the area is not decreasing greatly, which is consistent with the constant decrease in volume mentioned earlier. If this is true, and the drop footprint is not shrinking, then it can be assumed that the contact line of the drop is pinned. These pinned contact lines can lead to the phenomenon of coffee staining, where solute segregation occurs at the pinned line during drying. The rate of decrease in drop volume is greatest in

the samples that have spread the most. This suggests that the majority of the mode of volume of loss is due to evaporation, a hypothesis that is supported by the similarity in the rate of loss of volume across all samples, despite each sample having a different level of porosity.

It is clear from these results that the contact area of the drops remains constant throughout the measurement time with the volume of the drops decreasing at a roughly linear rate. The speed of the decrease in the sessile volume appears to be related to the roughness of the surface as explained above, with the faster spreading occurring on the smoother surfaces. The rather similar drop volume change with time suggests that the dominant mass loss mechanism is evaporation. If penetration or absorption was the dominant mechanism a bigger variation in the rate of volume decrease might be expected because of the different pore morphologies between samples. Each drop is approximately 200 µl in volume and only 1.5 mm in diameter at the widest point. It is expected that the volume would drop in such a short time due to the small volumes involved and the small drops. These experiments are using 500 to 1000 drops per sample so the printing of a single drop would lead to a more rapid drying rate than is shown here. These results give an indication of how a PBS fluid behaves on the electrode surface, including its rate of spreading and that of absorption or evaporation.

5.4.2. Effect of the enzyme sugar solution on the electrode – fluid interactions.

In order to gain a realistic impression of the behaviour of the solution when enzyme and the stabilising sugar solution are present, the same experiments were repeated using the 1 mm^2 surface area electrodes, but now with an enzyme in solution and the stabilising sugar solution used as the buffer. The resulting contact angle and PCM analysis would show whether any surfactants or anti-foaming agents were required in addition to the initial formulation to achieve the desired fluid - electrode interaction.

Images of the PBS solution on the carbon surfaces show relatively high contact angles on the 1 mm^2 surface area electrode (figure 5.31 (a)). The contact angle of the GOX enzyme on

the same electrode is much lower and the drop is seen to spread further across the electrode surface (Figure 5.31 (b)).

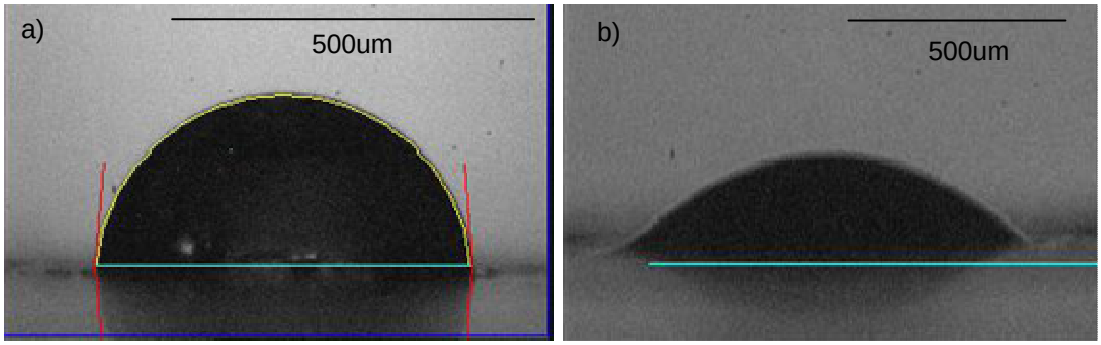

Figure 5.31. Contact angle images of solutions on a 1 mm^2 surface area electrode: (a) PBS (b) GOX. (The blue line is a point of reference showing the carbon surface).

The interaction of the GOX solution with the 1 mm^2 surface area electrode was then measured over a 2 minute period to assess the amount of drying encountered as well as the level of spreading. The GOX solution was a 600 U ml^{-1} solution in a sugar stabilisation buffer supplied by AET Ltd. There were 500 drops printed in a single trigger from a Microfab printhead at a voltage of 60 V with a pulse width of 25 µs and a fall and rise time of 3 µs. A frequency of 5000 Hz was also used, which equated to a print time of slightly less than 200 ms. This equated to a printed concentration of approximately 3 U. These results are shown in figure 5.32.

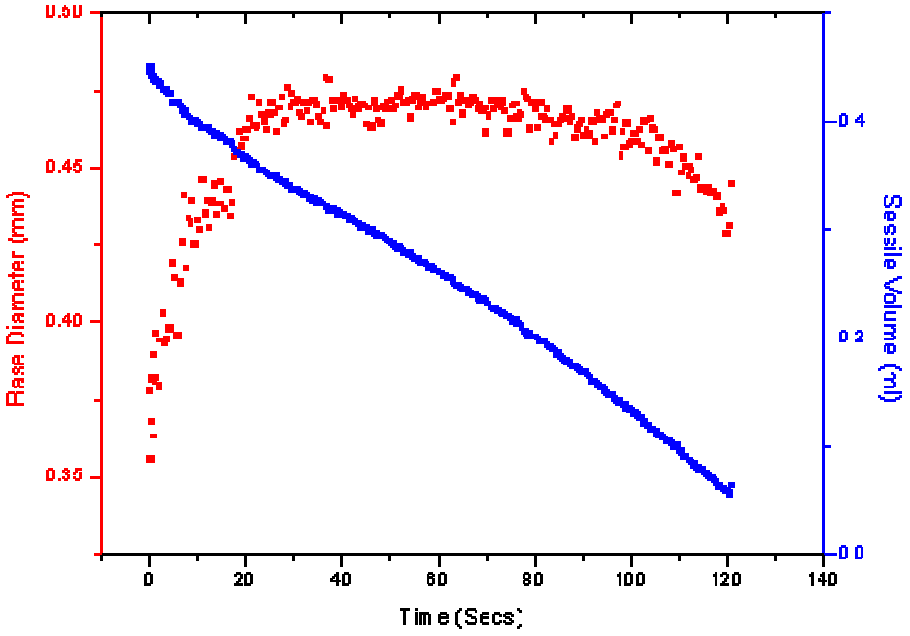

Figure 5.32. Spreading of a GOX plus stabilising solution sessile drop

The behaviour of the drop once on the electrode surface is similar to that of the PBS solution with an approximately linear decrease in the volume of the sessile drop with time. The spread length and volume are much smaller as a smaller number of drops were printed in this experiment (500 in comparison to 999 in the previous results). However, for the first 20 to 30 seconds, the GOX solution spreads quite dramatically with a growth of about 0.2 mm in the diameter of the drop across its base. The reason for the lower base diameter in these results is due to the smaller electrode onto which it is being deposited limiting the spreading of the solution.

The behaviour of the GOX shows the contact line pinning explained earlier, with the diameter of the drop remaining constant whilst the volume of the drop decreases. In order to confirm that contact pinning and therefore coffee staining occurs, PCM images of the dried electrode after printing 999 drops were obtained (fig 5.33).

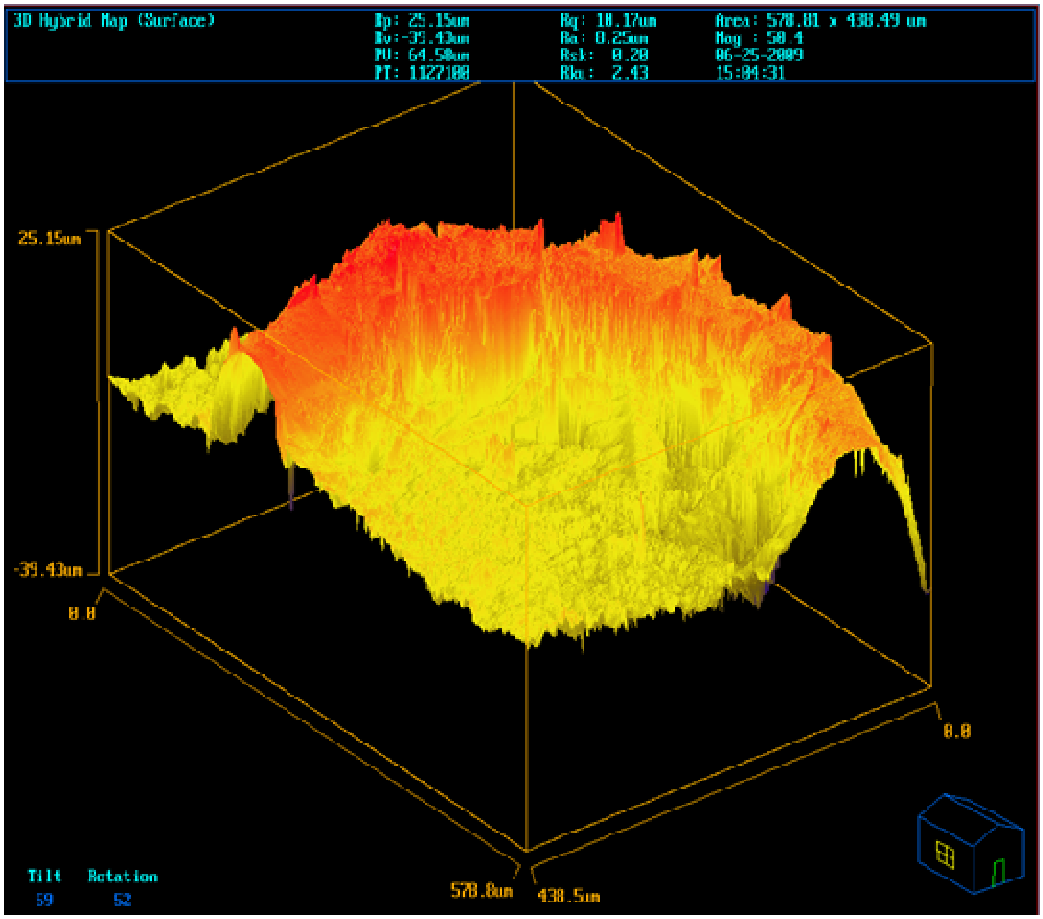

Figure 5.33. PCM image of the dried GOX solution on the electrode surface.

Figure 5.33 shows the surface morphology of the dried GOX solution on the electrode surface, which shows a distinct ring. We interpret this as showing solute segregation during drying, which is often termed the coffee stain effect or coffee staining [134] [135]. This effect is problematic for the electrode and the properties which are required of it. This is because the circular conformation of the dried enzyme gives a low overall surface area on which the analyte can be placed for detection. This will in turn give a low rate of reaction between the enzyme and the analyte and could therefore reduce the effectiveness and reliability of the electrode as part of a glucose biosensor.

The reason for this circular 'coffee staining' effect is thought to be due to the higher contact angle and therefore lower spreading of the solution over the electrode upon printing. The drying temperature and period is also thought to have an effect on the conformation of the dried solution on the electrode surface. Thus, a series of experiments were carried out to

assess the drying protocol, including trying new drying methods that may give different properties to the dried solution, and whether the addition of a surfactant would help in encouraging spreading of the solution on the electrode, thus reducing the coffee staining effect.

5.4.3. Effect of the addition of a surfactant to the enzyme solution

A surfactant is a solution that is able to reduce the surface tension of a liquid and therefore enable a greater amount of spreading. They are normally amphiphilic which means that they possess both hydrophobic groups (tails) and hydrophilic groups (heads). Use of a surfactant for this purpose, therefore, should create a solution with a lower surface tension, which should spread across the electrode surface more easily and thus dry more evenly. The drop in surface tension was shown earlier in figure 5.2 in comparison to the normal solutions. The surfactant chosen for this purpose was Triton-X 100 as it is known to not interfere with the electrochemical properties of the electrodes and is already widely used in the sensor market [161].

However, in order to confirm that this was the case, the electrochemistry of the GOX solution was tested in its normal form and after addition of the surfactant with both solutions pipetted onto the electrode at a concentration of 3.19 units (figure 5.34). This concentration was chosen due to the current enzyme concentration recognised by AET on the sensor surface being this figure and because of its suitability for physiological conditions (such as pH).

The surfactant was used at a concentration of 0.005% vol vol^{-1} to ensure that the spreading was kept within the limits of the electrode. Electrochemistry was only used at this point in the experimentation as the primary focus of work to this point was the definition of the solution properties to enable deposition of the correct enzyme concentration onto the electrode surface. Chronoamperometry was used from this point forward as it was important to ensure that all printed samples gave a reliable current response that was comparable to a hand pipetted sample.

It can be seen from figure 5.34 that there is no obvious difference when the surfactant is added to the GOX solution in terms of the electrochemical response. The response itself is reasonably linear with a good current response through to 6 mMol of Glucose. The addition of surfactant to the solution does lead to a slight fluctuation in the results but nothing to cause concern. There is no rise in the electrochemical response as expected. It was theorised that the surfactant allows the solution to spread across the electrode more evenly and therefore should have given an increased surface area for the enzyme to act over and increase the current response. It is postulated that this is not the case because the concentration of surfactant is not high enough in relation to the overall volume of the fluid. Thus some experiments were carried out to characterise the percentage of surfactant required to spread the GOX solution over the whole electrode surface without compromising the reference electrode on the 1 mm^2 surface area electrode sheet.

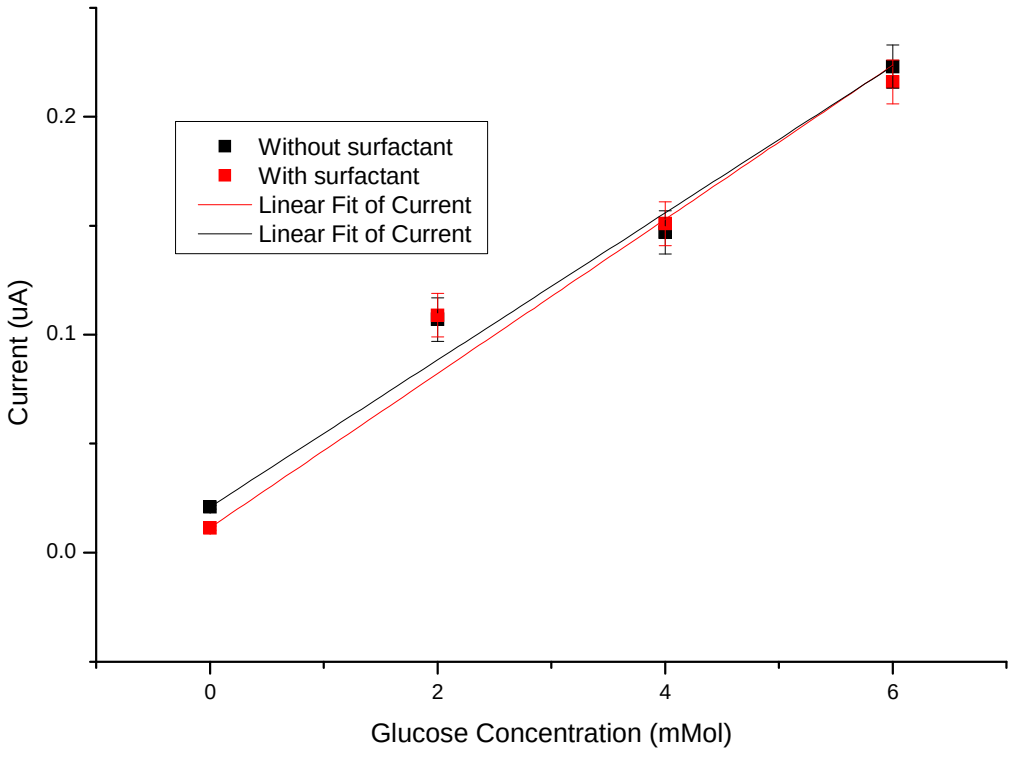

Figure 5.34. Electrochemical comparison of the GOX solution both with and without surfactant.

The relative percentage of surfactant in the GOX solution was calculated using the results of the GOX solution on the carbon electrodes. From the images, videos and results, it was

possible to approximate how much spreading was needed and then design the experiments around this. These results indicated that a spreading of approximately 100% would need to occur for the drop to spread across the whole electrode area, so the drop needs to double in size in order to achieve this. Having used a surfactant percentage of just 0.005% vol vol^{-1} in the electrochemical testing shown above, it was decided to try higher surfactant percentages than this at 0.01%, 0.05% and 0.1% as the spreading at 0.005% was not adequate but could be used as a baseline. If it was found that these concentrations of surfactant were not sufficient then further concentrations could be tested between these to find the correct percentage of surfactant necessary. The solution was deposited as 999 drops off one trigger at the same printer settings as before. The spreading of the solution was once again measured over 2 minutes and they were all plotted to allow for direct comparison. These results can be seen in figure 5.35.

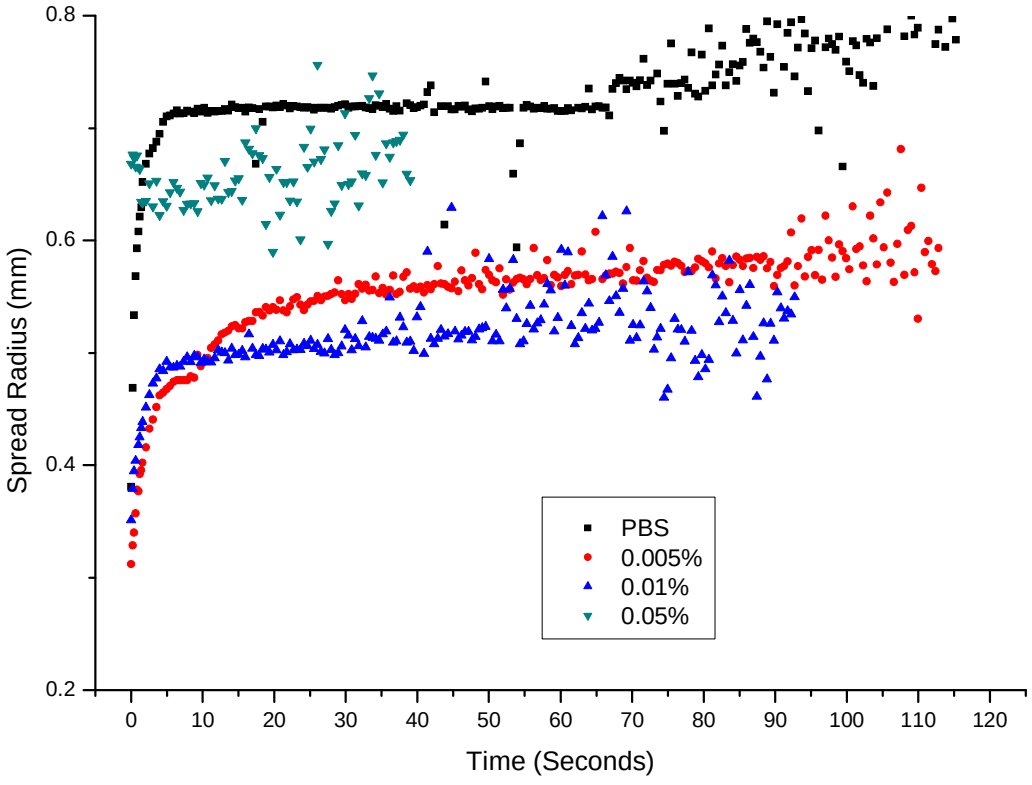

Figure 5.35. Graph showing the degree of spreading encountered when surfactant was added to the enzyme solution in terms of contact angles.

There is seen to be a degree of contact pinning encountered at all concentrations of surfactant whereby the solution spreads to the edge of the electrode but does not possess

enough surface energy to overcome the height of the sample at the edge and spread onto the polyester. At concentrations of surfactant over the 0.05% tested here this spreading is not prevented and therefore makes them unusable.

The surfactant concentration chosen for use with the solution was therefore set at 0.05% as it offered the appropriate amount of spreading over the electrode surface and did not cause the solution to spread over the edge of the working electrode onto the polyester substrate and the reference electrode. The next consideration to be made is how the contact angle and spreading properties of the solution on the electrode surface will be affected by the addition of more fluid onto the initially printed drops. In order to deposit the required 3.19 units of enzyme onto each electrode, working with a concentration of 12,000 U ml^{-1} of enzyme in the sugar solution with 0.05% of surfactant added, approximately 2,000 drops need to be deposited, depending on the initial activity of the enzyme. With the printer only able to deposit 999 drops per trigger in its current set up, the procedure must be repeated 3 – 4 times depending on the exact number of drops required. Thus, we must consider the influence of printing further solution onto dried, or partially dried, deposits.

Several methods were attempted to assess the implications of placing the second series of printed drops onto the electrode including: depositing it immediately after the initial printing run, allowing the first drop to dry in ambient conditions before depositing the second drop and placing the electrodes into a 4^0C controlled temperature environment overnight before printing again. All of these methods resulted in the next drop of fluid, consisting of 999 individual drops from 1 trigger of the printhead, spreading beyond the edge of the electrode (the electrode diameter is marked with the blue line in figure 5.36). The reason for this is thought to be that the electrode is already saturated after the original deposition.

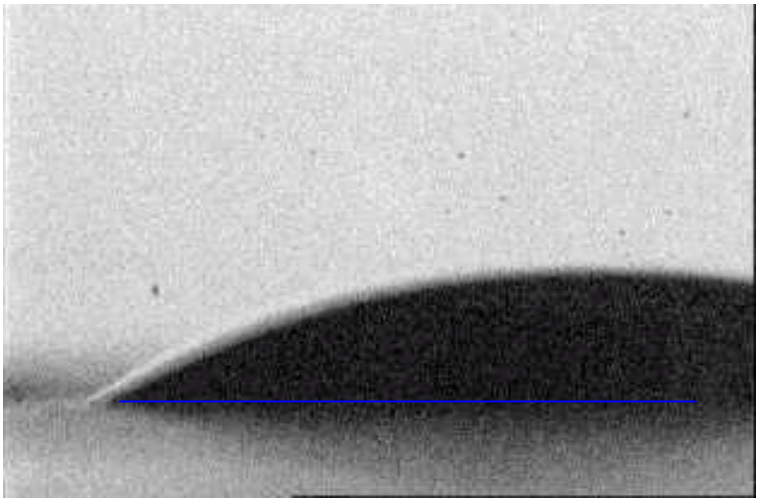

Figure 5.36. Contact angle analysis of the second drop placed on a saturated electrode. Blue line shows the extent of the electrode.

Therefore, a new method for the deposition of the fluid onto the electrode needed to be devised in order to prevent the spreading of the solution onto the polyester and the reference electrode. The root cause of this problem is that the enzyme concentration is insufficient to allow the electrode to be fabricated in a single pass; hence multiple printing runs having to be performed to deposit the correct amount of enzyme. When PCM was carried out on the same electrodes it was clear that the drying had not prevented the spreading, with a large concentration of the dried enzyme and sugar to be found on the reference electrode or the polyester (figure 5.37).

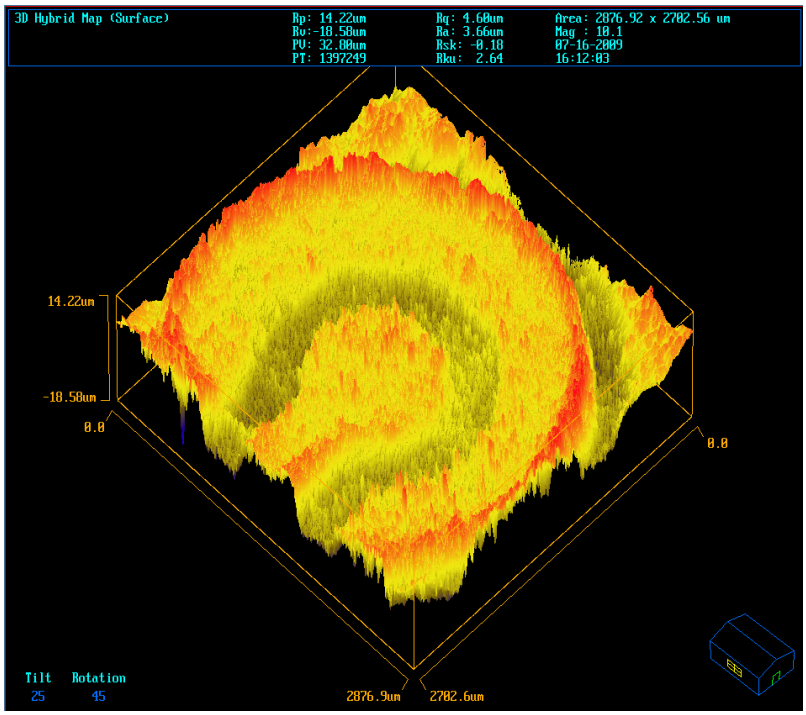

Figure 5.37. PCM image of dried enzyme on electrode surface showing the enzyme to have spread beyond the original electrode and onto the surrounding reference electrode.

Clearly, increasing the concentration of the enzyme in solution so that the enzyme can be deposited on the electrode in a single printing run of < 999 droplets would correct the problem. Currently 3,000 to 4,000 droplets of the enzyme solution are printed. Thus the concentration of the solution would have to be at least tripled to allow single pass printing. A series of samples were made up at 2x, 3x and 4x the normal concentration of GOX (concentrations of 24000, 36000 and 48000 U ml^{-1} of GOX in the sugar solution). These samples were then mixed and left overnight at 4^0C to see if any would come out of solution. It was found that the only solution that had remained 100% in solution was at a concentration of 24000 U ml^{-1}. This concentration was used for all future experiments which meant that at least 2 printing runs would still have to be made in order to deposit the correct amount of solution onto the electrode surface.

An alternative approach to increasing the GOX enzyme solution concentration is to reduce the amount of units deposited onto the electrode surface so that only one printing run is required. However, this may have an adverse effect on the electrode properties and reduce

the electrochemical effectiveness of the electrode making it unreliable. After discussion with AET, this approach was discarded.

The final method available to print suitable electrodes in a single printing pass is to study the effect of the solution drying process on the electrode surface. The interaction of the droplet with the surface is controlled by a combination of drying, absorbing and evaporation processes. It is possible that we can reduce the amount and extent of spreading by controlling the drying process and thus preventing spreading beyond the electrode surface.

5.4.4. Drying conditions and optimal concentrations

As previously discussed, it is postulated that the drying process may have an influence on the properties of the dried solution on the electrode surface and how much spreading occurs. We have already noted that the drying process influences the morphology of a dried drop and can introduce the phenomenon of coffee staining. Analysis of the electrode surface morphology after printing and a range of drying conditions will help identify the influence of drying conditions on deposit morphology. Each electrode was printed using a 60 µm Microfab printhead at 60 V with a pulse width of 25 µs and a frequency of 5000 Hz. The enzyme solution was at a concentration of 24000 U ml^{-1} in the sugar solution Q2090113D3 with a 0.05% vol vol^{-1} surfactant added and two runs of 999 drops were deposited onto the electrode in order to give approximately 3 units present on the surface. These were then dried under three different sample conditions, each having one set of samples in air and one set in a desiccator. The conditions were; at 37^{o}C, at room temperature and at 4^{o}C, all in uncontrolled ambient humidity. These samples were dried for 24 hours at these conditions before being analysed with PCM. The results of these drying experiments are given in figure 5.38.

The PCM method gives an indication of the different heights within a sample and, as such, can give a representation of where the enzyme is present on the electrode surface. In these images, and when they are compared to figure 5.27 shown earlier, the regions of enzyme deposition and drying are indicated by the red peaks. When the electrode has been dried at

4^{o}C (figure 5.38a) it can be seen that the enzyme has dried across both the working and reference electrode, with a defined wall like circular boundary being shown. This is significant as it shows that the enzyme has not dried evenly across the surface but has obviously spread beyond the confines of the working electrode where it is required. Comparing this to the samples dried at room temperature (figure 5.38b) it can be seen that both of the samples have behaved in a similar way with the solution spreading beyond the working electrode surface and drying into a circular rim, just as explained earlier by the coffee staining effect. This does not appear to be the case with the sample made at the 37^{0}C, which shows a more even spread of the solution and a higher surface area. However, the solution has still spread onto the reference electrode in this case too.

All of these experiments were repeated and the same results obtained showing that it was not possible to contain the second printing to the electrode area. It was thought that the lack of control of the ambient moisture content may have been a contributing factor, because this could impede a high rate of evaporation and therefore result in sufficient time for the sample to remain fluid and spread beyond the electrode. By removing this moisture and holding the samples at the same temperature it was hoped that the drying would occur on the working electrode and not the reference electrode. The samples were again prepared under identical conditions to before but were dried in a dessicator to remove the moisture at the same temperature and condition in order to test this hypothesis.

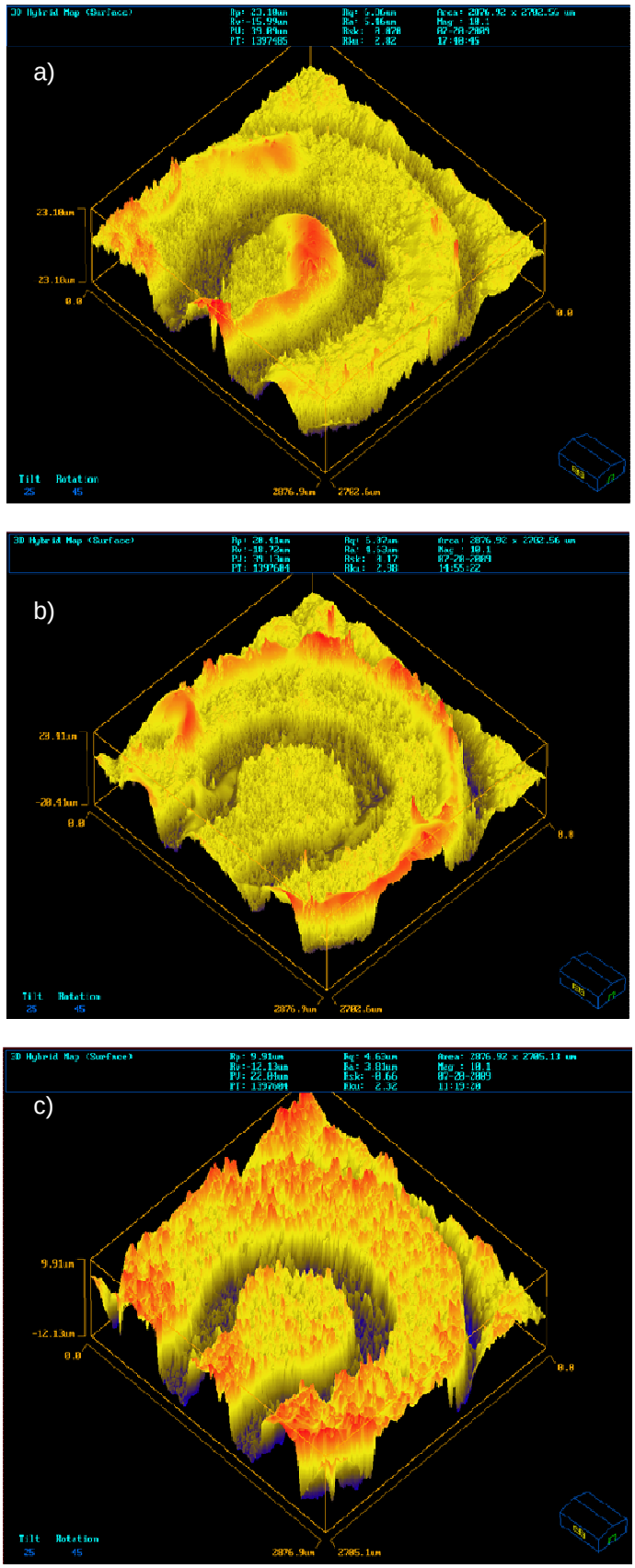

Figure 5.38. PCM images after drying of the electrodes at (a) 4°C (b) Room temperature (c) 37°C

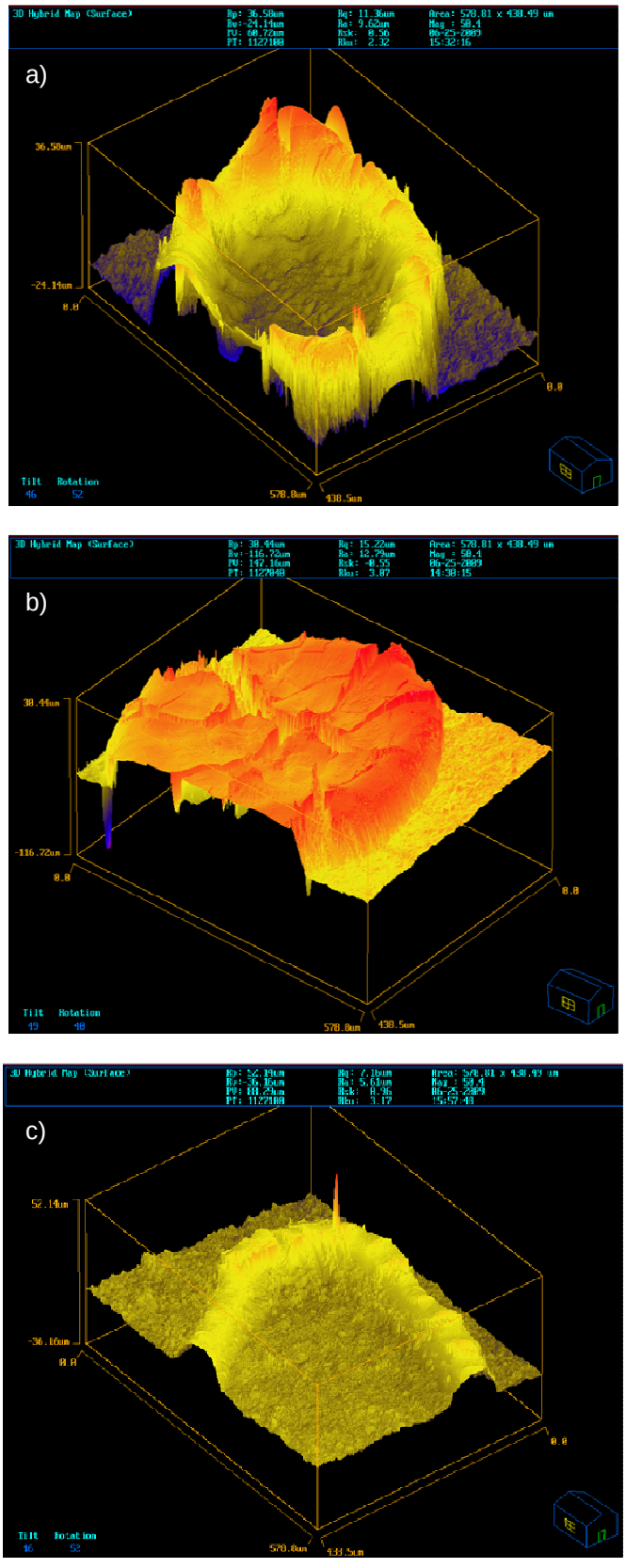

Figure 5.39. PCM images of electrodes dried in a dessicator at (a) 4^{o}C (b) Room temperature (c) 37^{o}C

Figure 5.39 shows PCM images of the dried printed enzyme solution after removal from a dessicator. This process results in more rapid drying and therefore the dried deposit covers a smaller area than was found with drying under ambient humid conditions. Drying in the dessicator resulted in a dramatic decrease in drop spreading and the fluid was now confined to the working electrode. The images displayed in Figure 5.39 are hence enlarged to show the central 1 mm^2 surface area electrode only. The ideal drying conditions from these images appears to be at room temperature, because this condition results in an even spread of the enzyme over the entire surface of the electrode, although the deposit has cracked during the drying process. However, at both 4^oC and at 37^oC the enzyme is not uniformly deposited over the electrode and there is a pronounced ring or coffee staining effect.

The mechanism that leads to optimum performance at an intermediate temperature is not clear. Soltman and Subramanian [162] found that reducing the physical substrate temperature reduced coffee staining and proposed that this was because heat was retained by the thicker drop centre and that the enhanced central evaporation would eliminate coffee staining, however our data suggests that at very low temperatures, coffee staining reappears as a phenomenon during drying. The mechanism for this behaviour clearly needs further investigation but is not considered further in this thesis.

The important considerations here are that the solution dries onto the working electrode only and provides as high a surface area as possible for the enzyme substrate interactions. One technique that can be used to quantify the benefit of this drying process and that drying at room temperature in a dessicator is beneficial, is to test the electrochemical properties of the electrodes after drying as this is to be the end use of the electrodes in the glucose sensing or protein array market.

The electrochemical method enables a measurement to be taken which gives an idea as to the conductive properties of the carbon electrode and the reliability of the enzyme in cleaving the glucose analyte once attached to the surface. These readings are amperometry readings that give a current response based on the concentration of the glucose placed onto the

surface, as outlined in the methods section. This current response is recorded after being held for 40 seconds at a constant voltage. This can be repeated for each concentration numerous times with a new electrode to determine the standard error involved in the process and therefore the reliability and accuracy of the enzyme that has been dried onto the surface. Figure 5.40 shows the results with the samples dried under different conditions.

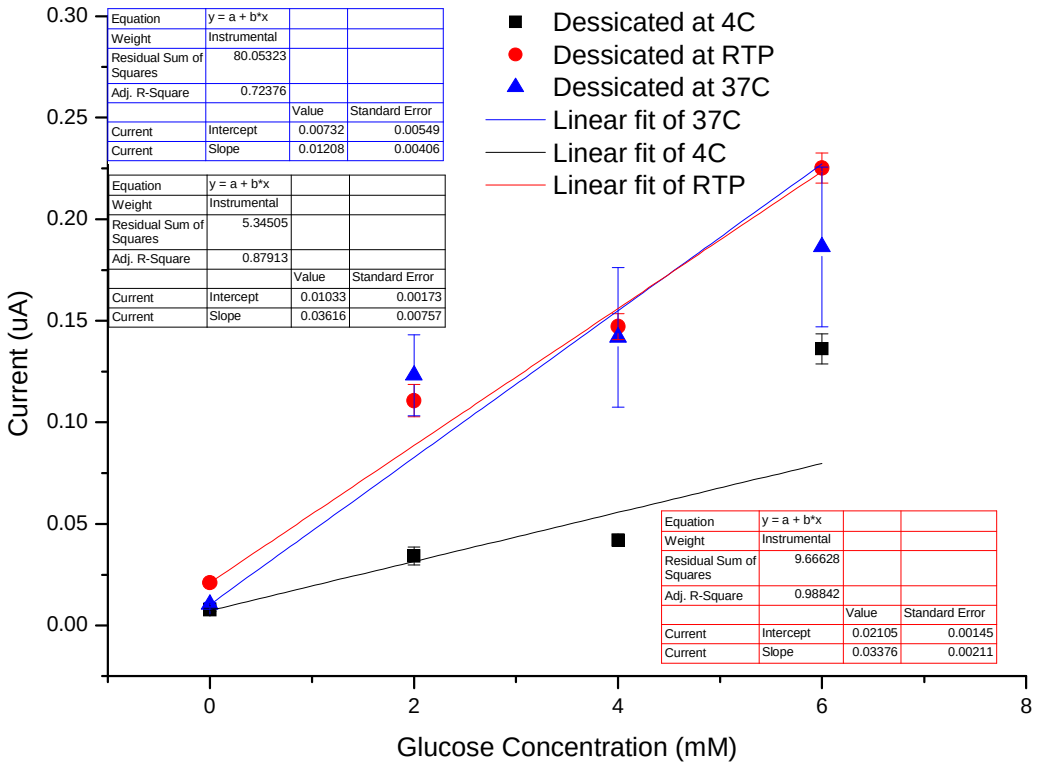

Figure 5.40. Electrochemical properties of the electrodes that were dried in a dessicator at 4^{o}C, Room temperature and 37^{o}C.

This figure shows the current response with different concentrations of Glucose placed onto the electrode surface with a Ferricyanide mediator. The electrode that was dried at 4^{o}C has an obvious drop in the current response in comparison to the other two electrodes. This is not ideal due to the electrode needing to be as sensitive as possible so that minor fluctuations in glucose levels can be read and an accurate reading produced. The electrode dried at 37^{o}C has a much higher response but is very erratic with the readings, as shown by the linear best fit line which produces an r value of just 0.73, making it unreliable for a biosensor system. Finally, the electrode dried at room temperature seems to possess the best properties for a biosensor application with a good r value, showing adequate linearity,

and points that are giving reasonably high current response thus making it reliable and able to detect fluctuations.

Although it has been shown that drying at room temperature is the most effective way to achieve good electrochemical properties and an even distribution of the enzyme, the electrochemical properties of the biosensor are still not fully researched or understood. The final section in this chapter will aim to explore whether it is possible to fine tune the electrode properties to achieve a linear electrochemical current response from the electrode and, if so, to suggest a possible final protocol for the production of the electrodes using a drop on demand inkjet printing technique.

5.5. Method for Production of a Biosensor using Drop on Demand Inkjet Technology

The analysis of the drying conditions and enzyme conformation on the surface of the electrode allow for an initial protocol to be drawn up for the production of Glucose Oxidase electrodes using a Drop on Demand Piezoelectric inkjet printer. To achieve this, further refinement can be carried out to optimise the electrochemical properties of the electrodes and hence the production protocol.

5.5.1. Refining the electrochemical properties of the electrode.

With the current glucose sensor design, 3.19 units of enzyme are deposited onto the electrode surface using a 24000 U ml^{-1} enzyme solution in a sugar buffer with a 0.05% surfactant concentration. With inkjet printing of the sensors, the number of printed drops required to achieve the desired concentration is calculated from the number of units per milligram of enzyme. This is known to vary from batch to batch. In order to optimise the electrochemical properties it is first necessary to check what proportion of enzyme is found on the surface of the electrode at each different concentration of enzyme, namely 1, 2, 3 and 4 units. This was done using PCM images to assess the coverage achieved over the electrode surface as well as whether there was any coffee staining encountered after drying at room temperature. These images are shown in figure 5.41.

The PCM images indicate the location of the enzyme on the electrode surface. The 4 unit sample, shown in figure 5.41d, has obviously spread over the boundaries of the working electrode onto the reference electrode and is therefore deemed to be unsuitable for this process. The remainder of the printed electrodes (figures 5.41a-c) appear to have a similar morphology, with a small ridge appearing on the working electrode representing the enzyme sugar solution. There is a similar distribution of enzyme across the electrodes at the different concentrations with the 2 and 3 unit samples appearing to show a more even distribution and less coffee staining. The PCM images show the contact pinning that was mentioned earlier in section 5.4.1; this is believed to occur when the drop energy is sufficiently large to overcome the boundary between the raised carbon sample and the polyester substrate.

To further characterise the influence of the number of units of enzyme deposited onto each electrode, it is necessary to test the electrodes electrochemically. This will determine whether the number of units deposited has any effect on the current response, as is predicted, and whether this effect is sufficient to consider depositing a higher number of units. To see if this is a commercially viable route requires a more complete cost/benefit analysis. The deposition of the higher number of units of enzyme will require more runs of the printer to print sequential deposits in the same location. This would however increase the production time per electrode sheet when using an inkjet printer.

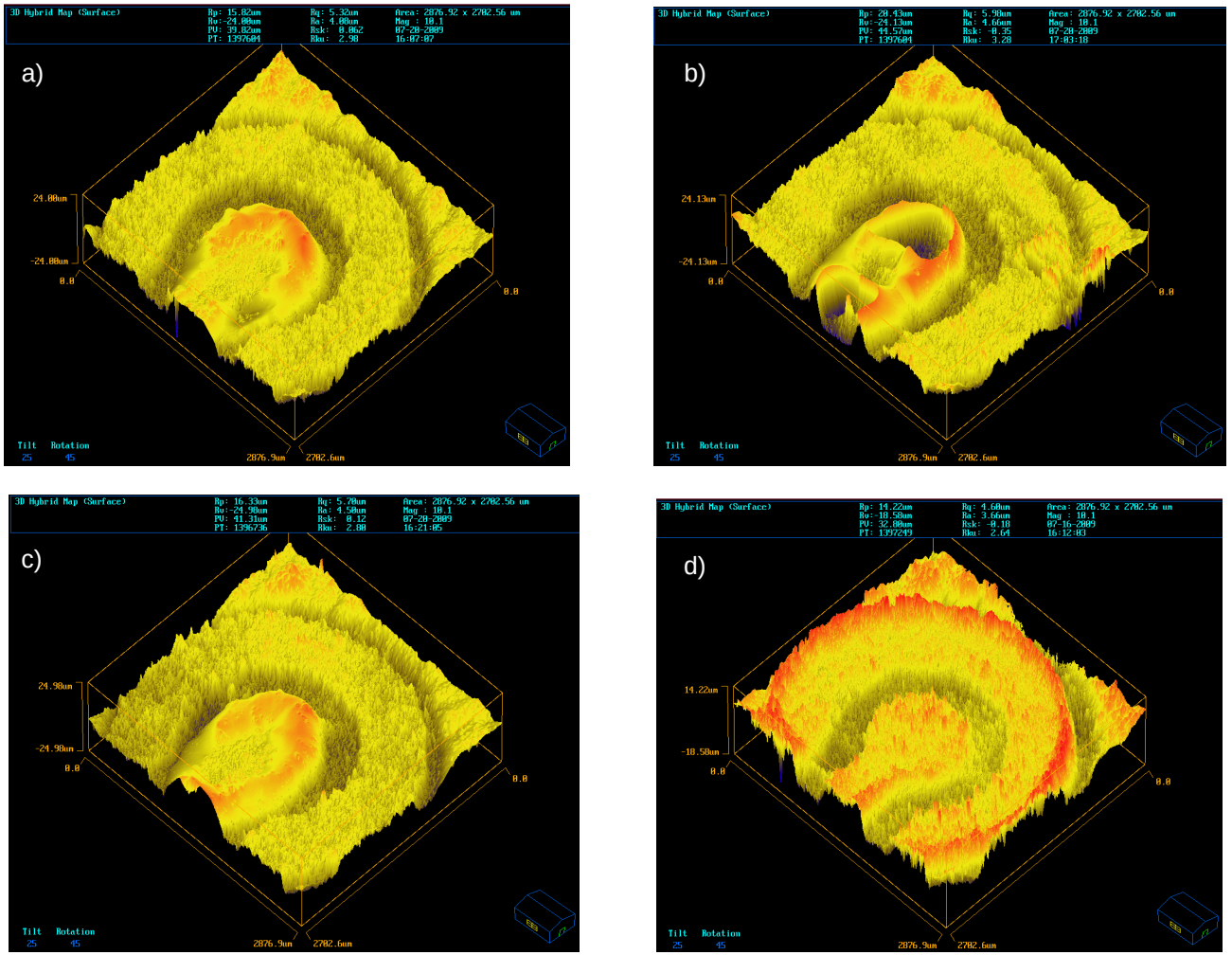

Figure 5.41. PCM images of enzyme deposited onto electrode surface at (a) 1 unit (b) 2units (c) 3 units (d) 4units

The electrochemical response of the electrodes is shown in figure 5.42. The samples were deposited using a Microfab printhead at a frequency of 5000 Hz and a pulse width duration of 25 µs with a 60 V amplitude. The enzyme solution was at 24000 U ml^{-1} in a sugar buffer solution with a 0.05% concentration of surfactant. The frequency of drops deposited with each trigger was adjusted for the number of units being deposited onto the sensor surface. Each electrode was dried at room temperature in a dessicator.

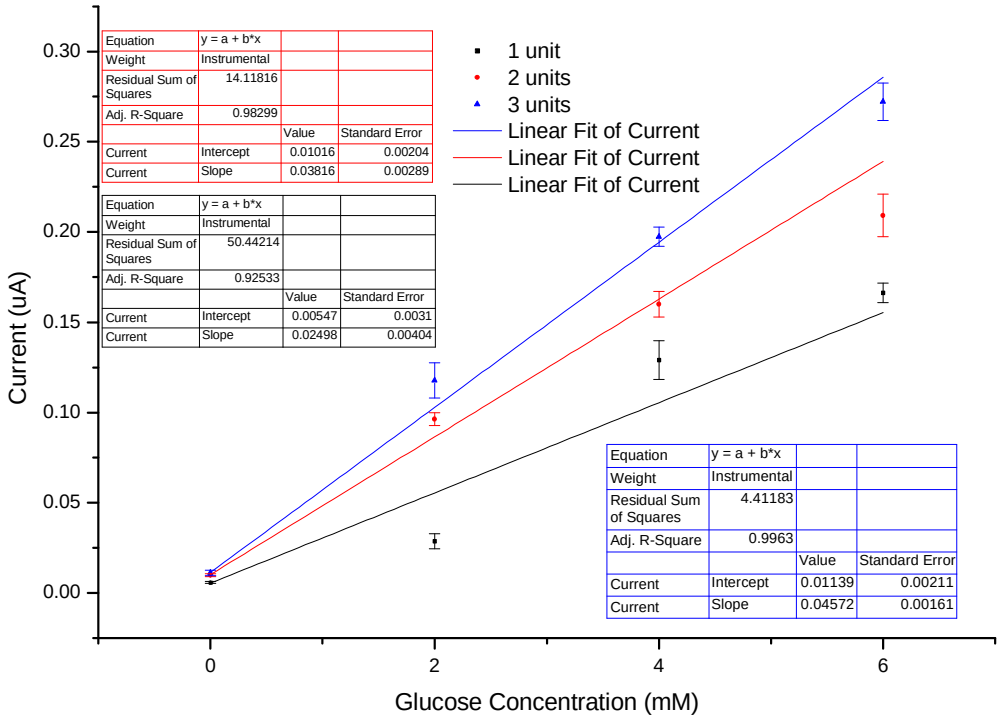

Figure 5.42. Electrochemical analysis of the electrodes with different concentrations of enzyme on the surface.

The electrochemical response as a function of glucose concentration for the different printed electrodes is displayed in figure 5.42. This is found to be dependent upon the number of units of enzyme present on the electrode surface. The response of the electrode to glucose concentration is expected to show a linear relation as each glucose unit converted generates an electron and the rate of conversion will be proportional to the glucose concentration. The more units of enzyme present, the greater the number of glucose molecules that can be converted. If there is insufficient enzyme present the time response of the reaction may result in the rate saturating and thus give too low readings at higher concentrations.

At 1 unit, the current response is low and does not appear to be linear. This non-linearity may be because the number of units printed is low and therefore the relative error between printing runs in terms of protein content would be greater than would be the case with the larger number of units. At 2 units of enzyme, there is a higher current response as would be expected with more enzyme present on the electrode, but there is also less variability in the readings at different glucose concentrations and a more linear trace is evident in figure 5.42.

The same behaviour is observed when the number of units of enzyme deposited is increased to 3 units. The linearity of the current response is also improved when the number of units is increased. This is important as it means that the electrochemistry of the electrode will be more consistent and produce more accurate data at any glucose concentration with a higher number of units of enzyme. However, the maximum number of units that can be deposited cannot exceed 3 because the printed enzyme will spread beyond the electrode pad. Printing too large a number of units will also significantly increase the manufacturing time and reduce the cost effectiveness of the printing route. Thus, it is the recommendation of this report and thesis that the number of units used should be set at approximately 3, with a margin of error of 0.2.

5.5.2. Protocol for the Production of Electrodes using Inkjet Printing.

This section will detail the protocol for the production of the electrodes as determined by this investigation. This protocol is designed specifically for use with the Microfab Printhead which is a drop – on – demand piezoelectric printhead with a single nozzle of 60µm diameter. The protocol is also specific to the Glucose Oxidase enzyme using a sugar buffer solution produced by AET (Applied Enzyme Technologies, Monmouth, Wales, UK). Other enzymes could be substituted into this protocol and although they should not experience any change in structure or conformation, there is no guarantee that the number of units to be printed or the proportion of surfactant in solution will be appropriate for other enzymes.

- Make up a solution of 24000 U ml^{-1} using the GOX enzyme and the chosen sugar buffer solution (from AET). Add 0.05% vol vol^{-1} of Triton X-100 surfactant to the solution.
- Ensure the solution is homogenised completely before progressing.
- Set the Microfab printhead settings to have a pulse width of 25 µs, pulse amplitude of 60 V, frequency of 5000 Hz and a rise and fall time of 3 µs. Also ensure that the drops per trigger are set to 500 and external trigger is selected (only if a motion controller is being used).
- If the head needs to be cleaned then keep the above settings but ensure that the head is set to continuous jetting and jet a solution of de-ionised water through the head.
- Once clean, attach the syringe containing the enzyme solution to the head with some flexible tubing. Ensure that the meniscus of liquid is approximately 2 cm below the head level and secure (if not using a pressure controller).
- Prepare a dessicator with some fresh silica gel.
- Switch on the motion software programme (if available) and the pressure controller (if available). Load the 'electrode' sub programme on the motion controller and ensure that the pressure controller is able to maintain a meniscus of fluid in the nozzle of the printhead. If not then adjust as applicable.
- Place an electrode sheet on the physical substrate plate and secure in the correct position.
- Ensure the motion control software is set to print the correct number of runs for the deposition of 3 units onto the electrode based on the number of units of enzyme per milligram of enzyme.
- Start the motion control software and leave it to complete the programme.
- If not using the motion control software, manually trigger the printhead to print as well as move the electrode sheet in between triggers. It is preferable to print all electrodes before beginning a second run so there is some time for drying to occur.

- Once printed, visually inspect the electrodes to ensure that the printhead has triggered during the printing. If not, repeat the above procedure or refer to a troubleshooting guide.
- If printing has occurred satisfactorily, place the electrodes into a dessicator ensuring they are kept flat to prevent any spreading of the solutions.
- Leave in a dessicator at room temperature for 24 hours to dry completely.
- Once dried, visually inspect the electrodes again to ensure that drying has occurred completely.
- The electrodes are now ready for use.

The exact number of drops required can be calculated based on the number of units per milligram of the enzyme. If the enzyme has an activity of 200 units per milligram and the solution is at 24000 U ml^{-1}, then there will need to be 120 milligrams in a 1 ml solution. To print approximately 3 units, then 3/24000 will give the volume of solution required. In this case it is 0.000125 ml or 125 nl. Based on a probable drop volume of 250 pl, then 500 drops are required to deposit 3 units. However, it is also known that about 50% of the predicted volume of enzyme is actually printed. To counter this, then double the amount of drops need to be printed, so 1000 drops are required to print 3 units. With one trigger producing 500 drops, then 2 runs are necessary to deposit the correct activity onto the electrode surface.

CHAPTER 6: CONCLUSIONS AND FURTHER WORK

The conclusions drawn from this study have inevitably led to a body of potential further work and improvements; as such this section will acknowledge the improvements required and identify areas of interest for the advancement of this technique.

The re-consideration of the aims of this work will help in defining the outcomes and success of this project as well as inform what extra work can be carried out. The aims, as outlined in the introduction, were to:

- Outline the current technologies used in the deposition of biological macromolecules for the purposes of manufacturing electrochemical sensors and the considerations that must be made when designing a new deposition technique,
- Justify the requirement and need for a new deposition technique in business and economic terms,
- Understand the effect the deposition technique may have on the protein macromolecules which are to be deposited onto the sensors and, if necessary, ameliorate the effect,
- Analyse the characteristics of the physical substrate surface both before and after deposition of the biological macromolecules,
- Analyse the reproducibility and repeatability of the deposition of the biological macromolecules, especially with regards to the properties of the completed sensor,
- Conclude whether or not the deposition technique is viable for the purpose of depositing biological macromolecules for use in electrochemical sensors and why,
- Recommend further work that should be carried out to enable the technique to be taken to market.

These aims will be assessed one at a time to assist in defining the overall success of the project and report what further work can be carried out to produce a marketable product.

6.1. Technical Aspects

6.1.1. Current Technologies

This work has demonstrated that there are several technologies that have been developed for the deposition of biological macromolecules onto physical substrates. These techniques can be classified as either contact or non contact printing techniques and use several different technologies, which vary in terms of the method they use to deposit the solution onto the physical substrate whether physical stamping or charging of a stream of drops to deposit them in specific areas of a physical substrate.

This work specifically focussed on the technologies used in the biosensor commercial sector, with an extra emphasis on those used in the deposition of enzymes in the glucose sensing market. The technology currently most used in the biosensor market for the deposition of biological macromolecules is Biodotting. This deposits µl of the required macromolecule onto the physical substrate surface accurately and repeatably. The technique has proved to be a successful and reliable method for the deposition of biological macromolecules onto a biosensor substrate surface. Inkjet printing technology, which was chosen for this work, has been proven to offer the opportunity to deposit biological macromolecules accurately, repeatably, and quickly onto the physical substrate through various previous pieces of work [146]. The challenge in this study was to ensure that these same qualities existed when depositing an enzyme solution onto a biosensor surface.

In order to demonstrate this technology, it was important to consider the following; the ability to deposit enzymes without damaging or denaturing their structure, the ability to accurately deposit the enzyme onto the biosensor surface to at least the same degree as the current technology, the ability to deposit aqueous solutions, and the ability to up-scale the technique to be used for large scale manufacturing of the biosensors or increased.

In order to continue to develop the knowledge already referenced in this work, it is important to maintain a working knowledge of the current techniques and research ongoing in this

specific market. The work can also be continued by carrying out a comparison study between the current technique and that demonstrated in this work to justify the use of it and demonstrate its advantages in a wider market environment and context.

6.1.2. Market Requirement

This work has shown the requirements and opportunities that exist for a new technology in the biosensor market. It is already known that an enzyme deposition technique is required to deposit enzymes in an accurate, repeatable manner and that the survivability of the enzyme is a key concern, especially in a technique such as piezoelectric inkjet printing. However, this work has also gone further and addressed the real market requirement of the technology, in so much as to say how it offers increased profitability and advantages over the existing technology.

Piezoelectric inkjet printing has the potential to deposit volumes of liquid in the pl range. Although there is no requirement for such small volumes of sample to be deposited in the blood glucose market, due to limitations in the blood sample required to get an accurate reading, it does offer the capability to meet a separate and potentially more valuable requirement, that of multi enzyme sensors. These sensors would offer the opportunity for diagnosis of several conditions with a single sensor. The accuracy and resolution of the inkjet printing technique would allow multiple enzyme sensors to be produced in large numbers, at speed and low cost. This work has proven the opportunity that exists for this and for the sponsoring companies to enter this market with a fairly developed and proven technology. This is explored further in section 6.2.

Despite this piece of work concluding that there is a market requirement for a technology such as inkjet printing to be made available for the prototyping and manufacture of multi enzyme sensors, there is very little data and figures available in the public domain to reinforce this conclusion. It is therefore important that as a result of this work, more research is carried out into the applicability of the technology to the multi enzyme sensor and the true market potential. The commissioning of a market research study may assist in (dis) proving

the conclusions drawn from this piece of work and help outline the true market value for the technology, both in the glucose market and the market for the testing of multiple analytes.

6.1.3. Effect of the printing technique on the enzyme

One of the major considerations of this piece of work was the effect of the printing technique, and the shear strains induced in the printhead, on the proteins. Therefore, this work dedicated a large amount of resource and time to analysing the true effect of the printing technique on the protein structure and conformation, using light scattering, analytical ultracentrifugation and circular dichroism. Although these techniques are commonplace in the analysis of proteins, there had not been any such in depth study of the effect of the printing process on enzyme characteristics before when a literature search was carried out.

The conclusions drawn from this element of the work demonstrate that although there is seen to be a drop in activity of the protein upon printing when testing through a simple fluorescence assay, there is not seen to be any lasting effect on the protein structure or conformation, as shown by the analytical ultracentrifugation and circular dichroism technique. The results disagreed with those found when testing the same samples through a light scattering technique, however this was proven to be due to the light scattering technique not being sensitive enough. The most important parameters, molar mass and hydrodynamic radius, remain unchanged after passage through the printhead.

It was therefore concluded that the reasons for the drop in enzyme activity were due to environmental factors and not caused by any printer related parameters. This was not an unexpected result due to work carried out before by Nishioka [146] and Setti [144] but it was also shown that the use of the stabilisation solutions assisted in improving the ability to print the enzyme onto the biosensor substrate.

In order to improve this work and build on the conclusions found herein, a more in-depth analysis of the printing technique, including the determining and controlling the exact shear strains found within the head, could be carried out. The protein could be exposed to the

same shear strains as found in the printhead whilst being monitored in one of the analytical techniques. This would allow the true effects of the shear strain to be understood and may lead to more targeted solutions that could be developed by AET to ameliorate any effect.

6.1.4. Surface characterisation

The surface characterisation element of this project was focussed on two main points; firstly, analysis of the properties of the sensor surface including the reproducibility of the sensors, and secondly, analysis of the drop properties when on the sensor surface, including the properties as the solution dries onto the surface.

The electrode surface itself was found to be repeatable between samples, demonstrating the suitability of the screen printing technique for the production of the sensors themselves. The surfaces were also found to be fairly smooth, with some low levels of impurities present within the surface, none of which were thought to interfere with the electrochemical properties of the sensor.

The properties of the drop on the surface of the electrode were found to be mostly dependent upon the concentration of the surfactant within the solution and the number of drops and therefore volume of solution deposited. In order to ensure that the drop did not spread beyond the bounds of the working electrode, experimentation determined the correct surfactant concentration and number of drops to be deposited.

During drying, the drop was found to drop in volume mostly due to evaporation, rather than large amounts of absorption, a finding that was common across all samples tested, despite there being different levels of porosity across the sample set. This did, however, have a separate effect of contact line pinning which led to solute segregation at the pinned line during drying, known as coffee staining. Further analysis on this effect revealed that treatment of the sample with the correct drying conditions helped negate this effect in the majority of samples.

Although this element of the work was carried out in a thorough manner, it addressed the problem from an engineering perspective to design a procedure that worked, and is therefore limited in its extent. In order to strengthen the conclusions drawn in this section of the work more analysis is required of the drying effect and the associated coffee staining encountered. This should be done with special relevance to the Marangoni flow and the surface contaminants on aqueous samples that reduces the Marangoni number and encourages coffee staining.

It would also be beneficial to the work, to replicate the studies carried out using PCM and SEM on the surface characterisation of the electrode with a method that is more able to differentiate the electrode surface from the dried enzyme solution on the surface. Such a technique would assist in proving whether or not the dried enzyme solution is coffee staining and what form it takes once dried onto the surface.

6.1.5. Reproducibility and Repeatability

This section refers to proving the capability of a sensor made using a piezoelectric inkjet deposition technique. This takes the form of electrochemical testing and proving that when electrochemical testing is undertaken, the results taken are repeatable and reproducible over several representative samples. In terms of repeatability, it refers to all of the measurements being within one standard error of the average measurement, and all of these falling within the correct band on the Clarke error grid. The reproducibility refers to these measurements being reproducible over several different batches, and hundreds of samples.

The work contained within this document has proved the principle of an inkjet printer being used for the deposition of enzymes onto a biosensor surface in terms of the provisioning of the ability to manufacture a biosensor which gives an adequate electrochemical response. However, and more importantly, it has also shown that this electrochemical response is repeatable across a small sample size, and the degree of error is low. This needs to be compared to a Clarke error grid to understand the results against industrial standards.

In terms of taking this technique to market, the degree of reproducibility of the deposition technique, especially with reference to the electrochemical response of the samples, needs to be analysed. This needs to be done over a large sample size, and needs to be done to demonstrate the reproducibility especially when attempting to up-scale the technique to mass market manufacture. This should also be carried out to test that the printing process itself is repeatable in terms of drop size and placement.

6.1.6. Overall Conclusions

The overall success of this work can be judged by measuring the outcomes against the aims. It is the conclusion of the author that this work has been successful in demonstrating the principle of the use of an inkjet technology for deposition of the glucose oxidase protein onto a biosensor for use in glucose sensing.

However, the project did not address the potential for using this technology in a much wider market such as multiple enzyme sensors or for infectious diseases. The background work carried out here in terms of protein analysis after printing has gone some way to address the problems and to make a case for the technology being used more widely in protein applications but there still needs to be a much wider sample size analysed to confirm that the results encountered here are similar when the protein type and structure is varied.

This work did not address the applicability of this process in a manufacturing environment rather than a prototyping environment. This means that the use of this technique for mass production of enzyme sensors of any type would require a printer with multiple heads and large solution reservoirs to be able to test the reproducibility of the technique over many thousands of sensors and hours of printing.

An associated problem with this that may be encountered is the operational and shelf life stability of the enzyme due to the large timescales and samples required. Again, this work has addressed the problem, and suggested a solution with the use of AET stabiliser solutions, but has not carried out a mass analysis of several different samples to prove that

the use of these would prevent the loss of activity and protein stability that was encountered when the first fluorescence analysis was carried out at the start of this project.

Therefore, in conclusion, whilst this work has begun to answer many questions about the suitability of the inkjet printing process to the biosensor market, there are many other issues and questions that have come to light. The next section will cover what further work should be considered to assist in answering these new questions.

6.1.7. Further work and Recommendations

This section will aim to summarise what further work could be carried out to enhance the knowledge gained from this project and move towards a more complete understanding of the use of inkjet printing for the deposition of enzymes for biosensors. This work is extra to the work mentioned in the above sections and attempts to capture the major recommendations from the overall conclusions captured in section 6.1.6.

Begin to investigate the use of inkjet printing for infectious diseases, array technology and lab on a chip technologies. The first step will be to understand the effect the printing has on a much larger group of proteins that could be used in this market by initially using the Light Scattering and AUC analysis carried out herein. The use of AET stabilisation solutions then needs to be considered if it is found that the proteins are more susceptible to damage than the GoX protein was found to be.

Analyse the effectiveness of the printing technique for deposition of multiple enzymes onto a sensor surface with the aim of developing tests for multiple analytes that can be used in lab on a chip or in array technology. This would require the use of a large scale industrial printer with large reservoirs and multiple heads. A more in depth investigation would be required into the correct parameters for the printing process for each protein.

Finally, it would be necessary to carry out some investigations into the shelf life of the solution both prior to printing and post printing to ensure that stability of the protein would not

be affected in a large scale manufacturing situation. There is an opportunity to develop some novel solutions with AET, using their current protein stabilisation solutions as a base, to use and market alongside the printer for the manufacture of the biosensors.

6.2. Business outcomes

The business outcomes for this project were primarily aimed at producing a marketable and useable product for one or more of the companies involved in the project consortium. Therefore, the projects business outcomes have been split into sections detailing the outcomes for each consortium member as well as some summary information detailing possible dissemination options for this technology. The companies involved in the consortium were Xaar (the printhead supplier), Applied Enzyme Technologies Limited (the enzyme provider) and Ellis Developments (the provider of woven substrates).

6.2.1. Xaar

Unfortunately, the business outcomes for Xaar do not deliver a marketable product, mainly due to the problems outlined earlier on in the document including the poor aqueous compatibility of the printheads due to a lack of a parylene coating on the head internals. However, the project has proven that there is a capability for the printing of proteins using a piezoelectric inkjet printer which is a similar technology to that used by Xaar in their printheads.

The technology used in this project has mainly been the Microfab printhead which is a single nozzle piezoelectric head using a radial compressive force from a tubular actuator. The Xaar printhead that was intended to be used was the XJ126 printhead which is a more complex printhead with 126 nozzles. This uses a shear wall actuation with shared walls between each nozzle, meaning that only one third of the nozzles can trigger at once with a small time delay between the sets of nozzles firing. This shared wall technology is primarily to make a compact device.

With this in mind, it is reasonable to assume that the Xaar technology will still abide by the principles that have been studied in this project and could therefore be marketed as a protein compatible printhead. The only issues with this are that the main production quality printheads are for oil based inks and therefore do not work well with aqueous fluids. In order to combat this Xaar would need to Parylene coat the heads in order to prevent damage to the heads when using aqueous fluids. This was another outcome of the project that was not able to be completed due to issues with the contributions of Xaar during the project life.

6.2.2. AET Ltd

With AET being the largest contributor in terms of raw materials and knowledge to this project it is no surprise that the company also benefits from the largest output of all of the companies in the conglomerate. The major outputs for AET Ltd from the project was to prove that the inkjet printing technique could be used to produce electrodes and that the solutions used to produce these electrodes were using the AET buffer solutions which are specially formulated to confer extra stability to the enzyme from both temperature and shear strain forces.

With the success of the printing of the electrodes using the AET buffer solutions, it is reasonable to state that the solutions are ‘printer friendly’ and can be used in conjunction with proteins for deposition by piezoelectric inkjet printing. Whether the buffer solutions confer extra stability onto the enzyme through printing and over time is something which AET is continuing to study and which looks positive. With this proof of principle combined with the proof of the printability of the buffer solutions, AET have a product which can be used to compliment the printing process and hopefully the enzyme survivability.

There is also the opportunity for AET to work alongside the University to develop a printing platform and associated stabilisation solution that can be used for the deposition of multiple different solutions onto a single physical substrate for the development of lab on a chip or array technology.

6.2.3. Ellis Developments

Ellis Developments were originally part of the consortium with the aim of producing a woven physical substrate for use with the cell printing technology. Although there has been some previous work carried out on the cell printing aspect of this project, no meaningful results have been generated as yet due to the lack of printing support from Xaar and the collapse of an early project partner who were to provide the cell lines for printing. Thus, no meaningful outcomes have been generated for Ellis Developments, though it is hoped that the remaining time on the project will deliver some outcomes which will lead to further work and sponsored projects.

6.2.5. Project Dissemination

The future of biosensor technology is widely believed to be either in the constant detection and supply area where the patient has an implant which can constantly monitor glucose levels and supply insulin accordingly, or in the development of detecting multiple analytes which can detect for multiple different conditions with a single sample.

The specific outcomes for each project partner have been outlined above and this section aims to outline how the technology used in this project may be disseminated to make maximum use of it and to enable maximum profitability for the companies involved. The dissemination of the technology mainly revolves around the buffer solutions provided by AET. These solutions have been proven to be inkjet compatible and can therefore be sold as such. They are also proven to give good electrochemical properties when deposited along with the protein onto a sensor.

In order to maximise their impact in the market place it would be recommended to partner the buffer solutions with a printhead provider so that they can be sold and are recognised as suitable for inkjet printer heads. Whether this provider could be Xaar would depend on the outcomes of the project with respect to the use of their heads with aqueous solutions. There could also be a dissemination event whereby the technology could be demonstrated to potential investors and buyers of the technology. Finally, further funding could be applied for

in order to carry out further work to develop a printing platform for use in multiple array technologies as well as developing an associated stabilising solution to help the operational and shelf life stability of the protein to position the overall product squarely at the manufacturing of biosensors area.

CHAPTER 7: REFERENCES

1 Alper J., Biology and Inkjets, Science, 305, p. 1895, 2005.

2 Eggins B., Biosensors: An Introduction, 2 ed, John Wiley and Sons, 212, 1997.

3 Leech D., Affinity Biosensors, Chemical Society Review, 205, 1994.

4 Hall E.A.H., Biosensors, Open University Press, Milton Keynes, 1990.

5 Meier H., L.F., Tran C.M., Application and automation of Flow Injection Analysis (FIA) using fast responding enzyme glass electrodes to detect Penicillin in fermentation broth and Urea in human serum, Journal of Automated Chemistry, 14, 137, 1992.

6 Wang J., Electrochemical Glucose Biosensors, Chemical Reviews, 108, 2, 814-825, 2008.

7 Crouch E., Cowell D.C., Hoskins S., Pittson R.W., Hart J.P., Amperometric, Screen Printed, Glucose Biosensor for Analysis of Human Plasma Samples Using a Biocompatible, Water-based Carbon Ink Incorporating Glucose Oxidase, Anal Biochem, 347, 17-23, 2005.

8 Sprules S.D., Hart J.P., Pittson R., Wring S.A., Evaluation of a new disposable Screen Printed sensor strip for the measurement of NADH and its modification to produce a Lactate biosensor employing microlitre volumes, Electroanalysis, 8, 539-543, 1996.

9 Gilmartin M.A.T., Hart J.P., Development of one shot Biosensors for the measurement of Uric acid and Cholesterol, Anal Proc, 32, 341-345, 1995.

10 Hart J.P., Serban S., Jones L.J., Biddle N., Pittson R., Drago G.A., Selective and Rapid Biosensor Integrated into a Commercial Handheld Instrument for the measurement of Ammonium ions in sewage effluent, Anal Letts, 39, 1657 - 1667, 2006.

11 Honeychurch K.C., Hart J.P., Recent developments in the design and application of Screen Printed electrochemical sensors for monitoring Metal pollutants in Biomedical, Environmental, and Industrial samples, Trends in Anal Chem, 22, 456-459, 2003.

12 Guell R., Aragay G., Fontas C., Antico E., Merkoci A., Sensitive and stable monitoring of Lead and Cadmium in Seawater using Screen Printed Electrode and Electrochemical stripping analysis, Analytica Chimica Acta, 627, 219-224, 2008.

13 Seddon B.J., Shao Y., Girault H.H., Printed Microelectrode array and Amperometric Sensor for Environmental monitoring, Electrochimica Acta, 39, 2377-2386, 1994.

14 GEM website: Technical Information: Screen printing (accessed on 28/03/2011).

15 http://www.andrew.cmu.edu/course/39-801/theory/theory.htm (accessed on 28/03/2011)

16 Brett C.M.A., Brett A.M.O., Electroanalysis, Oxford Chemist primers, ISBN 0-19-8541816-8, 2005.

17 Menshykau D., Huang X., Rees N.V., del Campo F.J., Munoz F.X., Compton R.G., Investigating the Concept of Diffusional Independence. Potential step transients at Nano and Micro Electrode arrays: theory and experiment, Analyst, 134, 343-348, 2009.

18 Gilmartin M.A.T., Hart J.P., Patton D.T., Prototype, solid-phase, Glucose Biosensor, Analyst, 1973-1981, 1995.

19 Kahlert H., Reference Electrodes, Electroanalytical methods, 3, 291-308, 2010.

20 Kissinger P.T., Heineman W.R., Cyclic voltammetry, Journal of Chemical Education, 60, 702-706, 1983.

21 Wang J., Analytical Electrochemistry - 3rd edition, John Wiley & Sons Inc, New Jersey, 2006.

22 van Benschoten J.J., Lewis J.Y., Heineman W.R., Roston D.A., Kissinger P.T., Cyclic Voltammetry Experiment, Journal of Chemical Education, 60, 772-775, 1983.

23 Bhatt A., Dryfe R.A.W., Hydrodynamic Voltammetry at membrane covered Electrodes, Journal of electroanalytical chemistry, 584, 2, 131-140, 2005.

24 Scholz F., Electroanalytical methods, Springer, ISBN 3540422293, 2002.

25 Ruzicka J., Hansen E.H., Flow Injection Analyses: Part 1. A new concept of fast continuous flow analysis, Analytica Chimica Acta, 78, 145-157, 1975.

26 Ruzicka J., Hansen E.H., Retro-view of flow-injection analysis, Trends in analytical chemistry, 27, 390-393, 2008.

27 Compton R.G., Fisher A.C., Tyley G.P., The Wall-jet Electrode and the study of Electrode reaction mechanisms: the EC reaction, Journal of Applied Electrochemistry, 20, 912-915, 1990.

28 Schmid R.D., Kunnecke W., Flow Injection Analysis based on Enzymes or Antibodies, applications in the life sciences, Journal of Biotechnology, 14, 3-31, 1990.

29 Milardovic S., Kruhak I., Ivekovic D., Rumenjak V., Tkalcec M., Grabaric B.S., Glucose Determination in Blood samples using Flow Injection Analysis and an Amperometric Biosensor based on Glucose Oxidase immobilised on Hexocyanoferrate modified Nickel electrode, Analytica Chimica Acta, 350, 91-96, 1997.

30 Stephens S.K., Tothill I.E., Warner J., Turner A.P.F., Detection of Silage effluent pollution in River Water using Biosensors, Water Research, 31, 41-42, 1997.

31 Serban S., Danet F.J., El Murr N., Rapid and Sensitive Automated method for Glucose monitoring in wine processing, Journal of agricultural and food chemistry, 52, 5588-5592, 2004.

32 Home S.P., Home test market reaches $1.4 billion, US Pharmacist, 23, 3, 1998.

33 Lipsitz R., Pregnancy tests, Sci Am, 283, 110-1, 2000.

34 Quattrochi E., Hove I., Ovulation & pregnancy: home testing products, US Pharmacist, 23, 9, 1998.

35 Rosenthal W.M., Briggs G.C., Home Testing and Monitoring devices, In: Berardi R.R., DeSimone E.M., Newton G.D., Oszko M.A., Popovich N.G., Rollins C.J. et al, eds. Handbook of nonprescription drugs, 13th ed, Washington DC: R.R. Donnelley and Sons, 1017-48, 2002.

36 Lee-Lewandroski E., Lewandroski K., Selected topics in point-of-care testing: Urinanalysis, Pregnancy testing, Microbiology, Foecal Occult Blood, and other tests, Clin Lab Med, 21, 389-404, 2001.

37 Wilcox A.J., Baird D.D., Dunson D., McChesney R., Weinberg C.R., Natural limits of Pregnancy testing in relation to the expected Menstrual period, JAMA, 286, 1759-61, 2001.

38 Ascheim S., Zondek B., The Hormone of the Anterior lobe of the Hypophysis and the Ovarian hormone in the Urine of pregnant womenz, Klin Wochenschr, 6, 1322, 1927.

39 Tietz N.W., Comparative study of Immunologic and Biologic Pregnancy tests in early Pregnancy, Obstet. Gynaecol. 25, 197-200, 1965.

40 Rees L.H., Holdaway I.M., Kramer R., McNeillt A.S., Chard T., New bioassay for Luteinizing Hormone, Nature, 244, 232-234, 1973.

41 Wide L., Gemzell C.A., An immunological pregnancy test, Acta Endocrinol, 35, 261-267, 1960.

42 Pierce J.G., Parsons T.F., Glycoprotein hormones: structure and function, Annu Rev Biochem, 50, 465-468, 1981.

43 Wehmann R.E., Blithe D.L., Flack M.R., Nisula B.C., Metabolic clearance rate and Urinary clearance of purified Beta-core, J Clin Endocrinol Metab, 69, 510-517, 1989.

44 Chard T., Pregnancy tests: a review, Human reproduction, 7, 5, 701-710, 1992.

45 Norman R.J., Lowings C., Chard T., Dipstick method for Human Chorionic Gonadotrophin suitable for emergency use on whole Blood and other fluids, Lancet, 1, 19-20, 1985.

46 Vaitukaitis J.L., Braunstein G.D., Ross G.T., A RIA which specifically measures hCG in the presence of LH, Am J Obstet. Gynecol., 113, 751-757, 1972.

47 Clark L.C. Jr., Lyons C., Electrode Systems for Continuous monitoring in Cardiovascular surgery, Ann. N.Y. Acad. Sci, 102, 29,1962.

48 Guilbault G.G., Lubrano G.J., An Enzyme Electrode for the Amperometric determination of Glucose. Anal. Chim. Acta., 64, 439, 1973.

49 Mullen W.H., Keedy F.H., Churchouse J.S., Vadgama P.M., Glucose enzyme electrode with extended linearity: Application to undiluted Blood measurements. Anal. Chim. Acta., 183, 59, 1986.

50 Miyabayashi A., Mattiasson B., An Enzyme Electrode based on Electromagnetic entrapment of the Biocatalyst bound to Magnetic beads. Anal. Chim. Acta., 213, 1-2, 121, 1988.

51 Wang J., Glucose Biosensors: 40 years of advances and challenges, Electroanalysis, 13, 12, 2001.

52 Malitesta C., P.F., Torsi L., Zambonin P., Glucose fast-response Amperometric Sensor based on Glucose Oxidase immobilized in an Electropolymerized poly(o-phenylenediamine) film, Anal. Chem., 62, 24, 1990.

53 Zhang Y., H.Y., Wilson G.S., Moatti-Sirat D., Poitout V., Reach G., Elimination of the Acetaminophen Interference in an Implantable Glucose Sensor. Anal. Chem., 66, 7, 1994.

54 Wang J., Liu J., Fang L., Chen L., Highly Selective Membrane-Free Glucose Membranes, Anal. Chem., 66, 3600, 1994.

55 Chi Q., Dong S., Amperometric Biosensors based on the Immobilization of Oxidases in a Prussian blue film by Electrochemical codeposition, Analytica Chimica Acta, 310, 3, 1995.

56 Wang J., Wu H., Highly Selective Biosensing of Glucose utilizing a Glucose-Oxidase/Rhodium/Nafion Biocatalytic/Electrocatalytic/Permselective Surface Microstructure, J. Electroanal. Chem, 395, 287, 1995.

58 Reach G., Wilson G.S., Can continuous Glucose Monitoring be used for the treatment of Diabetes?, Anal. Chem., 64, 6, 1992.

59 Armour J.C., Lucisano J.Y., Mckean B.D., Gough D.A., Application of Chronic Intravascular Blood Glucose sensor in Dogs, Diabetes, 39, 12, 1990.

60 Wang J., Lu F., Oxygen-Rich Oxidase Enzyme Electrodes for Operation in Oxygen-Free Solutions, Am. Chem. Soc., 120, 5, 1998.

61 D'Costa E.J., Higgins I.J., Turner A.P.F., Quinoprotein Glucose Dehydrogenase and its application in an Amperometric Glucose sensor, Biosensors, 2, 2, 1986.

62 Cass A.E.G., Davis G., Francis G.D., Hill H.A.O., Aston W.J., Higgins I.J., Plotkin E.V., Scott L.D.L., Turner A.P.F., Ferrocene-mediated Enzyme Electrode for Amperometric determination of Glucose, Anal. Chem., 56, 4, 1984.

63 Frew J.E., Alan H., Hill O., Electrochemical Biosensors, Anal. Chem., 59, 15, 1987.

64 Kirk J.K., Rheney C.C., Important features of Blood Glucose meters, J Am Pharm Assoc (Wash), 38, 2, 1998.

65 Varghese D., Deshpande M., Xu T., Kesari P., Ohri S., Boland T., Advances in tissue engineering: Cell printing, The Journal of Thoracic and Cardiovascular Surgery, 129, 2, 470-472, 2005.

66 Livache T., Fouque B., Roget A., Marchand J., Bidan G., Teoule R., Mathis G., Polypyrrole DNA chip on a Silicon Device: example of Hepatitis C virus genotyping, Analytical Biochemistry, 255, 188-194, 1998.

67 www.chromatography-online.org, accessed on 21/08/06.

68 Pauling L., Corey R.B., Configurations of Polypeptide Chains with favoured Orientations around Single Bonds; Two new pleated sheets, Proc. Natl. Acad. Sci. USA., 37, 11, 729-40, 1951.

69 http://fr.academic.ru/pictures/frwiki/65/AlphaHelixProtein_fr.jpg, accessed on 28th June 2010.

70 Branden C., Tooze J., Introduction to Protein Structure, 2 ed, Garland Publishing, 1999.

71 http://wiki.chemprine.chemeddl.org/images/1/1a/Parallel_antiparallel_beta_sheet.GIF, accessed on 28th June 2010.

72 Hecht H.J., Schomburg D., Kalisz H., Schmid R.D., The 3D structure of Glucose Oxidase from Aspergillus niger; Implications for the use of GOD as a Biosensor Enzyme, Biosensors and Bioelectronics, 8, 3-4, 197-203, 1993.

73 Haim A., Catalysis: New Reaction Pathways not just a lowering of the Activation Energy, Journal of Chemical Education, 66, 935, 1989.

74 Curtis H., Sue Barnes N., Biology: Fifth edition, Worth Publisher Inc, 1989.

75 Rossman M.G., Moras D., Olsen K.W., Chemical and Biological Evolution of Nucleotide Binding Protein, Nature, London, 250, 194-199, 1974.

76 Michaelis L., Menten M.L., The Kinetics of Invertase Activity, European Journal of Biochemistry, 49, 334-336, 1913.

77 Berg J.M., Tymozcko J.L., Stryer L., Biochemistry 5th Edition, WH Freeman, New York, Ch 8.4, 2002.

78 Eisenthal R., Cornish-Bowden A., The Direct Linear Plot - A new Graphical Procedure for Estimating Enzyme Kinetic Parameters, Biochemistry Journal, 139, 715-720, 1974.

79 Palmer T., Understanding Enzymes, second edition, Ellis Horwood Publisher, Chapter 6: Kinetics of single substrate Enzyme catalysed reactions, 1985.

80 Calvert P., Inkjet Printing for Materials and Devices., Chem. Mater., 13, 3299-305, 2001.

81 de Gans B.J., Duineveld P.C., Schubert U.S., Inkjet Printing of Polymers: State of the art and future developments., Adv. Mater., 16, 203-13, 2004.

82 Derby B., Bioprinting: Inkjet Printing of Proteins, Cells and Cell-containing Hybrid structures, J. Mater. Chem., 18, 5717 – 5721, 2008.

83 Mironov V., Reis N., Derby B., Bioprinting: a Beginning, Tissue Engineering, 12, 631-634, 2006.

84 Morozov V.N., Morozova T.Y., Electrospray Deposition as a Method for Mass Fabrication of Mono and Multicomponent Microarrays of Biological and Biologically Active substances. Analytical Chemistry, 71, p. 3110 - 3117, 1999.

85 Barbulovic - Nad I., Lucente M., Sun Y., Zhang M., Wheeler A.R., Bussmann M., Bio-Microarray Fabrication Techniques- A review, Critical Reviews in Biotechnology, 26, p. 237-259, 2006.

86 Wang X.H., Istepanian R.S.H., Song Y.H., Microarray Image Enhancement by denoising using Stationary Wavelet Transform, IEEE transactions on Nanobioscience, 2, p. 184-189, 2003.

87 Rose D., Microfluidic Technologies and Instrumentation for printing DNA microarrays, in Microarray Biochip Technology, Ed: Schena M., Eaton Publishing: Natick MA. p. 19-38, 2000.

88 Zhao X.M., Xia Y.N., Whitesides G.M., Soft Lithographic Methods for nano-fabrication, Journal of Materials Chemistry, 7, p. 1069-1074, 1997.

89 Kumar A., Whitesides G.M. Features of Gold having Micrometer to Centimetre dimensions can be formed through a combination of Stamping with an Elastomeric Stamp and Alkanethiol ink followed by Chemical Etching, in Applied Physics Letters, 1993.

90 Martin B.D., Gaber B.P., Patterson C.H., Turner D.C., Direct Protein Microarray Fabrication using a Hydrogel 'stamper', Langmuir, 14, p. 3971-3975, 1998.

91 Bernard A., Delamarche E., Schmid H., Michel B., Bosshard H.R., Biebuyck H., Printing patterns of Proteins, Langmuir, 14, p. 2225 - 2229, 1998.

92 Morozov V.N., Protein Microarrays: Principles and Limitations, in Protein Microarrays, Ed: Schena M., Jones and Bartlett Publishers Inc: Sudbury MA, p. 71-106, 2005.

93 Libioulle L., Bietsch A., Schmid H., Michel B., Delamarche E., Contact-inking Stamps for Microcontact Printing of Alkanethiols on Gold, Langmuir, 15, p. 300-304, 1999.

94 Chang Yen D.A., Myszka D., Gale B.K., A novel PDMS Microfluidic Spotter for Fabrication of Protein Chips and Microarrays, Proceedings of SPIE, 5718, p. 110-120, 2006.

95 Tseng F.G., Kim C.J., Ho C.M., A High-Resolution, High-Frequency Monolithic top-shooting Microinjector free of satellite drops - Part 1: Concept, Design and Model, Journal of Microelectromechanical systems, 11, p. 427 - 436, 2002.

96 Wadu-Mestrighe K., Xu S., Amro N.A., Liu G.Y., Fabrication and Imaging of Nanometer-sized Protein patterns, Langmuir, 15, p. 8580 - 8583, 1995.

97 Lee K.B., Park S.J., Mirkin C.A., Smith J.C., Mrksich M., Protein Nanoarrays generated by dip-pen Nanolithography, Science, 295, p. 1702 - 1705, 2002.

98 Piner R.D., Zhu J., Xu F., Hong S.H., Mirkin C.A., 'Dip-pen' Nanolithography, Science, 283, p. 661-663, 1999.

99 Tseng F.G., Lin S.C., Yao D.J., Huang H., Chieng C.C., Technological aspects of protein microarrays and nanoarrays, in: Protein Microarrays, ed: Schena M, Jones and Bartlett Publishers Inc: Sudbury, MA, 2005.

100 Blawas A.S., Reichert W.M., Protein Patterning, Biomaterials, 19, p. 595-609, 1998.

101 Lom B., Healy K.E., Hockberger P.E., A Versatile Technique for Patterning Biomolecules onto Glass coverslips, Journal of Neuroscience Methods, 50, p. 385-397, 1993.

102 McGall G.H., Barone A.D., Diggelmann M., Fodor S.P.A., Gentalen E., Ngo N., The Efficiency of Light-directed Synthesis of DNA Arrays on Glass substrates, Journal of the American Chemical Society, 119, p. 5081 - 5090, 1997.

103 Pirrung M.C., How to make a DNA chip, Angewandte Chemie- International edition, 41, p. 1277 - 1289, 2002.

104 Heller M.J., Forster A.H., Tu E., Active Microelectronic Chip Devices which utilize controlled Electrophoretic Fields for Multiplex DNA Hybridisation and other Genomic Applications, Electrophoresis, 21, p. 157 - 164, 2000.

105 Ringeisen B.R., Wu P.K., Kim H., Pique A., Auyeung R.Y.C., Young H.D., Chrisey D.B., Krizman D.B., Picoliter-scale Protein Microarrays by Laser Direct Write, Biotechnology Progress, 18, p. 1126-1129, 2002.

106 Schwarz A., Rossier J.S., Roulet E., Mermod N., Roberts M.A., Girault H.H., Micropatterning of Biomolecules on Polymer Substrates, Langmuir, 14, p. 5526 - 5531, 1998.

107 Zeng J., Deshpande M., Kan H.C., Gilbert J.R., A Dynamic Spotting Method for Split-pin based Microarrays, Micro Total Analysis Systems (MicroTAS) Conference, p. 143 - 144, 2001.

108 Madou M.J., Fundamentals of Microfabrication, New York: CRC Press, 2002.

109 Blazdell P., Solid Free-forming of Ceramics using a Continuous Jet Printer, Journal of Materials Processing Technology, 137, p. 49 - 54, 2003.

110 Le H.P., Progress and Trends in Inkjet Printing Technology, Journal of Imaging Science and Technology, 42, p. 49 - 62, 1998.

111 Ballarin B., Fraleoni-Morgera A., Frascaro D., Marazzita S., Piani C., Setti L., Thermal Inkjet Microdeposition of PEDOT:PSS on ITO coated glass and Characterisation of the obtained film, Synthetic Metals, 146, p. 201 - 205, 2004.

112 Hart A.L., Turner A.P.F., On the use of Screen and Inkjet Printing to produce Amperometric Electrodes for Lactate, Biosensors and Bioelectronics, 11, p. 263 - 270, 1996.

113 Xu T., Petridou S., Lee E.H., Roth E.A., Vyavahare N.R., Hickman J.J., Boland T., Construction of High-density Bacterial Colony Arrays and Patterns by the Inkjet Method, Biotechnology and Bioengineering, 85, p. 29 - 33, 2004.

114 Allain L.R., Askari M., Stokes D.L., Vo-Dinh T., Microarray Sampling Platform Fabrication using Bubble-jet Technology for a Biochip System, Fresenius Journal of Anals of Chemistry, 371, p. 146 - 150, 2001.

115 Sirringhaus H., Kawase T., Friend R.H., Shimoda T., Inbasekaran M., Wu W., Woo E.P., High-resolution Inkjet Printing of all Polymer Transistor Circuits. Science, 290, (2123), 2000.

116 Chen P.H., Chen W.C., Chang S.H., Bubble Growth and Ink Ejection process of a Thermal Inkjet Printhead, Int. Journal of Mech. Sci., 39, 6, p. 683 - 695, 1997.

117 Asai A., Hara T., Endo I., One-dimensional Model of Bubble Growth and Liquid flow in Bubble Jet Printers, Japan Journal of Applied Physics, 26, p. 1794 - 1801, 1987.

118 Asai A., Hirasawa S., Endo I., Bubble Generation Mechanism in the Bubble jet Recording process, Journal of imaging technology, 14, p. 120 - 124, 1988.

119 Asai A., Application of the Nucleation Theory to the Design of Bubble jet Printers, Japan Journal of Applied Physics, 28, p. 909 - 915, 1989.

120 Asai A., Bubble Dynamics in Boiling under High Heat Flux Pulse Heating, ASME Journal of Heat Transfer, 113, p. 973 - 979, 1991.

121 Asai A., Three-dimensional Calculation of Bubble Growth and Drop Ejection in a Bubble jet Printer, ASME Journal of Fluids Engineering, 114, p. 638 - 641, 1992.

122 Brunahl J., Physics of Piezoelectric Shear Mode Inkjet Actuators, in Condensed Matter Physics, Royal Institute of Technology: Stockholm, p. 109, 2003.

123 Kyser E.L., Sears S.B., Method and Apparatus for Recording with Writing Fluids and Drop Projection, Siliconic Inc, US, 1976.

124 Mikalesen A., Apparatus and Method Employing Phase Change Ink, D. Corp, US, 1988.

125 Derby B, Inkjet Printing of Functional and Structural Materials- Fluid Property Requirements, Feature Stability and Resolution, Ann Rev Mater Res, 40, 395 - 414, 2010.

126 Martin G.D., Hoath S.D., Hutchings J.M., Inkjet Printing - the Physics of Manipulating Liquid Jets and Drops, J Phys: Conf Ser, 105, 012001, 2008.

127 Fromm J.E., Numerical Calculation of the Fluid Dynamics of Drop-on-demand Jets, IBM J Res Dev, 28, 322-333, 1984.

128 Reis N., Derby B., Inkjet Deposition of Ceramic Suspensions: Modelling and Experiments of Droplet Formation, In: Materials Development for Direct Write Technologies, MRS Symposium Proceedings, Mater Res Soc, vol 624, 65-70, 2000.

129 Duineveld P.C., de Kok M.A., Buechel M., Sempel A.H., Mutsaers K.A.H., et al, Inkjet Printing of Polymer Light Emitting Devices, In: Proceedings of the conference on organic light-emitting materials and devices V, vol 4464, SPIE-Int Soc Opt Eng, 59-67, 2001.

130 Stowe C.D., Hadfield M.G., An Experimental Investigation of Fluid Flow Resulting from the Impact of a Water Drop with an unyielding Dry Surface, Proc R Soc Lond Ser A, 373, 419-41, 1981.

131 Derby B., Inkjet printing ceramics: From drops to solid, Journal of the European Ceramic Society, doi:10.1016/j.jeurcermsoc.2011.01.016, 2011.

132 Yarin A.L., Drop Impact Dynamics: Splashing, Spreading, Receding, Bouncing, Annu Rev Fluid Mech, 38, 159-92, 2006.

133 Tanner, L.H., The Spreading of Silicone Oil drops on Horizontal Surfaces, J. Phys. D: Appl. Phys., 12, 1473-1484, 1979.

134 Deegan R.D., Bakajin O., Dupont T.F., Huber G., Nagel S.R., Witten T.A., Capillary Flow as the cause of Ring Stains from Dried Liquid Drops. Nature, 389, 827-9, 1997.

135 Deegan R.D., Bakajin O., Dupont T.F., Huber G., Nagel S.R., Witten T.A., Contact Line Deposits in an Evaporating Drop, Phys Rev E, 62, 756-65, 2000.

136 Smith P., Derby B., Reis N., Wallwork A., Ainsley C., Measured Anisotropy of Alumina Components produced by Direct Inkjet Printing, In: Mandal H, Ovecoglu L, editors, Eur Ceram VIII, Pts 1-3, vol 264-8, p693-6, Key Eng Matters, 2004.

137 ven den Berg A.M.J., de Laat A.W.M., Smith P.J., Perelaer J., Schubert U.S., Geometric Control of Inkjet Printed features using a Gelating Polymer, J Mater Chem, 17, 677-83, 2007.

138 de Gans B.J., Schubert U.S., Inkjet Printing of well-defined Polymer dots and arrays, Langmuir, 20, 7789-93, 2004.

139 Zhang Y., Yang S., Chen L., Evans J.R.G., Shape Changes during the Drying of Droplets of Suspensions, Langmuir, 24, 2752-8, 2008.

140 Noguera R., Lejeune M., Chartier T., 3D Fine Scale Ceramic Components formed by Inkjet Prototyping Process, J Eur Ceram Soc, 25, 2055-9, 2005.

141 Hu H., Larson R.G., Marangoni Effect reverses Coffee Stain Depositions, J Phys Chem B, 110, 7090-4, 2006.

142 Davis S.H., Moving Contact Lines and Rivulet Instabilities, 1; The static rivulet, J Fluid Mech, 98, 225-42, 1980.

143 Allain L.R., Stratis-Cullum D.N., Vo - Dinh T., Investigation of Microfabrication of Biological Sample Arrays using Piezoelectric and Bubble jet Printing technologies. Analytica Chimica Acta, 518, p. 77 - 85, 2004.

144 Setti L., P.C., Bonazzi S., Ballarin B., Frascaro D., Fraleoni - Morgera A., Giuliani S., Thermal Inkjet Technology for the Microdeposition of Biological Molecules as a Viable Route for the Realization of Biosensors, Analytical Letters, 37, 8, p. 1559 - 1570, 2004.

145 Setti L., Fraleoni-Morgera A., Ballarin B., Fillipini A., Frascaro D., Piana C., An Amperometric Glucose Biosensor Prototype Fabricated by Thermal Inkjet Printing, Biosensors and Bioelectronics, 20, 10, p. 2019 - 2026, 2005.

146 Nishioka G.M., Markey A.A., Holloway C.K., Protein Damage in Drop on Demand Printers, Journal of the American Chemical Society, 126, p. 16320 - 16321, 2004.

147 Kaushik J.K., Bhat R.J., Why is Trehalose an exceptional Protein Stabiliser? An Analysis of the Thermal Stability of Proteins in the presence of the compatible Osmolyte Trehalose. Journal of Biological Chemistry, 278, p. 26458 - 26465, 2003.

148 Newman J.D., Turner A.P.F., Home Blood Glucose Biosensors: A Commercial Perspective, Biosensors and Bioelectronics, 20, p. 2435 - 2453, 2005.

149 MicroFab Technologies, I., MicroFab Technote 99-03 Drive Waveform Effects on Ink-Jet Device Performance. www.microfab.com, 2006.

151 http://www.ap-lab.com/circular_dichroism.htm. accessed in 2009.

152 Schuck P., Size-Distribution Analysis of Macromolecules by Sedimentation Velocity Ultracentrifugation and Lamm Modelling. Biophysical Journal, 78, 3, p. 1606-1619, 2000.

153 Compton L.A., Johnson W.C.Jr., Analysis of Protein Circular Dichroism Spectra for Secondary Structure using a Simple Matrix Multiplication. Analytical Biochemistry, 155, 1, p. 155-167, 1986.

154 Goldstein J., Newbury D.E., Joy D.C., Lyman C.E., Echlin P., Lifshin E., Sawyer L., Michael J.R., Scanning Electron Microscopy and X-ray Microanalysis, Springer, ISBN: 9780306472923, 2003.

155 http://www.microscopyu.com/articles/phasecontrast/phasemicroscopy.html, accessed in 2009.

156 Yao S.J., Chemistry and Potential Methods for In Vivo Glucose Sensing, in Bioinstrumentation and Biosensors, Ed: Wise D.L., Marcel Dekker: New York, p. 229 - 248, 1990.

157 Sahai H., Ageel M.I., The Analysis of Variance; fixed, random, and mixed models, Springer, ISBN: 0817640126, 2000.

158 Saunders R.E., Gough J.E., Derby B., Delivery of Human Fibroblast Cells by Piezoelectric Drop on Demand Inkjet Printing, Biomaterials, 29, 2, p. 193 - 203, 2008.

159 Perez-Ramirez B., Smales J.J., Therapeutic Proteins: Methods and Protocols, Ed: J.D.C. Smales C.M., Humana Press Inc: Totowa, New Jersey, p. 301 - 318, 2005.

160 Gouda M.D., Singh S.A., Rao A.G.A., Thakur M.S., Karanth N.G., Thermal Inactivation of Glucose Oxidase: Mechanism and Stabilisation using Additives,J. Biol. Chem., 278, 24324, 2003.

161 Liu X., Xu Y., Ma X., Li G., A third-generation Hydrogen Peroxide Biosensor fabricated with Haemoglobin and Triton X-100, Sensors and Actuators B: Chemical, 106, 1, 284-288, 2005.

162 Soltman D., Subramanian V., Inkjet-Printed Line Morphologies and Temperature Control of the coffee ring effect, Langmuir, 24, pp 2224-31, 2008.